Morphology control of the hair-cell bundle for frequency-selective auditory detection

Atitheb Chaiyasitdhi

HAL Id: tel-03518699
https://pastel.hal.science/tel-03518699

Submitted on 10 Jan 2022

THÈSE DE DOCTORAT
DE L'UNIVERSITÉ PSL

Préparée à Institut Curie

Morphology control of the hair-cell bundles for frequency-selective auditory detection

Contrôle de la morphologie de la touffe ciliaire des cellules mécanosensorielles ciliées pour une détection auditive sélective en fréquence

Soutenue par
Atitheb CHAIYASITDHI
Le 21 Septembre 2021

Ecole doctorale n° 474
Frontières de l'Innovation en Recherche et Éducation

Spécialité
Biochimie, biologie cellulaire et moléculaire, physiologie et nutrition

Composition du jury:

Martin, LENZ
Directeur de recherche, Université Paris-Saclay — *Président*

Peter, BARR-GILLESPIE
Professeur, Oregon Health & Science University — *Rapporteur*

Jennifer, GALLOP
Professeure, University of Cambridge — *Rapporteur*

Julie, PLASTINO
Directrice de recherche, Institut Curie — *Examinateur*

Alphée, MICHELOT
Chargé de recherche, Université d'Aix-Marseille — *Examinateur*

Christine, PETIT
Professeure, Institut de l'Audition — *Examinateur*

Pascal, MARTIN
Directeur de recherche, Institut Curie — *Directeur de these*

Acknowledgements

During four years of my PhD studies, many people lent their supports to me academically and emotionally. I would like to dedicate these pages to express my heartfelt thanks to them.

First of all, I would like to thank my supervisor, Pascal Martin, for investing his time and effort in me. This project would not have been possible without him. Pascal is not only the person who always strikes for rigorous conduct of science (and asks you to perform difficult experiments) but he is also a caring advisor who helps you to become a better scientist through his support and guidance. I would like to also thank my co-supervisor, Christine Petit, who put trust in me. The discussions I had with you always give new insights and provide a new aspect to look at my experiments.

I would like to thank members of the thesis advisory committee, Nicolas Michalski, Nadine Gérard, and Julie Plastino for their valuable comments and suggestions. Many interesting experiments happened as a result of the discussions we had during the thesis advisory committee meeting.

This project relies heavily on electron microscopy and I would like to thank Vincent Michel at Institut Pasteur who taught me scanning electron microscopy since the beginning of my PhD. I also spent a lot of time working on the ultrastructure of the stereociliary cores using transmission electron microscopy and for this I am deeply grateful for the support from Ilse Hurbain, Aurelie Di cicco and Daniel Levy. I am gratefully acknowledging Leroy Olivier for his support on fluorescence microscopy at the PICT-IBiSA imaging platform here at Institut Curie.

I thank members of the team MARTIN and also members of the UMR168. When I first arrived, the team was already small. Melanie Tobin was leaving and Marie Pochitaloff-Huvale was in the last year preparing for her PhD defense. There was also one point where I was the only member in the team for almost a year. Small lab is nice because it means there are a lot of interaction between the student and the advisor but I am also grateful that at the point of writing this thesis the team has grown to 5 members with Achille Joliot, Laure Stickel, and Henri Ver Hulst joining the lab!

Lastly, I would like to thank my family and especially my wife, Soonyata Mianlamai, who has gone through up and downs with me on my side.

I would like to end my acknowledgements with the first sentence from 'the Analects'.

學而時習之、不亦說乎。

Is not it a pleasure to study and practice what you have learned?

It is indeed my pleasure to study and practice what I have learned but without the people I mentioned here, *'the pleasure to study and practice what I have learned'* would not have been possible.

Contents

General Introduction

Hearing allows animals to communicate with each other and sense their acoustic environment with great efficiency. This technical prowess is the result of the operation of hearing organs over large dynamic ranges of sound intensities and frequencies. In particular, humans can hear sound intensities that span 6 orders of magnitude in sound-pressure levels (0 to 120 dB SPL)[1] and up to 3 orders of magnitude in sound frequencies (20 Hz to 20 kHz). Some vertebrates like bats and whales (and even some exotic frogs!) can hear sounds with frequencies as high as 100 kHz, corresponding to temporal variations of the air pressure over timescales that can be as small as 10 μs. Remarkably, the threshold of hearing for the faintest sound corresponds to mechanical vibration in the inner ear comparable to that of the Brownian motion; the ear thus operates down to a physical limit set by its own thermal fluctuations. These remarkable features make hearing a very exquisite sensory system.

Hearing in vertebrates is based on the operation of mechanosensory hair cells that are located in the inner ear. Hair cells are each endowed with a bundle of a few tens to a few hundred microscopic microvilli-like protrusions called stereocilia (the 'hairs' of the hair cells) that project from the apical surface of the cells. Hair cells act as mechano-electrical transducers that convert sound-evoked vibration into electrical signals. The hair bundle operates as a mechanical antenna: mechano-electrical transduction is initiated by the deflections of the hair bundle. In auditory organs, the morphology of the hair bundles is tightly coupled to their function as frequency-selective sensors. Hair bundles at the basal region of the cochlea, which is devoted to the detection of high frequencies are shorter and composed of more stereocilia than those detecting low frequencies at the apical region.

The morphology of the hair bundle is imposed by that of the actin core of its stereocilia. The stereociliary core is made of a parallel network of heavily cross-linked actin filaments. Incorporation of newly synthesized cytoplasmic actin into the polymerized barbed-end of the paracrystalline actin core is essential for maintaining the stereociliary structure, over the lifespan of the animal. In the mature hair cells, the stereociliary structure is remarkably stable along most of its length except ~ 0.5 μm near the tip, where actin incorporation takes place. The stereociliary

---

[1] Sound-pressure level (SPL) is a measure of the sound pressure P relative to the reference sound pressure P_o at the threshold of hearing (20 μPa), where $SPL = 20 \log_{10} (P/P_o)$. At the threshold of pain or the loudest sounds human can percieve (120 dB SPL), the sound pressure is 20 Pa or 6 order of magnitude greater than the threshold of hearing.

tip is also where the transduction channels are located. Indeed, it has been shown in cochlear hair cells from mice that perturbing the mechano-electrical transduction (MET) machinery results in stereocilia remodelling, suggesting that the actin core could become dynamic again. Such observations led to the hypothesis that the mechanotransduction, perhaps as the result of a Ca^{2+} influx, regulates the dynamics of actin polymerisation in the stereocilia and thus that there might be feedback between mechano-electrical transduction and the hair bundle morphology.

During my PhD, I further explored the hypothesis that there is feedback between the mechano-electrical transduction and the hair bundle morphology using vestibular hair cells of the frog. My objective was to test whether the regulation of the actin dynamic in the stereocilia by mechano-electrical transduction is employed across species and also to probe the mechanisms that may be involved in the maintenance of the hair bundle.

The manuscript is organized into four main chapters. In the first chapter, I provide a general introduction to the hair cells, starting from their anatomy and function as mechano-electrical transducers to then present the current knowledge about the role of actin dynamics on the development and maintenance of the stereociliary architecture. I provide comparative descriptions of actin dynamics and maintenance between the stereociliary structure and that of other actin-based protrusion, such as microvilli and filopodia. Finally, I then describe the available evidence indicating that mechano-electrical transduction may regulate the actin dynamic in the stereociliary core.

In the second chapter, I describe the methods used throughout the work. Using saccular hair cells of the frog Rivan 92, I perturbed the mechano-electrical transduction machinery by either blocking the transduction channels or disrupting the tip links with pharmacological drugs. By combining the scanning and transmission electron microscopy, I studied the morphology of the hair bundle and its stereociliary actin core under the control condition and after perturbing mechanotransduction. I also used mechanical stimulations of the hair bundles to characterize their stiffness under these two conditions. Finally, I studied the localization of actin nucleator formins and the effects of inhibiting formins on the morphology of the hair bundles.

In the third chapter, I describe the results obtained during my PhD study. My original contribution to this field was to demonstrate that stereocilia of the frog saccular hair bundle widen (and also shorten) as a result of pharmacological perturbation of the mechano-electrical transduction machinery and that these morphological changes to an increase of the number of actin filaments in the stereociliary core. Furthermore, I also found that formins are likely localized

at the stereociliary tips of the frog saccular hair bundles, and may be involved in the stereocilia widening observed upon blocking of the transduction channels.

In the last chapter, the results will be discussed within the context of the relevant literature.

Chapter I

I. Introduction

Contents

A. Hair-cells: the mechano-electrical transducers

A.1 Morphology and function of hair cells across vertebrate species

Hearing in all vertebrates is based on the operation of mechanosensory hair cells in the inner ear. The presence of hair cells in both lampreys (modern jawless fish) and modern gnathostomes (jawed vertebrates) indicates the evolutionary origin of vertebrate hair cells in a common ancestor from at least ~400 million years ago when the two lineages separated from one another (Coffin et al. 2004). Hair cells work as sensory receptors not only for hearing but also for other sensory modalities. Hair cells are used to detect fluid flows in the fish's lateral line system for rheotaxis, prey detection and schooling, sense head in the vestibular system for balance, and detect sound-evoked vibrations in the auditory organs for hearing (Fig. I-1).
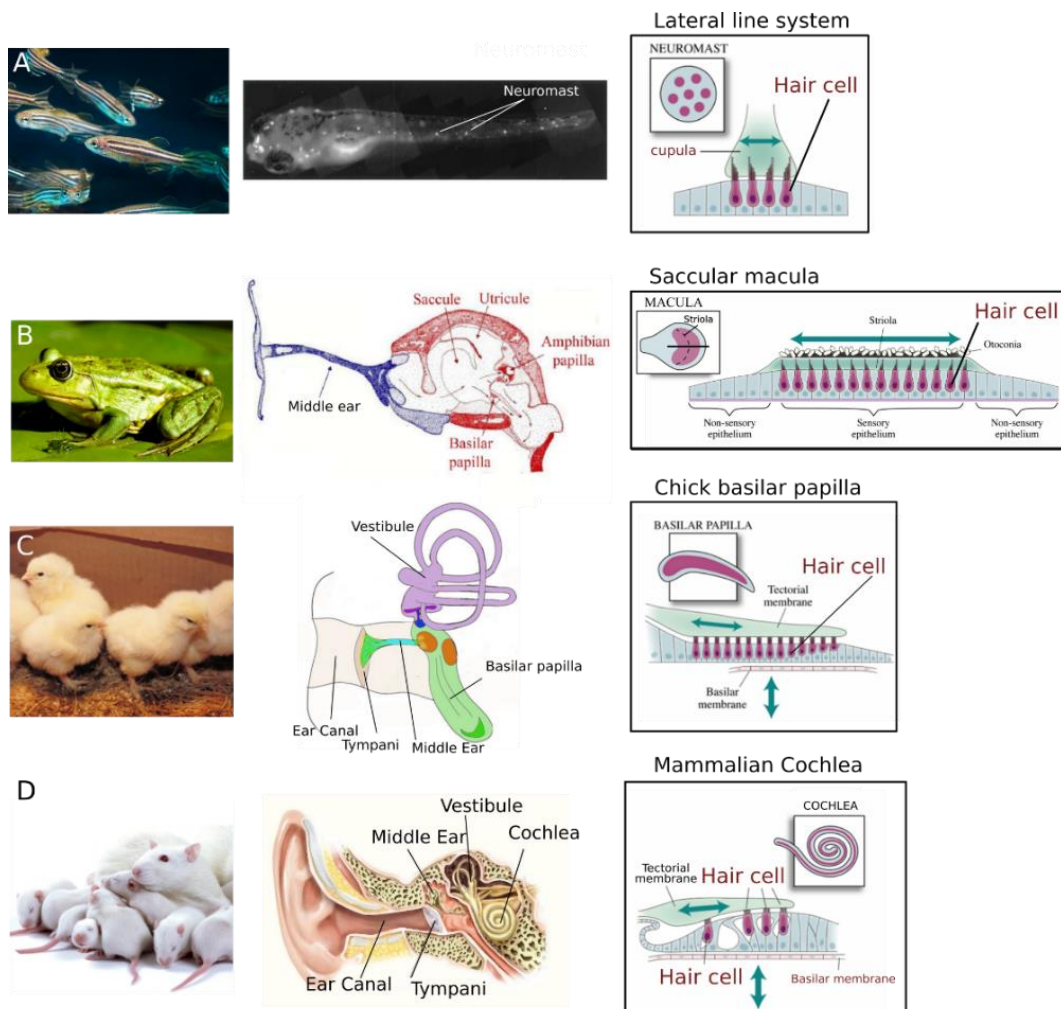
Figure I-1: HAIR CELLS ACROSS VERTEBRATES SPECIES. Diverse modalities of mechanosensation are based on sensory hair cells. Hair cells take their name from a specialized organelle projecting from their apical surface and composed of microscopic 'hairs': the hair

bundle. *The lateral line system* - **(A)** In fish, the lateral line system detects surrounding fluid flows. The lateral line is composed of sensory units called neuromasts that are located along the fish body, as shown in the fluorescence image (Middle panel). Each neuromast is a cluster of about ten hair cells with their hair bundles embedded in a jelly-like sheath called the cupula. *Vestibular organs* - **(B)** In the vestibular system of the inner ear, here from the frog, the saccular macula is used for detecting linear acceleration of the head. (Right panel) A cross-section of the saccular macula shows hair bundles embedded in the otolithic membrane. On top of the membrane are calcium carbonate ($CaCO_3$) crystals called otoconia that act as an inertial mass when the head accelerates up and down, thereby creating shearing movements that deflect the hair bundles. *Auditory organs* - The basilar papilla (in frogs and birds), the amphibian papilla (in frogs), and the mammalian cochlea are fluid-filled tubes. The mammalian cochlea is coiled into a spiral shape resembling the shell of a snail; hence the name 'cochlea' or snail shell in Latin. The tube is divided into chambers by an inner partition called the organ of Corti and supported by the basilar membrane; this is where mechanosensory hair cells are located. In auditory organs, sound-evoked vibrations generate vertical movements of the basilar membrane that supports the sensory tissue, resulting in a shearing movement between the tectorial membrane and the apical surface of the hair cells and thus in a deflection of the hair bundles. **(C)** The auditory hair cells from the chick basilar papilla. (Right panel) A cross-section of the chick basilar papilla shows hair cells with varying heights. **(D)** The auditory hair cells from the mammalian cochlea. (Right panel) A cross-section of the mammalian cochlea shows three outer hair cells (OHC) and a single inner hair cell (IHC).

Hair cells are cylindrical cells that are each endowed with a bundle of a few tens to a few hundred apical protrusions called stereocilia that are arranged into rows of increasing height a (Fig. I-2.A-B). Each stereocilium within the hair bundle is 1 to 10 µm tall and has a diameter of a few hundred nanometres (Lewis G Tilney and Saunders 1983). Each stereocilium is connected to its taller neighbour by an oblique link, called the tip link, that transmits force to mechanosensitive ion channels residing near the stereociliary tip (J.O. Pickles, Comis, and Osborne 1984; Assad, Shepherd, and Corey 1991; Beurg et al. 2009) (Fig. I-2.C). A deflection of the hair bundle results in shearing between adjacent stereocilia, which modulates tension in the tip links and in turn the open probability of the transduction channels. Channel opening elicits an increased influx of cations, mainly K^+ ions but also Ca^{2+} ions, corresponding to the transduction current (Fig. I-3.A).
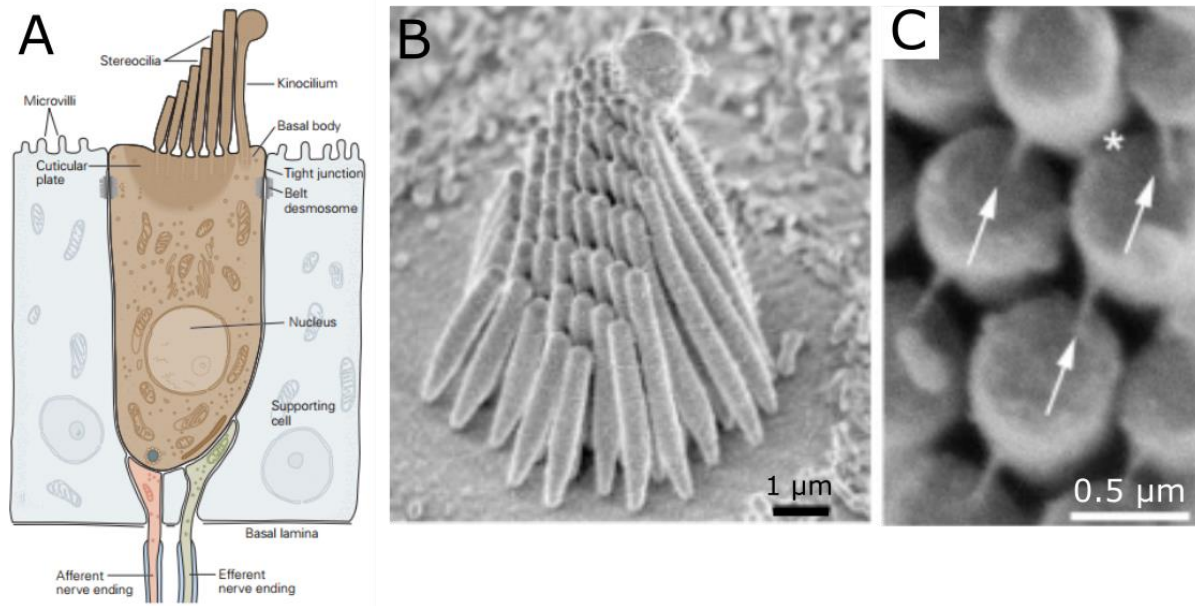
Figure I-2: HAIR CELL AND ITS HAIR BUNDLE. (A) Schematic representation of a typical hair cell within a sensory epithelium (here from the frog saccule). The hair cell is surrounded by supporting cells that are endowed with short actin-based protrusions called microvilli on their apical surface. On top of each hair cell is a hair bundle, a tuft of specialized elongated microvilli called stereocilia that arrange themselves into rows of increasing height. Next to the tallest stereocilia is the kinocilium, a microtubule-based protrusion composed of an array of 9 microtubule doublets surrounding a central microtubule pair (9 + 2 axoneme). The electrical signal from a hair cell is transmitted to the brain along the afferent nerve fibres while efferent nerve fibres bring signals from the central nervous system to the hair cell. Figure from Martin, P., Manley, G.A. (2020) Auditory processing by the cochlea (Principles of Neural Science 6th Edition). **(B)** This electron micrograph shows the arrangement of the stereocilia in rows of graded height, resembling a staircase. Mechano-electrical transduction results from deflections of the hair bundle along a horizontal axis within the vertical plane of mirror symmetry of the bundle. **(C)** Tip links (arrows) that interconnect the tip of the shorter stereocilia to their taller neighbours. The links transmit force to mechanosensitive ion channels residing near the stereociliary tip. Figures (B-C) are from (Tompkins et al. 2017).

The relation between the current I that flows through the channels and the deflection X of the hair bundle is sigmoidal (Fig. I-3.B). Remarkably, the current rises from near zero to a saturating value for a hair-bundle movement that spans only a couple hundred nanometers, a distance comparable to the diameter of a single stereocilium. The resting position of a hair bundle sits near the steepest region of the curve. Correspondingly, about 15 - 50% of the transduction channels are

open at rest and there is thus a continuous influx of cations even in the absence of a mechanical stimulus (Johnson et al. 2011; Hudspeth 2014; Pascal Martin and Hudspeth 2021). Although this condition imposes a metabolic load on the hair cell ("what comes in must come out"), it is necessary to ensure that even a small deflection of the bundle evokes a significant change in the opening probability of the transduction channels and thus a significant transduction current (Fig. I-3.B). The open probability of the transduction channels at rest defines the operating point of the hair bundle.
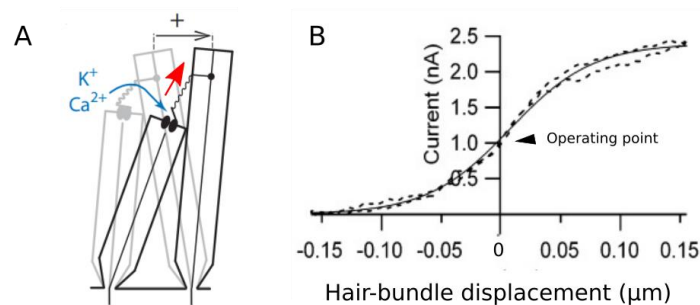
Figure I-3: MECHANO-ELECTRICAL TRANSDUCTION BY A HAIR CELL. (A) Schematic representation of two stereocilia interconnected by a tip link that acts as "gating spring" (D. Corey and Hudspeth 1983; J. Howard and Hudspeth 1988). At the lower end of the tip link is the transduction channel and at the upper end of the tip link is the myosin motor complex that tenses and modulates tension in the tip link (arrow indicates tip-link tension). A deflection of the hair bundle towards the tallest stereocilia, defined as the positive direction, lead to the openings of the mechanosensitive ion channels—the transduction channels, thus allowing for an increased cation influx, mainly K^+ but also Ca^{2+} ions. **(B)** The relation between the current that flows through the transduction channels and the hair-bundle displacement is sigmoidal. For negative deflections, the transduction channels are all closed (no current), whereas, for large positive deflections, the transduction channels are all open (the current saturates). At the operating point (no deflection), a large fraction (here about 50%) of the transduction channels remain open; there is thus a significant inward current at rest (here 1 nA). Figure B is adapted from (Johnson et al. 2011).

When the tip links are chemically disrupted, the hair bundle moves in the positive direction and the transduction channels close (Tobin et al. 2019). These observations indicate that the transduction channels are inherently more stable in a close state and that the tip links are under tension at rest. The resting tension pulls on the tip links to partially open the transduction channels and set the operating point of the hair bundle (Fig. I-3.A and I-4). The resting tip-link tension in frog saccular hair bundles was estimated to be 57 pN for the whole bundle and 8 pN per tip link (using a single compartment chamber at 100 μM Ca^{2+}). In a recent study by Alonso et al. (2020) using a two-compartment chamber (250 μM Ca^{2+} artificial endolymph and 2 mM Ca^{2+} artificial perilymph), the resting tension is found to be ~ 20 pN per tip link for oscillating hair bundles and

8 pN for quiescent hair bundles. Myosin motors located at the upper end of the tip link, perhaps Myosin-1c or Myosin-7a, (Holt et al. 2002; Stauffer et al. 2005b; Grati and Kachar 2011; Li et al. 2020), have been proposed to set the tip links under tension and set the operating point of the hair bundle (Hudspeth and Gillespie 1994b).
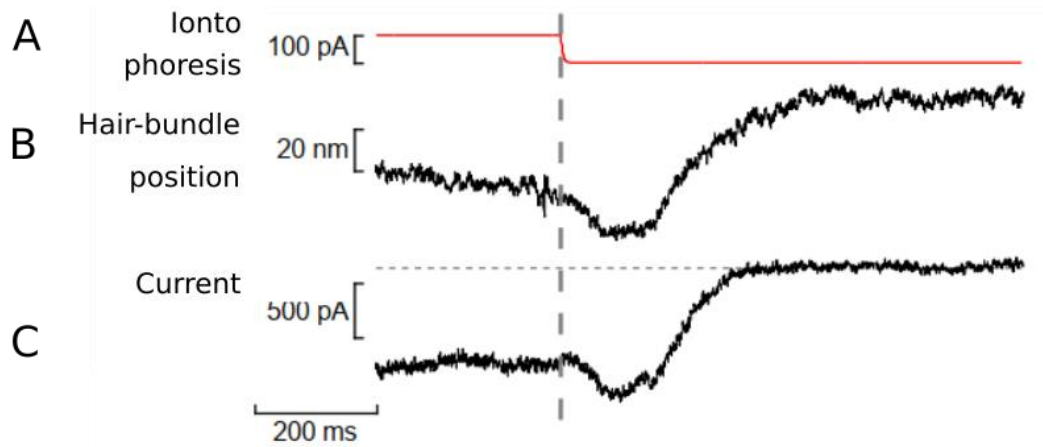
Figure I-4: TENSION IN THE TIP LINKS. Chemical disruption of the tip links with EDTA iontophoresis betrays tension in the tip links of the rat cochlea hair bundles. **(A)** The command signal for iontophoresis as a function of time. The vertical dashed line indicates when the calcium chelator EDTA is applied. **(B)** Hair-bundle position as a function of time. Tip-link disruption evokes a positive offset of the hair-bundle position. **(C)** Current flowing through the transduction channels as a function of time. After the tip links break, the inward current goes to zero (horizontal dashed line, due to channel closure upon tip-link disruption. Note that the onset of EDTA iontophoresis, the bundle first moves in the negative direction and the channels open, resulting in an increased inward current; this is because the tension in the tip links first increases at the Ca^{2+} concentration drops before the concentration is so low that the tip links break. Figure from the thesis manuscript of Mélanie Tobin (2017).

In the cochlear hair cells, the resting tensions at the level of single tip links vary along the tonotopic axis[2] (Tobin et al. 2019). Hair cells that respond to higher sound frequencies are endowed with higher tip-link tension. This gradient in tip-link tension gradient implies its role in mechanical tuning for frequency discrimination. Intriguingly, the relationship between the characteristic frequency and the single tip-link tension exhibits a steeper gradient in outer hair cells than in the inner hair cells (Tobin et al. 2019). This may reflect the division of labour between the inner hair cells that propagate nervous signals to the brain and the outer hair cells that are thought to amplify the signal.

---

[2] Tonotopic axis refers to the spatial arrangement that each sound frequency stimulates hair cells at a specific region within the cochlea. Hair cells at the base of the cochlear detect high sound frequencies whereas those at the apex of the cochlea detect low frequencies.

How does the brain know that a hair bundle has been deflected by an external stimulus? Opening of the transduction channels depolarizes the hair cell, i.e. increases the transmembrane potential of the cell (D. P. Corey and Hudspeth 1983). This leads to the release of neurotransmitter chemicals at synapses (about 10 per hair cell) between the soma of the hair cell and afferent nerve fibres and an increased firing rate of action potentials in the nerve fibres that then transmit the signal to the brain. Closure of the channels does the opposite, i.e. cell hyperpolarization, decreased release of neurotransmitters, and decreased rate of firing in afferent nerve fibres.

A.2 Architecture and mechanics of the hair bundle

a.   Morphological features of the hair bundle

The hair bundle is composed of a few tens to a few hundred stereocilia that are arranged in rows of increasing height, forming a staircase pattern. Next to the tallest stereocilia, there is also sometimes a kinocilium, which is a "true" cilium comprising an axonemal core, i.e. 9 circumferential doublets of microtubules and a pair of singlet microtubules at the centre. The kinocilium is present at the early stages of hair-bundle development and may play a role in defining the polarity of the hair bundle (Denman-Johnson and Forge 1999; Tona and Wu 2020). In the mammalian and bird cochlea, the kinocilium then regresses and disappears at a later developmental stage but remains in mature vestibular organs and vestibular and auditory organs of non-mammalian species (Lewis G Tilney et al. 1986; Denman-Johnson and Forge 1999). Each bundle displays a vertical plane of mirror symmetry. The hair cell is maximally sensitive for deflections along a horizontal axis within this plane (Shotwell, Jacobs, and Hudspeth 1981). Vertebrate hair bundles, regardless of their sensory systems, are all 'built' after this blueprint.
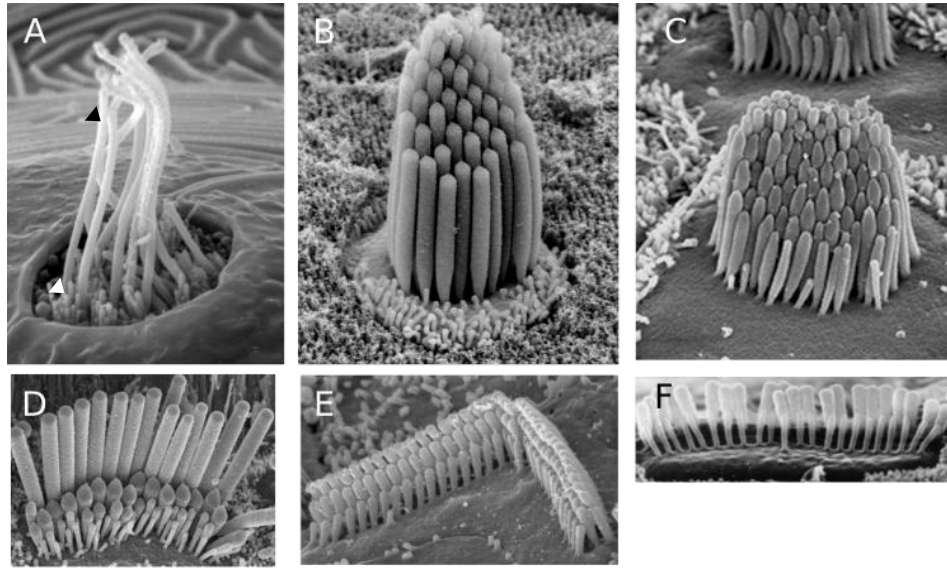
Figure I-5: HAIR-BUNDLE MORPHOLOGY. (A) The neuromast from the fish's lateral line system is a cluster of mechanosensory hair cells centrally located inside the cavity. Each hair cell is endowed with a long kinocilium (▲) and several shorter stereocilia (∆). Figure by A. Forge. **(B)** A frog saccular hair bundle with a few tens of stereocilia; bundle is used for detecting linear accelerations of the frog's head. I studied this type of hair bundle during my PhD. Figures by B. Kachar. **(C)** A chick cochlear hair bundle with a few tens of stereocilia, from the low-frequency region of the organ. Figure by P. Barr-Gillespie and K. Spinelli. **(D-E)** In the mammalian cochlea, here from the rat, hair cells come in two flavours: inner hair cells (D) and outer hair cells (E). Both types of hair bundles show three prominent rows of stereocilia. In outer hair cells, the hair bundle has a characteristic V-shape, whereas those of inner hair cells are planar. **(F)** A bat cochlear hair bundle of an inner hair cell in the high-frequency region. The bundle shows only two rows of stereocilia, the minimum configuration required for mechanotransduction. Figures D-F by C. Hackney and D. Furness from (Fettiplace and Kim 2014).

The morphology of the hair bundle is tightly coupled to its function as a mechanosensory antenna. In neuromasts from the fish's lateral line system at the surface of the skin, a cluster of mechanosensory hair cells senses local fluid flows. Each hair cell within a neuromast has a very long kinocilium (~15 µm) accompanied by several short stereocilia (Fig. I-5.A). A long kinocilium may serve as a flexible antenna that is very sensitive to drag forces exerted by a fluid flow along the fish, thus perpendicular to the long axis of the kinocilium. A long kinocilium is less stiff and exposes a larger area to fluid flow, thus increasing the operating range of the hair cell (Spoon and Grant 2011). In the frog's saccular macula, a vestibular organ used for detecting linear accelerations of the head, hair bundles show kinocilia that are comparable in height to the tallest stereocilia (Fig. I-5.B). These bundles respond to shearing movements of an overlying membrane called the otolithic membrane, to which the kinociliary tips are attached, with respect to the apical surface of the hair cells (Fig. I-6). These frog hair bundles are also very cohesive (Kozlov, Risler, and Hudspeth 2007) and thus move as a single unit, maximizing the sensitivity of mechano-electrical transduction by ensuring concerted gating of the transduction channels. During my PhD, I studied the hair bundle of this type.
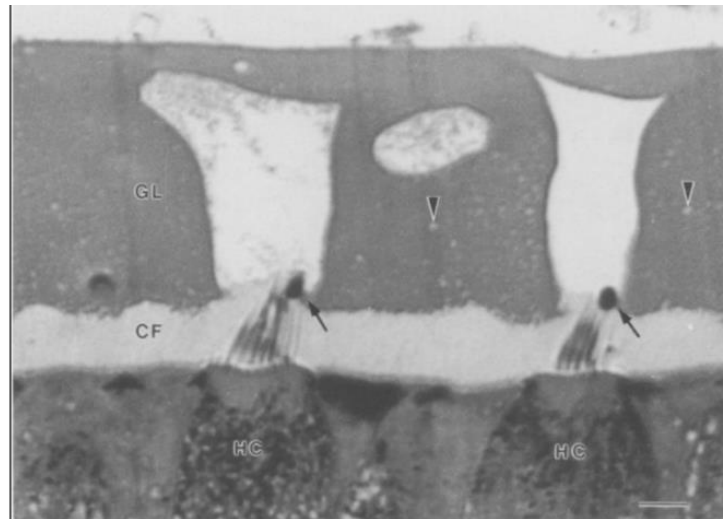
Figure I-6: FROG SACCULAR HAIR-BUNDLE. Light micrograph of a vertical section of the sensory epithelium of the bullfrog sacculus. The gelatinous sheath layer (GL) forms large cavities above the hair cells (HC). Each hair cell is surrounded by supporting cells and the top of the kinocilia (black arrows) are attached to the overlying gelatinous sheath layer of the otolithic membrane. Figure from (Bechara Kachar, Parakkal, and Fex 1990).

In contrast to frog (Fig. I-5.B and Fig. I-6) and chick hair bundles (Fig. I-5.C), which are directly attached to an overlying membrane, the hair bundles of inner hair cells (IHCs) in the mammalian cochlea are free-standing. These bundles adopt a planar shape (Fig. I-5.D and F) that may maximize drag and increase sensitivity to radial fluid flow hypothesized to stimulate the bundles in the cochlea. In contrast, the characteristic V-shape (or U-shape) of the hair bundles of outer hair cells (OHCs), whose tips are embedded in the overlying tectorial membrane, is believed to reduce viscous resistance to cross flow, thus increasing IHC stimulation (Ciganović, Wolde-Kidan, and Reichenbach 2017) (Fig. I-5.E). The two types of hair cells in the mammalian cochlea—inner and outer hair cells—are associated with different functions: inner hair cells are thought to be the true sensors of the organ, sending information about cochlea vibrations to the brain, whereas outer hair cells are believed to serve as mechanical amplifiers of the input to the inner hair cells (Dallos 2008). As described here, this division of labour is associated with different morphologies of the corresponding hair bundles in different modes of bundle stimulation. Interestingly, mammals tend to hear higher sound frequencies than non-mammals (Fay and Popper 1994; 1999), a property associated with hair bundles with a smaller number of rows, often down to only three and even only two in some bats (Fig. I-5.F).
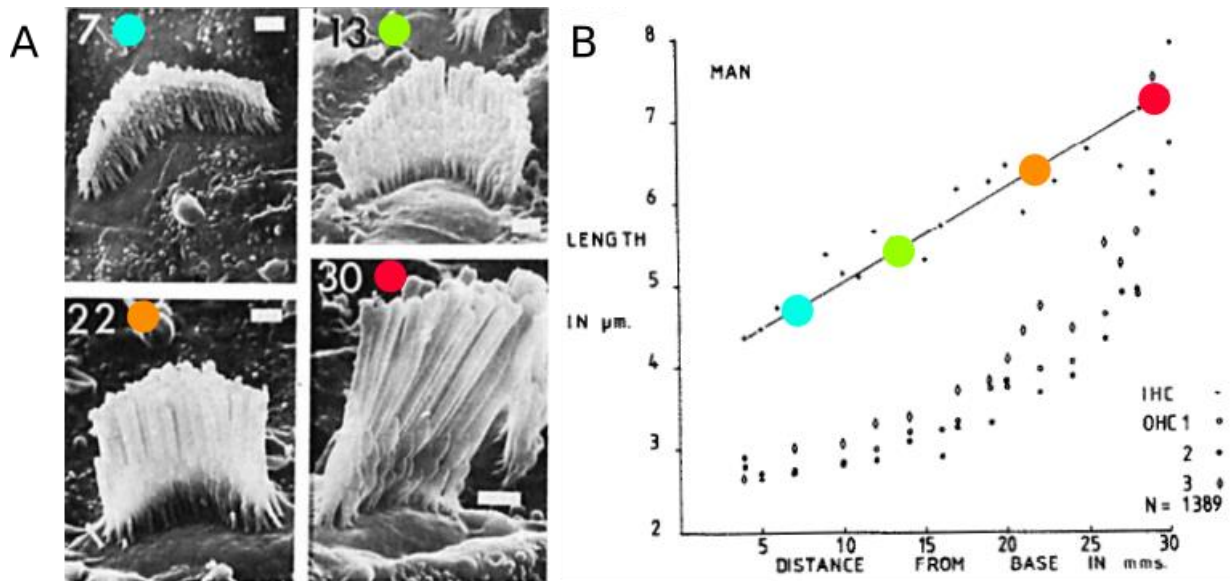
Figure I-7: MORPHOLOGICAL GRADIENTS OF HAIR BUNDLES IN AUDITORY ORGANS. (A) Scanning electron micrographs of human hair bundles at each corresponding position (in mm from the base of the cochlea). Short hair bundles at the basal region detect high sound frequencies, whereas long hair bundles at the apical region detect lower sound frequencies. The morphological gradient is steeper for outer hair cells than for inner hair cells. Scale bar 1 µm. Figure from (Wright 1983). **(B)** Length of the tallest stereocilia in hair bundles from inner hair cells (IHC) and outer hair cells (OHC) along the longitudinal axis of the human cochlea (Wright 1984).

The cochlea works as a frequency analyser: high-frequency sounds elicit vibrations near the base of the cochlea, where they are detected by the hair cells residing there, whereas lower-frequency sounds are detected at progressively more apical regions of the organ. This frequency map is called the tonotopic map. One ubiquitous feature of auditory organs is that tonotopy is associated with morphological gradients of the hair bundle: the number of stereocilia, the stereociliary width, and the stereociliary height all vary monotonically along the length of the organs (Lewis G Tilney and Saunders 1983). Hair cells that detect high sound frequencies, at the basal end of the organ, are endowed with shorter hair bundles and more stereocilia than hair cells are dedicated to the detection of lower frequencies; the height and number of stereocilia in a hair bundle vary monotonically along the tonotopic axis (Fig. I-7.A). Regulation of the hair bundle size is so tight that one can locate the position of a particular hair cell by knowing only the dimensions of its hair bundle[3] (Lewis G Tilney and Saunders 1983). The study of hair-bundle height in the human cochlea suggests that the precision with which the hair cell regulates the size of its hair bundle is within the range of a few nanometres because the difference in height between

---

[3] Remarkably, it was shown that the amount of polymerized actin in the hair bundles of chicken cochlear hair cells remains nearly the same along the tonotopic axis of the cochlea (G. Tilney and Tilney 1988).

the most basal and most apical outer hair bundles, corresponding to a distance along the cochlear axis of about 3.5 cm, is only about 3-4 µm (Wright 1984) (Fig. I-7.B).

The gradient in hair-bundle height is expected to result in a passive gradient of hair-bundle stiffness along the cochlea. Indeed, the pivotal stiffness K_{sp} of a hair bundle ought to vary as $1/h^2$, if h is the hair bundle height where the force is applied (J. Howard and Ashmore 1986). For a simple harmonic oscillator, for which the natural frequency $\omega_{natural} \sim \sqrt{K_{sp}}$, it would make sense that shorter hair bundles are 'built' to respond best at high frequencies, and vice versa. Indeed, mechanical gradients have been observed already in the early 1980s with hair bundles from both inner and outer hair cells from the guinea pig cochlea (Strelioff and Flock 1984). A recent study confirmed the existence of such a passive mechanical gradient with hair cells from the rat cochlea (Tobin et al. 2019). However, frequency discrimination cannot happen via passive mechanical resonance alone, for which the hair bundle would build up a sensitive response by accumulating energy from cycle to cycle of the sound stimulus; the hair bundles are overdamped (Crawford and Fettiplace 1985a; Denk, Webb, and Hudspeth 1989). Still, the tight regulation of the hair-bundle size along the cochlea suggests that the morphological gradient might serve physiological purposes involving frequency discrimination by hair cells.

b.   Organization of actin filaments in the core of stereocilia

A stereocilium is made of a parallel network of a few hundred heavily cross-linked actin filaments that stretch from a few nanometres below the stereociliary tip to a dense disorganized network of actin filaments called the cuticular plate underneath the apical surface of the hair cell (Fig. I-8.A-B). There are two types of actin filament packing in the stereociliary core: liquid and hexagon. the liquid packing of actin filaments has been observed in mouse inner hair cells (Mogensen, Rzadzinska, and Steel 2007), in mouse utricular hair cells (Krey et al. 2016), and lizard cochlea hair cells (L G Tilney, Derosier, and Mulroy 1980) whereas chick cochlea and utricles exhibit hexagonal packing (L G Tilney, Derosier, and Mulroy 1980). In the shaft region of a stereocilium, adjacent actin filaments are spaced by about 10 nm (L G Tilney, Derosier, and Mulroy 1980) (Fig. I-18.C-D). Near their insertion into the apical surface of the hair cells, in a region that spans a micrometre or so above the surface, the stereocilia taper, i.e. their diameter progressively decreases. A few tens of actin filaments with denser packing penetrate the cuticular plate, where they form a so-called 'rootlet' (Fig. I-8.B and I-9). As a result, when the hair bundle

is deflected a stereocilium behaves like a stiff rod that pivots about its insertion point; the stereocilium does not bend (Crawford and Fettiplace 1985b).
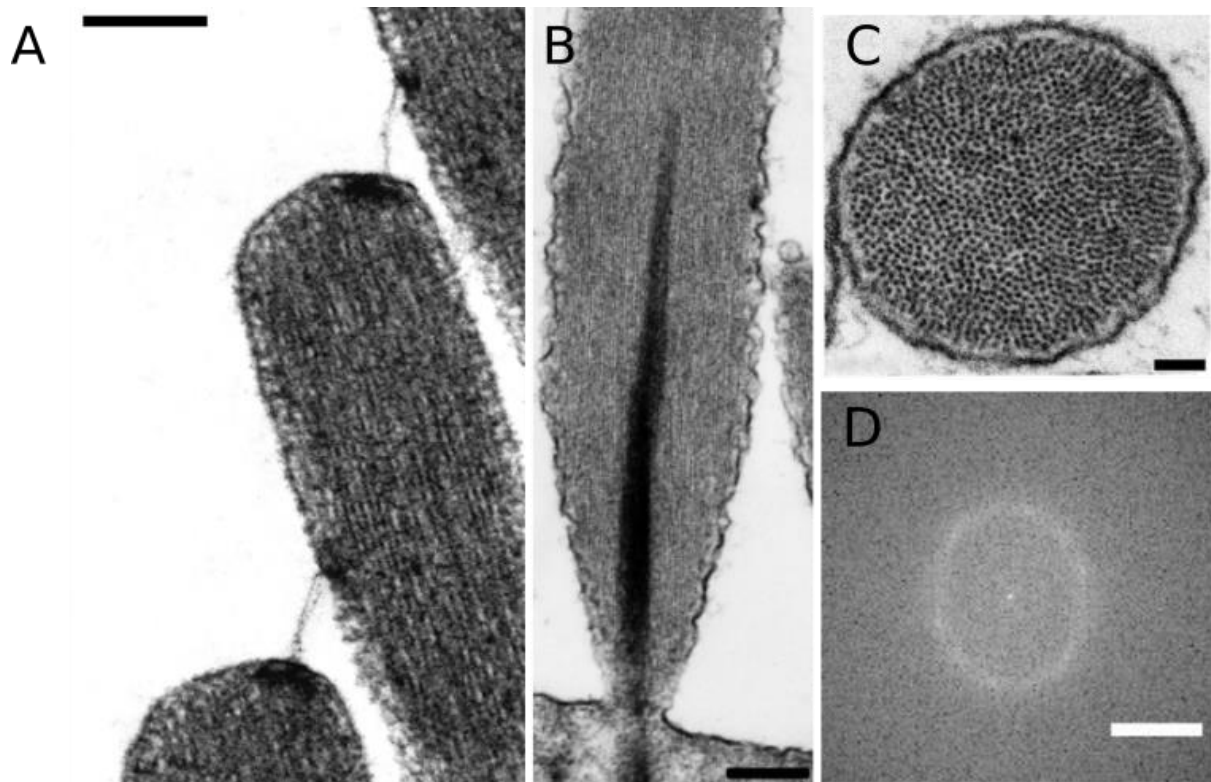
Figure I-8: ORGANIZATION OF ACTIN FILAMENTS IN THE CORE OF STEREOCILIA. (A) Each actin-filled stereocilium is connected by an oblique proteinaceous tip link (arrow heads) that gates mechanosensitive ion channels located at the stereociliary tip near the lower end of the tip link. Transmission electron micrograph by A. J. Hudspeth from (Pascal Martin 2007). **(B)** Each stereocilium is made of a parallel network of actin filaments. From the stereociliary taper, some of the filaments form a rootlet that inserts into the cuticular plate. The densely-packed stereociliary rootlet (arrow head) can be seen in a vertical section along the stereociliary height. Scale bar 250 nm. **(C)** The transverse section of the stereociliary core above its taper reveals cross-sections of actin filaments. Scale bar 60 nm. **(D)** The 2D Fourier transform of the image shown in (C) shows a ring-like pattern indicating that the actin filaments in the stereociliary core are organized according to a liquid packing with an inter-filament spacing of ~10 nm. Scale bar 10 nm^{-1}. Figures B-C from (Mogensen, Rzadzinska, and Steel 2007).

c. Stereociliary rootlets and pivotal stiffness of stereocilia

The stereociliary rootlet is a densely packed array of actin filaments that extends from around the stereociliary taper into the cuticular plate underneath the cell apical surface. In transmission electron micrographs (TEM) of longitudinal sections of the stereocilia, the osmophilic rootlets appear as a dark region (Fig. I-9.B). In transverse sections near the stereociliary insertion, the rootlet appears as a region with more tightly-packed actin filaments than in the periphery (Fig. I-9.C-D). Removing the hair bundle by either pushing with an eyelash or blowing pressurized air reveals the imprints of the stereocilia at the insertion site (Fig. I-9.E). A detailed in the result

section, I have extensively used this trick in my work to characterize the size of the rootlet insertions as well as their organization.

The pivotal stiffness of a stereocilium is thought to be dictated by elastic resistance to bending of actin filaments in the stereociliary rootlet over a short region near its insertion (J. Howard and Ashmore 1986; Jonathon Howard 2001). In a simple description, this region can be modelled as a cylindrical beam of radius a and length l, the latter being much shorter than the length L of the whole stereocilium $(L \gg l)$. Introducing the flexural rigidity EI and radius r of a single actin filament and assuming that the actin filaments are crosslinked, the pivotal stiffness κ_{SP} of a stereocilium is then estimated as

$$\kappa_{SP} = \frac{nEI}{lL^2} \frac{a^2}{r^2}, \qquad\qquad \text{(I-1)}$$

where n is the number of actin filaments at the insertion of each stereocilium (Fig. I-9.F). Within this framework, the pivotal stiffness of a stereocilium is largely determined by the number n of actin filaments at the insertion and the height of the stereocilia L. Any change in these parameters would result in a dramatic change of the hair bundle's pivotal stiffness. The pivotal stiffness K_{sp} was reported in the range of 200 to 650 μN·m^{-1} for the saccular hair bundle of the American bullfrog (Jaramillo and Hudspeth 1993; Marquis and Hudspeth 1997) and 150 to 550 μN·m^{-1} for the rat cochlear hair bundles (Tobin et al. 2019). Assuming that $N \simeq 50$ stereocilia contribute equally to this measured stiffness, the estimate of the pivoting stiffness of a single stereocilium is $\kappa_{SP} \simeq 4 - 15$ μN/m, corresponding to a rotational stiffness $\kappa_{SP}^R = L^2 \kappa_{SP} \simeq 0.06 - 0.35$ fN·m·rad^{-1} if $L = 5$ μm is an average length for the stereocilia in these hair bundles. Using typical parameter values, $EI = 4 \, 10^{-26} \, N \cdot m^2$, $a = 50 \, nm$, $r = 5 \, nm$, $l = 1 \, \mu m$, $L = 5 \, \mu m$, and $n = 30$, leads to theoretical estimates $\kappa_{SP} \simeq 5 \, \mu N \cdot m^{-1}$ and $\kappa_{SP}^R \simeq 0.12$ fN·m·rad^{-1} that are consistent with experimental estimates. Note that in the absence of crosslinking, the stereocilia would be much softer, with $\kappa_{SP} = nEI/(lL^2)$, corresponding to stiffness that is about 100-fold smaller than that with cross-linking.
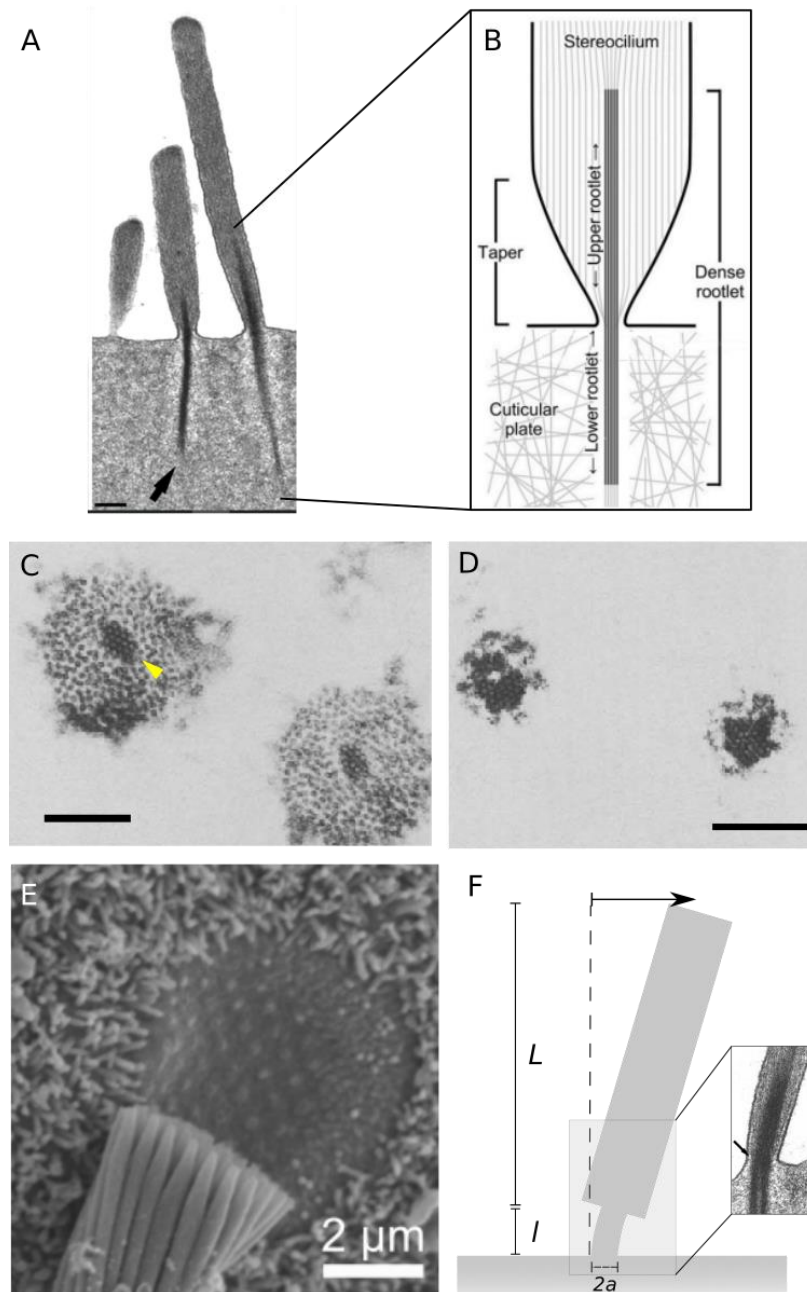
Figure I-9: THE STEREOCILIARY ROOTLETS. (A) A transmission-electron micrograph of a vertical section of a rat OHC bundle reveals the stereociliary rootlets. They appear as dark regions extending from around the taper region of the stereocilia into the cuticular plate beneath the hair cell's apical surface. Scale bar 200 nm. Figure adapted from (David N. Furness et al. 2008). **(B)** Schematic representation of the rootlet structure of a single stereocilium. The stereociliary rootlet consists of a few tens of densely packed actin filaments inserted into the cuticular plate. Figure adapted from (Pacentine, Chatterjee, and Barr-Gillespie 2020). Transmission-electron micrographs of the transverse sections of stereocilia from guinea pig cochlea **(C)** at the taper region and **(D)** at the stereociliary insertions. **(C)** Near the stereociliary insertion, actin filaments appear as dots that are more tightly packed in the rootlet (arrow head) than within the peripheral region. Scale bar (A-B) 100 nm. Figures adapted from (Itoh 1982). **(E)** Scanning-electron micrograph of the apical surface of a frog saccular hair cell after the hair bundle was broken at its base by pushing against it with an eyelash or by blowing pressurized air. The stereociliary imprints reveal the stereociliary rootlets at the site of insertions. **(F)** Schematic representation of a single stereocilium that behaves like a cantilevered beam with a flexible base where a displacement X is imposed at the tip of the beam. The inset shows the stereociliary rootlet of a single stereocilium at the site of insertion. Figure adapted from (J. Howard and Ashmore 1986).

The pivoting stiffness of a hair bundle is not only imposed by the stereociliary rootlets. Horizontal lateral links interconnecting the stereocilia, as well as the oblique tip links, actually contribute a significant fraction of the hair-bundle stiffness (Bashtanov et al. 2004). In intact hair-bundles from the bullfrogs' sacculus, the experimentally measured hair-bundle stiffness is in the range of 680 to 1,200 $\mu N \cdot m^{-1}$ (Marquis and Hudspeth 1997; P. Martin, Mehta, and Hudspeth 2000). The contribution of tip links the total hair-bundle stiffness is about 20% on average but can go up to 50% in rat cochlea hair bundles (Tobin et al. 2019), 80% in Mongolian gerbils (Chan and Hudspeth 2005), and around 50-80% in the frog saccular hair bundles (Marquis and Hudspeth 1997). Having the tip links contribute a large fraction of the hair-bundle stiffness is advantageous to convey the energy of the stimulus to the transduction machinery associated with the tip links (Chan and Hudspeth 2005).

A.3 The mechano-electrical transduction machinery

The molecular identity of the ion channel that mediates mechanoelectrical transduction in the hair cell—the transduction channel—has been resisting identification and extensive research efforts for many years. This is in part due to the small number of hair cells in auditory organs (only a few thousand) and of transduction channels per hair cells (2-4 per tip link (Beurg et al. 2009; 2018), corresponding to a few hundred molecules per hair cell). However, over the past 30 years, genetic studies of deafness in mammals helped to identify several molecules implicated in mechanotransduction of hair cells (see the reviews of (Michalski and Petit 2015) and (W. Zheng and Holt 2021) regarding the genetic studies of the mechano-electrical transduction machinery).

The mechano-electrical transduction (MET) machinery consists of the tip link, the transduction channel itself located near the lower end of the tip link, and the myosin motor complex located at the upper end of the tip link. Conventional Transmission Electron Microscopy reveals that both ends of the tip link connect to dark osmophilic regions called the upper tip-link density (UTLD) and the lower tip-link density (LTLD) (Figure I-8.A).
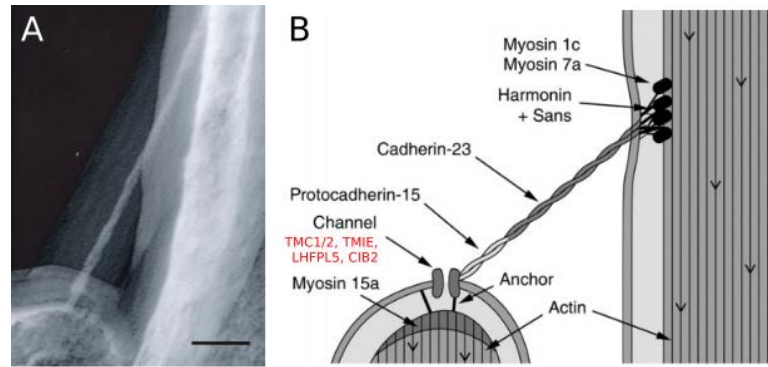
Figure I-10: MECHANOTRANSDUCTION MACHINERY OF THE HAIR CELLS. (A) A high-resolution image of the tip link using freeze-etch electron microscopy reveals its right-handed helical structure. The tip link is about 5 nm in diameter and 180 nm in length and is made of the heterophilic association of dimers of unconventional calcium-dependent adhesion proteins, one dimer of protocadherin-15 and one dimer of cadherin-23. Scale bar 50 nm. Figure from (B. Kachar et al. 2000). **(B)** Schematic representation of the mechano-electrical transduction (MET) machinery. The MET machinery comprises the tip link connected in series with the transduction channel itself and the myosin motor complex, located at the lower and upper end of the tip link, respectively. Figure from (James O. Pickles 2012).

a. The tip links

The oblique tip link is made of the heterophilic association of one dimer of protocadherin-15 (PCDH15) and one dimer of cadherin-23 (Cdh23), which together form a right-helical strand interconnecting two stereocilia in adjacent stereociliary rows, from the tip of the shorter stereocilia to the flank of its taller neighbour (Fig. I-10.A). The tip link seen by Scanning Electron Microscopy is ~ 8-11 nm wide and ~150-300 nm long. The short stereocilium contributes a dimer of protocadherin-15 molecules with 11 extracellular (EC) domains, while the longer stereocilium contributes a dimer of cadherin-23 molecules with 27 EC domains, corresponding to about 1/3 and 2/3 of the tip link, respectively (B. Kachar et al. 2000). Because cadherin proteins are calcium-dependent adhesion proteins, the tip link can be disrupted by applying calcium chelators, such as BAPTA[4], to lower the Ca^{2+} concentration and disconnect protocadherin 15 from cadherin 23 (Assad, Shepherd, and Corey 1991) (Fig. I-11.B).

---

[4] 1,2-bis(o-aminophenoxy)ethane-N,N,N′,N′-tetraacetic acid.
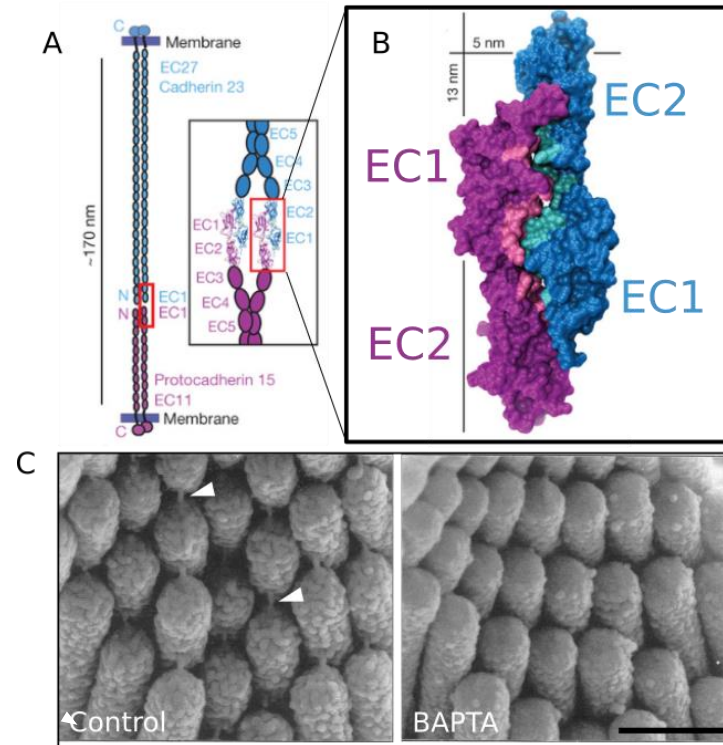
Figure I-11: TIP LINKS. (A) Schematic representation of the molecular constituents of the tip link. The tip link is made of two parallel protofilaments forming cis-homodimers of protocadherin-15 at the lower portion of the tip link and cadherin-23 at the upper portion. The opposing extracellular (EC) repeats of protocadherin-15 and cadherin-23 interact through a 'molecular handshake', forming a *trans* interaction at the last two-terminal domain (EC1-EC2) of the cis-homodimers. **(B)** Surface representation of protocadherin-15 (in purple and pink) and cadherin-23 (in blue and cyan) at the site of the molecular handshake. Figures B-C adapted from (Sotomayor et al. 2012). **(C)** Tip links are sensitive to chemical disruption by tetracarboxylic calcium chelators, such as BAPTA. Assad *et al.* demonstrated that tip links and mechanotransduction can be chemically disrupted by replacing a high Ca^{2+} standard perilymph (Right panel) with a 5 mM BAPTA solution for 10 s (Left panel). Scale bar 500 nm. Figures from (Assad, Shepherd, and Corey 1991).

The tip link was initially proposed to be the 'gating spring' that pulls on the transduction channel, as introduced in the gating spring model of mechanoelectrical transduction (D. Corey and Hudspeth 1983). However, molecular dynamic (MD) simulations based on structural data later indicated that the tip link is likely too rigid to be the gating spring (Sotomayor, Corey, and Schulten 2005; Sotomayor et al. 2010; 2012), and thus that the 'gating spring' may be composed of other elastic elements connected in series with the tip link. Nevertheless, the conclusion was recently re-evaluated based on MD simulations (Araya-Secchi, Neel, and Sotomayor 2016) and force spectroscopy of a portion and the whole tip link (Bartsch et al. 2019; Mulhall et al. 2021). Within a physiological tension range, a single protocadherin-15 molecule shows a low stiffness but the stiffness can go up to ~ 10 mN·m^{-1} at very high tension as a result of strain stiffening (Bartsch et al. 2019). These recent studies bring back the question regarding the identity of the tip link as the long-sought 'gating spring'.

Disrupted tip links can regenerate. Normal transduction is mostly restored within 24 hours (Zhao, Yamoah, and Gillespie 1996). Regeneration happens first with Pcdh15-Pcdh15 links at ~12 h. Then Cdh23 replaces Pcdh15 at the upper end of the tip link at ~36 h (Indzhykulian et al. 2013). Pulling on the tip-link connection containing extracellular (EC) domains EC1-5 has recently revealed a mean lifetime of 9 s for the tip-link bound at a resting tension of 10 pN (Mulhall et al. 2021) but the lifetime reduces to about 500 µs at the tension of 40 pN, a high-tension value that may be physiological in the cochlea (Tobin et al. 2019). The tip-link bond seems to be much more dynamic than originally thought. Interestingly, it was also recently shown that applying a sinusoidal force to the hair bundle or pushing the bundle towards the negative direction to facilitate encounter of the tip link fragments evoked tip-link recovery within seconds after disruption (Alonso et al. 2020). These remarkable observations suggest that mechanical stimulation may facilitate the reconstitution of functional tip links, which may help explain why normal hearing is restored after temporary hearing loss due to loud sound exposure.

b.   The transduction channels

The MET channel is located at the lower end of the tip link where (Beurg et al. 2009). TMC1/2, TMIE, LHFPL5, and CIB2 were identified as components of the transduction channel (Fig. I-12). TMC1/2 are believed to work as pore-forming proteins (Pan et al. 2013; Kurima et al. 2015; Jia et al. 2020). Another transmembrane protein, TMIE is likely to be a subunit of the transduction channel and binds to LHFPL5 (Cunningham et al. 2020). LHFPL5, which binds to the lower end of the tip link through protocadherin-15, may transmit tension in the tip link to the transduction channels (Xiong et al. 2012; Beurg et al. 2015). CIB2 has an affinity for Ca^{2+}, a prominent ionic signal in the hair cells, and was reported to bind to the MET channel (Giese et al. 2017). Based on their homologs in *Caenorhabditis elegans,* CIB2 was also proposed to link the stereociliary actin core to the transduction channel through ankyrin proteins (Tang et al. 2020). However, direct evidence of such arrangement (TMC1/CIB2/Ankyrin) has yet to be confirmed in vertebrate hair bundles.
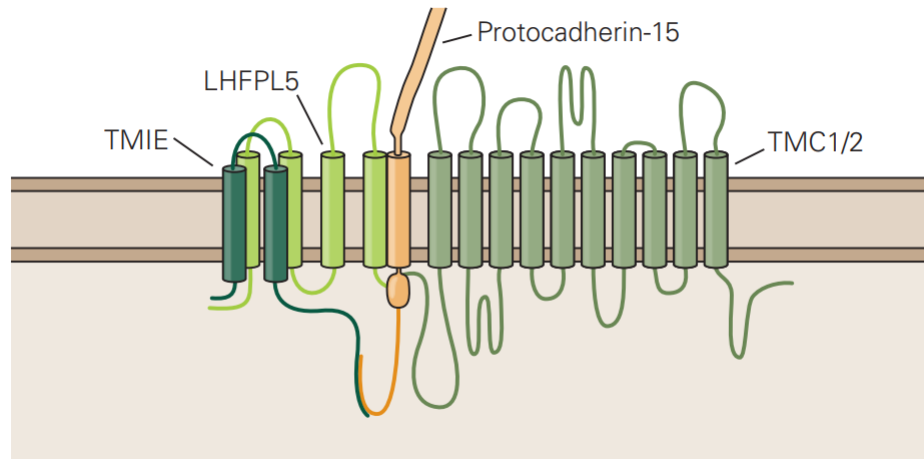
Figure I-12: MOLECULAR CONSTITUENTS OF THE MECHANO-ELECTRICAL TRANSDUCTION (MET) CHANNEL. Figure from Martin, P., Manley, G.A. (2020) Auditory processing by the cochlea (Principles of Neural Science 6th Edition).

TMC1/2

Transmembrane channel-like proteins 1 and 2 or TMC1/2 have been shown to be pore-forming proteins and are accepted as the main determinant of the conductive pathway for the transduction channel (Jia et al. 2020; Pan et al. 2013). Immunofluorescence and immunogold labelling localize the two proteins at the tip of the stereocilia shorter rows of mice hair bundles, where the mechanotransduction channels are located, but not at the tallest (Kurima et al. 2015). Both TMC1 and TMC2 are required for mechanotransduction and both are detected at early postnatal stages in mouse hair cells. TMC2 expression reaches its peak during the first postnatal week, around the onset of the mechanotransduction, and then declines to be undetectable at P10. During this time, TMC1 expression, which starts 2 - 3 days later than TMC2 expression, overcomes TMC2 expression around P6 - P7 (Kawashima et al. 2011). TMC1 expression then reaches saturation. The developmental switch between TMC2 and TMC1 is tightly coupled to properties of mechanotransduction and expression of important actin-binding proteins (Krey et al. 2020), as will be described further.

TMC1 molecules assemble as dimers (Pan et al. 2018). The transduction channels of OHCs and IHCs in the mouse cochlea show multiple conductance states in 50-pS increments (Beurg et al. 2018). In addition, it was shown in the same study for OHCs that the number of TMC1 molecules per MET complex increases from ~ 8 at the apex to ~ 20 at the base of the cochlea. Thus, there seems to be a varying number of channels per tip link and each MET complex is composed of multiple TMC1 molecules, with a gradient along the tonotopic axis of auditory organs for OHCs (but not for IHCs).

In mammalian hair cells, the single-channel conductance of the transduction channel was reported to be in the range of 50-300 pS (Beurg et al. 2018; 2006; Géléoc et al. 1997; K. X. Kim et al. 2013; Pan et al. 2018; 2013) while the single-channel conductance of purified TMC1 and TMC2 in liposomes is 40 pS and 35 pS (Jia et al. 2020), respectively. TMC1 and TMC2 also show distinct permeation properties. Hair cells expressing only TMC1 have a smaller single-channel conductance and lower Ca^{2+} permeability than those expressing only TMC2 (K. X. Kim and Fettiplace 2013). The developmental switch from TMC2 to TMC1 at the onset of the mechanotransduction may result in reducing the Ca^{2+} influx in the mature hair cells.

TMIE

Transmembrane inner ear expressed protein or TMIE is a transmembrane protein that was identified from deaf mice and deaf humans (DFNB6) (Shabbir et al. 2006). TMIE has two transmembrane domains. TMIE localizes at the stereociliary tip and is first expressed in the shorter stereocilia of mice cochlear hair cells during the first postnatal week, around the onset of the mechanotransduction (Cunningham et al. 2020).

Deletion of *TMIE* eliminates mechanotransduction and the loss of mechanotransduction can be rescued by expressing wild-type *TMIE*. Point mutations in different regions of the N- or C-cytoplasmic domains also result in disrupted mechanotransduction currents. As a result, TMIE is believed to be a subunit of the transduction channel. Further study reveals that TMC1 traffic from the cell body to the stereociliary tip is disrupted in *TMIE* knockout mice. While TMC1 is not transported to the stereociliary tip, TMC2 localisation in the stereocilia is only slightly affected (Cunningham et al. 2020). Moreover, in TMIE zebrafish mutants, both TMC1 and TMC2 cannot be delivered to the stereociliary tip (Pacentine, Chatterjee, and Barr-Gillespie 2020). These observations indicate that TMIE is required for trafficking of at least TMC1 to the stereociliary tip.

LHFPL5

Lipoma HMGIC Fusion Partner-Like 5 Protein, or LHFPL5, is another transmembrane protein (Kalay et al. 2006), like TMIE, that regulates TMC1 localisation to the stereociliary tip in mice cochlear hair cells. LHFPL5 belongs to a family of transmembrane proteins with four transmembrane domains. During the first postnatal week, at the onset of mechanotransduction, LHFPL5 is expressed at the stereociliary tip in all rows and the expression level reaches a peak.

The expression level then declines by P12 and LHFPL5 localisation is restricted to only the tip of the shorter stereocilia rows (Beurg et al. 2009).

Deletion of *LHFPL5* results in a severe impairment of mechano-electrical transduction (the current magnitude is reduced by 90%) and TMC1 is not trafficked to the stereociliary tip. Interestingly, the number of tip links in Lhfpl5-null mice is also reduced significantly (Xiong et al. 2012). Consistent with the later result, biochemical assays show that LHFPL5 can physically interact with PCDH15, the tip-link protein at the lower end of the tip link (Beurg et al. 2015; Xiong et al. 2012). Within this framework, LHFPL5 may connect the tip link to the transduction channel. However, co-immunoprecipitation assays failed to reveal a physical interaction between LHFPL5 and TMC1 (Beurg et al. 2015).

CIB2 and Ankyrin proteins

Calcium and Integrin Binding Family Member 2, or CIB2, belongs to a family of proteins that are known to contain multiple EF-hand domains that bind Ca^{2+}. Mutations in CIB2 are associated with human nonsyndromic deafness DFNB45 and Usher syndrome type 1J. A null mutation or a point mutation in CIB2 also results in profound hearing loss in mice (Giese et al. 2017; Yanfei Wang et al. 2017; Michel et al. 2017). TMC1 and TMC2 localisation at the shorter-row stereociliary tips is normal in the absence of CIB2, suggesting that CIB2 may not be involved in transporting TMC1 and TMC2 to the stereociliary tips. However, CIB2 interacts with the cytoplasmic N-terminus of TMC1 and TMC2 and this interaction disappears after a missense mutation in CIB2 (Giese et al. 2017). Deletion of *CIB2* also entirely eliminates the transduction current indicating that CIB2 is an integral part of the transduction channel.
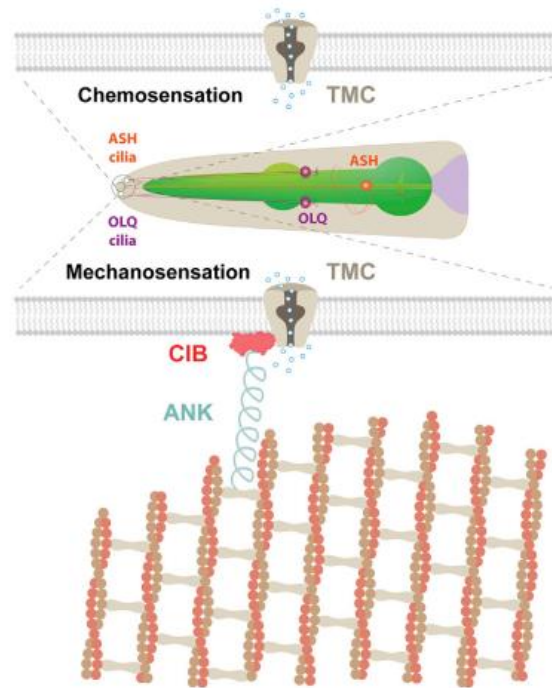
Figure I-13: TMC-1/CIB/ANKYRIN/SPECTRIN/ACTIN COMPLEX IN THE MECHANOSENSORY NEURONS OF *C. ELEGANS*. The protein complex composed of TMC-1/CIB/ankyrin/spectrin/actin cytoskeleton found in *C. elegans* is proposed to be a likely candidate of a Ca^{2+} binding structure that physically links the mechanotransduction channel to the actin cytoskeleton in stereocilia although it is unclear whether the ankyrin gene is expressed in cochlear hair cells. Figure from (Tang et al. 2020).

Ankyrin belongs to a family of proteins that serve as an attachment or scaffold between integral membrane proteins, such as ion channels and signalling receptors, to the spectrin-actin based membrane cytoskeleton. Although it is unclear whether the ankyrin gene is expressed in mammalian cochlear hair cells, UNC-44 which is the homolog of ankyrin in *Caenorhabditis elegans* can bind to CALM-1, the CIB homolog in *C. elegans* (Tang et al. 2020). Moreover, the UNC-44/ankyrin complex also connects to TMC-1 via CALM-1/CIB and both are required for TMC-1-mediated mechanoreception of nociceptive quadrant outer labials (OLQ) neuron in *C. elegans* (Fig. I-13). This TMC-1/CIB/ankyrin/spectrin/actin cytoskeleton complex provides an attractive candidate of a Ca^{2+} binding structure that physically links the mechanotransduction channel to the actin cytoskeleton in stereocilia.

Remarkably, in direct relevance to my PhD work, CIB2 deficiency leads to over-elongation of shorter-row stereocilia in the mouse cochlea (Giese et al. 2017). This observation suggests that CIB2 directly or indirectly plays a role in the regulation of the stereociliary structure.

c. The myosin complex

The myosin motor complex is located at the upper tip-link density (ULTD). Myosin-1c (MYO1C) and myosin-7a (MYO7A) were proposed as candidate motors that set the tip links under tension. MYO1C was shown to be involved in the adaptation of transduction currents in vestibular hair cells (Holt et al. 2002; Stauffer et al. 2005a). MYO7A is localized at the upper insertion point of the tip link in mature cochlear hair cells (Grati and Kachar 2011; Li et al. 2020) and mutation sin MYO7A case Usher syndrome type 1, characterized by combined deafness and blindness (Boeda 2002). The exact role of MYO7A remains unclear because the knockout and knockdown mouse model of *Myo7a* affect hair bundle development, thus rendering the functional study difficult to interpret. The recent work from *Li et al. 2020* showed that several isoforms of *Myo7a* are expressed in cochlear hair cells. In genetically engineered mice where a specific isoform of *Myo7a* (*Myo7a-ΔC*) has been deleted, the expression level of *Myo7a* is severely reduced in IHC bundles and affected tonotopically in OHC bundles, although the hair bundles develop normally (Fig. I-14.A). Mutant IHC hair bundles show a reduced resting open probability of their transduction channels and a slowed onset of transduction currents (Fig. I-14.B-C). These results provide some (but not definitive) support for MYO7A as a candidate for the myosin motor that tensions the tip links in cochlear hair cells (Li et al. 2020), although measurements of tip-link tension in the mutant mice are lacking to reinforce this conclusion.
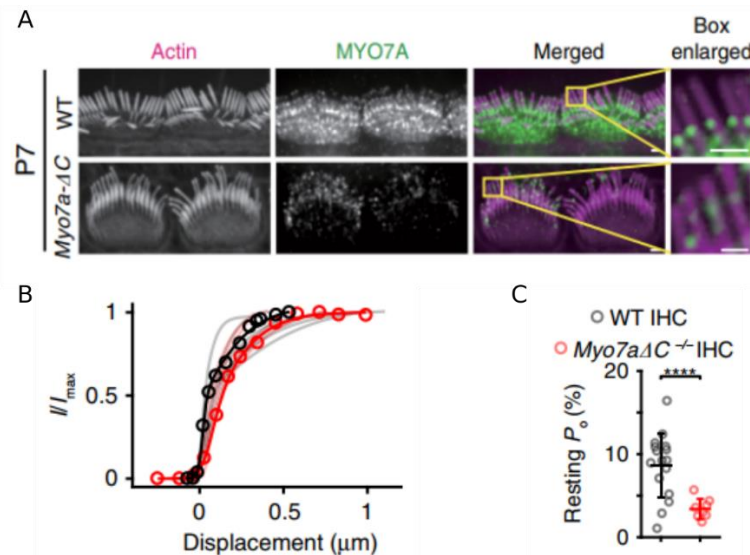
Figure I-14: LOCALIZATION OF MYO7A AND EFFECTS OF DELETING AN ISOFORM OF MYO7A ON THE MET CURRENT IN COCHLEAR HAIR CELLS. (A) Immunofluorescence labelling localizes MYO7A at the upper end of the tip links in the IHC stereocilia of wild-type (WT) mice. Immunoreactivity of *Myo7a* is strongly reduced and more diffusive in mutant mice where a specific isoform of *Myo7a* (*Myo7a-ΔC*) is deleted. Scale bar 1 μm. **(B)** Normalized I-X curves (I/I_{max} vs Displacement) reveal a significant rightward shift of the normalized I-X curves from that of the wild-type mice (in black) to that of the mutant *Myo7a-ΔC* mice (in red). The rightward shift indicates a reduced resting open probability (P_o) in **(C)**. Figure adapted from (Li et al. 2020).

# B. The architecture of the actin core and actin dynamics in the stereocilia

The actin cytoskeleton is a network of semi-flexible filaments that are active polymers. The filaments can elongate or shrink depending on the surrounding environment. As a result, the network can continuously reorganize to adapt to changing conditions. The actin cytoskeleton is involved in various key cellular processes such as motility, morphogenesis, polarity, transport and cell division (see the reviews of (Laurent Blanchoin et al. 2014) and (Banerjee, Gardel, and Schwarz 2020) regarding the adaptive nature of the actin cytoskeleton in various biological systems). The hair bundle provides a striking example of an actin-based structure that must be tightly regulated during development and maintained at mature stages according to its function as a frequency-selective detector of periodic mechanical stimuli.

B.1 Introduction to actin polymerization and its dynamics

a. Actin structure

The actin protein exists in two forms: the monomeric globular form (G-actin) and the polymerized filamentous form (F-actin). The actin monomer is a 43-kDa globular protein (G-actin) composed of 4 sub-domains that bind to the nucleotides ATP and ADP as well as to Mg^{2+} ions (Kabsch et al. 1990). G-actin, which has a diameter of ~5-6 nm (Jonathon Howard 2001), is asymmetrical. When individual monomers assemble into a proto-filament, the subunits are orientated in the same direction in a head-to-tail manner. This gives rise to the polarity of the actin filament; the ends of the filament are structurally different. Two parallel F-actin filaments form a double-stranded helix with a 37-nm repeat and a diameter of an equivalent cylinder of about 8 nm. Sub-domains 1 and 3 of a monomer are called the plus (+) or barbed end and sub-domains 2 and 4 constitute the minus (-) or pointed end. The addition of an actin monomer to a filament extends the overall length by 2.7 nm (Jonathon Howard 2001; Phillips 2013) (Fig. I-15.A-C). The assembly of an actin filament induces a conformational change in the actin subunit: G-actin has a twisted conformation whereas F-actin has a flat conformation, obtained by a rotation of 20 degrees of subdomains 1-2 with respect to subdomains 3-4 (Fig. I-15.D-E). The flat conformation is essential for the stability of helical F-actin (Oda et al. 2009).
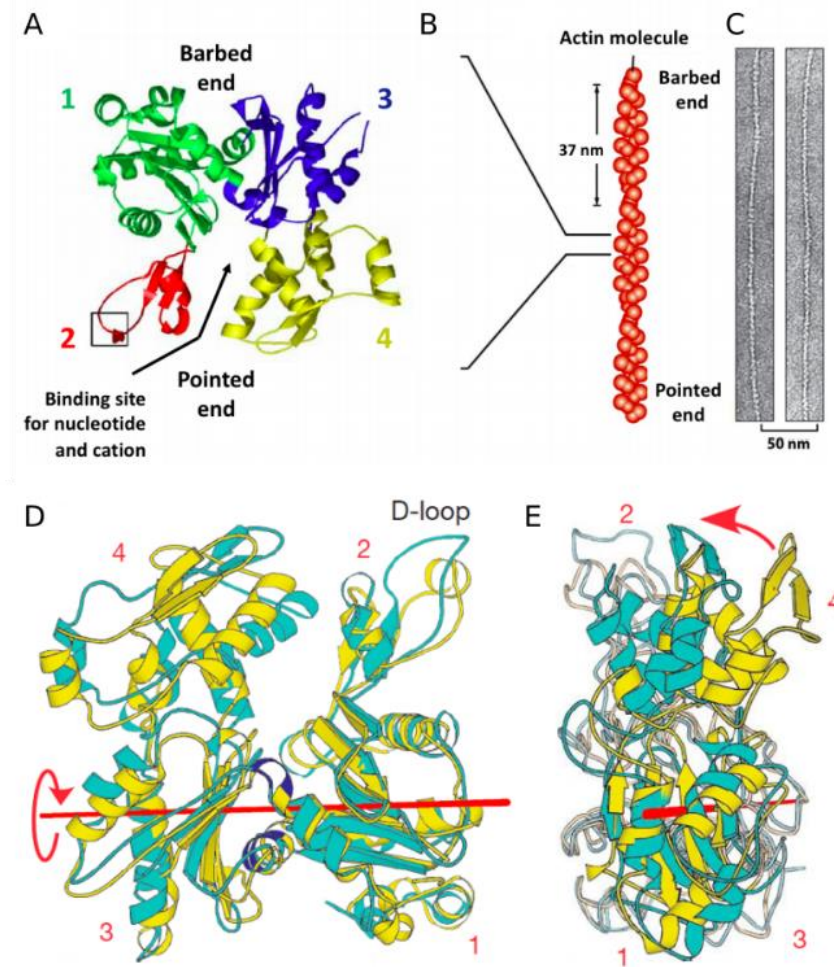
Figure I-15: STRUCTURE OF GLOBULAR (G-ACTIN) AND FILAMENTOUS ACTIN (F-ACTIN). (A) The asymmetric topology of G-actin, with its 4 subdomains represented in different colours. Subdomains 1 and 3 form the fast-growing "barbed end" while subdomains 2 and 4 form the slow-growing "pointed end" of the actin filament. Adapted from (M. Kim, Jang, and Jeong 2006). **(B)** The polymerization of monomers in filament results in a double helix of two proto-filaments, with a 37-nm repeat and a diameter of about 8 nm. **(C)** Electron micrograph of the negatively stained actin filament. Figures B-C adapted from (Alberts 2008). **(D)** Front view. The structures of the subunits in F-actin (cyan) and the G-actin (yellow) forms are superimposed, which subdomains 1 and 2 aligned in the two forms. Subdomains 3 and 4 are rotated by ~20 degrees with respect to subdomains 1 and 2 about the rotational axis indicated by the red line in the direction indicated by the red arrow. **(E)** Side view from the left-hand side of subdomains 3 and 4 in (D). Figures (D-E) adapted from (Oda et al. 2009).

b. Actin polymerization kinetics

The polarity of an actin filament is associated with different kinetics of polymerization and depolymerisation at both ends. At saturating concentrations of G-actin (~mM), the barbed end is the fast-growing end, whereas the pointed end is the slow-growing end. Correspondingly, the association rate of ATP-G-actin (k_+) is ten times higher at the barbed end than that at the pointed end (T D Pollard 1986). The association and dissociation rates that tune polymerization and depolymerisation at both ends of the actin filament are controlled by the nucleotides (Fig. I-16).

In cells, where ATP molecules are abundant, actin filaments are mostly assembled from ATP-G-actin since G-actin has a strong affinity for ATP. Upon incorporation into a filament, an actin subunit hydrolyses its nucleotide at a relatively fast rate of $0.3\ s^{-1}$ (Laurent Blanchoin and Pollard 2002). ATP-F-actin is then transformed into ADP-P_i (P_i: inorganic Phosphate) F-actin and then into ADP-F-actin. The release of P_i, which is 100 times slower than ATP hydrolysis (Carlier and Pantaloni 1986).
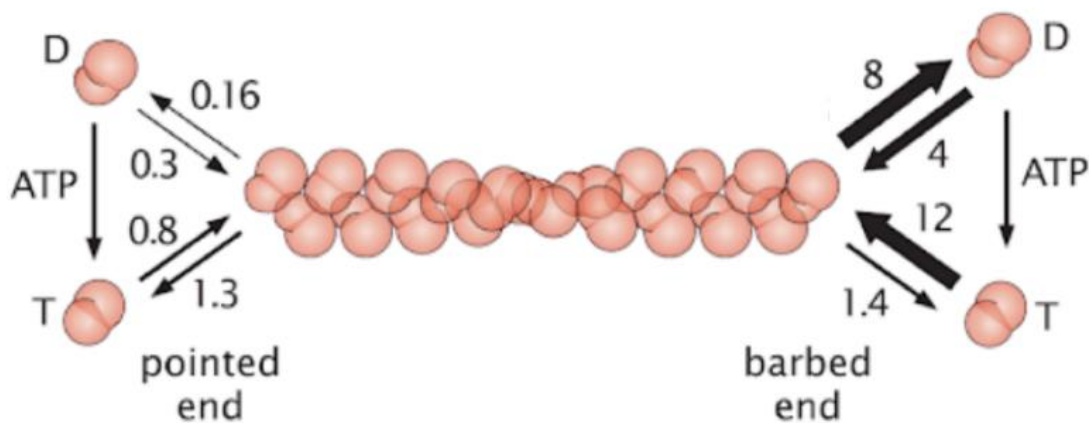
Figure I-16: ACTIN POLYMERIZATION. Association/dissociation rates of actin. G-actin is bound to ATP (respectively ADP) represented by the letter T (D). The association rates have units of $\mu M^{-1}.s^{-1}$. Dissociation rates have units of s^{-1}. At each end, the ratio of the dissociation and association rates gives C_c, the critical concentration beyond which a filament elongates and below which a filament retracts. Figure adapted from (Thomas D. Pollard and Borisy 2003).

The assembly of actin monomers into a filament requires energy to overcome a kinetic barrier that prevents spontaneous nucleation. The critical nucleus size or the smallest oligomer that is more likely to grow into an actin filament is an actin trimer (T. D. Pollard and Cooper 1986; Sept and McCammon 2001).

c.   Actin nucleation

Actin nucleation is the first step of actin polymerization. Nucleation involves the formation of an actin nucleus composed of a G-actin trimer, or a complex of three actin monomers. The cytoplasm of cells shows a high concentration of G-actin-ATP, up to about 150 µM in the cytoplasm (Laurent Blanchoin et al. 2014; Carlier and Pantaloni 1986), as well as a high concentration of the protein profilin, as high as 100 µM. Profilin binds to the majority of G-actin

present within the cell, preventing the spontaneous nucleation of filaments. This is because, when actin monomers are bound to profilin, the concentration of free actin monomers available for filament elongation is decreased, so that spontaneous nucleation becomes unlikely (Carlsson et al. 1977). When profiling binds to actin monomers, the monomer can still add onto free barbed ends of an actin filament but at a slower rate compared to that of free G-actin. However, profilin affects the association and dissociation rates of G-actin to a filament by increasing the rate of nucleotide exchange by 1000-fold which replenish the pool of ATP-actin monomers (Goldschmidt-Clermont et al. 1991). In the presence of 8 µM of profilin and with an excess of ATP, the association rate at the barbed end decreases from 11.6 to 8 $\mu M^{-1}.s^{-1}$ and the dissociation rate increases from 1.4 to 2 s^{-1} (Gutsche-Perelroizen et al. 1999). In the presence of profilin, nucleation of actin filaments requires nucleation promoting factors. An actin filament may either elongate by interacting with formins or interact with the Arp2/3 complex to promote the formation of new filaments via branching.

Once the actin subunit is incorporated into the filament, profilin is released and the barbed end becomes available for the incorporation of new monomers. In summary, profilin sequesters a pool of monomeric actin and inhibits actin polymerization in the bulk by preventing the spontaneous nucleation of actin filaments in the cell. In the presence of profilin, nucleation factors are needed to promote de novo actin assembly.

The arp 2/3 complex

The Actin-Related-Protein 2 and 3 complex or Arp2/3 complex promotes branching from a pre-existing filament by forming a nucleation seed. The Arp2/3 complex is constitutively inactive but can be activated by nucleation promoting factors (NPF) from the Wiskott-Aldrich Syndrom Protein (WASP/WAVE) family (Machesky et al. 1999; Marchand et al. 2001). The nucleation of branched actin networks by the Arp2/3 complex requires the presence of nucleation-promoting factor (WASP), actin monomers and a pre-formed actin microfilament called a primer (Fig. I-17.A). New actin filaments appear at a 70-deg angle relative to the mother filament (Mullins, Heuser, and Pollard 1998) and elongate by the addition of actin monomers to the barbed end (Machesky et al. 1999; L. Blanchoin et al. 2000).
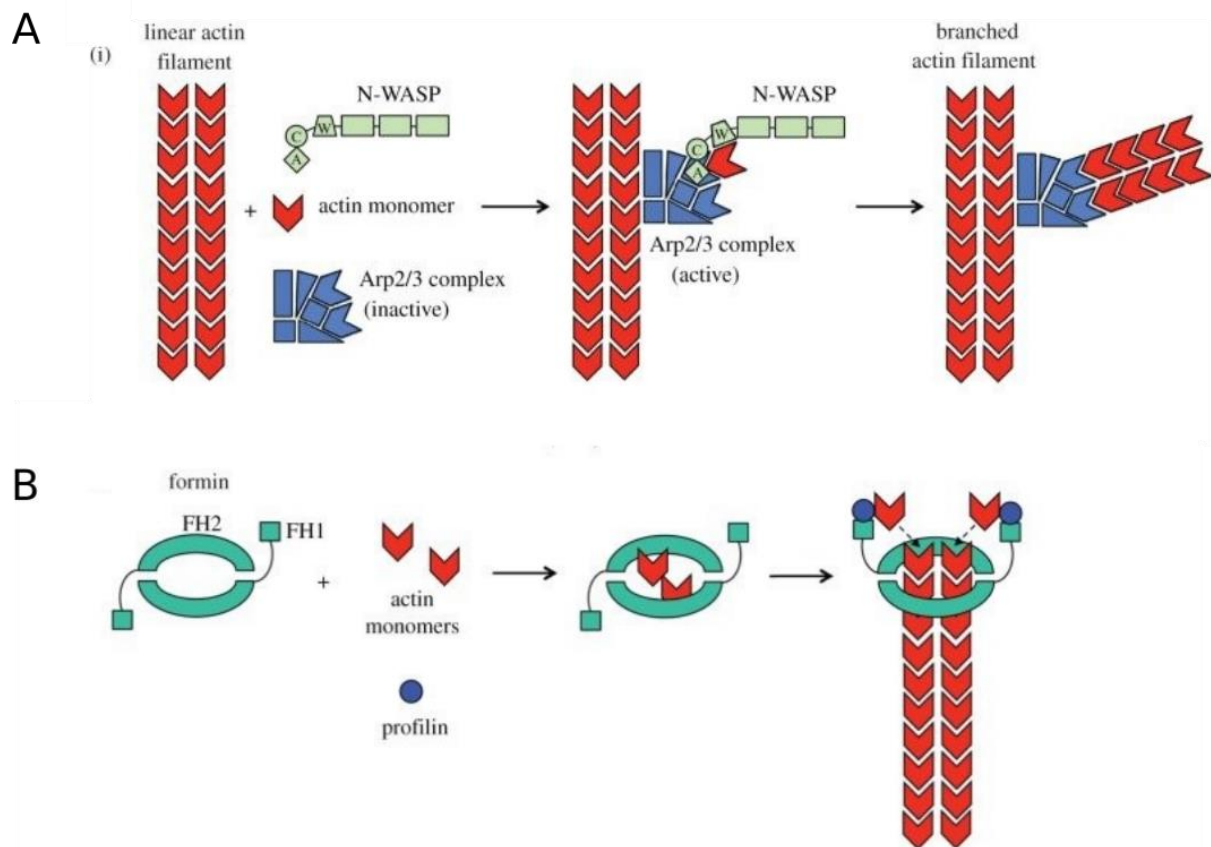
Figure I-17: ACTIN NUCLEATION BY THE ARP2/3 COMPLEX AND FORMIN. (A) Nucleation of branched actin networks by the Arp2/3 complex requires the presence of a nucleation-promoting factor WASP, actin monomers, and an actin microfilament called a primer. **(B)** Formin proteins work as dimers and use two domains to stimulate the assembly of linear actin filaments. The formin homology 2 (FH2) domain nucleates actin filaments and the formin homology 1 (FH1) domain delivers profilin–actin complexes to the filament's barbed end. Figures A-B adapted from (Ireton 2013).

Formins

Formins are a large and diverse class of actin-binding proteins that are involved in the nucleation and elongation of actin filaments (Courtemanche 2018; Paul and Pollard 2009a; Zigmond 2004); some formins also bundle actin filaments (Harris et al. 2006; Michelot et al. 2006; Schönichen et al. 2013) and bind to microtubules (Bartolini et al. 2008; Chesarone, DuPage, and Goode 2010; Gaillard et al. 2011). This wide range of functions indicates that formins may serve various roles in cells. Mutations in formins cause severe defects in cytokinesis, polarity, and cell and tissue morphogenesis (Mass et al. 1990; Jackson-Grusby, Kuo, and Leder 1992; Castrillon and Wasserman 1994; Kohno et al. 1996).

The C-terminal formin homology 1 and 2 domains (FH1, and FH2) of formins are much conserved. The FH1 contains proline-rich motifs that interact with the profilin–actin complex,

thereby recruiting actin monomers (Courtemanche and Pollard 2012; Paul et al. 2008). The FH2 domains form dimers that can nucleate actin filaments and mediate processive elongation at filament barbed ends of the filaments (Aydin et al. 2018; Courtemanche 2018; Goode and Eck 2007; Paul and Pollard 2009b). The combined action of FH1 and FH2 domains strongly accelerates filament growth.

Activated formins facilitate the elongation of actin filaments. They form a doughnut-shaped complex around the terminal actin subunits by orientating themselves towards the barbed end of the actin filament. The formin complex binds to the actin filament by its FH2 (formin homology 2) domains, removing capping protein from the end of the filament and preventing re-capping to allow continuing growth of filaments or cross-linked bundles. Each formin monomer binds and captures G-actin monomers bound to profilin. These monomers of ATP-G-actin are then added to the growing actin filament (Fig. I-17.B).

B.2 Actin dynamics in stereocilia.

Mammalian hair cells do not regenerate, which means that the hair-bundle must architecture must be maintained throughout the life of the animals. Maintenance and repair of the stereociliary structure result from the incorporation of cytoplasmic G-actin into the paracrystalline actin core. How dynamic is actin in stereocilia? Early studies based on transfection with β-actin-GFP of neonatal rata and mouse hair cells in culture had suggested that actin in stereocilia is continuously renewed in 48-72 hr by a treadmilling mechanism, with polymerization at the tip of the stereocilia and depolarization at the base (Schneider et al. 2002; Rzadzinska et al. 2004). Interestingly the treadmilling rate was observed to be proportional to the stereociliary length so that stereocilia of different lengths would be renewed in the same amount of time. However, this attractive model of dynamic maintenance was contested by more recent experiments from several groups and using various approaches in adult frog saccular hair cells and neonatal mice utricular hair cells. Instead, stereocilia were found to be remarkably stable over most of their length, with actin turnover happening only within about 0.5 µm from the stereociliary tips (Zhang et al. 2012; Drummond et al. 2015; Narayanan et al. 2015) (Fig. I-18). To reconcile these contrasting observations, it was proposed that the previously observed propagation of β-actin GFP from the tip to the base of the stereocilia (Schneider et al. 2002; Rzadzinska et al. 2004) might correspond to the incorporation

of actin into nascent stereocilia during the development of immature hair bundles or 'stereociliogenesis' (Drummond et al. 2015).
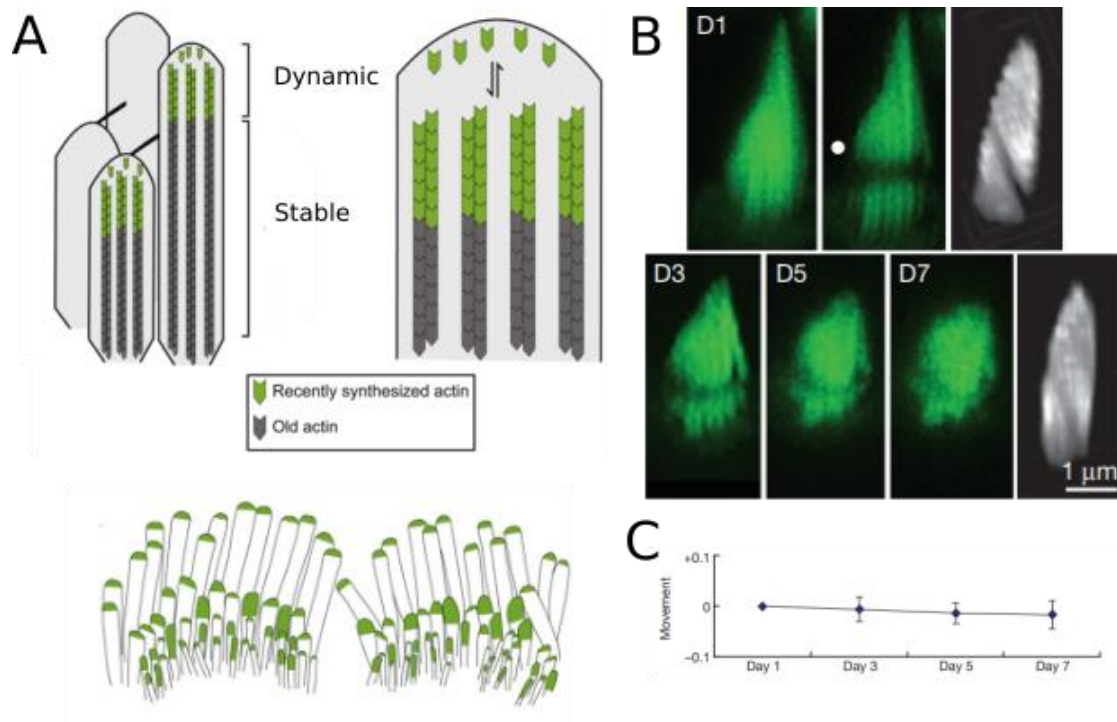
Figure I-18: ACTIN DYNAMICS IN THE STEREOCILIARY CORE. (A) The actin core of cochlear hair bundles is remarkably stable. Incorporation of new cytoplasmic actin into the polymerizing barbed ends happens only about half a micron near the stereociliary tips, where the transduction channels are located. Figure from (McGrath, Roy, and Perrin 2017). **(B)** The neonatal utricular macula in culture mice hair cells expressed b-actin– GFP. A bleaching profile (circle) of the b-actin–GFP indicates that actin turnover at the shaft region is stable (day 1 – day 7). **(C)** The bleaching line is remarkable stable and moves by a very small amount after 7 days. Figure (B-C) from (Zhang et al. 2012).

In the following sections, I will introduce the actin-binding proteins that have been involved in the development and maintenance of stereocilia, and describe the available evidence implicating mechanotransduction in the control of the hair-bundle morphology

B.3 Molecular constituents of the stereocilia

Maintenance of the stereociliary structure, like those of other actin-based protrusions, results from a complex interplay between several types of actin-binding proteins, including actin nucleators, cross-linkers, capping, severing proteins, and molecular motors (Fig. I-19). In this section, I will describe the main actin-binding proteins that have been identified in the hair bundle as well as their putative role.
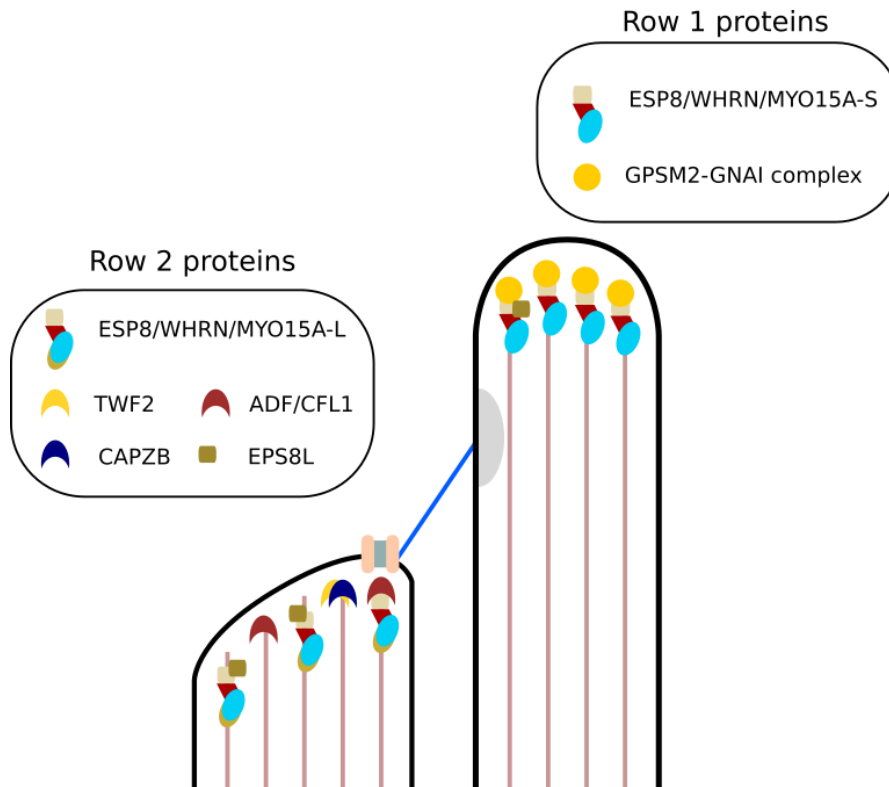
Figure I-19: SCHEMATIC REPRESENTATION OF IMPORTANT ACTIN BINDING PROTEINS AT THE STEREOCILIARY TIP OF MAMMALIAN COCHLEAR HAIR BUNDLES. Note that the proteins at the tips of the two rows are different, defining "row-identity proteins".

a. Actin

Stereocilia are made of both β-actin and γ-actin. These two isoforms differ by only four amino acid residues in the N-terminus region and are evolutionarily conserved from birds to mammals (Vandekerckhove and Weber 1978). Immunofluorescence microscopy of mice cochlear hair cells revealed that β-actin and γ-actin co-localize in the stereocilia and the lateral wall (Benjamin J. Perrin, Sonnemann, and Ervasti 2010) (Fig. I-20). In chick and guinea pig cochlear hair cells, γ-actin is expressed in the hair bundle, the cuticular plate, and the lateral wall, whereas β-actin localization is restricted to the hair bundle (Höfer, Ness, and Drenckhahn 1997; D.N. Furness et al. 2005).

Although the molecular differences between β-actin and γ-actin are small, the two isoforms cannot compensate for each other to develop normal hearing. In mice, knockout of the β-actin gene, *Actb*, results in early death during embryonic development (I. A. Belyantseva et al. 2009). Instead, knockout of the γ-actin gene, *Actg1*, results in early progressive hearing loss (Shawlot et al. 1998). Furthermore, in adult mice, immunolabeling of γ-actin reveals the presence of this actin isoform in gaps of the stereociliary core resulting from sound damage (I. A. Belyantseva et al.

2009). These observations suggest that β-actin is required for stereocilia formation during development and that γ-actin is involved in the maintenance and repair of the stereociliary structure (Benjamin J. Perrin, Sonnemann, and Ervasti 2010).
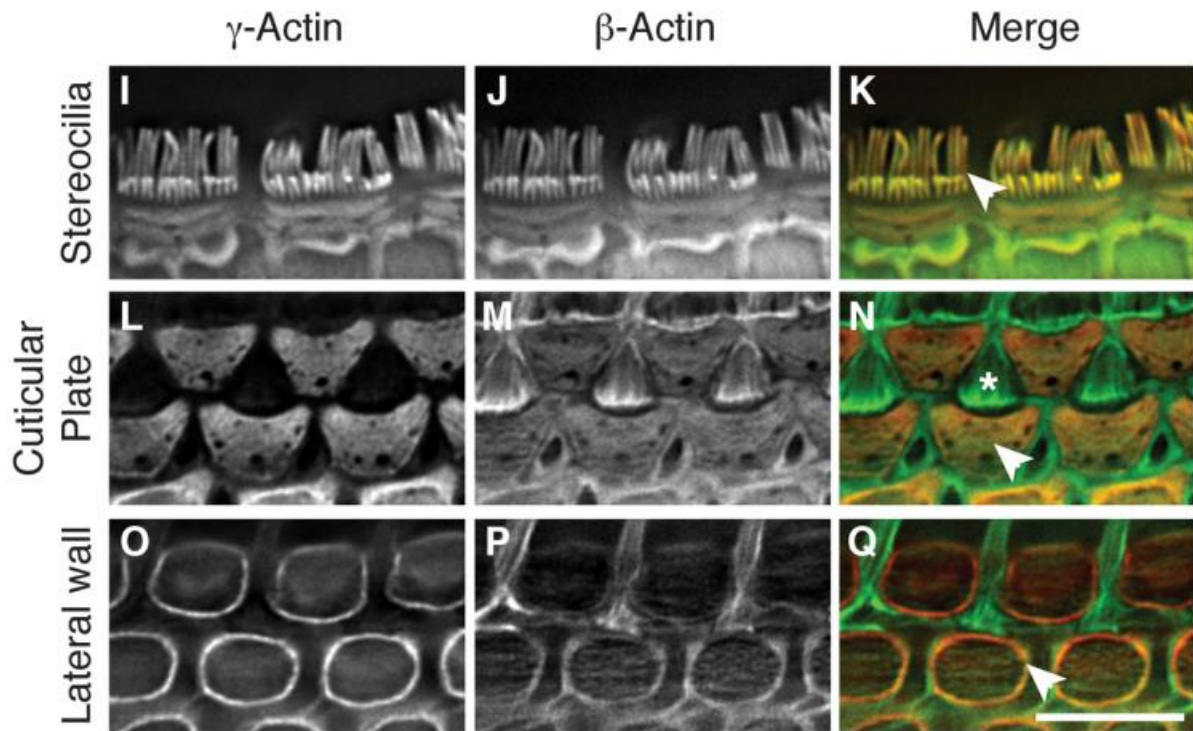
Figure I-20: CO-LOCALIZATION OF γ-ACTIN AND β-ACTIN IN COCHLEAR HAIR CELLS. Immunofluorescence microscopy reveals the localization of γ-actin and β-actin in the stereocilia, cuticular plate and lateral wall of outer hair cells. The γ-actin is more abundant in the lateral wall than the β-actin. Scale bar 5 μm. Figure from (Benjamin J. Perrin, Sonnemann, and Ervasti 2010).

b. Actin nucleators

Formins have been identified in chick or mice utricular hair bundles, although the number of molecules per stereocilium (~8) was very low and the evidence is thus not strong (Shin et al. 2013; Krey et al. 2015). Endogenous formins have also been identified in auditory hair cells, particularly at the apical junctional complex but not in the hair bundles, except when human DIAPH1 was over-expressed in mice (Ninoyu et al. 2020). Although formin localization in the normal stereocilia is not clear, over-expression of formin genes results in morphological defects (Fig. I-21 Overexpression of *DIAPH1* also results in morphological defects in inner hair cells where the hair bundles have fewer stereocilia and the remaining stereocilia get wider and longer, probably due to fusions of adjacent stereocilia (Fig. I-21.A). A similar effect was also observed upon overexpression of wild-type *Diaph3,* the murine homolog of human *DIAPH3*, in mice (Fig.

I-21.B) (Schoen, Burmeister, and Lesperance 2013). Not only do the stereocilia get wider, the cell apical surface, upon over-expression of both *DIAPH1* and *Diaph3*, also bulges. This observation suggests that over-expression of formins disrupt the normal maintenance of the hair bundle due to excessive nucleation of actin. However, a phenotype resulting from overexpression of exogenous formins does not provide definite evidence that formins actually play a role in normal stereocilia.
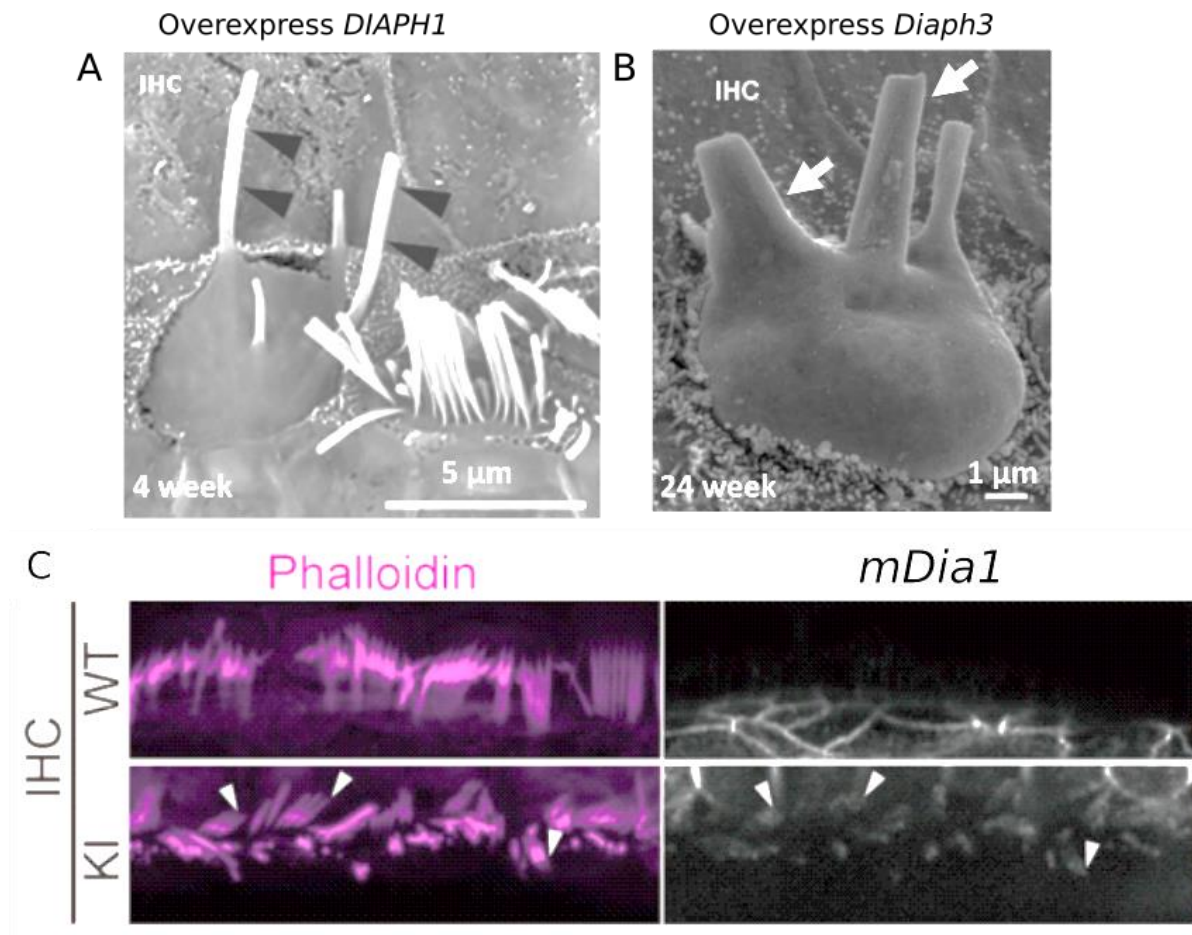
Figure I-21: EFFECTS OF OVEREXPRESSING FORMINS ON THE STEREOCILIARY STRUCTURE. Morphological defects of the hair cells as the result of overexpressing formins **(A)** overexpression of human DIAPH1 and **(B)** overexpression of mice Diaph3 in mice. **(C)** Using an anti-mDia1 antibody, the immunoreactivity of formins is observed at the stereociliary tips (arrow heads) after knock-in overexpression of human DIAPH1 in mouse cochlear inner hair cells. In the wild type, the labelling is prominent in the apical functional complex only. Figure (A and C) from (Ninoyu et al. 2020). Figure B from (Schoen, Burmeister, and Lesperance 2013) (B-C).

In addition, mutations in the formin genes have been linked to deafness. Non-syndromic deafness DFNA1 in humans is associated with mutations of the gene *DIAPH1*. Moreover, mutations in the genes *DIAPH3* are associated with hereditary deafness AUNA1 (Lynch 1997). In mice, endogenous Dia1 is expressed during and after the differentiation of the organ of Corti,

sensory epithelium and spiral ganglion neurons (SGNs), and is localized at the apical junctional complex (AJCs). The constitutively active mutant accumulates at hair cells' apical junctional complex and stereociliary tips in the *DIAPH1* knock-in mice (Ninoyu et al. 2020).

Another candidate for actin nucleation in the hair bundle comes the Arp 2/3 complex. The Arp2/3 complex and the Ena/vasodilator-stimulated phosphoprotein (VASP) family have been identified in the proteome of chick and mice utricular hair bundles (Shin et al. 2013; Krey et al. 2015). In mice, the estimated numbers of Arp2 (71) and Arp 3 (51) per stereocilium to reliably conclude that these molecules are present in the hair bundle of mice. However, no morphological defect related to the Arp2/3 complex has yet been reported. Nevertheless, mutations in the actin gene (γ-actin) that result in progressive autosomal dominant nonsyndromic hearing loss (DFNA20/26) have been found to be associated with Arp2/3 complex-dependent actin regulation. Two of the mutations, K118M and K118N are located near the putative binding site for the Arp2/3 complex (Kruth and Rubenstein 2012).

The possible roles of actin nucleators, such as formins and the Arp2/3 complex, on stereocilia maintenance, may have been underestimated and require further investigations. *mDia1* is also known to sense force and promote actin polymerization (Jégou, Carlier, and Romet-Lemonne 2013; M. Yu et al. 2017). If *mDia1* is involved in stereocilia maintenance, it may act as the mechanosensitive element that controls actin polymerization in the stereocilia.

c. Cross-linkers

Actin cross-linkers are proteins that bundle the actin filaments together. They provide stability against bending and buckling. According to equation (I-1), if the stereociliary actin core were not cross-linked, the pivotal stiffness of a single stereocilium would be much lower, by a factor $(a/r)^2 \simeq 100$, where $a \approx 50$ nm is the radius of the stereociliary taper and $r \approx 5$ nm is the radius of individual actin filaments (Jonathon Howard 2001). Three types of actin cross-linkers have been identified in the stereocilia: fimbrin was the first to be found (Flock, Bretscher, and Weber 1982), then espin (L. Zheng et al. 2000), and finally fascin (Chou et al. 2011). Fimbrin was later identified as a homolog of plastin (de Arruda et al. 1990).

Plastin - Plastins (plastin-1 (also called fimbrin),-2,-3) are encoded by three different gene. Plastin-1 (PLS-1) is the most abundant cross-linker in mouse vestibular hair cells (Krey et al. 2016; de Arruda et al. 1990). The spacing of actin filaments constrained by plastin-1 is ~9-12 nm (Matsudaira et al. 1983; Volkmann et al. 2001). In *Pls-1* knockout mice, the animals show reduced inner ear function with progressive hearing loss. In the stereocilia of utricular hair bundles of these

mutant mice, where espin is dominantly expressed, the stereocilia become shorter and thinner, and the actin spacing is reduced by ~ 1.1 nm compared to the control (Krey et al. 2016). This observation indicates that actin spacing in the stereociliary core is likely the result of an interplay between PLS-1 and espin, the latter favouring a network of tightly packed filaments (Fig. I-22). Moreover, PLS-1 may favour stereocilia widening and elongation.

Espin – Espin (ESPN) isoforms (1, 2A, 2B, 3A, 3B, 4) are encoded by a single gene *ESPN* and result from different transcriptional splice variants (Sekerková, Richter, and Bartles 2011). ESPN-1 and its paralog ESPNL are transported to the stereociliary tips by MYO3A and MYO3B (Ebrahim et al. 2016). Mutations in *ESPN* is associated with human deafness DFNB36 whereas mutations in its murine homolog, *Espn*, produces the so-called *jerker* mice (Naz et al. 2004; L. Zheng et al. 2000). In mice cochlear hair bundles, the expression levels of ESPN increase gradually during the elongation phase of stereocilia. This increase is also greater towards the cochlear apex where stereocilia are taller than at the cochlear base (Sekerková, Richter, and Bartles 2011). Although ESPN constitutes only 15% of the total cross-linkers in mice hair bundles, defect or deficiency in the *Espn* gene produces dramatic effects on the hair-bundle morphology. In jerker mice, where there is a missense mutation in the *Espn* gene, the stereocilia are bent and shortened, and later progressively disappear by P10 (Sekerková, Richter, and Bartles 2011). Knockout mice lacking *ESPN* have thin vestibular stereocilia that lose their staircase pattern (Ebrahim et al. 2016). These observations strongly indicate that ESPIN-1 may be required for stereocilia widening and elongation.

In contrast to ESPN, the role of ESPNL in stereocilia maintenance is not obvious. Knockout mice lacking *ESPNL* have apparently normal stereocilia except for the loss of row-3 stereocilia (the shortest row) in OHC hair bundles. Nevertheless, it has been proposed that ESPNL may play a role in stopping stereocilia elongation, based on the observation in filopodia that co-expression of *MYO3A* and *ESPNL* produces shortened stereocilia. The length of filopodia is also inversely proportional to the concentration of ESPNL et the tips (Ebrahim et al. 2016).
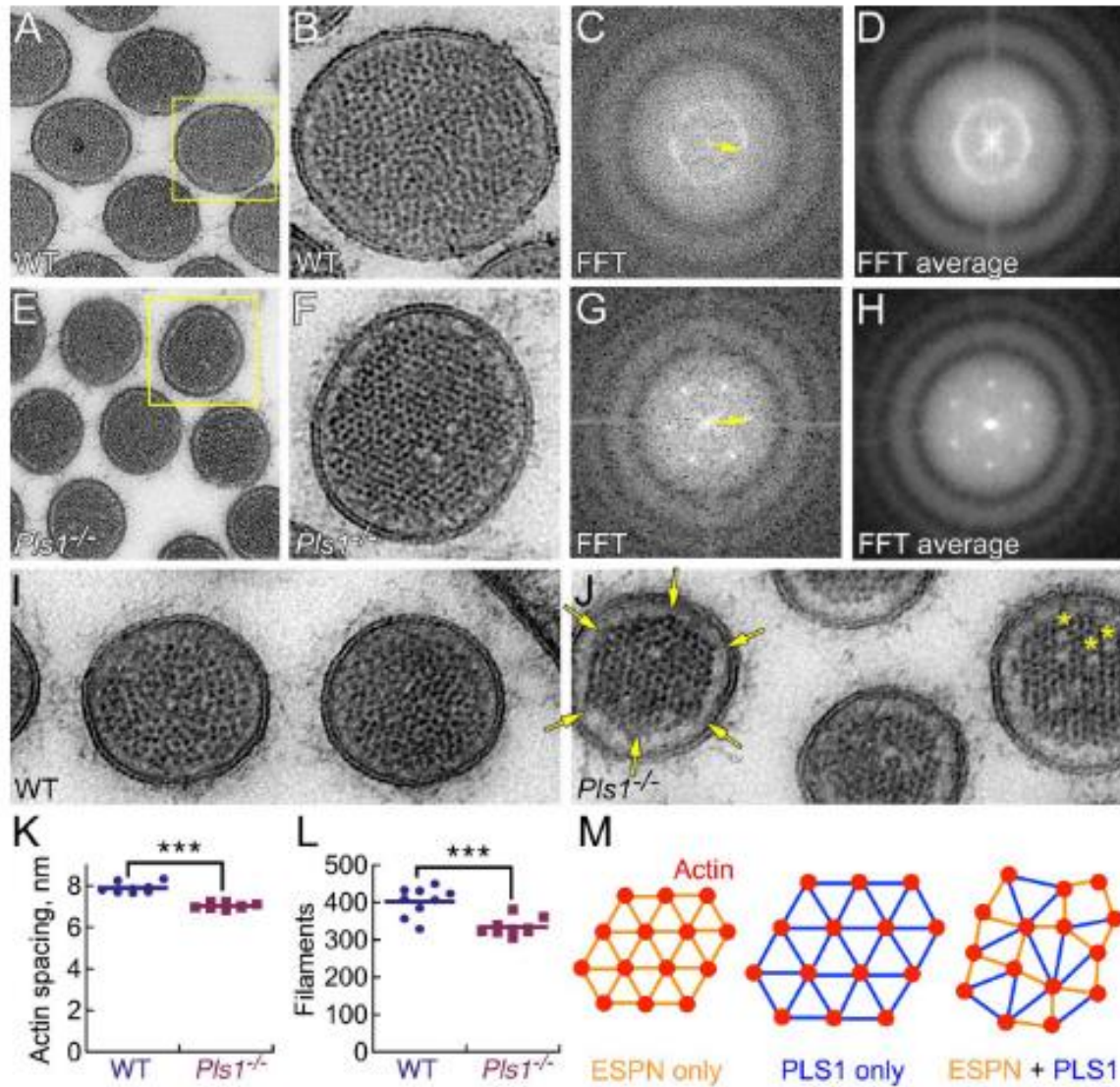
Figure I-22: INTERPLAY BETWEEN PLASTIN-1 AND ESPN FOR ACTIN-FILAMENT PACKING IN STEREOCILIA. (A-D) Transmission electron micrographs of a transverse section of stereocilia and 2D Fourier transform images of the corresponding micrographs from wildtype (WT). **(E-H)** Same as in (A-D) but for plastic-1 knockout mice (*Pls1*-/-). Transverse sections of the WT **(I)** and *Pls1*-/- **(J)** reveal that the stereociliary core of the mutant mice may have a reduced number of actin filaments with denser packing. Quantification of the number and inter-filament spacing of actin filaments indicate that the knockout mice indeed have denser **(K)** and fewer actin filaments **(L)**. **(M)** Schematic representation of actin-filament packing in different scenarios. In the presence of plastin-1, wild-type stereocilia adopt a more liquid packing, while in the absence of plastin-1 the stereocilia adopt a tight hexagonal packing due to constraints imposed by espin, another major actin cross-linker in the stereocilia. Figures from (Krey et al. 2016).

Fascin – There are 3 isoforms of fascin (Fascin-1, 2, and 3) that are encoded by 3 different genes. Although fascin-1 and 2 have a high degree of similarity (~73%) only fascin-2 has been reported in adult rat hair cells (Postnatal day 5, P5). In chick embryos (Embryonic day 20, E20), fascin-2 (FSCN-2) is the most abundant actin cross-linker in vestibular hair bundles (Shin et al. 2010; Avenarius et al. 2014) (Fig. I-23.A). Three-week-old mice with a missense mutation in the

Fscn2 gene (*Fscn2^{R109H}*) show reduced inner ear function with no apparent morphological defect in the hair bundles but stereocilia in row 2 and 3 later progressively shorten (~16 weeks after birth) (Fig. I-23.B). FSCN-2 is likely important for the maintenance of the stereociliary structure, rather than for stereocilia formation, and that FSCN-2 may favour stereocilia elongation (B. J. Perrin et al. 2013; Chou et al. 2011).
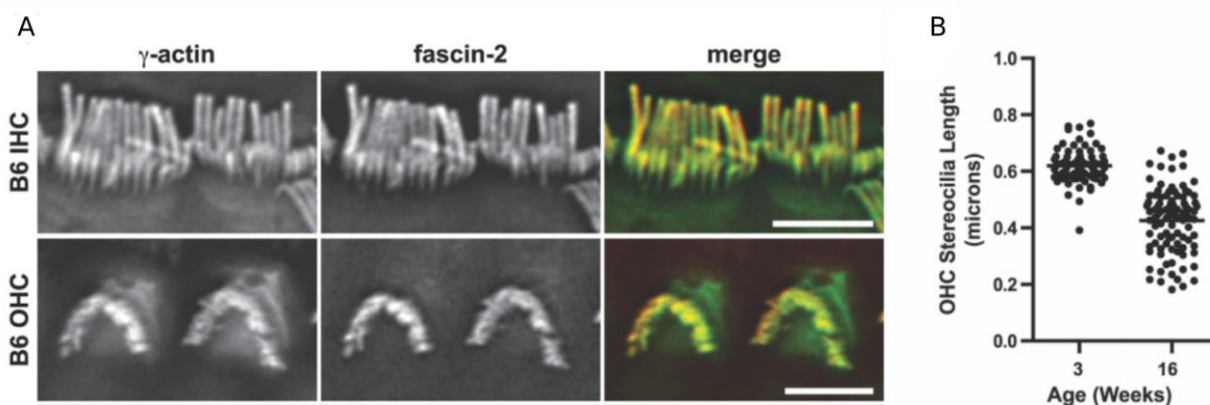
Figure I-23: LOCALISATION OF FASCIN-2 AND ITS ROLE ON STEREOCILIA MAINTENANCE. (A) In wildtype mice with B6 background, immunofluorescence microscopy shows the expression of *Fscn-2* along the stereociliary height in both IHC (top panel) and OHC (bottom panel). The immunoreactivity also shows co-localization of *Fscn-2* with γ-actin. Scale bar 5 μm. **(B)** Effects of a missense mutation in the *Fscn-2* (*Fscn2^{R109H}*) gene on the stereociliary height. Quantification of OHC stereociliary height indicates that *Fscn2^{R109H}* mice initially develop hair bundles with a more uniform stereociliary height at 3 weeks after birth. 16 weeks after birth, the stereociliary length is more variable and stereocilia are on average shorter by ~ 200 nm in the row 3 stereocilia. Figures from (B. J. Perrin et al. 2013).

d. Capping and severing proteins

Capping proteins control actin polymerization/depolymerisation by blocking the association or dissociation of actin monomers at the barbed end of actin filaments. Severing proteins generate new barbed ends at break points of each filament, thus increasing the availability of free barbed end for polymerization and depolymerization. Several capping and severing proteins have been identified in the stereocilia. These proteins are not only required for maintaining the proper stereociliary length but also for maintaining the stereociliary width. In stereocilia, capping proteins require myosin motors for transport to the stereociliary tips.

Eps8/Myosin-15/Whirlin - Under normal conditions, MYO15A co-localizes at the stereocilia tips with whirlin (WHRN), its cargo protein (Inna A. Belyantseva et al. 2005; Delprat et al. 2005). *Shaker-2* mice, which carry a mutation in the motor domain of MYO15A, have hair bundles that are abnormally short and have lost their staircase pattern. In the *whirler* mice, for which there is a mutation in the *WHRN* gene, stereocilia are shorter and wider than those of the control (Mogensen,

Rzadzinska, and Steel 2007). In the *shaker*-2 mice, the capping protein Eps8 fails to localize at the tips of the stereocilia tallest row suggesting that the MYO15A may be responsible for delivering Eps8 onto the barbed end at the stereociliary tip. In *Eps8* knockout mice, the hair bundles of both the inner and outer hair cells are abnormally short (Manor et al. 2011) (Fig. I-24). These observations suggest that Eps8/MYO15A/WHRN complex favours the elongation of stereocilia.
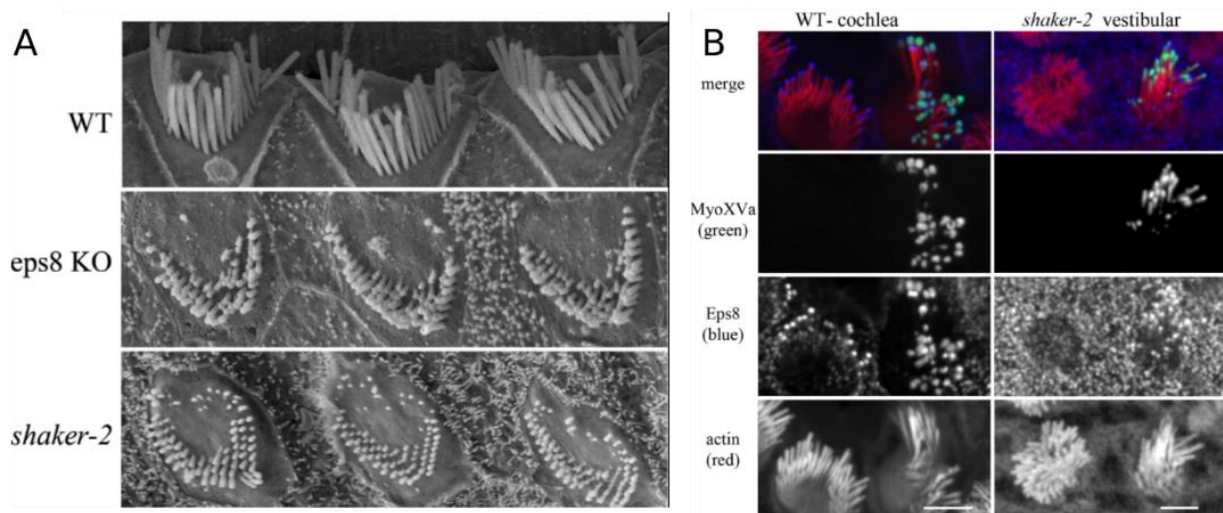
Figure I-24: ROLES OF EPS8 AND ITS TRANSPORTER MYOSIN-15 IN STEREOCILIA MAINTENANCE. (A) Scanning electron micrographs of hair bundles in wild type (WT), Esp8 knockout mice, and in *shaker-2* mice where there is a mutation in the motor domain of myosin-15. Both mutant mice show hair bundles with abnormally short stereocilia that have lost their unique staircase pattern. **(B)** Immunofluorescence labelling localizes myosin-15a and Esp8 at the stereociliary tip of wild type cochlear hair bundles (left panel), while, in the *shaker-2* mice, the capping protein Esp8 is absent from the stereociliary tips of the vestibular hair bundles even though its transporter Myosin-15a appeared at the stereociliary tips. Scale bar 5 μm. Figures adapted from (Manor et al. 2011).

A particular member of the Eps8 protein family, Eps8L2 has been identified in stereocilia but has less pronounced effects on the stereociliary height (David N. Furness et al. 2013). Eps8L2, however, is expressed more strongly at the tip of row-2 stereocilia. Both EPS8 and Eps8L2 are row identity proteins of the cochlea hair bundles that may likely play a role in controlling the stereociliary width during the widening phase of the hair-bundle development, close to the onset of mechanotransduction (~ P6-7.5) (Krey et al. 2020).

Signalling proteins GPSM2-GNAI – Mutations in GPSM2 is associated with sensorineural hearing loss Chudley-Mccullough syndrome in human (Mauriac et al. 2017). The molecule GPSM2 and its binding partner GNAI are expressed at the tips of the tallest stereocilia of both IHC and OHC in the mammalian cochlea. Both proteins require MYO15A and its cargo WHRN

for transport to the stereociliary tips, where they form a protein complex with EPS8 (Mauriac et al. 2017; Tadenev et al. 2019; Krey et al. 2020). Expression patterns of both GPSM2 and GNAI are nearly identical. GNAI accumulates at the tip of row-1 stereocilia as early as P2.5, reaches a peak of expression around the onset of mechano-electrical transduction in the second postnatal week, and then expression declines from P21.5 onwards. The expression of GPSM2 and GNAI coincides with the lengthening phase of the tallest stereocilia. Knockout mice lacking GPSM2 or mice with impaired GNAI have abnormally short stereocilia that lose their staircase pattern, resembling the hair bundles of *shaker-2*, *whirler*, and *EPS8* knock-out mice (Tadenev et al. 2019; Inna A. Belyantseva et al. 2005; Manor et al. 2011). These observations suggest that GPSM2 and GNAI are required for stereocilia elongation and their localisation to the stereociliary tip depends on functional mechanoelectrical transduction.

Twinfilin/Capzb - Twinfilin-2 (TWF2), has a dual role as capping and severing protein. It localizes at the tips of stereocilia shorter rows (Fig. I-25.A-B). It has been proposed that myosin-7a (MYO7A) delivers the capping protein to the stereociliary tips. However, other roles, such as anchoring TWF2 to the tip or increasing the activity of TWF2, are also possible (Rzadzinska et al. 2009). Moreover, if MYO7A tenses the tip links (Li et al. 2020), mutations of *MYO7A* in *shaker-1* mice may affect the open probability of the transduction channels (and in turn the magnitude of the Ca^{2+} influx) and localization of TWF2 at the stereociliary tip, which happens 4-5 days after the MET onset (Krey et al. 2020).

Overexpression of *Twf2* results in abnormally short stereocilia (Fig. I-25.C-D) while *shaker-1* mice that have mutations in the *Myo7A* gene have unusually long and disorganized stereocilia (Rzadzinska et al. 2009; Peng et al. 2009). These observations suggest that TWF2/MYO7A flavours stereocilia shortening.

TWF2 is also found to co-localize and interact with another capping protein CAPZB that regulates both the width and height of the stereocilia (Avenarius et al. 2017). In the same study, both auditory and vestibular hair bundles of *Capzb* knockout mice had shortened and thinned stereocilia that eventually disappeared. This observation suggests that CAPZB may favour stereocilia widening and elongation, an effect opposite to that of TWF2.

Although TWF2 and CAPZB may work in antagonistic fashions (shortening vs. elongation, respectively), they are co-localized and physically interact with each other. In mammalian cochlear hair cells, TWF2/CAPZB have enriched at the tip of stereocilia shorter rows during their

shortening phase (from P10 - 12 onwards) (Krey et al. 2020). Stereocilia may be able to shorten or elongate depending on whether TWF2 or CAPZB dominates.
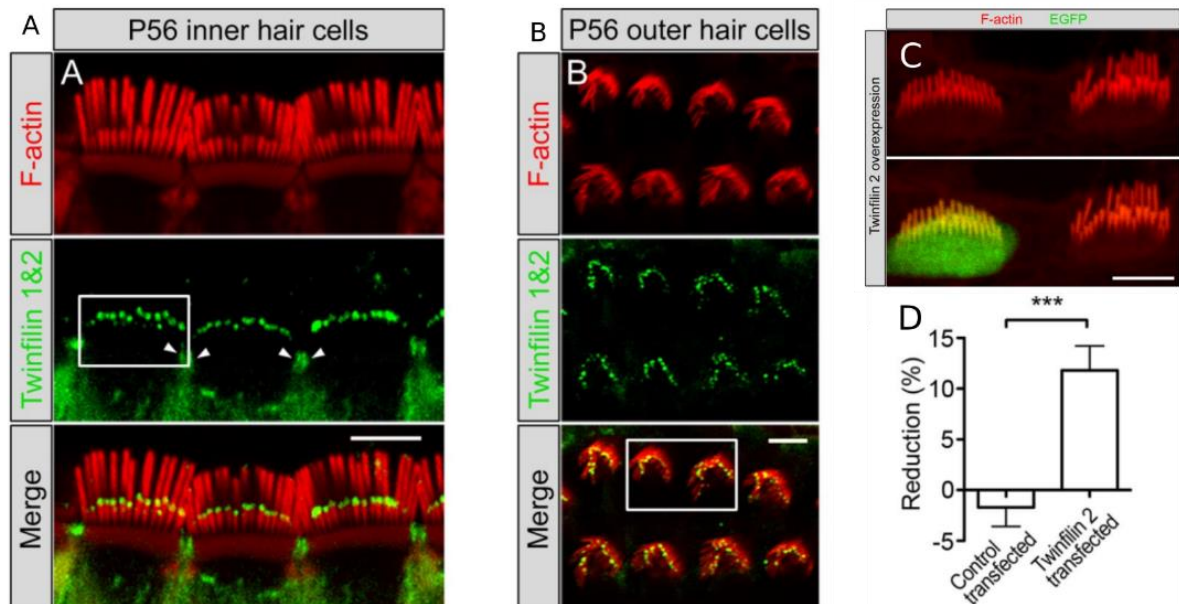
Figure I-25: LOCALIZATION OF TWINFILIN-2 AND ITS ROLE ON STEREOCILIA MAINTENANCE. Immunofluorescence labelling of twinfilin-2 in adult (post-natal day 56) mice in both IHC **(A)** and OHC **(B)** hair bundles. **(C)** Overexpression of twinfilin-2 results in significantly shorter tallest-row stereocilia (left) compared to the un-transfected neighbour where there is no twinfilin-2-EGFP signal (right). **(D)** Quantification of the stereociliary height of the tallest stereocilia indicated shortening by almost 13% in twinfilin-2 transfected bundles. Scale bar (A-C) 5 µm. Figures from (Peng et al. 2009).

Adf/Cofilin-1 – The severing protein actin-depolymerizing factor (ADF, or DSTN) and actin-interacting protein 1 (AIP1, or WDR1) have been identified in the stereocilia of the chick vestibule (Shin et al. 2013) and the mammalian cochlea (Narayanan et al. 2015). Knock-out mice lacking *Adf* gene or mice bearing a mutant allele of *Aip1* gene that results in reduced expression of AIP1 protein share a similar phenotype. Some stereocilia in the shorter rows are shorter than in the control, whereas the tallest row remains normal (Narayanan et al. 2015). Because cofilin-1 (CFL1) shares 70% sequence identity with ADF, the two proteins are likely to compensate for the loss of one of them. Both proteins are functionally and structurally similar to each other. They both sever actin filaments and allow for the new barbed ends they have produced to undergo actin assembly or disassembly depending on the conditions of the cells.

A recent study by *McGrath et al. 2021* showed that ADF/CFL1 localizes at the tip of row 2 stereocilia (Fig. I-26.A-B). Accordingly, the transducing row-2 stereocilia harbour more available barbed ends of actin filaments at their tips than the non-transducing row-1 stereocilia. Note a smart

47

technical trick: the number of available barbed ends at the stereociliary tips can be estimated from the fluorescence intensity of rhodamine-labelled actin that incorporates there.

The localization of ADF/CFL1 at the stereociliary tips relies on the myosin transporter MYO15a and its associated protein EPS8. *Shaker*-2 mice, which has a mutation in the motor domain of the *Myosin-15a*, and the *Eps8* null mice (*Esp8*^{-/-}) fail to deliver ADF/CFL1 onto the stereociliary tip. The immunoreactivity of ADF/cofilin-1 appears to be more diffusive and distributed to other stereocilia rows instead of being restricted to the tips of row 2 stereocilia as in the control (Fig. I-26.A-B). Correspondingly, in the *Eps8* null mice, the available barbed ends are also redistributed to the tallest stereocilia rows, as indicated by the increase of rhodamine-actin signal in the tallest stereocilia (Fig. I-26.C-D).

Interestingly, in direct relevance to my PhD work, pharmacological blocking of the transduction channels also results in similar redistribution of available barbed ends (Fig. I-34). Mice with the double knockout of both *Adf* and *Cfl1* develop hair bundles with complex phenotypes. The IHC bundles have shorter row-1 stereocilia and thinner row-3 stereocilia compared to those of the control, whereas the OHC bundles have wider stereocilia in all rows. Many hair cells in the double knockout mice have morphological defects in which the stereocilia fuse or disappear. Some are highly dysmorphic, where the hair cells are extruded (McGrath et al. 2021). These observations add to the available evidence (see below) that links the hair-bundle morphology to mechano-electrical transduction.
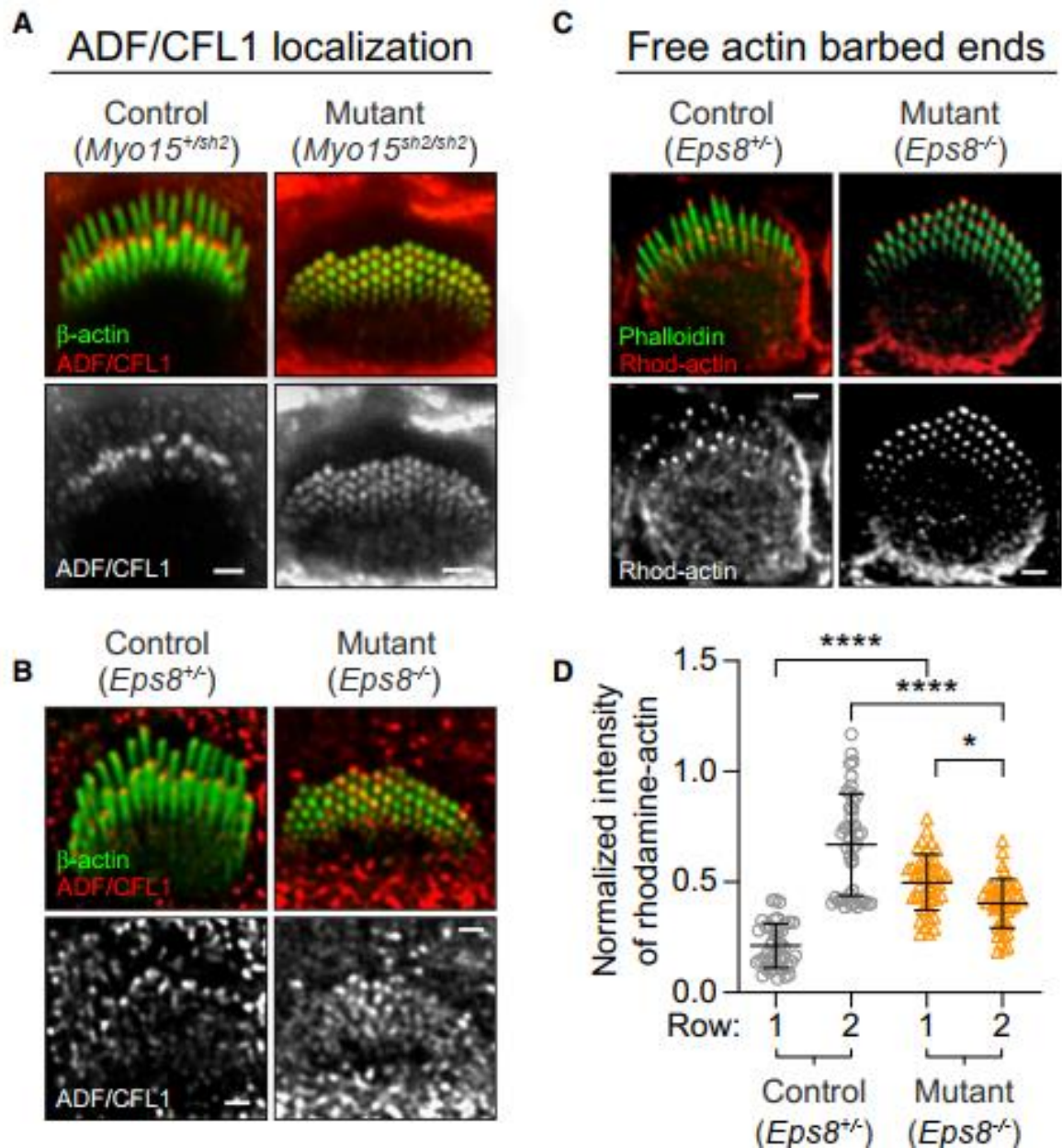
Figure I-26: LOCALIZATION OF ADF/CFL1 AND AVAILABLE BARBED-ENDS FROM RHODAMINE-ACTIN INCORPORATION IN MYO15$^{SH2/SH2}$ AND EPS8$^{-/-}$ MUTANTS. (A) Misplaced localization of capping and severing proteins ADF/CFL1 from row 2 stereocilia (row 1 being the tallest stereocilia row) to all rows of IHC bundles in *shaker*-2 (sh2) $Myo^{sh2/sh2}$ mice that have a mutation in the motor domain of MYO15. Hair bundles of the mutant mice also lose the staircase pattern and stereocilia in all rows become equally short. **(B)** Similar misplaced localization of ADF/CFL1 and morphological defects as in (A) are also observed in $Eps8^{-/-}$ mutant mice. **(C)** Rhodamine-actin intensity, which indicates the availability of free polymerizing-barbed ends and the incorporation of new actin subunits into the stereocilia, is more evenly distributed among stereocilia rows in the mutant $Eps8^{-/-}$ mice. **(D)** Quantification of the rhodamine-actin intensity demonstrated that the availability of free actin barbed ends was reduced in row 2 stereocilia and distributed to row 1 stereocilia in $Eps8^{-/-}$. Scale bar (A-C) 1 µm. Figure from (McGrath et al. 2021).
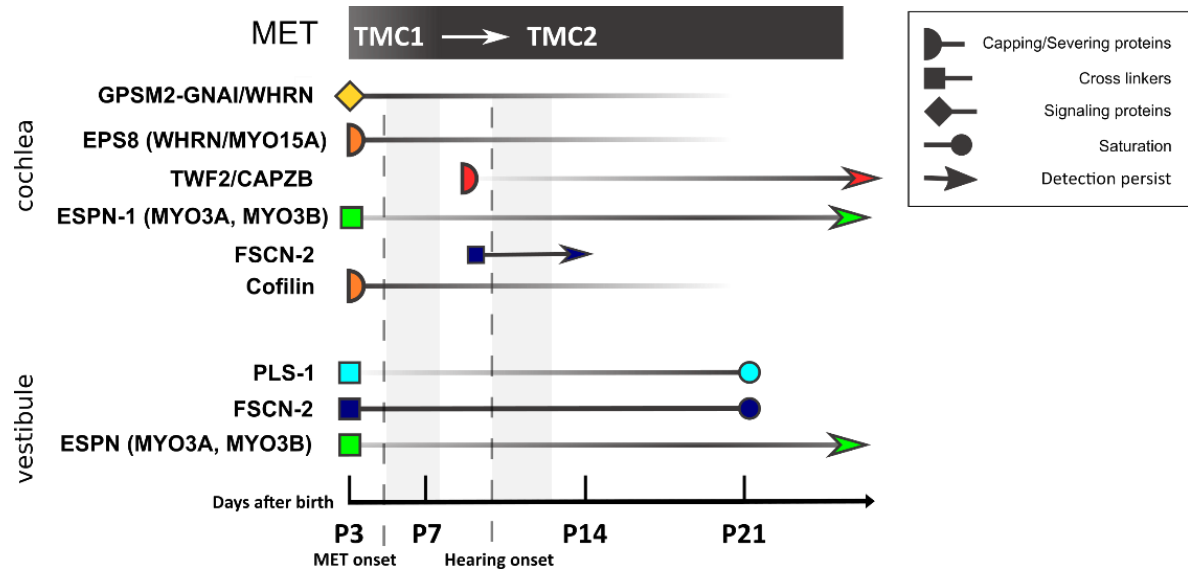
SUMMARY

The table (Table I-1) summarize the actin-binding proteins found in stereocilia and their hypothetical functions in stereocilia maintenance. The figure (Fig. I-27) indicates the timeline of expression of these actin-binding proteins.

| Type	Name	Deafness	Perturbation	Hair-bundle phenotype	Location
Nucle ators	DIAPH1	DFNA1	Overexpression	Elongated and fused stereocilia	n.a.
	DIAPH3	AUNA1			n.a.
Cross-linker	PLS-1	n.a.	Knockout	Short and thin stereocilia, reduced actin spacing, and the number of actin filaments.	Shaft
	ESPIN-1	DFNB36	Overexpression	Elongated stereocilia	Shaft
			Knockout	Loss of staircase pattern and thin vestibular stereocilia.	
			Mutation	Bent and short stereocilia	
	ESPNL		Knockout	Loss of row 3 stereocilia in OHC	Shaft
	FSCN-2	n.a.	Knockout	Short row 2 and 3 stereocilia in OHC	Shaft
	fascin 2b	n.a.	Overexpression	Elongated stereocilia	Shaft
Capping & Severing	EPS8	DFNB102	Knockout	Short cochlear stereocilia	Tip, row 1 & 2
	GPSM2-GNAI*	Chudley-Mccullough	Knockout	Loss of the staircase pattern of IHC and OHC	Tip, row 1
	TFW2	n.a.	Overexpression	Short cochlear stereocilia	Tip, row 2
	CAPZB2	n.a.	Overexpression	Loss of the staircase pattern and widen utricular stereocilia.	
			Knockout	Short and thin stereocilia	
	ADF	n.a.	Knockout	Short row 3 OHC stereocilia	Tip, row 2
	ADF /CFL1	n.a.	Double knockout	Short IHC row 1 stereocilia and thin row 3 stereocilia. OHC stereocilia widen	Tip, row 2
Myosin	MYO3A	DFNB30	Knockout	Similar to control	Tip
	MYO3B	n.a.	Knockout	Shortening of the tallest stereocilia and elongation of the shortest stereocilia.	Tip
	MYO6	*Snell's waltzer* mice	Mutations	Fused and branching cochlear stereocilia	haft and taper
	MYO7A	*Shaker-1* & Usher 1B DFNA22, DFNB37	Mutation	Abnormally long stereocilia	Tip links
	MYO15A	*Shaker-2* & DFNB3	Mutation	Very short stereocilia and the loss of staircase	Tip, row 1 & 2
Other	TRIOBP	DFNB28	Knockout	Stereocilia lacking rootlets that later fuse together	Rootlet
Table I-1: ACTIN BINDING PROTEINS AND THEIR HYPOTHETICAL FUNCTIONS IN STEREOCILIA MAINTENANCE.					
*(Signalling proteins associated with EPS8). (n.a., not available).					

Figure I-27: EXPRESSION TIMELINE OF ACTIN-BINDING PROTEINS IN MAMMALIAN HAIR BUNDLES. Summarized from (Peng et al. 2011; Krey et al. 2016; 2020).
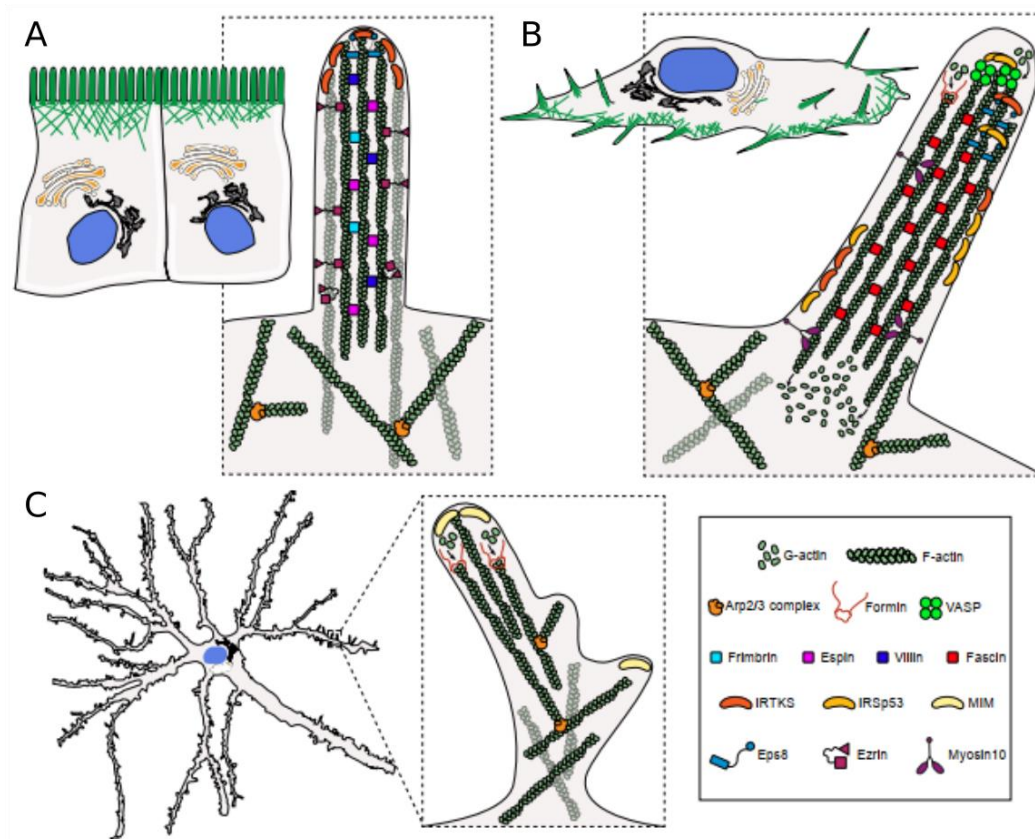
C. Other actin-based protrusions
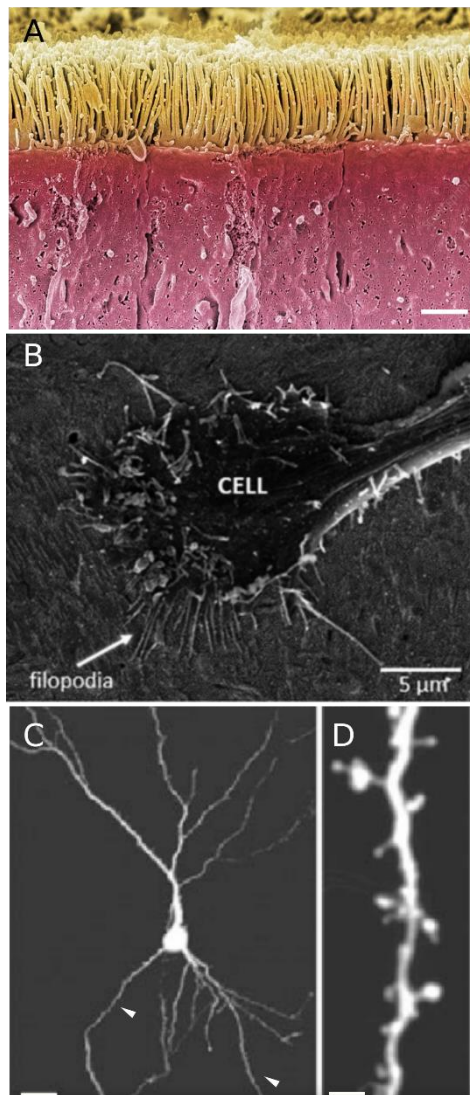
Figure I-28: ACTIN-BASED PROTRUSIONS. (A) Intestinal microvilli are numerous actin-based apical protrusions (1-2 µm in height) that project from the epithelial cells lining the surface of the intestinal tract. These microvilli increase the surface area and efficiency of nutrient absorption of the epithelial cells. Scale bar 1.25 µm. **(B)** Filopodia are actin-based cellular processes that extend by about a few hundred nanometers beyond thin-sheath membrane protrusions called lamellipodia, which are located at the leading edge of a motile cell. Cells employ filopodia as antennae for probing the surrounding environment. **(C)** Neurons show several spike-shaped processes that extend from the cell body called dendrites (white arrow heads). **(D)** Dendritic spines are bulb-like protrusions that form on the dendrites. At the head of a spine is a site where excitatory synapses take place. Figures from (Lippman and Dunaevsky 2005). Scale bar 20 µm for (C) and 2.7 µm for (D).

Actin-based cellular protrusions serve various purposes, from absorption and secretion of chemicals to probing surrounding chemical and physical environments. Among these protrusions are microvilli, filopodia, and dendritic spines, which all share a similar underlying structure made of a cross-linked actin core. Microvilli are finger-like protrusions that project from the apical surface of the epithelial cells, for instance in the intestinal tract (Fig. I-28.A), whereas filopodia are cellular processes that extend from the motile edge of migrating cells (Fig. I-28.B). Dendritic spines are bulb-like cellular protrusions that extend from dendrites, the sites of excitatory synapses (Fig. I-28.C) in neurons.

Similar to stereocilia, protrusions like microvilli, filopodia, and dendritic spines are all made of an array of polarized and cross-linked actin filaments. The actin filaments in these protrusions

are oriented so that the polymerizing-barbed ends are located at the tip of the protrusions. In contrast to the mature stereociliary structure that is stable along most of its length (Narayanan et al. 2015), actin remodelling in these protrusions employs highly dynamic treadmilling: these protrusions can entirely retract or elongate within a timescale of minutes (Gorelik et al. 2003; Oertner and Matus 2005).

Figure I-29: MOLECULAR CONSTITUENTS OF ACTIN-BASED PROTRUSIONS. (A) Microvilli (1-2 µm in length) comprised straight actin filaments bundled by various actin cross-linkers. **(B)** Filopodia (10 µm in length), like microvilli, are made of straight actin filaments that are predominantly bundled by fascin. **(C)** Dendritic spines found in neurons share similar underlying structures with microvilli and filopodia but they also have branched actin filaments mediated by the Arp2/3 complex. The branching of actin filaments produces a bulb-like shape in the dendritic spines. Figure adapted from (Ljubojevic, Henderson, and Zurzolo 2021).

In these protrusions, the actin remodelling process that initiates elongation and stabilization of crosslinked actin filaments is tightly controlled by mechanisms that involve several actin-binding proteins. Some of these proteins or their homologs are also present in the stereocilia (Fig. I-29).

For example, maintenance of these protrusions requires actin cross-linkers, such as fascin, fimbrin, espin, Eps8, and villin to stabilize a bundle of a few tens of actin filaments within the protrusions against buckling. Stereocilia employ fimbrin, espin, and fascin as actin cross-linkers

(Flock, Bretscher, and Weber 1982; L. Zheng et al. 2000; Chou et al. 2011) but lack villin (Flock, Bretscher, and Weber 1982), the major actin cross-linker identified in intestinal microvilli (Anthony Bretscher and Weber 1979). Espin and fimbrin were also identified in microvilli (Bartles et al. 1998; A Bretscher and Weber 1980). The filopodia largely rely on fascin (Vignjevic et al. 2006), another major actin cross-linker employed by hair cells for stereocilia maintenance (Chou et al. 2011; B. J. Perrin et al. 2013).

Actin cross-linkers like Eps8 can also work as a capping protein (Hertzog et al. 2010) that could be employed to control the length of the protrusions. In Eps8 knockout mice, the intestinal microvilli length is reduced (Tocchetti et al. 2010). As discussed above, stereocilia from outer hair cells in *Eps8* knockout mice also have shorter stereocilia and the unique staircase pattern of the hair bundles is also disrupted (Manor et al. 2011). These observations suggest that Eps8 in these two systems may favour elongation. Intriguingly, deletion of Eps8L1, another member of the Eps8 family, leads to excessive elongation of microvilli, while overexpression produced an opposite effect (Zwaenepoel et al. 2012). Eps8L2, which was also identified in stereocilia has a less pronounced effect on the stereociliary height (David N. Furness et al. 2013). These distinct effects may reflect the complexity of the interplay between the Eps8 family and other actin-binding proteins or may arise from different roles played by members of the Eps8 family themselves.

Although intestinal microvilli and mammalian cochlear hair bundles may control their lengths through the Eps8-based tip complex, another type of tip complex, based on formins, is used in filopodia and dendritic spines. This reflects the diversity of mechanisms that actin-based protrusions may employ to develop and maintain their structures.

The interplay between different actin-binding proteins described here in the microvilli, filopodia, and dendritic spines, provides one example showing how actin-based protrusion could employ different schemes to develop and maintain their structures. Many proteins identified in other actin-based protrusions share a similar function to those found in the stereocilia. Understanding the functions of these proteins in systems like microvilli, filopodia, and dendritic spines may help to provide more insights regarding the development and maintenance of the stereociliary structure.

D. Control of stereocilia dimensions by mechanotransduction
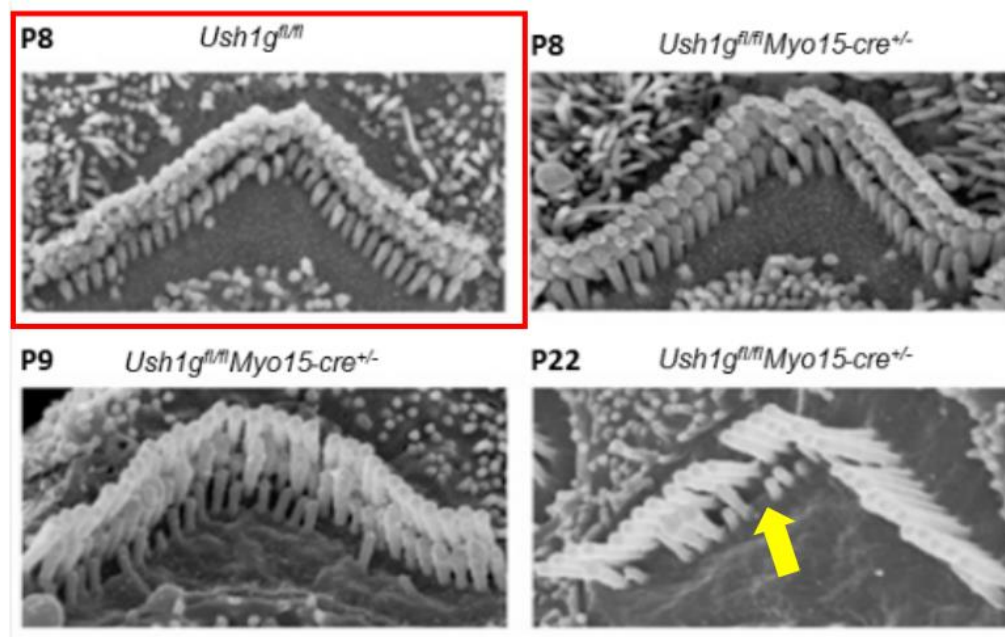
Figure I-30: STEREOCILIA SHORTENING AS A RESULT OF GENETIC DELETION OF TIP LINK PROTEINS. In conditional knockout mice, *Ush1g$^{fl/fl}$Myo15-cre$^{+/-}$*, the tip-link proteins SANS and cadherin-23 are post-natally deleted. The hair bundles of the mutant mice initially develop normally compared to the control *Ush1g$^{fl/fl}$* mice (red) and then the stereocilia in the shorter rows (row 2 and 3), but not in the tallest row (row1), shorten or even completely disappear. Note that only stereocilia if the shorter rows are expected to be equipped with transduction channels are their tips; loss of the tip links must have resulted in the loss of a Ca^{2+} influx through these channels. Figure from (Caberlotto et al. 2011).

In the hair bundle, incorporation of new actin monomers appears to happen mainly within about 0.5 µm from the stereociliary tips. Remarkably, in cochlear hair cells, the tips of stereocilia in the second row, which are endowed with transduction channels, are more dynamic than those of stereocilia of the tallest row, which are not (McGrath, Roy, and Perrin 2017). Does mechanotransduction or the proteins that contribute to the MET machinery play any role in stereocilia maintenance? Although the stereociliary structure in mature hair cells is remarkably stable, there is a growing bulk of evidence showing that perturbing the mechano-electrical transduction can result in dramatic changes of the hair-bundle morphology.

In the pioneering work of *Caberlotto et al. 2011*, the authors developed conditional knockout mice to delete the Usher 1G protein *SANS*, a putative scaffold protein at the upper tip-link density, as well as the tip-link protein cadherin-23, after normal development of the hair bundle. In *Ush1g$^{fl/fl}$Myo15-cre$^{+/-}$* mice, which are defective for the protein *SANS*, stereocilia develop normally until about one week after birth (Fig. I-30). However, later on, the stereocilia in the shorter rows of both IHC and OHC bundles get shorter, but not those of the tallest row. This

deference is remarkable remembering that only the stereocilia of the two shorter rows are thought to be endowed with transduction channels at their tips (Beurg et al. 2009). By P22, a few stereocilia from the shortest stereociliary row have almost disappeared. Additionally, the number of tip links is also reduced in the knockout mice (Caberlotto et al. 2011).

These results have been interpreted as evidence that the MET machinery is essential for maintaining the stereociliary structure. However, it remained unclear whether the current flowing through the transduction channels was involved in stereocilia maintenance or whether protein deletion of components of the transduction machinery generated a remodelling of the stereocilia due to perturbation of their interactions with other proteins. Knockout of genes of the MET machinery may have produced off-target effects on the molecular constituents in the stereocilia.
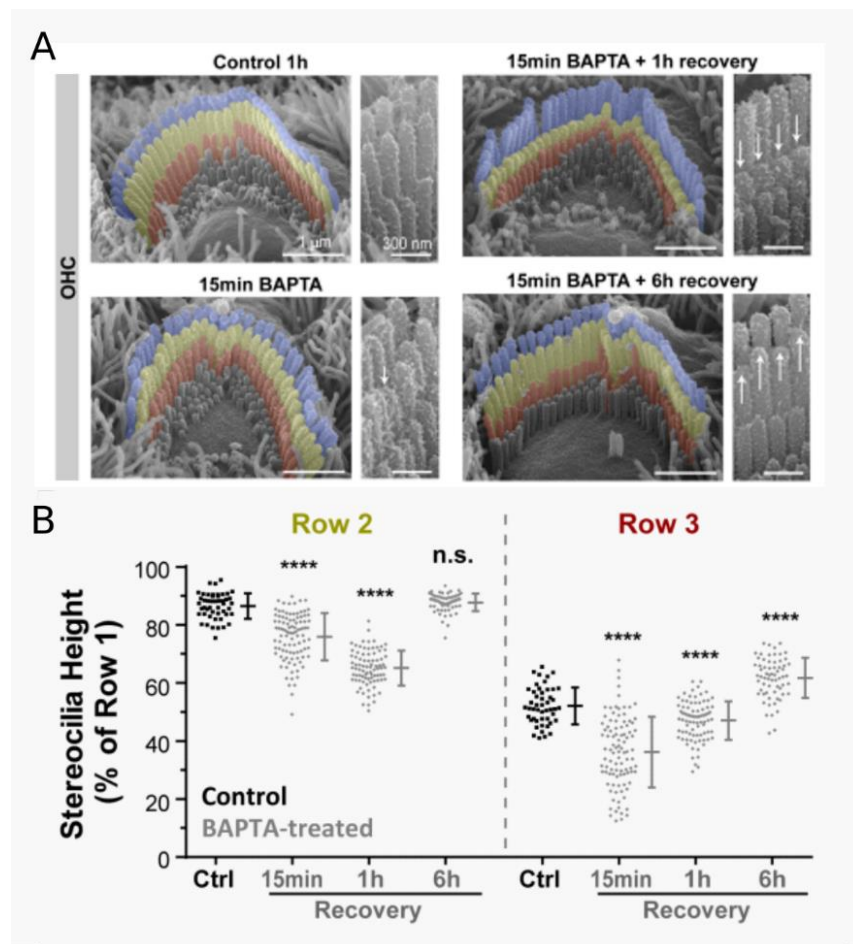
Figure I-31: STEREOCILIA SHORTENING AS A RESULT OF CHEMICAL DISRUPTION OF TIP LINKS. (A) Scanning electron micrographs of the OHC bundles. Upon chemical disruption of tip links by exposure to a solution with 5 mM BAPTA, the transducing shorter row stereocilia recede. Actin remodelling is reversible and recovered within 1 – 6 hr after washing out the calcium chelators. **(B)** Quantification of the stereociliary height indicates that both shorter rows 2 & 3 (where row 1 being the tallest stereocilia row) shorten within 15 min after application of BAPTA and later recovered. Figures from (Vélez-Ortega et al. 2017).

More recently, blocking the transduction channels or disrupting the tip links that pull them open has provided more direct evidence for the implication of the mechanotransduction current (Fig. I-31 and I-32) (Vélez-Ortega et al. 2017). Again, although the composition of the transduction channels remained unaffected in this study, the transducing stereocilia of rows 1 and 2 of mice cochlear hair cells were observed to shorten but not those in the tallest non-transducing row. Furthermore, retrospective examination of several other studies of mice with defective MET machinery proteins also shows the same effects (Vélez-Ortega and Frolenkov 2019). Importantly, actin remodelling observed upon chemical disruption of tip links is reversible. The stereociliary height recovers within 1-6 hr and may reflect the slow restoration of tip links and mechanotransduction (Assad, Shepherd, and Corey 1991).
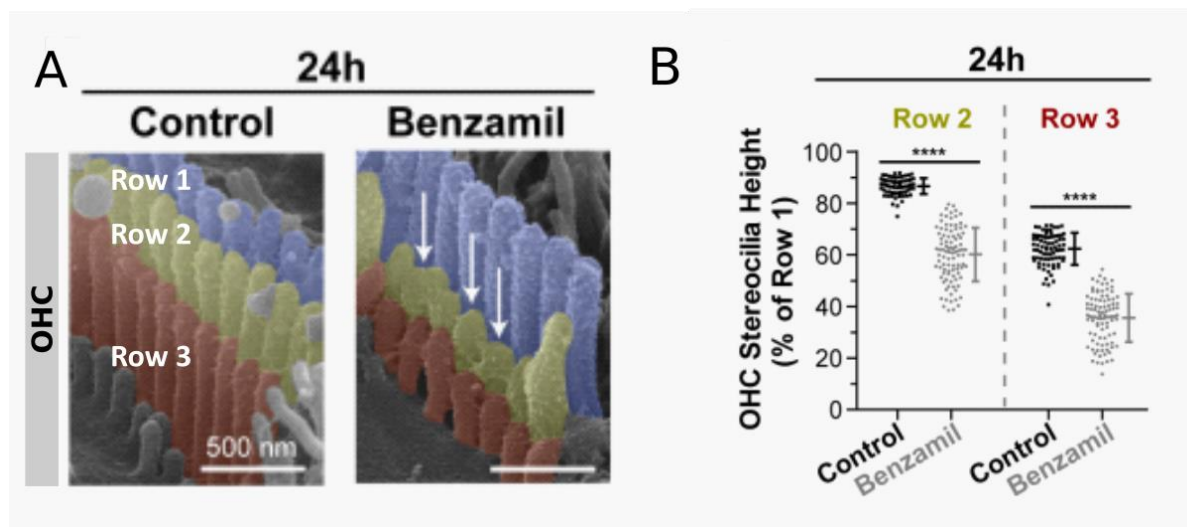
Figure I-32: STEREOCILIA SHORTENING AS A RESULT OF BLOCKING THE MET CHANNELS. (A) Scanning Electron micrographs of the OHC rows 1, 2 and 3, where row 1 is the tallest stereocilia row. Upon pharmacological blocking of the MET channels (with 30 µM benzamil), stereocilia in row 2 recede. **(B)** Quantification of the stereociliary height in OHC indicates that after 24 h of blocking MET channels, the transducing stereocilia in the shorter rows get shorter relative to those in the tallest stereocilia row 1. Figures from (Vélez-Ortega et al. 2017).

Disrupting the tip links or blocking the MET channels both results in a reduced influx of cations, especially Ca^{2+}, which is known as a control signal of actin polymerization in other systems (Yin et al. 1981). If the Ca^{2+} influx is essential for actin remodelling, intracellular chelation of calcium should also affect the morphology of stereocilia. Indeed, the stereocilia get thinner, prominently at the stereociliary tip, with intracellular Ca^{2+} chelation using BAPTA (Vélez-Ortega et al. 2017). Altogether, these observations reinforced the hypothesis that there is

a feedback between actin remodelling of the stereociliary structure and mechano-electrical transduction, probably mediated by the influx of Ca^{2+}.

Mechanotransduction not only seems to play an important role in hair-bundle maintenance but also hair-bundle development (Krey et al. 2020). Tilney had already suggested that mechanotransduction correlates with stereocilia elongation (L. G. Tilney, Tilney, and Cotanche 1988). In addition, it was shown in IHC bundles from mice that stereocilia widening coincides with the maturation of mechanotransduction (Fig. I-33.A-B). Genetic knockouts of genes encoding subunits of the transduction channel (TMC1 and TMC2, or TMIE) or pharmacological blocking of the transduction channels produce bundles of stereocilia that develop with more uniform diameters in between rows (thinner rows 1-2, thicker row 3) and a shallower staircase pattern. Remarkably, these morphological defects are associated with the redistribution of row-identity proteins (Fig. I-33.C) (Krey et al. 2020). Recently, it was shown that blocking the transduction channels (at P6) also leads to a redistribution of the severing proteins ADF/CFL1 from row 2 to row 1, of the row identity protein EPS8 from row 1 to row 2, and of a reduction of the availability of the free polymerizing barbed-end at the stereociliary tips of row 2 (McGrath et al. 2021) (Fig. I-34). It is proposed that the availability of free polymerizing barbed-end relies on severing proteins ADF/CFL1 that are enriched in row 2 stereocilia. However, how these effects might explain morphological changes of the hair bundle remains unclear.

In one study (Krey et al. 2020), blocking transduction channels mostly affected the stereociliary width (wider row 3 and thinner row 2 stereocilia), whereas the main effect reported in the earlier study (Vélez-Ortega et al. 2017) was that the transducing rows get shorter (Fig. I-31 and Fig. I-32). However, the former study was performed using relatively immature hair cells from the apical cochlear region at P4.5, whereas the latter was performed with more mature hair cells from mid-cochlear regions, at P4 - P6. The pattern of expressions of actin-binding proteins is quite different at these two developmental changes (Fig. I-33.A), possibly explaining why the two studies led to different observations.
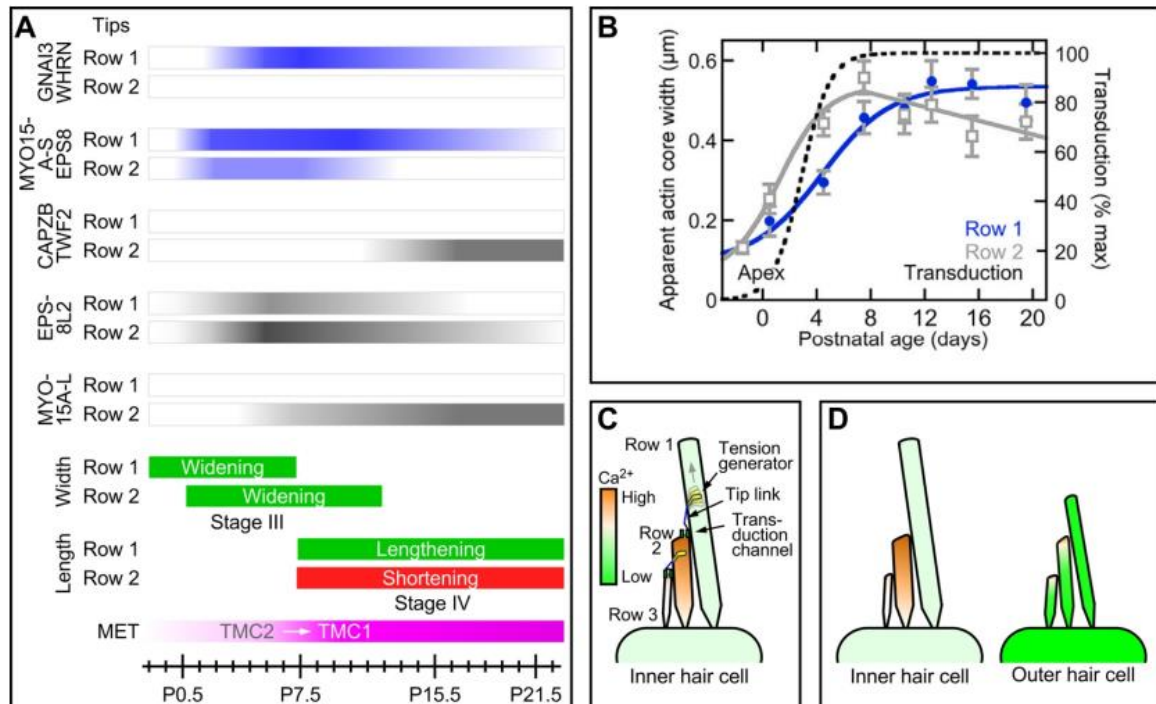
Figure I-33: ROW IDENTITY PROTEINS AND MECHANOTRANSDUCTION. (A) Expression patterns of row identity proteins in relation to the maturation of mechanotransduction. **(B)** Change of the stereociliary width in row 1 and row 2 after birth. The onset of the widening phase starts roughly at about the same time as the mechanotransduction. **(C)** A hypothetical model of an IHC bundle with different resting intracellular Ca^{2+} concentrations in row 1 and row 2 due to differential tensions in the tip links and comparison with an OHC bundle in **(D)**. Figure from (Krey et al. 2020).

Krey et al. (2020) also proposed a model to explain why row dimensions may be differentially controlled by mechanotransduction (Fig. I-33.C-D). In this model, the tensioning motor in the tallest row, which lacks a transduction channel, may see a lower Ca^{2+} concentration than the motor controlling the row 3 channel. Low Ca^{2+} in row 1 stereocilia should increase tip-link tension leading to a higher opening probability for the row 2 channel. The motor controlling the row 2 channel may be weakened by Ca^{2+} that diffuse down the shaft leading to the reduction in the open probability of row 3 channels. Within this framework, the resting Ca^{2+} concentration should be higher in row 2 than in row 1 and row 3. It is suggested that the differential resting Ca^{2+} concentration should be observed in IHCs because they have much less concentration of mobile Ca^{2+} and lower density of Ca^{2+} pumps than in the OHCs (Krey et al. 2020). Altogether, the work of *Krey et al. (2020)* provides insight into how row identity proteins and mechanotransduction may differentially control the stereociliary dimensions of the mammalian hair bundles.
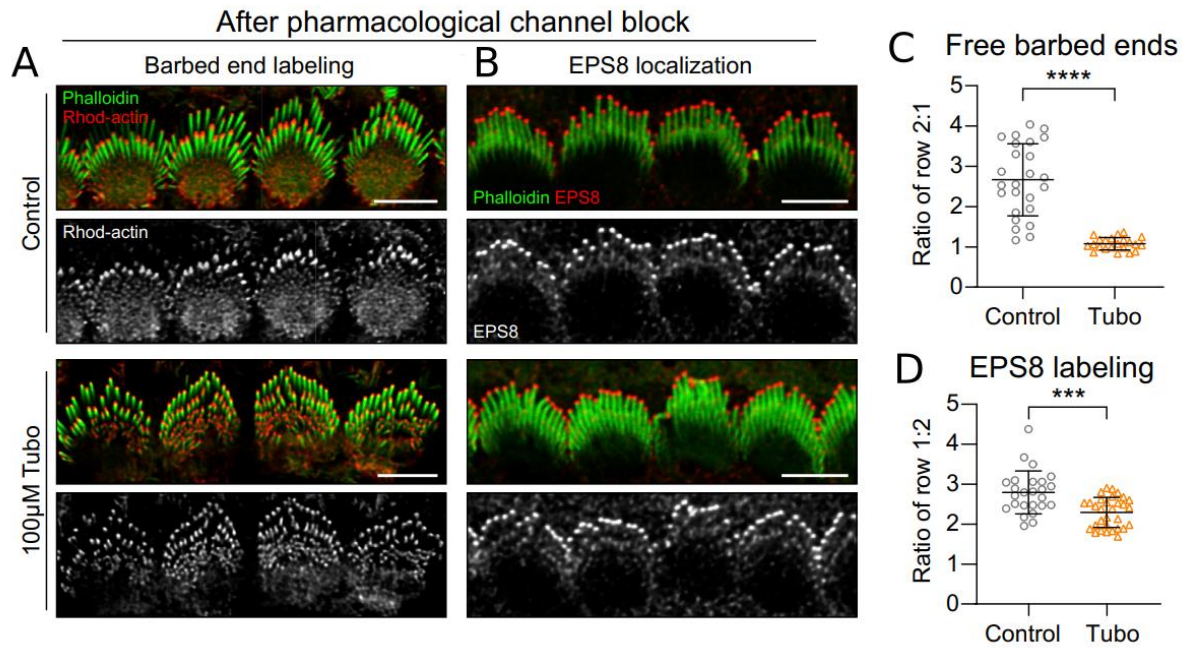
Figure I-34: EFFECTS OF PHARMACOLOGICAL BLOCKING OF THE MECHANO-ELECTRICAL TRANSDUCTION CHANNELS ON AVAILABLE BARBED ENDS. (A) Immunofluorescent labelling of rhodamine-actin indicates actin incorporation at the free barbed ends of actin filament at the stereociliary tip. In the control (upper panel), the rhodamine-actin signal is more restricted to the tip of the row 2 stereocilia (row 1 being the tallest stereocilia row. Upon pharmacological blocking of MET channels (lower panel) with 100 μM tubocurarine, the rhodamine-actin signal was distributed to other rows indicating that there were free barbed ends. **(B)** Eps8, which is the row identity protein of the row 2 stereocilia, was also distributed to other stereocilia row upon blocking the MET channels. Quantification of the free barbed ends as a ratio between row 2 & row 1 **(C)** and EPS8 labelling as a ratio between row 1:2 **(D)**. Scale bar (A-B) 5 μm. Figure from (McGrath et al. 2021).

All this evidence suggests that the mechano-electrical transduction and its transduction machinery are essential for the control of the hair-bundle morphology, both during the maintenance and the development. Calcium influx through the transduction channels is thought to regulate activities of actin-binding proteins that are essential for the morphology of the hair bundles.

In my Ph.D. study, I further explored feedbacks between the mechano-electrical transduction and the morphology of the hair bundles in the vestibular organ of the frogs. In this thesis, I characterized hair-bundle morphology and the ultrastructure of stereocilia after the mechano-electrical transduction of hair cells were perturbed by either exposing the hair cells to pharmacological drugs that block the mechano-electrical transduction or calcium chelators that break tip links. I also tested the implication of actin nucleator formins in the maintenance of hair-bundle morphology.

Chapter 2

II.Materials and Methods

Contents

A. Experimental preparation of the sensory tissues

Ethical Statement – The frogs are sheltered in an approved animal facility (certification C75-05-16) that ensures the animals' health and well-being. The experimental project consists of an ex-vivo analysis of inner ear tissues of wild type frogs and thus does not need a ministerial project authorization. Only certified people having followed the regulation training in animal experimentation performed the sacrifice of the animals.
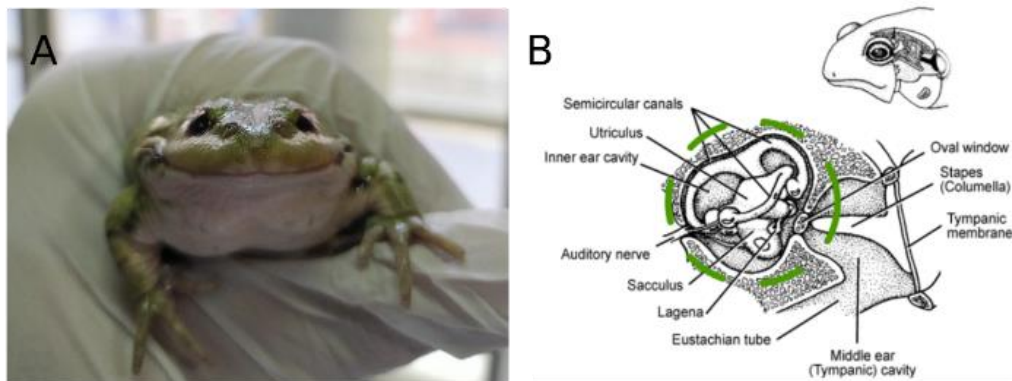
Figure II-1: FROG RIVAN 92 AND THE FROG INNER EAR. (A) The animal model was the frog Rivan 92, a hybrid variety from two frog species; *Pelophylax ridibunda* (formerly known as *Rana ridibunda*) and *Rana esculenta* (or 'green frog', known for its delicacy in the French cuisine) **(B)** The frog inner ear resides in a bone cavity of the skull, the otic capsule (in a circle). In my PhD, I studied the vestibular hair cells from the sacculus, the organ for detecting linear acceleration of the frog's head.

During my PhD, I worked with hair cells from excised preparations of the sacculus of the frog variety Rivan 92 (Fig. II-1). Rivan 92 is a hybrid species that was developed by the Institut National de la Recherche Agronomique (INRA) from two frog species; *Pelophylax ridibunda* (formerly known as *Rana ridibunda)* and *Rana esculenta* (commonly known as the 'green frog' or 'edible frog') (Neveu 2009). Rivan 92 can be fed by fish food pellets instead of living insects.

Frogs have long been a major animal model used by neuroscientists in the field of auditory and vestibular research. Studies of American bullfrogs (*Rana catesbeiana*)' saccular hair cells have provided many general insights into the physiology of mechanosensory hair cells. Due to restrictions on importing alien species like American bullfrogs into France, our lab has been using locally domesticated Rivan 92 as the animal model for several years.

The sacculus or the saccular macula is the vestibular organ that detects linear acceleration of the head in a vertical plane as well as gravity and low-frequency sound (Lewis, Leverenz, and Koyama 1982; X. L. Yu, Lewis, and Feld 1991). Unlike auditory organs, there is no tonotopic

organization of hair cells in the sacculus. The frog sacculus comprises a few thousand hair cells (~ 3000) on its sensory epithelium. Each hair-cell bundle has ~50 stereocilia that arranged, as in any hair bundle, into rows of increasing height, and there is also one true cilium, a kinocilium, that stands behind the tallest row. A kinocilium ends with a kinociliary bulb that attaches to the overlying gelatinous sheath of the otolithic membrane *in vivo* (Fig. I-6).

A.1 Dissection of the frog sacculus
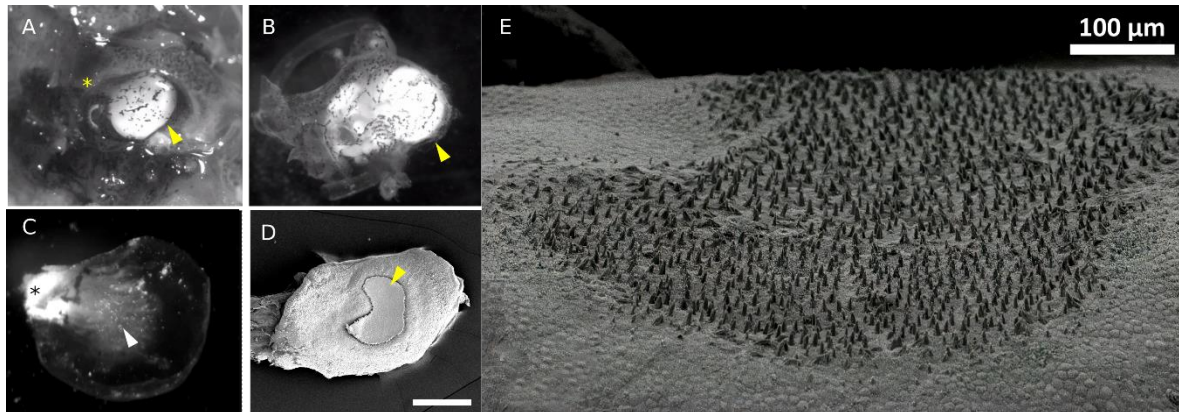
Figure II-2: PREPARATION OF THE FROG SACCULUS. (A) The frog inner ear (arrow) is partially exposed by shaving off the upper surface of the pro-otic bone and **(B)** shown after being removed from the otic capsule, the white mass corresponds to otoconia on top of the saccular macula. The VIIIth cranial nerves can be seen (asterisk *). **(C)** The frog sacculus or saccular macula is oriented with the saccular nerve on the left (asterisk *). The sensory epithelium, where the hair cells reside, is located at the middle of the macula (arrow) under the semi-transparent otolithic membrane. Small crystalline particles of Calcium carbonate ($CaCO_3$), or the otoconia, deposited on the otolithic membrane can be seen as white spots. 60x magnification. **(D)** Scanning electron micrograph (SEM) of a frog saccular macula with the otolithic membrane intact (arrow). Scale bar 400 μm. **(E)** Scanning electron micrograph of the sensory epithelium of the sacculus after the otolithic membrane has been removed. Numerous saccular hair bundles (~ 3,000) can be seen protruding from the surface of the sensory epithelium.

Before performing any physiological experiments or morphological studies of the frog's hair bundle, the frog was sacrificed and the frog's inner ears were removed from the otic capsule, the bony outer wall of the inner ear. All experimental procedures were approved by the Ethics committee on animal experimentation of the Institut Curie; they complied with the European and French National Regulation for the Protection of Vertebrate Animals used for Experimental and other Scientific Purposes (Directive 2010/63; French Decree 2013–118). The frogs were sacrificed by inserting a pitching needle into the brain through the foramen magnum, a small opening at the base of the skull, and then into the spinal cord. The animal was then immediately decapitated and dissected under a stereomicroscope.

After the pro-otic bone was shaved tangentially, the underlying otic capsule with the membranous labyrinth of the inner ear was partially exposed. The sacculus could readily be seen

at this stage by its large white otolithic sac (Fig. II-2.A). The VIIIth cranial nerves are severed and then the inner ear labyrinth is removed from the otic capsule and transferred to artificial frog perilymph (Fig. II-2.B). Table II-1 indicates the chemical compositions of the artificial perilymph used in experiments.

The frog sacculus was surgically removed from the inner ear labyrinth while bathing in the oxygenated artificial frog perilymph. The sacculus was then mounted with magnetic pins in a chamber containing artificial perilymph (sodium-rich, 4 mM [Ca^{2+}]). Then the links between the hair bundles and the otolithic membrane were digested by proteolytic incubation of the sacculus in 67 mg·L^{-1} subtilisin (Protease XXIV, Sigma P8038) for 20-30 min at room temperature. The otolithic membrane was then carefully removed with fine forceps after replacing the protease solution with artificial perilymph.

Contents	Artificial Perilymph (concentrations in mM)
Na^{2+}	110
K^+	2
Ca^{2+}	4
Cl^-	~122
HEPES	5
D-(+)-glucose	3

Table II-1: CONTENTS OF THE ARTIFICIAL FROG PERILYMPH. The pH is adjusted to 7.3~7.5 with NaOH for perilymph. The osmotic strength is ~ 230 mOsmol·kg^{-1}. Solutions were oxygenated before experiments.

A.2 Cell culture

To study the frog sacculus over a long duration (3 - 24 hr), I developed with the help of Fanny Tabarin (the Biochemistry, Molecular Biology and Cells Platform, UMR168, Institut Curie) a frog culture medium based on the mammalian cell culture medium L-15 (Leibovitz) (L5520, Sigma-Aldrich). Unlike Wolf-Quimby medium which has been used with the frog sacculus (Wolf and Quimby 1964; Steyger et al. 2003; Hordichok and Steyger 2007), L-15 does not rely on the usual bicarbonate-CO_2 buffering system to maintain the pH at the physiological level (7.3-7.5). Instead, L-15 contains HEPES, phosphate buffers and a high concentration of free-base amino acids as a

buffering system. This gives us flexibility since the tissue can be manipulated and maintained without requiring a CO_2 incubator.

L-15 provides essential amino acids and vitamins for amphibian cells. The base L-15 medium is diluted to adjust the osmotic strength of the medium to a level adequate for amphibian cells (~ 230 mOsmol·kg^{-1}). Fetal bovine serum (FBS) is also supplemented to help promote the proliferation of the amphibian cells (Freed and Mezger-Freed 1970). The non-ototoxic antibiotics ciprofloxacin is also added to prevent bacterial infections (Steyger et al. 2003). The hair cells incubated in the modified L-15 culture medium at 25 °C remain healthy (i.e. show no morphological defects, exhibit spontaneous oscillations) for at least 24 hr without replacing the culture medium. Table II-2 indicates the chemical compositions of the modified L-15 medium for frog sacculus.

Contents	Concentration
L-15 medium (Leibovitz) without L-glutamin	45.5%
FBS	6.5%
L-glutamin	1.3 mM
HEPES	3.25 mM
Ciprofaxacin	65 μM

Table II-2: CONTENTS OF THE MODIFIED L-15 MEDIUM (LEIBOVITZ) FOR FROGS SACCULUS. The pH is ~ 7.5 and the osmotic strength is ~ 230 mOsmol·kg^{-1}. The final concentration of Ca^{2+} in the modified L-15 is 0.57 mM and can be supplemented to desirable levels. Galactose is used as the carbon source instead of glucose.

B. Pharmacological perturbation of the mechano-electrical transduction machinery

Blocking the transduction channels – One can block the ion channels that mediate the mechano-electrical transduction using pharmacological drugs, such as benzamil or tubocurarine (Rüsch, Kros, and Richardson 1994; Farris et al. 2004). Channel blocking is demonstrated by measuring the transduction current of a hair cells upon the application of the pharmacological drugs. Stimulating a hair bundle under the control conditions elicits an inward transduction current (up to a few hundreds of picoampere) but in the presence of channel blockers, the transduction current is diminished (Fig. II-3.A). The drugs are thought to work as open channel blockers, meaning that they plug the channels' pores. Some of these drugs, e.g. benzamil (Fig. II-3.B), may still work as a permeant blockers because the transduction current does not entirely vanish even at high concentration of the drugs.

During my PhD, I incubated for 1 hr the excised sensory tissue in artificial perilymph supplemented with benzamil, a derivative of amiloride, at a concentration of 30 µM or tubocurarine at a concentration of 100 µM) (Sigma Aldrich). For a longer experiment (incubation time 1 - 48 h), I used instead the culture medium described before. The concentration used was based on the dose-response curves to block more than 90% of the MET current (Rüsch, Kros, and Richardson 1994; Farris et al. 2004) (Fig. II-3.B and C). After the incubation, the tissues were rinsed then fixed for electron microscopy or for physiological studies.
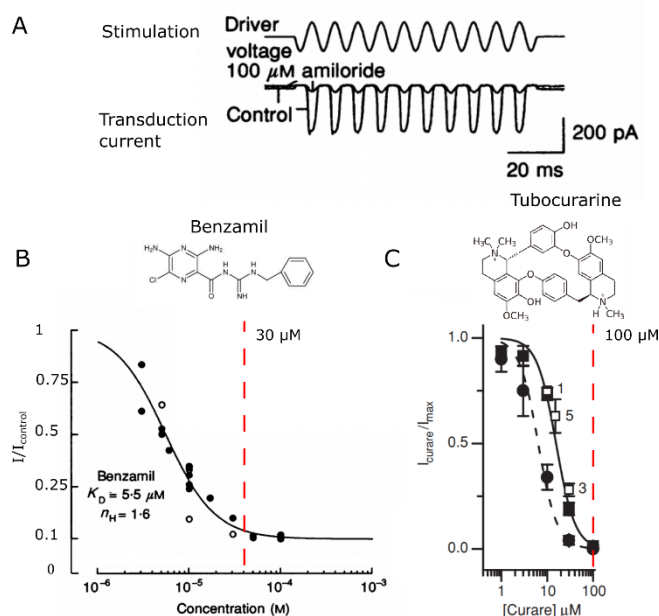
Figure II-3: BLOCKING THE TRANSDUCTION CHANNELS. (A) The transduction current measured while stimulating a hair bundle is diminished upon application of a pharmacological drug, amiloride (Rüsch, Kros, and Richardson 1994). Dose-response curves of transduction channel blocking by benzamil, the derivative of amiloride, in **(B)** and tubocurarine in **(C).** The concentration used in this thesis (30 µM for benzamil and 100 µM

for tubocurarine) indicates in dashed red lines. The half-blocking dose (IC$_{50}$) is 5.5 μM for benzamil and 16 μM (steady-state, continuous line) for tubocurarine. Figure A adapted from (Rüsch, Kros, and Richardson 1994). Figure B is adapted from (Farris et al. 2004).

Disrupting tip links - The excised frog sacculus was incubated for 15 min in artificial perilymph with no Ca^{2+} added, supplemented with 5 mM of Ca^{2+} chelator, 1,2-bis(o-aminophenoxy)ethane-N,N,N',N'- tetraacetic acid, BAPTA (Sigma-Aldrich)[5]. BAPTA has a half-saturation concentration (IC$_{50}$) for Ca^{2+} binding of about 100 nM (or 10^{-7} M) (Tsien 1980). After incubation, the tissues were rinsed with high calcium artificial perilymph then fixed for electron microscopy. Tip links can be disrupted by exposing the hair cells to a Ca^{2+} chelator (Assad, Shepherd, and Corey 1991).

C. Mechanical stimulation of hair bundles

C.1 Experimental setup

Mechanical stimulation experiments were under an upright microscope (Olympus BX51WI) with a 60x immersion objective (N.A. = 0.9) in series with a 1.25x relay lens. A CCD camera (IDS μEye CP) is connected to the microscope to allow for observations of the preparation during the experiments on a computer screen. An experimental chamber is clamped on a stage in which XY translation and rotation in the full 360 ° can be done. An image of a hair bundle or a flexible fibre is normally projected onto a two-quadrant photodiode with a magnification of 1000x to measure displacement in the nanometre range. The microscope and the setup mentioned here are installed on an anti-vibration table.

Signals generated and acquired during an experiment are under the control of an in-house user interface program written for LabView software (version 2011, National Instruments). Command signals sending to piezoelectric actuators of a flexible fibre were produced by a 16-bit interface card (PCI-6733, National Instruments), while acquisitions of signals from the photodiode were done by another 16-bit interface card (PCI-6250, National Instruments). All generated and acquired signals can be conditioned with an 8-pole Bessel anti-aliasing low-pass filter below the Nyquist frequency, a cut-off frequency at half of the sampling rate. The sampling rate for all the signals is set to 2.5 kHz.

---

[5] BAPTA has a dissociation constant (K$_D$) of Ca^{2+} = 10^{-7} M at pH = 7.0, 20 °C and an ionic strength of 0.1 N (Naraghi 1997).

C.2 Stimulation with flexible fibres and stiffness measurement

The hair-cell bundles can be mechanically stimulated by using a flexible glass fibre of a known stiffness. A flexible fibre is fabricated by pulling a 1.2 mm Ø borosilicate glass capillary (TW120F-3, World Precision Instruments) perpendicular to the axis of the shaft by a micro forge. The fibres are 0.5 - 1 μm in diameter and have a length of 100 - 500 μm. Sputter-coating of the fibres with gold-palladium was done to improve their optical contrast. In an experiment, a flexible fibre is attached to a piezoelectric actuator and submerged under a liquid (artificial perilymph or endolymph). An image of the fibre is then projected onto the centre of a two-quadrant photodiode to measure displacements at a nanometre range (Fig. II-4). The stiffness K_f and drag coefficient ζ_f of fibre can then be extracted from a spectral analysis of the fibre's Brownian motions by fitting with a Lorentzian function (Fig. II-5). The stiffness and drag coefficient of fibres used in this study is in the range of 200 - 400 μN$\cdot$m^{-1} and 200 - 250 nN$\cdot$s$\cdot$m^{-1}.
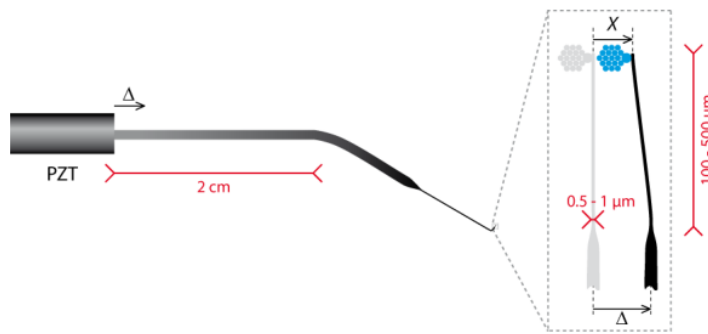
Figure II-4: MANIPULATION OF A FLEXIBLE FIBRE. The fibre's tip is attached to the kinociliary bulb of the hair bundle (right). A movement Δ applied at the fibre's base results in a force applied at the bundle's top, which is then deflected by X. The force at steady state is given by $F = K_f(\Delta - X)$, where K_f is the stiffness of the fibre. Figure adapted from the thesis of JY. Tinevez (2006).
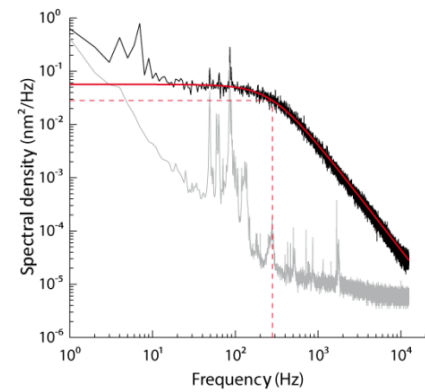
Figure II-5: SPECTRAL DENSITIES OF THE FLEXIBLE FIBER. Spectral density of the tip (black) and the base (grey) of a flexible fibre freely fluctuating in water. The fibre's stiffness is K_f = 176 μN $\cdot$ m^{-1} and the fibre's drag is ζ_f = 57 nN $\cdot$ s $\cdot$ m^{-1}. (Red) The fit of the fibre's spectrum with a Lorentzian function.

To measure hair-bundle stiffness, a calibrated flexible fibre was attached to the kinociliary bulb without imposing any offsets to the position of the hair bundle. Before sending any command signals to the piezoelectric actuator, the fibre was manually moved slightly to ensure that the kinociliary bulb is properly attached before returning it to the initial position. The fibre can be treated with a lectin type IV (Concanavalin-A Sigma-Aldrich) extracted from jack-bean (*Canavalia ensiformis)* to improve its adhesiveness. Then, a series of command steps were sent to move the base of the fibre, and the displacement at the tip of the fibre was measured (Fig. II-6).

When the base of the fibre was displaced by Δ, this movement resulted in a force F that applied to the top of a hair-cell bundle and moved the tip of the fibre by X. At a steady-state, the force F can be calculated from $F = K_f(\Delta - X)$, where K_f is the characteristic stiffness of a fibre. The stiffness of a hair bundle (K_{HB}) is the slope of the force-displacement relation.
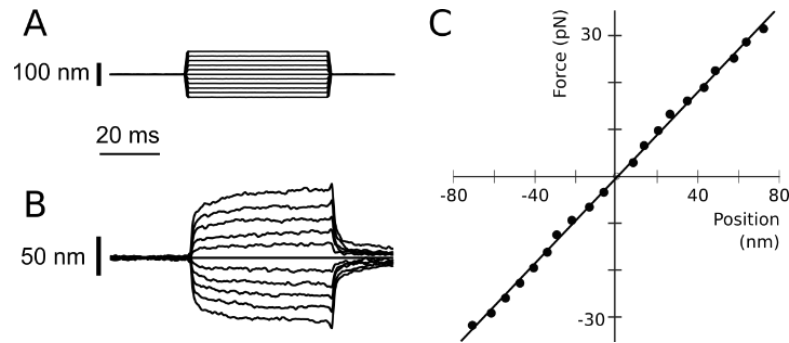
Figure II-6: MECHANICAL STIMULATION OF THE HAIR BUNDLE. (A) Command displacement at the base of the calibrated flexible fibre. **(B)** Hair-bundle position measured the tip of the flexible fibre. **(C)** The force-displacement (F-X) relationship of mechanical stimulation of a hair bundle. The slope is corresponding to the stiffness of a hair bundle. In this example, the stiffness of a hair bundle is 0.48 mN/m.

D.   Scanning electron microscopy

I am grateful to Vincent Michel (Institut Pasteur) for teaching me sample preparation and Scanning Electron Microscopy.

D.1 Sample preparation and imaging

The excised saccular explants were fixed for 1 hr at room temperature or 4 °C overnight by immersion in a solution containing 2.5% glutaraldehyde and a 0.1-M sodium cacodylate buffer at pH = 7.5. Glutaraldehyde crosslinks proteins as it slowly penetrates the tissue, preserving the structure of the sample. The fixed tissues were then contrasted for Scanning Electron Microscopy with osmium tetroxide/thiocarbohydrazide according to the OTOTO procedure (Chissoe, Vezey, and Skvarla 1995). Osmium tetroxide (OsO_4) stains lipids, whereas the osmiophilic thiocarbohydrazide stains carbohydrates. The tissues were dehydrated by successive immersions in ethanol solutions of graded concentrations (35, 50, 70, 80, 90, and 100%) and then in hexamethyldisilazane (HMDS) (Shively and Miller 2009). For detailed protocols on the sample preparation, see the Appendix (p. 116).

Samples were mounted on a stub and sputter-coated with gold-palladium. They were then analysed by field emission scanning electron microscopy operated at 5-7 kV (Jeol JSM6700F) at the Ultrastructural BioImaging Platform (Institut Pasteur) or variable-pressure scanning electron

microscopy (Hitachi SU1510) at the Bioimaging platform of the Hearing Institute. Images were analysed using (Fiji) ImageJ software (NIH, USA).

In the experiments where I characterized the stereociliary insertions into the apical surface of the hair cell, I shaved off the hair bundles by gently rubbing an eyelash against the surface of the sensory epithelium or blowing short bursts of pressurised air from an air duster spray. The technique was first described by Tilney and Saunders (Tilney and Saunders 1983).

D.2 Estimating stereociliary height in scanning electron microscopy

Scanning electron micrographs are projected images in the plane of the electron beam. To estimate the stereociliary height, scanning electron micrographs are taken at two different angles (α and $\alpha + \tau$) by tilting the microscopic stage by τ degree, where α is the angle between the surface and the stereocilium. The projected stereociliary heights at each angle (p_1 and p_2) are measured and the estimated stereociliary height h is determined by solving the system of equations (Fig. II-7).

$$h = \frac{p_1}{\sin(\alpha)} \tag{II-1}$$

$$h = \frac{p_2}{\sin(\alpha + \tau)} \tag{II-2}$$

$$\alpha = \cot^{-1}\left[\frac{(p_2/p_1)}{\sin \tau} - \cot \tau\right] \tag{II-3}$$
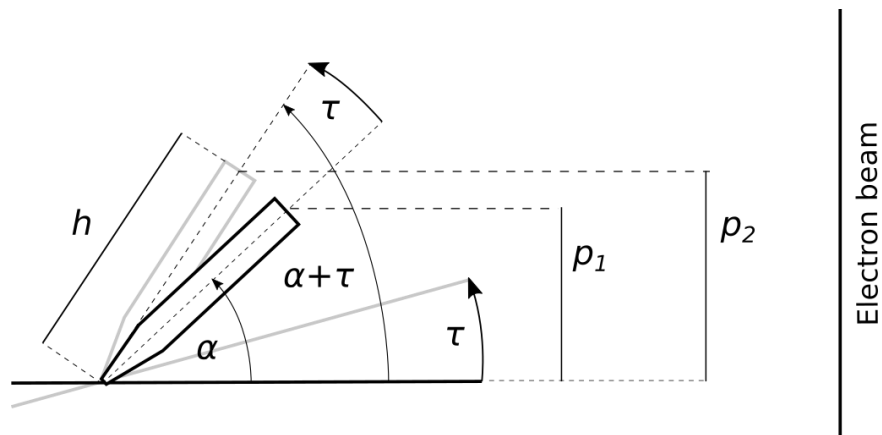
Figure II-7: SCHEMATIC REPRESENTATION OF THE ESTIMATION OF STEREOCILIARY HEIGHT H IN SCANNING ELECTRON MICROSCOPY BY THE METHOD OF TRIANGULATION. The scanning electron micrographs are taken at two different angles (α and $\alpha+\tau$) by tilting the microscope stage by τ degree, where α is the angle between the surface and the stereocilium. The projected stereociliary heights at each angle (p_1 and p_2) are measured and the estimated stereociliary height h is determined by solving the system of equations (II-3).

E.   Transmission electron microscopy

I am grateful to Ilse Hurbain (Institut Curie) for teaching me sample preparation for transmission electron microscopy. I am also grateful to Ilse, Daniel Levy, and Aurelie Di cicco for teaching me transmission electron microscopy.

E.1 Sample preparation and imaging

For fixation, the excised tissues were immersed for 1 hr at room temperature or overnight at 4 °C in a solution containing 2.5% glutaraldehyde, 0.5% paraformaldehyde, and a buffer of 0.1 M sodium cacodylate at pH ~ 7.5. This solution was supplemented with 0.5 mM $CaCl_2$ and 100 µM tannic acid. Tannic acid stained the peripheral region of actin filaments, whereas their central region appears relatively unstained; the actin filaments thus appeared as if they were negatively stained (LaFountain et al. 1977). I found that adding tannic acid greatly improved the contrast of the actin filaments, which was critical to quantify the inter-filament spacing (Fig. II-8).
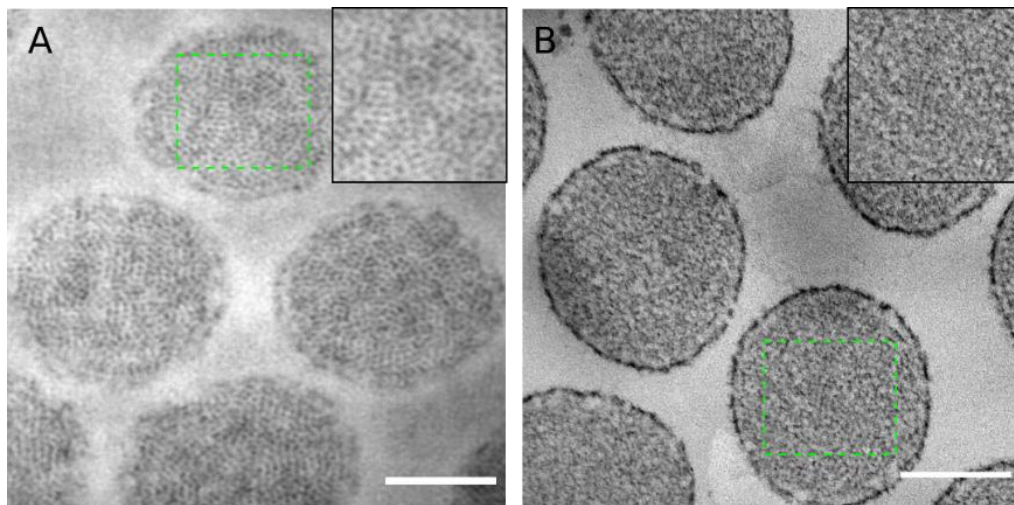
Figure II-8: IMPROVING THE CONTRAST OF ACTIN FILAMENTS. Transmission electron micrographs of the transverse sections of stereocilia with **(A)** tannic acid and **(B)** without tannic acid added during the fixation. Inset figures are magnified from the corresponding area in dashed squares. Scale bar 200 nm.

The fixed samples were stained with 1% osmium tetroxide (OsO_4) for 1 hr and then with 0.5% uranyl acetate for 3 hr at room temperature. Both staining solutions were prepared in a 0.1-M sodium cacodylate buffer. The tissues were dehydrated by successive immersions in ethanol solutions of graded concentrations (35, 50, 70, 80, 90, and 100%) and then in 100% acetone. They were then embedded in Epoxy resin, which hardened in the oven at 60 °C for 48 hr. Ultrathin sections (~ 90 nm) were cut on a Reichert Ultracut S microtome (Leica, Milton Keynts, UK) or a

Leica Ultracut UCT Ultra-microtome (Leica, Milton Keynts, UK), mounted on a pioloform-treated 0.1-mm hole copper-nickel grid (G2010-Cu, Ni, EMS, USA), counterstained by immersion in 1% aqueous uranyl acetate for 7 min and then in Reynold's Lead citrate for 1 min. For detailed protocols on the sample preparation, see the Appendix (section Transmission electron microscopy).

All transmission electron micrographs were taken at 20 kV (Tecnai Spirit) at the Cell and Tissue Imaging Platform (PICT-IBiSA), Institut Curie. Images were analysed using (Fiji) ImageJ software (NIH, USA).

E.2 Measuring actin inter-filament spacing in stereocilia

The actin inter-filament spacing can be measured from transmission electron micrographs of the transverse sections of stereocilia (Fig. II-9.A-B) in the Fourier space by using the fast-Fourier transform (FFT) tool in the image processing software (Fiji) ImageJ. The 2D-FFT produces a ring-link pattern that indicates that actin filaments in the stereociliary core adopt a liquid packing where neighbouring actin filaments are located in random orientations. The average radius of the ring-like patterns nevertheless indicates the average actin inter-filament spacing (Fig. II-9.C-D).
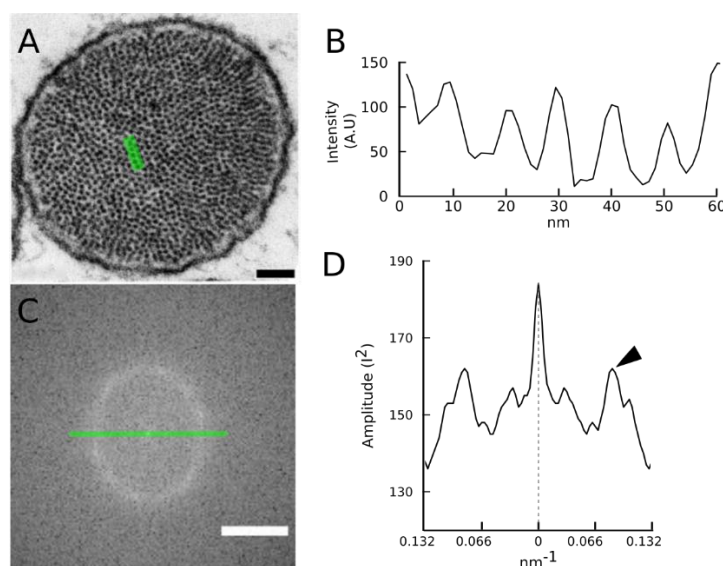
Figure II-9: MEASURING ACTIN INTER-FILAMENT SPACING IN STEREOCILIA. (A) Transverse section of a stereocilium from transmission electron microscopy. Scale bar 60 nm. **(B)** The intensity profile along the yellow line in (A) shows valleys of intensity where actin filaments are. The distance between the valleys is ~ 10 nm. **(C)** The 2D fast-Fourier transform of (A) shows a ring-like pattern where the ring's radius is the average actin inter-filament spacing. Scale bar 0.1 nm^{-1}. **(D)** The intensity profile along the yellow line in (C) shows peaks corresponding to the inter-filament spacing of ~ 10 nm. Figures A and C from (Mogensen, Rzadzinska, and Steel 2007).

F.   Immunolabelling and immunofluorescence microscopy

F.1 Antibodies

To immunolabel formins in the frog saccular hair bundles, I used DIAPH1 (DIA1) polyclonal antibody (PA5-27607, Fisher Scientific) raised in rabbits against a region within amino acids 981 and 1272 (aa. 981 – 1272) of human DIAPH1 at 2 µg/ml (1:500 dilution). The specificity of the antibody was tested by observing its labelling pattern in HeLa cells: the signal colocalized with the mitotic spindle, in agreement with specific labelling because DIAPH1 is known to reside there (Kato et al. 2001). However, there was no negative control with knockout samples. Goat anti-Rabbit IgG, Alexa Fluor 594 (A-11012, Fisher Scientific) at 10 µg/ml (1:200 dilution) and 4 µg/ml (1:500 dilution) was used as the secondary antibody for rabbit anti-Human DIAPH1 polyclonal antibody. Actin filaments were stained with Alexa Fluor 488-conjugated phalloidin.

F.2 Sample preparation and imaging

The excised saccular explants were fixed with 3.7% glutaraldehyde in PBS for 1 hr at room temperature or 4 °C overnight. The tissues were then washed with PBS and incubated with a blocking solution made of 0.1% Triton X-100 and 1% bovine serum albumin (BSA) in PBS. Then, the tissues were stained with the primary antibody for 1 hr at room temperature or 4 °C overnight and then incubated with the secondary antibody and Alexa Fluor 488-conjugated phalloidin. The samples were mounted on a glass slide with the mounting media Fluoroshield (F6057-20ML, Sigma-Aldrich).

All confocal images were taken on an upright spinning disk confocal microscope (Roper/Zeiss) at the Cell and Tissue Imaging Platform (PICT-IBiSA), Institut Curie. Confocal z-stacks were obtained using a 100x oil immersion objective (NA = 1.46, Carl Zeiss). Images were acquired with CoolSnap HQ2 CCD camera at 440 nm (for Alexa Fluor 488-conjugated phalloidin) and 561 nm (for Alexa Fluor 568 and 594-conjugated secondary antibodies) using MetaMorph (Molecular Devices, US) and analysed using (Fiji) ImageJ software.

G. Inhibition of formins

To inhibit the activity of formins, I used a formin inhibitor SMIFH2 or 1-(3-Bromophenyl)-5-(2-furanylmethylene)dihydro-2-thioxo-4,6(1H,5H)-pyrimidinedione   (S4826-5MG,   Sigma-Aldrich). This compound was found to inhibit the actin nucleation through the formin homology

domain 2 (FH2) of formins (Rizvi et al. 2009). Since the FH2 is conserved in most formins, the compound SMIFH2 provide an inhibition with broad-specificity to formins. The effect of SMIFH2 on actin nucleation is also concentration-dependent. The half-maximal inhibition (IC_{50}) of the formin mDia1 in the actin filament assembly assay is~ 15 µM (Rizvi et al. 2009), whereas the IC_{50} of the actin-activated ATPase of human nonmuscle myosin 2A required a higher concentration of ~50 µM (Nishimura et al. 2021). In my experiments, I used 250 µM SMIFH2 in DMSO.

Chapter 3

III. Results

Contents

A. Morphological characterization of saccular hair bundles of the frog Rivan 92

In the literature, morphological descriptions of frog's saccular hair bundles were done mostly using hair cells from the American bullfrog, *Rana Catesbeiana* (Jacobs and Hudspeth 1990; Bechara Kachar, Parakkal, and Fex 1990). In this study, I used instead saccular hair bundles from the frog Rivan 92, a hybrid species derived from *Rana ridibunda* and *Rana esculenta* (see Materials and Methods). Here, I will describe the architecture of the hair bundle and the ultrastructure of the stereociliary actin core in this species. Unless otherwise noted, the results below are quoted as mean ± standard deviation (SD) over an ensemble of *N* samples.

A.1 Hair-bundle and stereocilia dimensions

a. Dimorphism of saccular hair cells based on the size of their apical surface

The saccular macula of the frog's ear is endowed with a few thousand hair cells that are distributed more or less homogeneously across the sensory epithelium. The hair bundles vary in size and shape (Fig. III-1.A), and like the hair bundle themselves, the size of the hair-bundle imprints and the cells' apical surface also varies (Fig. III-1.B). In the central region of the macula[6], a typical hair bundle is composed of 33 ± 9 stereocilia ($N = 70$ cells) arranged into 5-9 stereociliary rows of increasing height, and a single kinocilium. The distal end of the kinocilium shows a bulbous structure—the kinociliary bulb, which is connected to the overlying otolithic membrane *in vivo* (Fig. III-1.A). Remarkably, as also reported in the bullfrog (Jacobs and Hudspeth 1990), the apical surface of a hair cell is typically convex along the axis of mechanosensitivity (Fig. III-1.B). The stereocilia may thus be pushed together by the curved cuticular plate into which they insert, resulting in elastic loading. This feature has been proposed to help the hair bundle move as a unit, promoting concerted gating of the transduction channels (Kozlov, Risler, and Hudspeth 2007).

The diameter D_{apical} of the cells' apical surface clearly showed a bimodal distribution that could be fitted by the sum of two Gaussian distributions (Fig. III-2.A-B and D). The hair cells could thus be parsed in two populations—"small" and "large", corresponding to apical-surface diameters of 3.22 ± 0.43 µm ($N = 29$) and 6.03 ± 0.49 µm ($N = 30$), respectively. A hair cell with an apical-surface diameter that fell within three standard deviations of the mean of a given

---

[6] At the peripheral region of the saccular macula, hair cells show small and short bundles and very long kinocilia. These cells are easy to distinguish from hair cells in the central region; they were excluded from my study.

population ("small" or "large") was attributed to this population. The cells whose apical-surface diameter fell in the overlapping region of the bimodal distribution were discarded from further analysis (Fig. III-2.A-B, and D). In the following, we thus considered two types of hair bundles—small and large—based on the diameter of the apical surface of the corresponding hair cells. All morphological features were analysed for each bundle type.
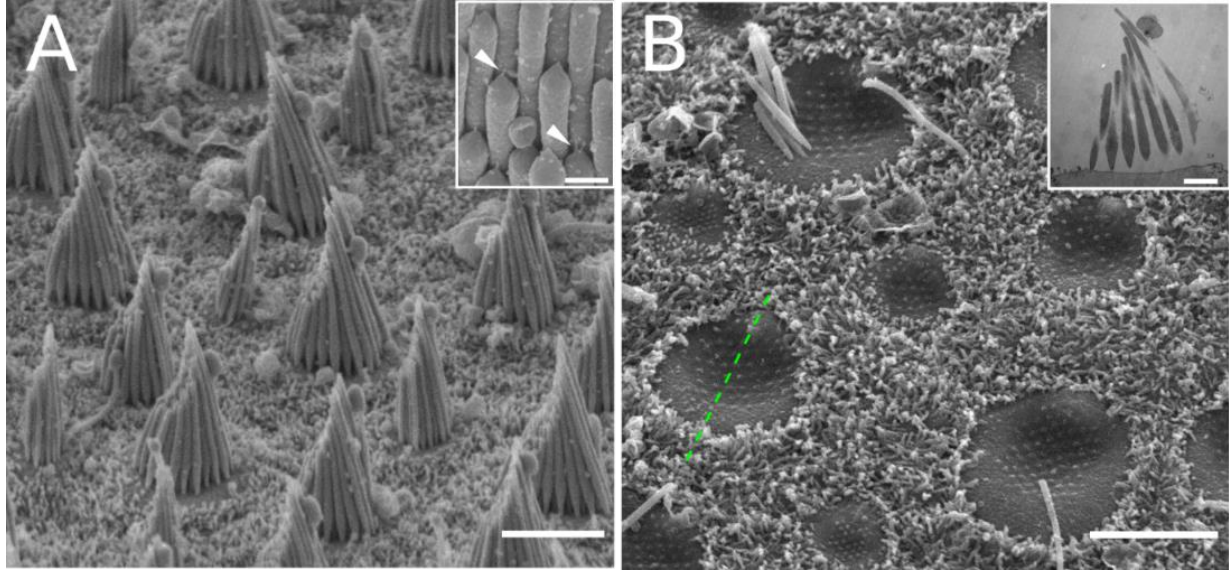
Figure III-1: FROG SACCULAR HAIR BUNDLES AND HAIR-BUNDLE IMPRINTS. Sensory epithelium of the saccular macula **(A)** before and **(B)** after the hair bundles have been removed. **(A)** A view from the side of the hair bundles shows stereocilia that form rows of increasing height. The stereocilia in the middle rows tend to be wider at the taper region than those of the shorter and the taller rows. The shorter stereocilia are connected to their taller neighbour by the thin oblique tip links (inset, see arrowheads) that gate the transduction channels. Scale bar (inset) 400 nm. The stereociliary tips showed tenting, possibly due to tension in the tip links. **(B)** The apical surface of each hair cell is left with the imprint of the corresponding hair bundle. The hair cells are surrounded by supporting cells decorated by numerous and short microvilli. The apical surface of the hair cells is convex along the axis of mirror symmetry of the hair bundle (i.e. the axis of mechanosensitivity; see dashed line). This curvature may help push the stereocilia together and facilitate the cohesiveness of the bundle. The inset image shows a transmission electron micrograph of a hair bundle and its convex apical surface. Scale bar (inset) 2 µm. Scale bar (A-B) 5 µm.

Using this classification (Fig. III-2.D), the imprint diameter $D_{imprint}$ of the hair bundle was 1.60 ± 0.24 µm (N = 29 cells) and 3.13 ± 0.43 µm (N = 30 cells) for small and large hair cells, respectively (Fig. III-2.E). Hair cells with a large apical surface were thus endowed with a bigger hair-bundle imprint than those with a small apical surface. Hair-bundles of the small hair cells had nearly isotropic imprints ($D_{imprint\ X}/D_{imprint\ Y} \simeq 1$), whereas those of the large hair cells were more extended along the axis of mechanosensitivity than perpendicular to it ($D_{imprint\ X}$: $D_{imprint\ Y} = 1.2$; Fig. III-2). Actually, the hair-bundle imprint occupied about 50 % of the apical-surface area for two types of cells. The width of the hair bundle was measured at the top of the stereociliary taper, where it is maximal (Fig. III-2.C). Although the hair-bundle width showed a broad distribution, classifying the hair cells according to the size of their apical surface, as described earlier, revealed

an underlying correlation between the size of the apical surface and the width of the bundle. The hair-bundle width was 2.00 ± 0.47 µm ($N = 35$ cells) and of 3.62 ± 0.44 µm ($N = 38$ cells) for small and large cells, respectively (Fig. III-2.C and F).
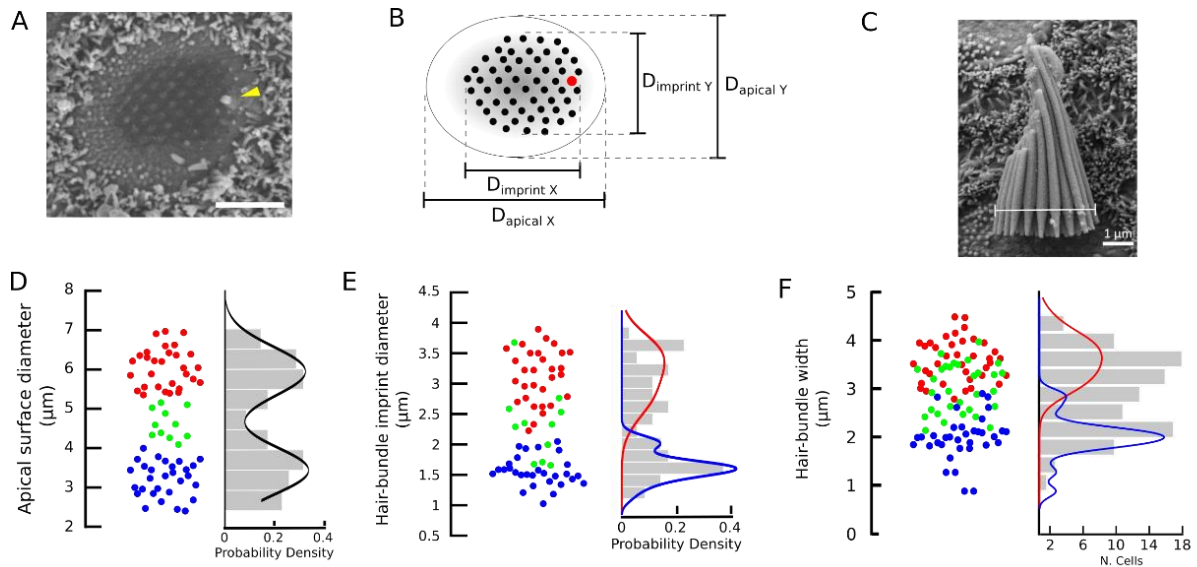
Figure III-2: DIMENSIONS OF THE HAIR-CELL APICAL SURFACE AND THE HAIR BUNDLE. (A) The hair-bundle imprint is oriented so that the kinocilium is on the right (see arrow). Scale bar: 2.5 µm. **(B)** Schematic representation of the hair cell's apical surface. Both the apical surface diameter D_{apical} and the hair-bundle imprint diameter $D_{imprint}$ were averaged from what was measured along two perpendicular axes, as indicated in the diagram. **(C)** A scanning electron micrograph of a hair bundle that was completely detached from the hair cell but that remained cohesive and lied flat on the cell's apical surface. The hair-bundle width was measured at the top of the taper region of the stereocilia, where it is maximal (white horizontal interval). **(D)** The beeswarm plot and the histogram of the apical-surface diameter show a bimodal distribution, corresponding to two populations of hair cells, "small" and "large". The distribution was well described by the sum of two Gaussian distributions The hair cells were attributed to a given population if their apical-surface diameter was within three standard deviations of one of the two peak diameters (large hair cells ●, small hair cells ●). Hair cells (●) that fell within the overlapping region of the two distributions were classified discarded from the analysis. The beeswarm plot and histograms of **(E)** the hair-bundle imprint diameter and **(F)** hair-bundle width are colour coded according to this classification. The colored lines in **E** and **F** are trend lines (polynomial fits) to the histograms for the two subpopulations of large and small hair bundles, in red and blue, respectively.

Within a given hair bundle, individual stereocilia are usually described as cylindrical rods with a diameter of a few hundred nanometres that taper towards their insertions into the apical surface (Jacobs and Hudspeth 1990; but see also Garcia et al. 1998). Stereocilia within the tallest stereociliary row generally adopted a cylindrical shape (Fig. III-3.D). However, here, the stereocilia of other rows in large hair bundles clearly adopted a biconical shape: they widen from the tip towards the base, reaching a maximal width before tapering toward their insertion into the cuticular plate. The effect is particularly pronounced in the stereocilia from the middle rows (Fig. III-3.D). For the population of large hair bundles, I found that the stereociliary width 440 ± 41 nm ($N = 16$ cells) in the middle row was larger than that 386 ± 41 nm ($N = 17$ cells) in the shortest

row and that 285 ± 21 nm ($N = 12$ cells) in the tallest rows. In addition, the stereociliary height grew from 3.08 ± 0.38 µm ($N = 17$ cells) in the shortest row to 7.13 ± 0.49 µm ($N = 17$ cells) in the tallest row (Fig. III-3). I also analysed the height of the taper and the volume of a stereocilium, but only in the stereocilia of the shortest row because tapers were most visible in this row. There, the taper height was 933 ± 141 nm ($N = 16$ cells) and the stereociliary volume was 0.25 µm^3 (Fig. III-3.C). Note that the small hair bundles were excluded from this analysis because their stereociliary widths are small and thus difficult to characterize.
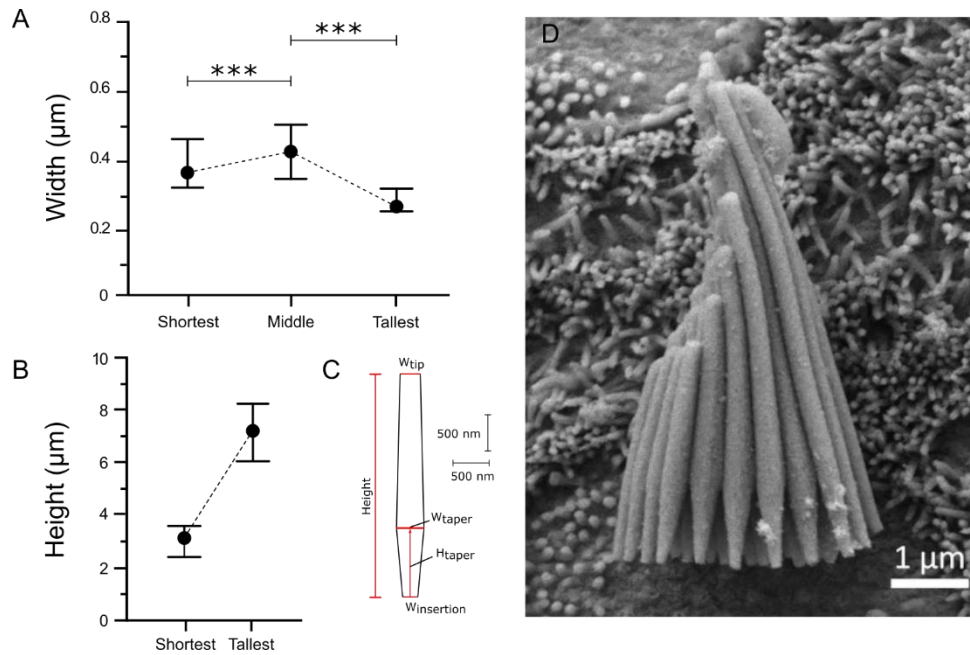
Figure III-3: STEREOCILIARY DIMENSIONS. (A) The maximal stereociliary width measured at the top of the taper region of the shortest, middle, and tallest rows. **(B)** The stereociliary height of the shortest and the tallest rows. The measurement was done in large hair bundles, only. Statistical significance was tested with Student's t-test, * for p-value ≤ 0.1, ** for p-value ≤ 0.01, and *** for p-value ≤ 0.001, whereas N.S. (non-significance) is for p-value > 0.05. **(C)** The average shape of the shortest stereocilia. A single stereocilium can be described as a truncated bicone[7]. To estimate the volume of a stereocilium, I measured additional geometric parameters in scanning electron micrographs of the hair bundle: the stereociliary width at the tip (W_{tip}) and the insertion ($W_{insertion}$), and also the height of the taper region (H_{taper}). In the plots shown in (A-C), the circles represent the medians and the error bars represent the 1st and the 3rd quartiles. **(D)** A scanning electron micrograph of a frog saccular hair bundle that was completely detached from the hair cell but remained cohesive and lied flat on the cell's apical surface. The hair bundle shows a typical non-monotonic variation of the stereociliary width where the middle row is the largest.

---

[7] A truncated bicone is created by joining two truncated cones base-to-base. The volume of a truncated cone is $V = \frac{1}{3}\pi(r_1^2 + r_1 r_2 + r_2^2)h$, where r_1 is the radius at the base and r_2 is the radius at the truncated top, and h is the height of the cone. If $r_1 = r_2$, the geometry becomes a cylinder instead of a cone.

b. Packing of the stereocilia

Packing symmetry. Hair-bundle imprints also provide information about the organization of the stereocilia within a hair bundle, which is generally described in the literature by a hexagonal lattice (Jacobs and Hudspeth 1990; Jacobo and Hudspeth 2014) (Fig. III-4.A-D). Hexagonal packing is indeed observed in the upper part of the hair bundle, where the stereocilia are in contact with one another[8] (Fig. III-4.G-H). However, at the site of stereociliary insertions into the cuticular plate, the stereociliary packing is less tight and the stereocilia may be allowed to adopt different arrangements.
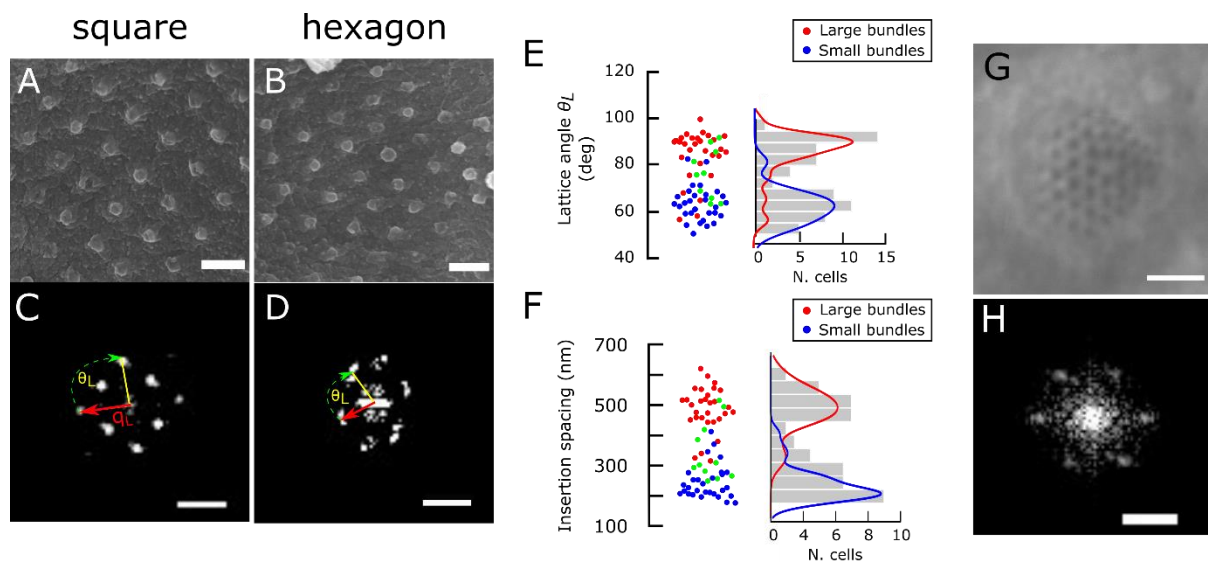
Figure III-4: STEREOCILIARY INSERTION PACKING. Hair-bundle imprints reveal stereociliary insertion packing that can be classified into 2 types: **(A)** square and **(B)** hexagonal, based on the corresponding 2D-FFT images (**C** and **D**). The lattice angle θ_L and the stereociliary spacing $S_{insertion} = 2\pi/q_L$ where the wavevector q_L is defined as indicated in panel C. Scale bar: (A-C) 500 nm, (D-F) 3.3 μm^{-1}. **(E)** Beeswarm plot (left) and histogram of lattice angle θ_L (right, grey). **(H)** Beeswarm plot (left) and histogram of the stereociliary insertion spacing $S_{insertion}$ (right, grey). In both (E) and (H), the data is colour coded according to the classification of hair cells into two populations (large hair bundles in red and small hair bundles in blue), with the corresponding distributions superimposed on the histogram for the whole ensemble of hair cells. **(G)** A light micrograph from the top of a hair bundle with a focal plane positioned at about half the bundle's height. **(H)** 2D-FFT image of the micrograph shown in G, indicating hexagonal packing. Scale bar: 2 μm in (G) and 1.77 μm^{-1} in (H).

The diffraction pattern observed in 2D-FFT images (Fig. III-4.C and D) from scanning electron micrographs (Fig. III-4.A and B) of the hair-bundle imprints revealed two main arrangements of the stereociliary insertions. Indeed, the lattice angles Θ_L measured between two principal axes of the diffraction pattern showed a bimodal distribution (Fig. III-4.E), with $\Theta_L = 89.6 \pm 3.7$ deg ($N = 25$ cells) or 62.3 ± 5.3 deg ($N = 35$ cells). Although there were some variations in the lattice

---

[8] Because hexagonal packing has the highest possible packing density (about 90%), tight packing of cylindrical rods results in a hexagonal arrangement (Appendix, **Figure V-1**) .

angle, these values were close to those of a square ($\Theta_L = 90$ deg) and a hexagonal lattice ($\Theta_L = 60$ deg), respectively. Only a few cells (2 out of 70 cells) showed neither a square nor a hexagonal arrangement, but rather a liquid packing. Interestingly, I found that the majority of large hair bundles (69 %, $N = 29$ cells) adopted a square packing of their stereocilia, whereas the overwhelming majority of the small hair bundles (83 %, $N = 29$ cells) showed hexagonal packing (Table III.1).

These results are summarized in Table III.1.

Hair-cell population	Small hair bundles (N = 29 cells)			Large hair bundles (N = 29 cells)		
Lattice Packing	Hexagon	Square	Intermediate	Hexagon	Square	Intermediate
Number of cells	24	2	3	4	20	5
% of cells	83 %	7 %	10 %	14 %	69 %	17%
Table III.1: CORRELATION BETWEEN HAIR-BUNDLE SIZE AND STEREOCILIARY PACKING.						

Spacing of stereociliary insertions. The diffraction pattern in the 2D-FFT image from the scanning electron micrograph of a hair-bundle imprint does not only provide the type of stereociliary packing but also information regarding the average spacing between stereociliary insertions within the lattice (Fig. III-4.F) along and perpendicular to the axis of mechanosensitivity. The stereociliary insertion spacing $S_{insertion}$ showed a clear bimodal distribution that was strongly correlated with the two hair-bundle types (Fig. III-4.F), with $S_{insertion}$ = 246 ± 58 nm ($N = 29$ cells) and 489 ± 75 nm (mean ± SD, $N = 23$ cells) for small and large hair bundles, respectively. The saccular hair bundles of the frog Rivan 92 appear to be more compact than those of the American bullfrog, for which the stereociliary insertion spacing measured from fixed tissues was shown to 940 ± 75 nm ($N = 14$ cells)(Jacobs and Hudspeth 1990), thus about twice the value reported here for large hair bundles.

c. Stereociliary insertion diameter

Stereociliary insertions (Fig. III-5.A-D) are the sites where the stereociliary rootlets insert into the cuticular plate, underneath the apical surface of a hair cell. The diameter of the stereociliary rootlets is expected to control the pivotal stiffness of individual stereocilia and in turn the passive stiffness of the hair bundle (Eq. (I-1). In a few stereocilia, I observed that the imprints of individual stereociliary insertions were hollow in the centre (Fig. III-5.D). In these stereocilia, the

stereociliary rootlet may have come off during the mechanical removal of the hair bundle from the sensory epithelium.
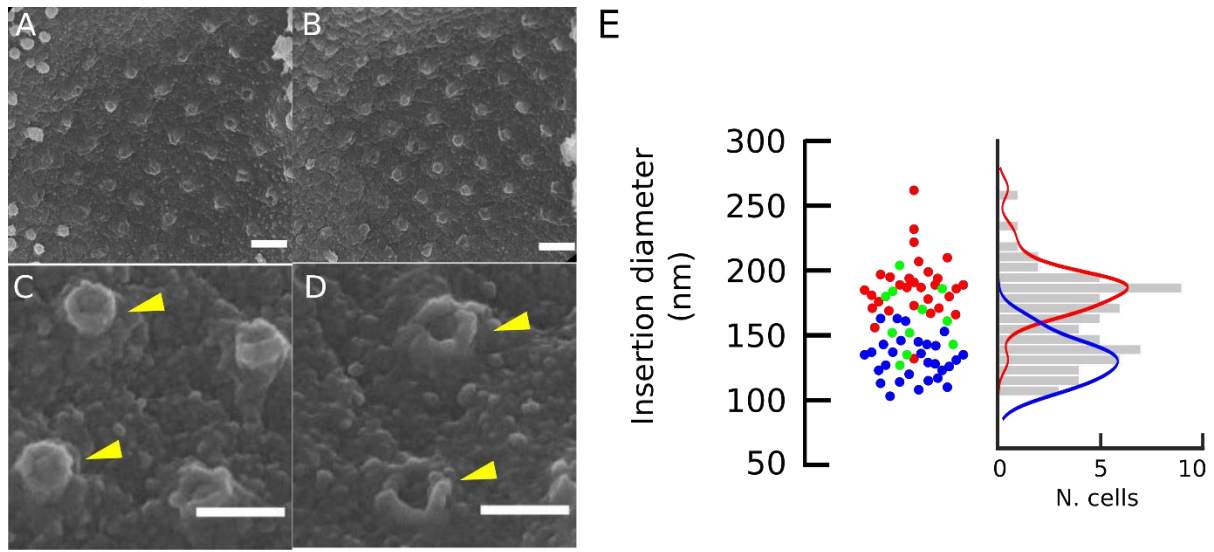
Figure III-5: STEREOCILIARY INSERTION DIAMETER. (**A** and **B**) Scanning electron micrographs of stereociliary imprints. Scale bar 500 nm. (**C** and **D**) Individual stereociliary insertions (see arrows). Scale bar 250 nm. (**E**) Distribution of the stereociliary insertion diameter for large (●), small (●), and (●) intermediate hair bundles. The histogram for the whole ensemble of hair bundles (no classification) is shown in grey. Taking the imprint-diameter histograms of two subpopulations (large vs small bundles) and fitting these histograms with a polynomial function results in the trend lines shown in red (for large bundles) and blue (for small bundles). Because the imprints of individual stereocilia were not perfectly circular, the stereociliary insertion diameters $D_{insertion} = 2\sqrt{(area/\pi)}$ reported here are effective diameters calculated from the area of individual stereociliary insertion imprints. I used the Particle Analyser plugin in the image processing software Fiji (ImageJ) to subtract the background and measure the area of individual stereociliary imprints from scanning electron micrographs.

The stereociliary insertion diameter $D_{insertion}$ for the two hair-bundle types was $D_{insertion} = 132 \pm 16$ nm ($N = 29$ cells) and 188 ± 24 nm (mean $\pm$ SD, $N = 30$ cells) for small and large hair bundles, respectively (Fig. III-5.E). In addition, the stereociliary insertion diameter was strongly correlated to both the hair-bundle imprint diameter (Pearson's $r = 0.7$, p-value < 0.001) and to the stereociliary insertion spacing (Pearson's r = 0.7, p-value < 0.001) (Fig. III-6.A-B). Because stereocilia are tightly packed at the upper part of a hair bundle, it makes sense that wider stereocilia result in a larger stereociliary insertion spacing and thus in a larger hair-bundle diameter. Of note, after parsing the data to account for the two populations ("small" and "large") of hair bundles (Fig. III-6.C-D), the correlations appeared to be weaker for the large hair bundles. As a result, one would expect that varying the size of stereociliary insertions may affect hair-bundle dimensions more dramatically for small and tight hair bundles than for large and loose hair bundles.
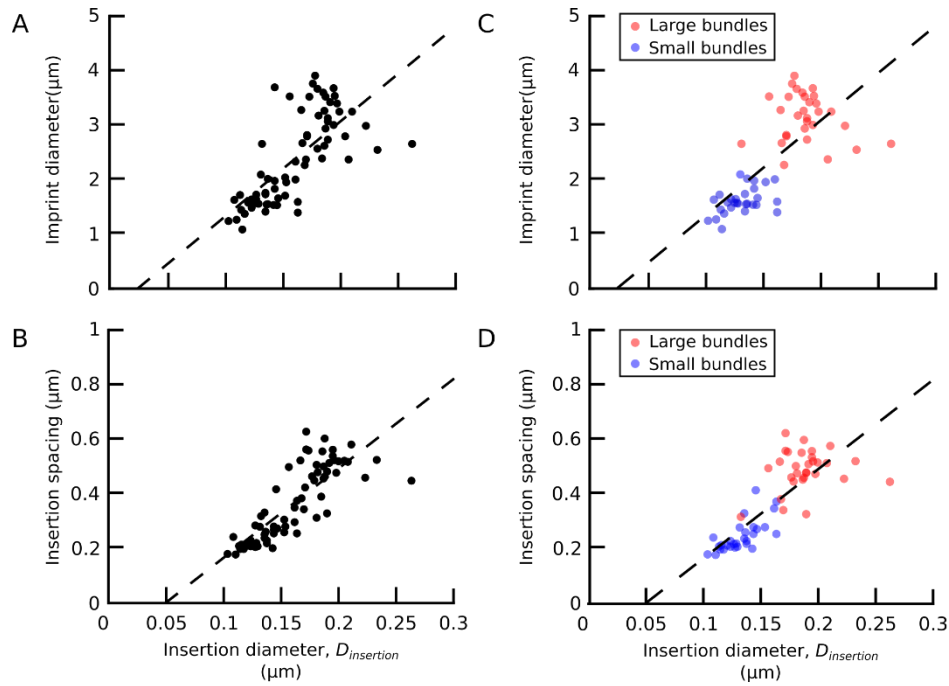
Figure III-6: DIMENSIONS OF HAIR-BUNDLE IMPRINTS AS A FUNCTION OF THE STEREOCILIARY INSERTION DIAMETER. Both the hair-bundle imprint diameter **(A)** and the stereociliary insertion spacing **(B)** showed strong positive correlations with the stereociliary insertion diameter $D_{insertion}$. Pearson's linear correlation coefficients r was 0.7 and 0.8, respectively, with a corresponding p-value < 0.001. The dashed lines corresponding to (A) $17 \cdot D_{insertion} - 0.42$ and (B) $3.3 \cdot D_{insertion} - 0.16$, where $N = 70$ cells. **(C-D)** Same data as in (A-B) after classification of the hair cells.

A.2 Actin core of the stereocilia

In transmission electron micrographs of ultrathin (~ 90 nm) transverse sections of hair bundles, the actin filaments appeared as dark spots in the section plane (Fig. III-7.A and B). When the actin filaments were not orientated perpendicular to the section plane, which happened most of the time, the filaments appeared instead as stripes; theses data were discarded. FFT analysis of the transmission electron micrographs showed ring-like patterns (Fig. III-7.D), indicating that the actin filaments adopted liquid packing, for which neighbouring actin filaments are randomly oriented. It is worth noting that the actin-filament packing in the stereocilia was not always uniformly liquid. FFT analysis of small regions within a stereocilium sometimes revealed hexagonal packing (Fig. III-7.C-E). The average radius of the ring-like patterns provided an average actin inter-filament spacing of 12.0 ± 0.5 nm ($N = 43$ stereocilia from 15 cells) (Fig. III-7.F). The actin inter-filament spacing reported here is 2-3 nm larger than those measured from mouse utricular (9.7 ± 0.8 nm) (Krey et al. 2016) or cochlear hair cells (~ $9 - 10$ nm) (Scheffer et al. 2015) using similar sample preparations.

Figure III-7: ACTIN INTER-FILAMENT SPACING. (A) Transmission electron micrograph of a transverse section of a hair bundle. **(B)** Higher magnification of the transverse section of the individual stereocilium enclosed by the dashed square shown in (A). **(C)** A small region within the stereocilium is shown in (B). **(D)** The corresponding 2D-FFT image of (B) reveals a ring-like pattern, corresponding to liquid packing of the actin filaments in the stereocilium. **(E)** FFT analysis of small regions within the stereocilia sometimes showed local hexagonal packing. **(F)** Boxplot of the actin inter-filament spacing. Scale bar (A-B) 200 nm, (C) 100 nm, and (D-E) 83 μm^{-1}.

SUMMARY

The results in this section are summarized in Table III.2.

	Small hair bundle	Large hair bundles
Number of stereocilia	**31 ± 7** ($N = 26$)	**35 ± 8** ($N = 26$)
Hair-bundle width (μm)	**2.00 ± 0.47** ($N = 35$)	**3.62 ± 0.44** ($N = 38$)
Hair-bundle height (μm)	n.a.	**7.13 ± 0. 49** ($N = 17$)
Kinociliary height (μm)	n.a.	**5.18 ± 0.44** ($N = 17$)
Insertion diameter(nm)	**132 ± 16** ($N = 29$)	**188 ± 24** ($N = 23$)
Insertion spacing (nm)	**246 ± 58** ($N = 29$	**489 ± 75** ($N = 23$)
Actin spacing (nm)	**12.0 ± 0.5** ($N = 15$)	
Lattice angle (deg)	**63 ± 7** ($N = 29$)	**85 ± 11** ($N = 29$)

Table III.2: DIMENSIONS OF HAIR BUNDLES AND THEIR STEREOCILIA IN THE SACCULE OF THE FROG RIVAN 92. N is the number of hair cells. n.a. (not available).

B. Effects of pharmacological perturbation of mechano-electrical transduction

In this section, I describe how blocking the transduction channels or disrupting the tip links affected the architecture of frog saccular hair bundles and the ultrastructure of their stereociliary actin core. The following figure (Fig. III-8) serves as a summary of the observed effects.
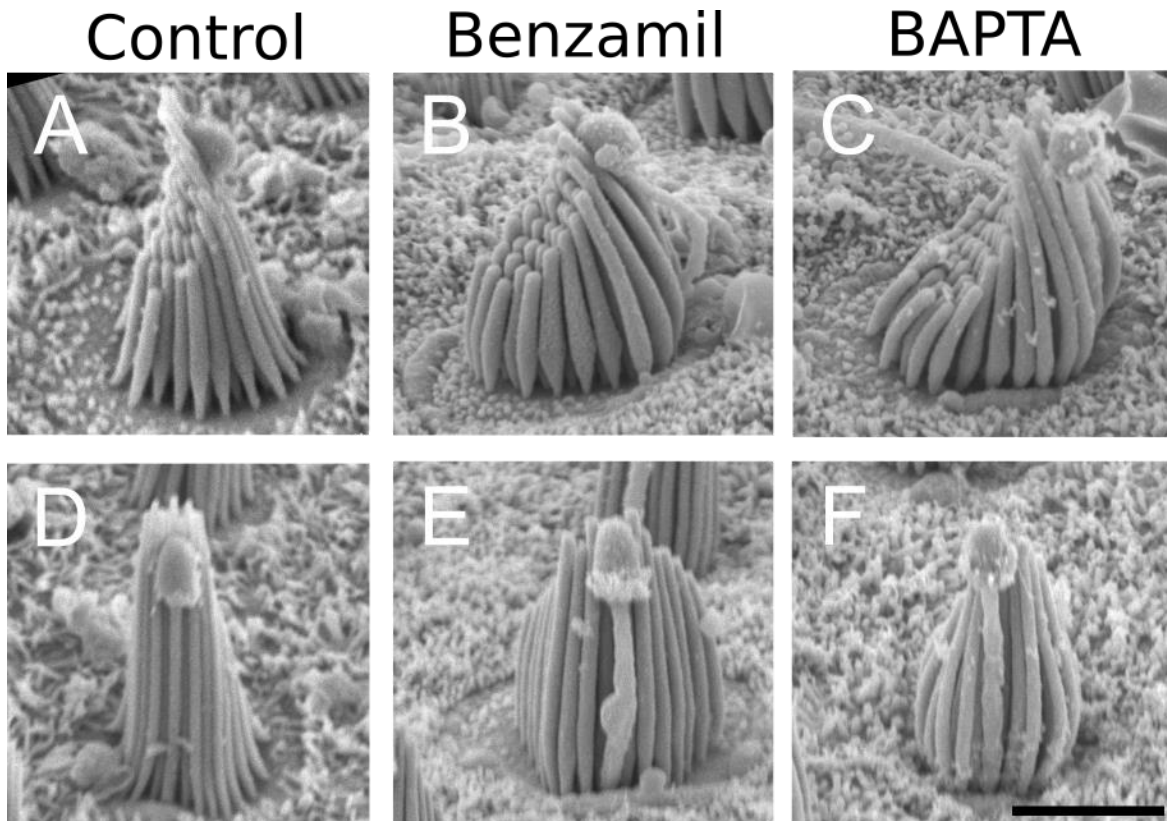
Figure III-8: SUMMARY - MORPHOLOGICAL EFFECTS OF PHARMACOLOGICAL BLOCKING OF TRANSDUCTION CHANNELS OR CHEMICAL DISRUPTION OF THE TIP LINKS. Scanning electron micrographs were taken from the lateral side of a hair bundle **(A)** under control condition, **(B)** after exposure for 1 hr to a pharmacological blocker (benzamil) of the transduction channels, and **(C)** after exposure for 15 min to a Ca^{2+} chelator (BAPTA) known to disrupt the tip links before washing and transferring the tissue to standard saline for 1 hr. **(D-F)** same bundles as in (A-C) seen from the front of the tallest row. Scale bar: 3 µm.

B.1 Hair-bundle morphology with impaired transduction

a. Blocking transduction channels

Based on previous observations in mouse and rat cochlear hair cells (Vélez-Ortega et al. 2017), I expected to see abnormally thin tips of the stereocilia upon blocking the transduction channels for only 1 hr. To my surprise, I instead observed a dramatic widening of the hair bundles, which adopted an 'onion-like shape (Fig. III-8.B and Fig. III-9). The tallest stereocilia were bent towards the middle stereociliary rows. Because I never observed similar stereocilia bending under control conditions, it is unlikely that the bending simply resulted from chemical fixation.
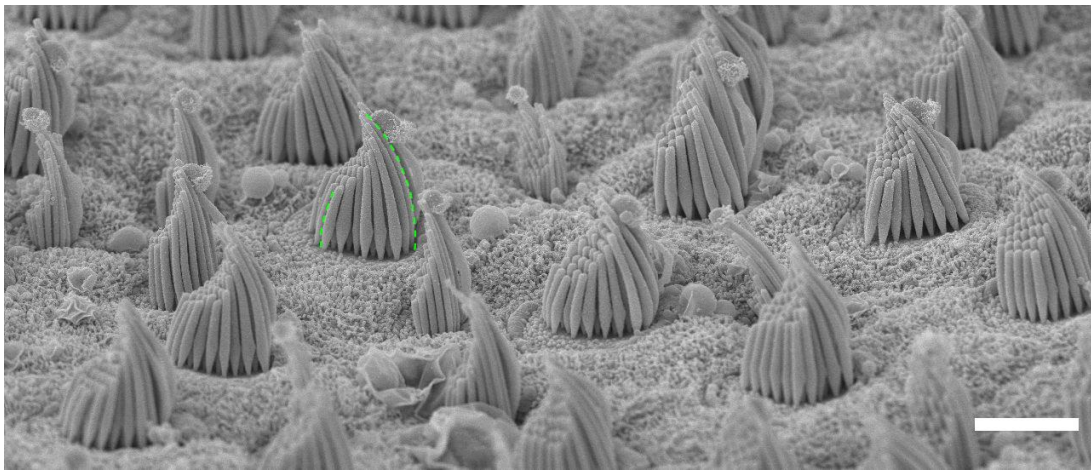
Figure III-9: HAIR-BUNDLE MORPHOLOGY AFTER BLOCKING THE TRANSDUCTION CHANNELS. Scanning electron micrograph of the saccular macula after incubation in perilymph containing 30 µM of the transduction-channel blocker benzamil for 1 hr. The hair-bundles adopted an onion-like shape, where taller stereocilia bent towards the middle of the hair bundle (dashed lines). Scale bar: 5 µm.

To quantify these changes, I measured the stereociliary width and height of the large hair bundles. The width was measured for the shortest, middle, and tallest rows, whereas the height was measured for the shortest and tallest rows only. The analysis demonstrates that the stereocilia widened by about 36 % in all three rows: from 386 ± 41 nm (control, $N = 17$ cells) to 535 ± 75 nm (benzamil, $N = 29$ cells) in the shortest row, from 440 ± 41 nm (control, $N = 16$ cells) to 592 ± 86 nm (benzamil, $N = 20$ cells) in the middle row, and from 285 ± 21 nm (control, $N = 16$ cells) to 384 ± 46 nm (benzamil, $N = 22$ cells) in the tallest row (Fig. III-10.A). The non-monotonic variation in stereociliary width from the shortest to the longest rows of stereocilia was preserved: the stereocilia in the middle row were wider than those in the shortest and tallest row, respectively by 11% and 54%. In addition, the height of the shortest stereocilia was also reduced from 3.08 ± 0.38 µm (control, $N = 17$ cells) to 2.77 ± 0.27 nm (benzamil, $N = 14$ cells), corresponding to a relative variation of only 11%. There was no significant change in height was observed in the

tallest stereocilia (Fig. III-10.B). Interestingly, the height of the taper region also increased by 22%, from $0.93 \pm 0.14\,\mu m$ (control; $N = 16$ cells) to $1.13 \pm 0.18\,\mu m$ ($N = 14$ cells) after benzamil treatment (Fig. III-10.C). As a result of the morphological changes, the estimated volume of a stereocilium increased. Using stereocilia of the shortest row, which are the most visible in scanning electron micrographs, the stereociliary volume increased by 60%, from $0.25\,\mu m^3$ (control) to $0.40\,\mu m^3$ (benzamil; channels blocked) (Fig. III-10.D). Overall, the main effect of blocking the transduction channels was thus to increase the width and volume of the stereocilia.
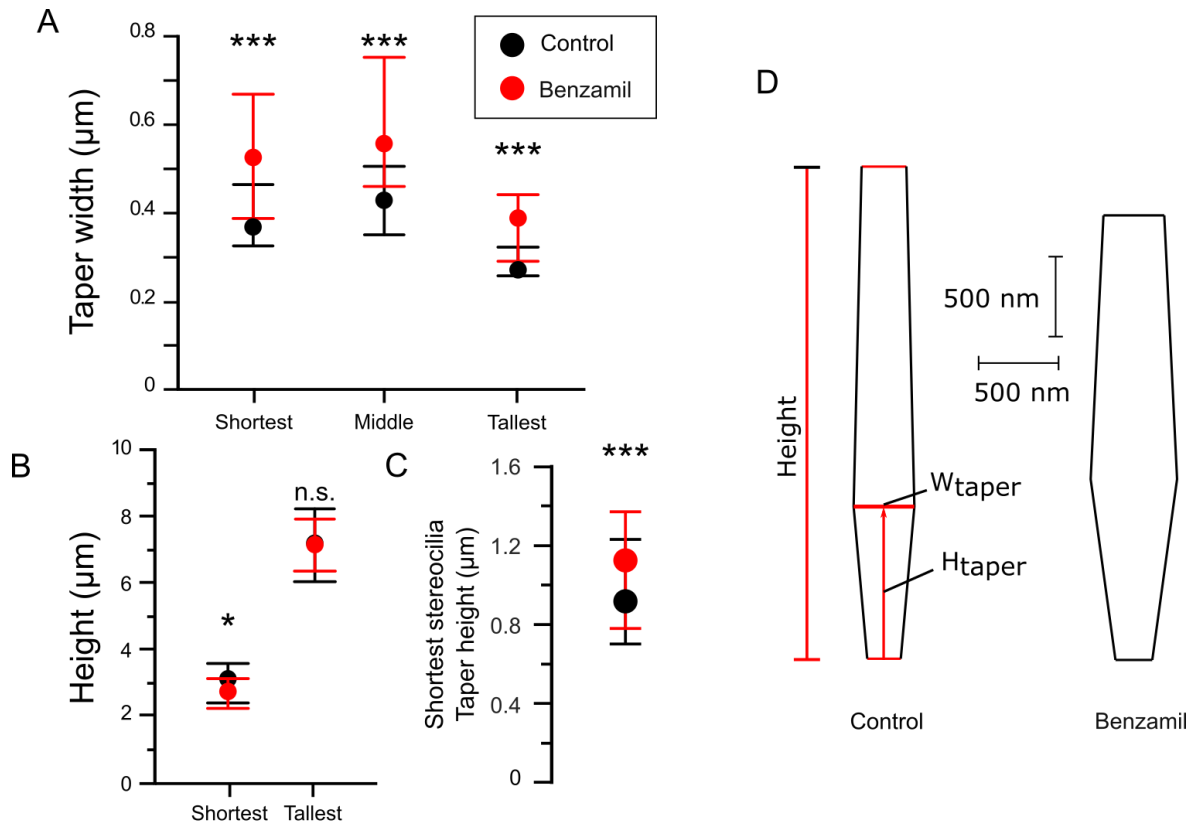
Figure III-10: STEREOCILIA WIDENING AND SHORTENING UPON BLOCKING TRANSDUCTION CHANNELS. Stereociliary width **(A)** and height **(B)** in the shortest, middle and the tallest rows under the control condition (●) and after exposure to the channel blocker benzamil for 1 hr (●). **(C)** The height of the taper region increased by 22 % upon blocking the transduction channels. **(D)** The average shape of stereocilia in the shortest row under control conditions and after the transduction channels were blocked. In the plots shown in (A-C), the circles represent the medians and the error bars represent the 1st and the 3rd quartiles. Statistical significance was tested with Student's t-test, * for p-value ≤ 0.1, ** for p-value ≤ 0.01, and *** for p-value ≤ 0.001, whereas N.S. (non-significance) is for p-value > 0.05.

To rule out that the observed morphological effects were specific to the channel blocker benzamil, I repeated the experiment with another well-documented channel blocker (Farris et al. 2004), tubocurarine. I observed similar effects with tubocurarine (100 µM for 1 hr) as those

described above with benzamil (30 µM for 1 hr; Fig. III-11). In these experiments, the stereociliary width of the shortest stereocilia increased by about 57 %, from 386 ± 41 nm (control, $N = 17$ cells) to 604 ± 61 nm (tubocurarine, $N = 16$ cells). The observed effect was actually larger than in our experiments with benzamil (+36 %).
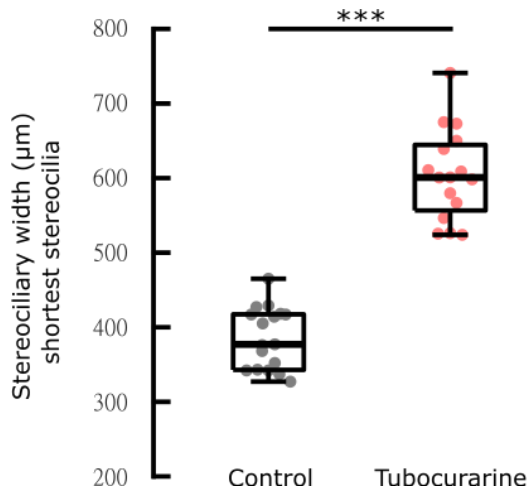
Figure III-11: STEREOCILIA WIDENING UPON BLOCKING THE TRANSDUCTION CHANNELS WITH TUBOCURARINE. As with benzamil, the width of the stereocilia in the shortest row increased after exposure for 1 hr to the channel blocker tubocurarine at 100 µM. Statistical significance was tested with Student's t-test, * for p-value ≤ 0.1, ** for p-value ≤ 0.01, and *** for p-value ≤ 0.001, whereas N.S. (non-significance) is for p-value > 0.05.

Are the effects of blocking the transduction channels reversible? In these experiments, I washed the channel blocker benzamil after 1-hr incubation in a culture medium and then transferred the saccule to a culture medium with no drug for another 5 hrs of incubation[9]. I observed partial recovery of the stereociliary width (Fig. III-12). After a 1-hr incubation in a cell culture medium supplemented with 30 µM benzamil, the stereociliary width of the shortest stereocilia had increased from 386 ± 41 nm (control, $N = 17$ cells) to 614 ± 45 nm (benzamil, $N = 26$ cells), thus by 59 %. Then, 5 hrs after washing out the channel blocker, the stereociliary width had decreased to reach a value of 513 ± 58 nm ($N = 46$ cells), corresponding to a 44 % recovery.

---
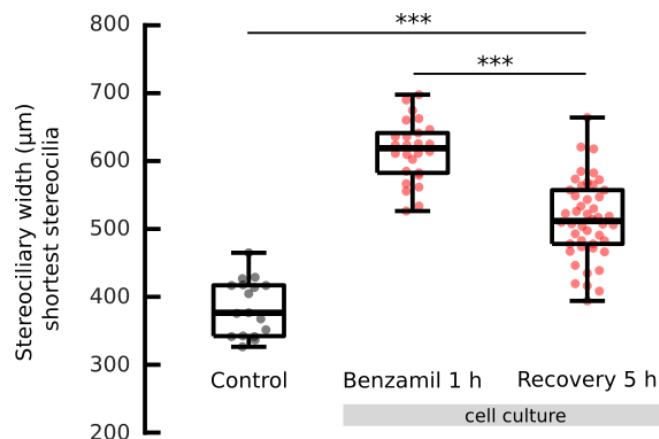
[9] I observed that incubating hair cells in perilymph with 4 mM Ca^{2+} for longer than ~3 hr had deleterious effects (i.e. morphological defects in the hair bundle and blebs at the cell apical surface). For this reason, I developed a frog culture medium (see Materials and Methods) that allowed me to study the hair-bundle morphology for longer durations.

Figure III-12: RECOVERY OF THE STEREOCILIARY WIDTH. After a 1-hr incubation in the cell culture medium supplemented with 30 µM benzamil, the stereociliary width had increased by 59 %. After washing out the channel blocker and incubating the saccules for 5 hrs in the cell culture medium, the stereociliary width partially recovered, by 44 %. Statistical significance was tested with Student's t-test, * for p-value ≤ 0.1, ** for p-value ≤ 0.01, and *** for p-value ≤ 0.001, whereas N.S. (non-significance) is for p-value > 0.05.

b. Disrupting tip links

Blocking the channels and disrupting the tip links both interrupt the mechanotransduction current, in particular the Ca^{2+} influx, but the stereociliary tips of all but those in the tallest stereociliary row are expected to remain under tension (Fig. I-3.A) under the former condition whereas tension ought to be released in the latter. Does it make a difference for hair-bundle morphology? Tip links can be chemically disrupted by reducing the extracellular Ca^{2+} concentration to sub-micromolar levels with the calcium chelators BAPTA (Assad, Shepherd, and Corey 1991).

Hair bundles with disrupted tip links showed stereocilia with oblate tips, as expected from the loss of tip-link tension. In these hair-bundle, I also observed clear stereocilia widening and onion-like shapes of the hair bundles (Fig. III-8.C and Fig. III-13). These morphological changes were similar to those described above upon blocking the transduction channels (Fig. III-8.B and Fig. III-9).
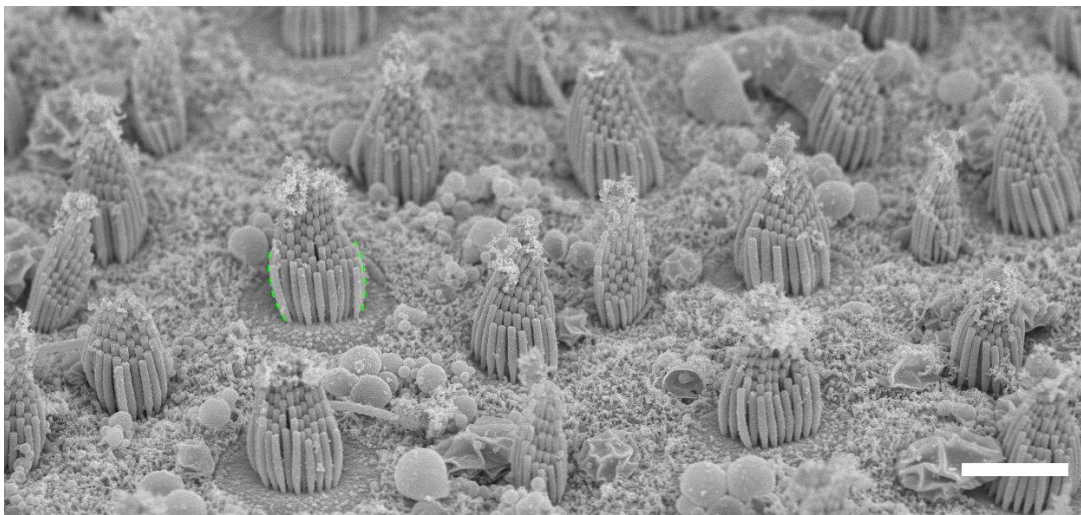
Figure III-13: HAIR BUNDLE MORPHOLOGY AFTER DISRUPTING THE TIP LINKS. The sensory epithelium was incubated in no Ca^{2+}-added artificial perilymph supplemented with 5 mM BAPTA for 15 min and then in 4 mM Ca^{2+} artificial perilymph for 1 hr. Similar to the effect observed after blocking transduction channels, the hair bundles adopted onion-like shapes (see dashed lines). Scale bar 5 µm.

The stereociliary width increased from 386 ± 41 nm (control, $N = 17$ cells) to 429 ± 44 nm (BAPTA, $N = 30$ cells) in the shortest row, from 440 ± 41 nm (control, $N = 16$ cells) to 505 ± 73 nm (BAPTA, $N = 29$ cells) in the middle row, and from 285 ± 21 nm (control, $N = 16$ cells) to

356 ± 46 nm (BAPTA, N = 22 cells) in the tallest row (Fig. III-14.A). However, the effect was only +17 % on average over the three rows, which was smaller than the +36-60 % widening observed after blocking the transduction channels (Fig. III-10, Fig. III-11, Fig. III-12). The stereocilia of the shortest row also shortened by 16 %, from 3.08 ± 0.38 µm (control, N = 17 cells) to 2.58 ± 0.4 nm (BAPTA, N = 16 cells). Again, no significant shortening was observed in the tallest stereocilia (Fig. III-14.B). The height of the taper region in the stereocilia of the shortest row actually decreased by 26%, from 0.93 ± 0.14 µm (control; N = 16 cells) to 0.69 ± 0.13 µm (N = 16 cells) after BAPTA treatment, an effect that was opposite to what observed after blocking the transduction channels (Fig. III-14.C). The estimated volume of a stereocilium in the shortest rows increased by 16%, from 0.25 µm³ (control) to 0.29 µm³ (BAPTA; disrupted tip links) (Fig. III-14.D). Thus, tip-link disruption resulted in a smaller increase of the stereociliary volume than in response to blocking the transduction channels, with less widening of the stereocilia.
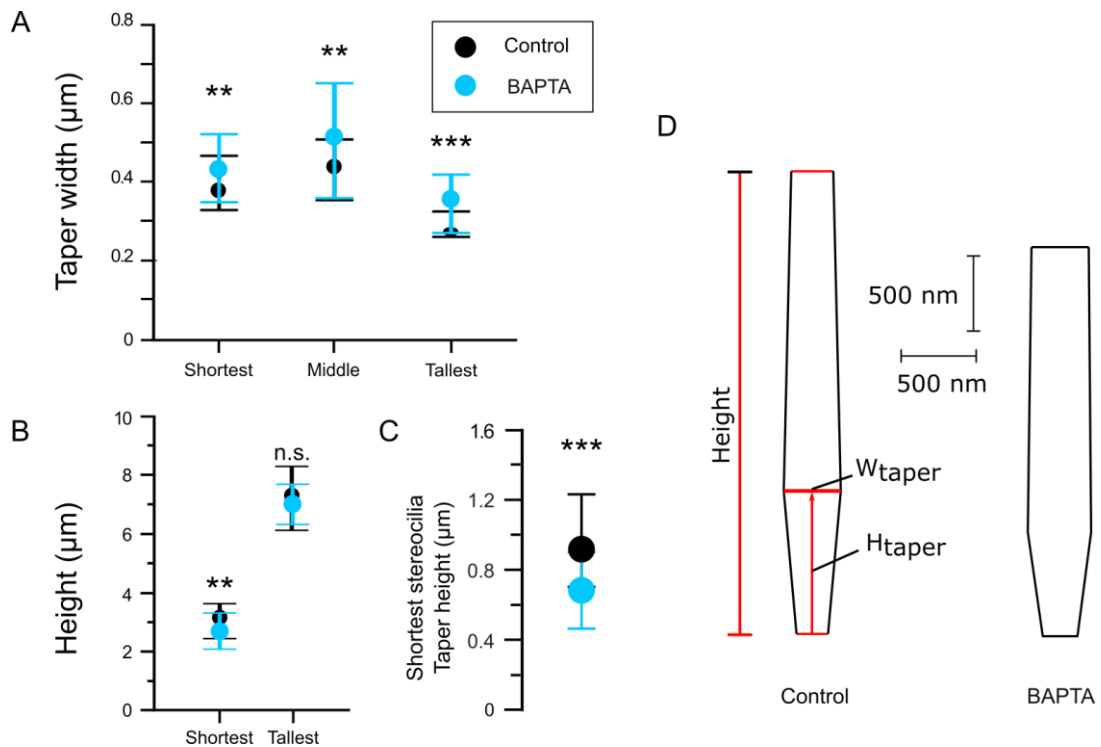
Figure III-14: STEREOCILIA WIDENING AND SHORTENING AFTER CHEMICAL DISRUPTION OF THE TIP LINKS. (A) Stereocilia widen in all rows after incubation in no-added Ca^{2+} perilymph containing 5 mM of the calcium chelator BAPTA for 15 min and in 4 mM Ca^{2+} perilymph for 1 hr. (Control ●, BAPTA ●).

(B) The shortest stereocilia shorten but not the tallest. **(C)** The height of the taper region was reduced by 26 % upon disrupting tip links. **(D)** The average shape of stereocilia in the shortest row under control conditions and after the tip links were disrupted. In the plots shown in (A-C), the circles represent the medians and the error bars represent the 1ˢᵗ and the 3ʳᵈ quartiles. Statistical significance was tested with Student's t-test, * for p-value ≤ 0.1, ** for p-value ≤ 0.01, and *** for p-value ≤ 0.001, whereas N.S. (non-significance) is for p-value > 0.05.

SUMMARY

The following figure (Fig. III-15) compares the average shape of a typical stereocilium in the shortest row under control conditions (Fig. III-15.A) and after pharmacological perturbation of the mechano-electrical transduction (Fig. III-15.B-C). Stereocilia dimensions are listed in Table III.3.
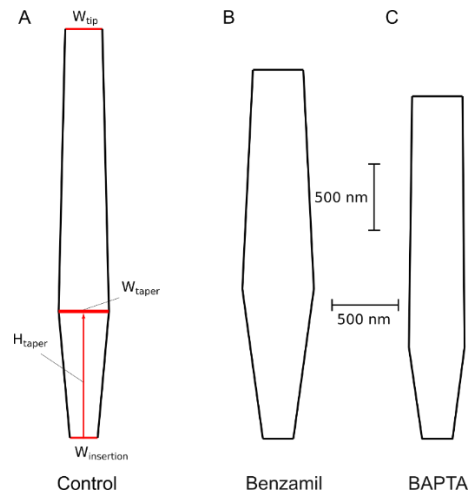
Figure III-15: AVERAGE SHAPE OF A STEREOCILIUM IN THE SHORTEST ROW. The average shape of the shortest stereocilia under control conditions (**A**), after blocking the transduction channels for 1 hr with benzamil (**B**), and 1 hr after disrupting the tip links (**C**).

Condition	Shortest stereocilia					Tallest stereocilia		Kinociliary bulb height (μm)
	Taper Width (μm)	Height (μm)	Taper Height (μm)	Tip Width (μm)	Insertion Width (nm)	Width (μm)	Height (μm)	
Control	0.39 ± 0.04 (N = 17)	3.08 ± 0.38 (N = 14)	0.93 ± 0.14 (*N* = 16)	0.28 ± 0.03 (*N* = 16)	0.20 ± 0.02 (*N* = 15)	0.29 ± 0.02 (N = 12)	7.13 ± 0.49 (N = 17)	5.18 ± 0.44 (N = 17)
Benzamil (Blocking channels)	0.54 ± 0.08 (N = 29)	2.77 ± 0.27 (N = 14)	1.13 ± 0.18 (*N* = 14)	0.38 ±0.03 (*N* = 14)	0.23 ± 0.03 (*N* = 12)	0.38 + 0.05 (N = 22)	7.10 ± 0.46 (N = 9)	5.52 ± 0.37 (N = 12)
BAPTA (Disrupting tip links)	0.43 ± 0.04 (N = 30)	2.58 ± 0.40 (N = 16)	0.69 ± 0.13 (*N* = 16)	0.35± 0.08 (*N* = 16)	0.22 ± 0.04 (*N* = 14)	0.36 + 0.05 (N = 22)	6.79 ± 0.55 (N = 16)	5.08 ± 0.52 (N = 14)

Table III.3: DIMENSIONS OF HAIR-CELL BUNDLES IN THE FROG SACCULUS IN CONTROL AND PERTURBED CONDITIONS.

B.2 Hair-bundle imprints and stereociliary insertions

a. Expansion of the cells' apical surface and the hair-bundle imprints

After blocking the transduction channels for 1 hr, both the diameter of the apical surface and the hair-bundle imprint had increased (Fig. III-16). The apical-surface diameter increased by the same relative amount for both small and large hair bundles, by +21% and +23 %, respectively. In contrast, the diameter of the hair-bundle imprints expanded much more for small hair bundles than for large hair bundles, by +39% and +26 %, respectively (Table III.4). Correspondingly, the stereociliary-insertion spacing displayed a larger relative increase for small than for large hair cells, by +37% and +12%, respectively (Table III.4). The hair-bundle imprint of the small hair bundles expanded more than the apical surface. The surface fraction occupied by the hair bundle thus increased significantly from 50 ± 7 % ($N = 29$ cells) under control conditions to 57 ± 6 % ($N = 23$ cells) after blocking the transduction channels. Interestingly, the imprint diameter increased more than expected from a homothetic expansion of the cuticular plate, for which imprint diameter would increase by the same amount as the diameter of the apical surface. Because the stereocilia are tightly packed at the hair bundle's top, the increased spacing of the stereociliary insertions may have resulted from the stereocilia pushing against each other as they got wider, forcing the stereocilia to move laterally within the cuticular plate.

Importantly, in fresh preparations examined with light microscopy, I did not find any significant change of the cell-body diameter, which was measured at 11.6 ± 1.2 µm ($N = 35$ cells) under control conditions and at 11.6 ± 0.7 µm ($N = 30$ cells) for benzamil-treated cells. These observations indicate that upon channel blocking with benzamil, the actin-rich apical surface of the hair cell and the hair-bundle imprint expanded but the cells did not swell.

Apical surface diameter	**Control**	**Benzamil**
Small hair bundles	3.22 ± 0.43 µm ($N = 29$)	3.90 ± 0.38 µm ($N = 23$), ***
Large hair bundles	6.03 ± 0.49 µm ($N = 30$)	7.40 ± 0.89 µm ($N = 43$), ***
Hair-bundle imprint diameter	**Control**	**Benzamil**
Small hair bundles	1.60 ± 0.24 µm ($N = 29$)	2.22 ± 0.94 µm ($N = 23$), ***
Large hair bundles	3.13 ± 0.43 µm ($N = 30$)	3.93 ± 0.50 µm ($N = 43$), ***
Stereociliary insertion spacing	**Control**	**Benzamil 1 h**
Small hair bundles	246 ± 58 nm ($N = 29$)	337 ± 89 nm ($N = 30$), ***
Large hair bundles	489 ± 75 nm ($N = 23$)	548 ± 74 nm ($N = 43$), ***

Table III.4: DIAMETER OF APICAL SURFACE, OF THE HAIR-BUNDLE IMPRINT, AND STEREOCILIARY INSERTION SPACING. Statistical significance (control vs. benzamil) was tested with Mann-Whitney U test, *** for p-value ≤ 0.001. N is the number of hair cells.
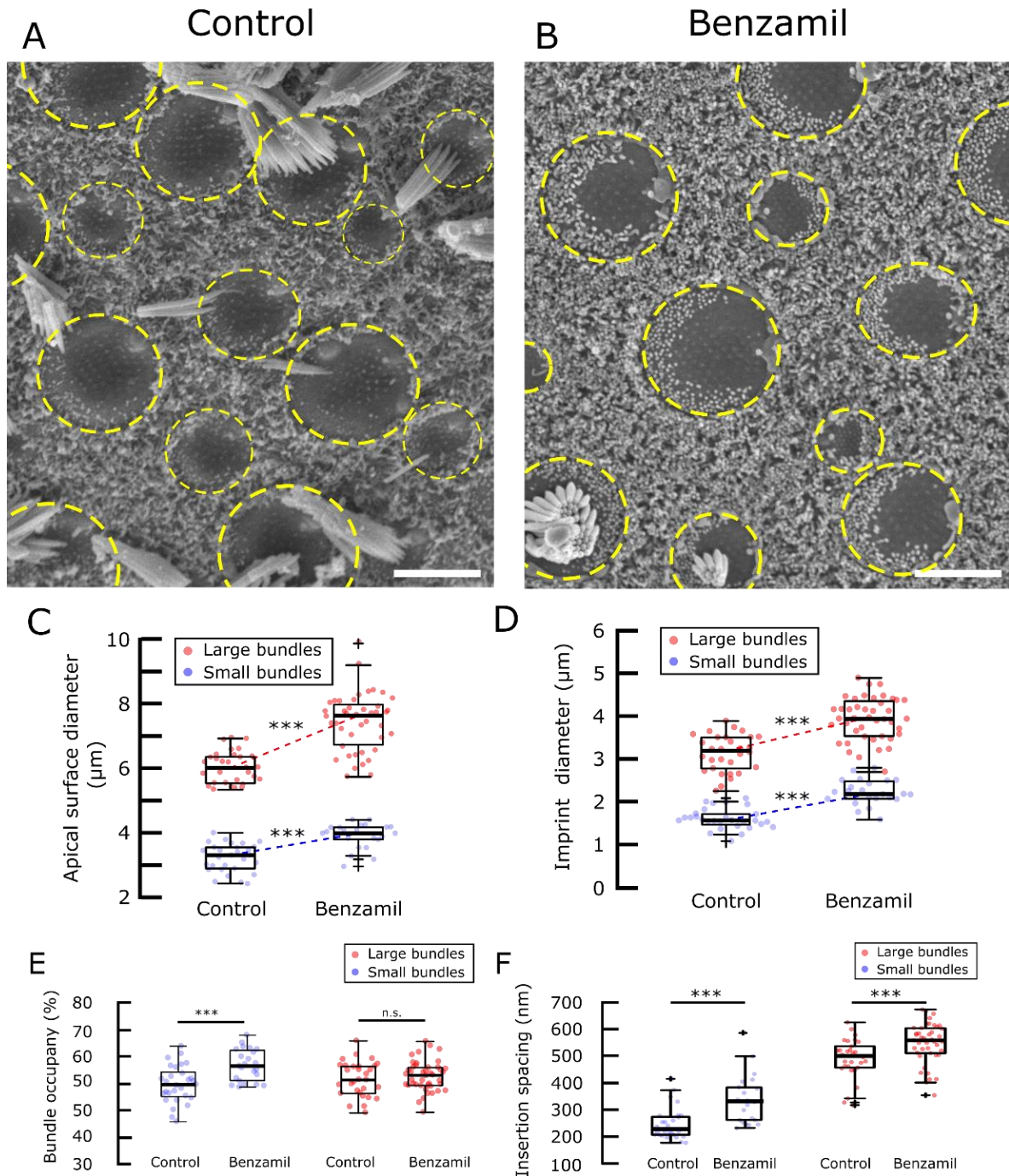
Figure III-16: EXPANSION OF THE APICAL SURFACE OF THE HAIR CELL AND THE HAIR-BUNDLE IMPRINT. Scanning electron micrographs of the sensory epithelium for **(A)** the control condition and **(B)** after incubation in perilymph containing 30 µM benzamil for 1 hr. Scale bar: 5 µm. **(C)** The apical surface diameter increased by 22 % for both hair bundle populations. **(D)** The hair-bundle imprint diameter increased by 39 % for large hair bundles and by 26 % for small hair bundles. **(E)** The hair-bundle occupancy increased from about 50% to 57% for small hair bundles but did not increase significantly not for large hair bundles. **(F)** The stereociliary-insertion spacing increased by 37 % for small hair bundles and by 12 % for large hair bundles. Statistical significance was tested with Mann-Whitney U test, * for p-value ≤ 0.1, ** for p-value ≤ 0.01, and *** for p-value ≤ 0.001, whereas N.S. (non-significance) for p-value > 0.1.

b. Widening of the stereociliary insertions

In addition to the increase of the hair-bundle imprint diameter, I also observed a substantial increase in the diameter of the stereociliary insertions (Fig. III-17), by 24 % for small hair cells and 13 % for large hair cells (Table III.5). Again, small hair bundles displayed a larger effect than large hair bundles.

Stereociliary insertion diameter	Control	Benzamil 1 h
Small hair bundles	132 ± 16 nm ($N = 29$)	164 ± 21 nm ($N = 23$), ***
Large hair bundles	188 ± 24 nm ($N = 30$)	212 ± 31 nm ($N = 43$), ***

Table III.5: STEREOCILIARY INSERTION DIAMETER. Statistical significance (control vs. benzamil) was tested with Mann-Whitney U test, *** for p-value ≤ 0.001. N is the number of hair cells.
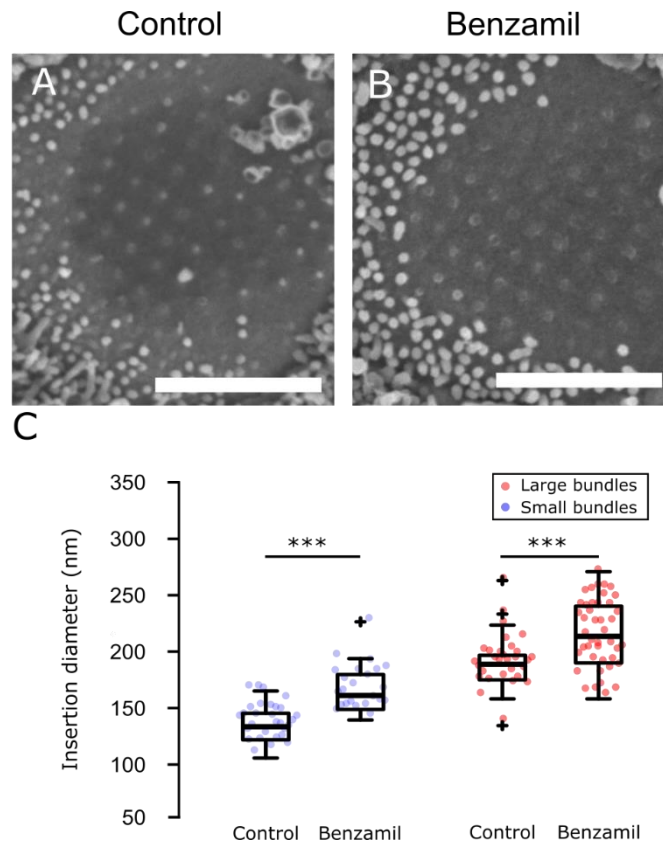
Figure III-17: STEREOCILIARY INSERTION DIAMETER. Imprints of the stereocilia insertions at the apical surface. **(A)** under control conditions and **(B)** for benzamil-treated hair cells. **(C)** The diameter of individual stereociliary insertions increased by 24 % for small hair bundles, and by 13 % for large hair bundles. Scale bar: 3 μm. Statistical significance was tested with Mann-Whitney U test, * for p-value ≤ 0.1, ** for p-value ≤ 0.01, and *** for p-value ≤ 0.001, whereas n.s. (non-significance) for p-value > 0.1.

I found no change in correlation (Fig. III-6) between the stereociliary-insertion diameter with the hair-bundle imprints (Fisher z-transformation, p-value = 0.77) or the stereociliary-insertion spacing (Fisher z-transformation, p-value = 0.28). The correlations only shifted upwards to the right as the stereociliary-insertion diameter increased (Fig. III-18).
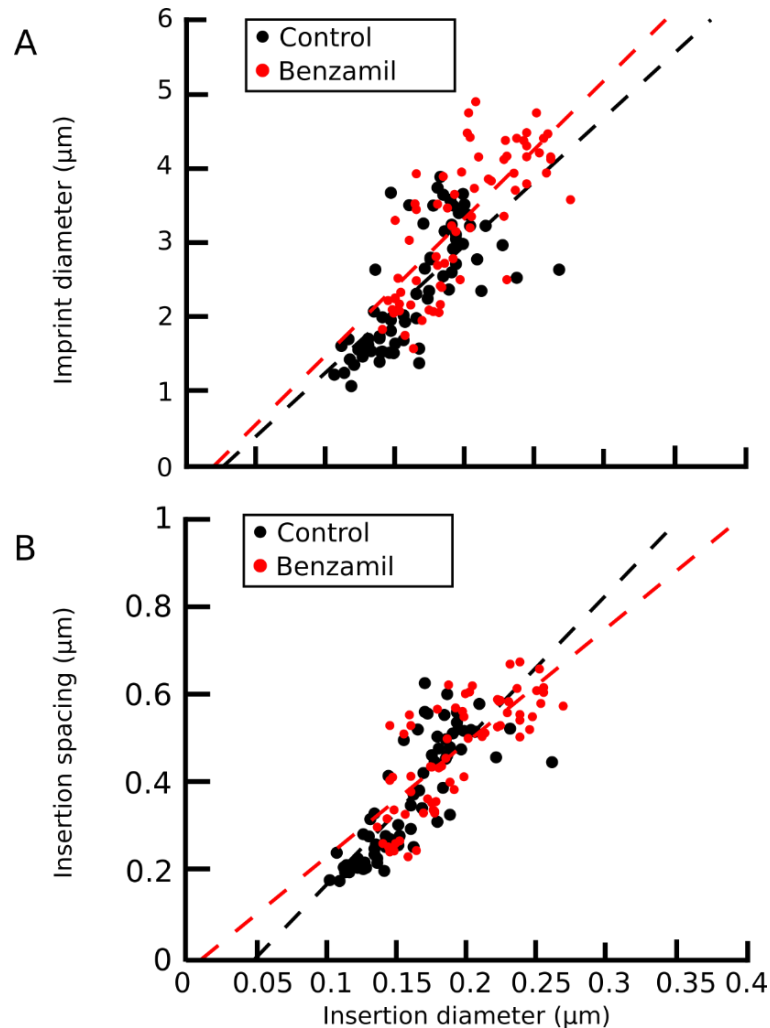
Figure III-18: DIMENSIONS OF HAIR-BUNDLE IMPRINTS AS A FUNCTION OF THE STEREOCILIARY-INSERTION DIAMETER. As the stereociliary insertions widened upon incubation in perilymph containing 30 μM of the channel blocker benzamil, their correlations with **(A)** the hair-bundle imprint diameter and **(B)** the stereociliary insertion spacing remained the same and only shifted upwards to the right (Pearson's $r = 0.7$ in both cases, p-values < 0.001. The dashed lines are correspond to **(A)** $17 \cdot D_{insertion}$ - 0.42 **(black)** and $19 \cdot D_{insertion}$ - 0.33 **(red)** in (A) and to $3.3 \cdot D_{insertion}$ - 0.16 **(black)** and $2.6 \cdot D_{insertion}$ - 0.03 **(red) in (B)**, with $N = 70$ cells. No significant difference was found between control conditions and after incubation in perilymph containing 30-μM benzamil for 1 hr (Fisher z-transformation, p-value = 0.77 and 0.28 for the correlations in A and B, respectively).

Although the stereocilia widened and the stereociliary-insertion spacing increased after blocking the transduction channels, I found that the proportion of hair bundles with stereocilia insertions arranged within a hexagonal or a square lattice did not change significantly (Table III.6).

Conditions	Small hair bundles		Large hair bundles	
	Hexagon	Square	Hexagon	Square
Control	24	2	4	20
Benzamil	21	1	8	30
Table III.6: LATTICE PATTERN AFTER 1 H BLOCKING OF THE TRANSDUCTION CHANNELS. Although the percentage of large hair bundles showing hexagonal lattice packing of their insertions slightly increased from 17% to 21% after prolonged blocking of the transduction channels, this increase was not statistically significant (two proportion z-test at the confidence level = 90%, z = 0.57).				

However, for small hair bundles, the median of the lattice angle came closer to the ideal lattice angle of 60° for hexagonal packing and the standard deviation of the lattice angle was markedly reduced (p-values < 0.001), with a median angle of 63.3 with an inter-quartile range of 8.1 ($N = $ 29 cells) under control conditions and a median angle of 60.1 with an interquartile range of 2.6 ($N = 23$ cells) for benzamil-treated cells. Widening of the stereocilia of the small hair cells thus resulted in stereociliary packing that was more precisely hexagonal.
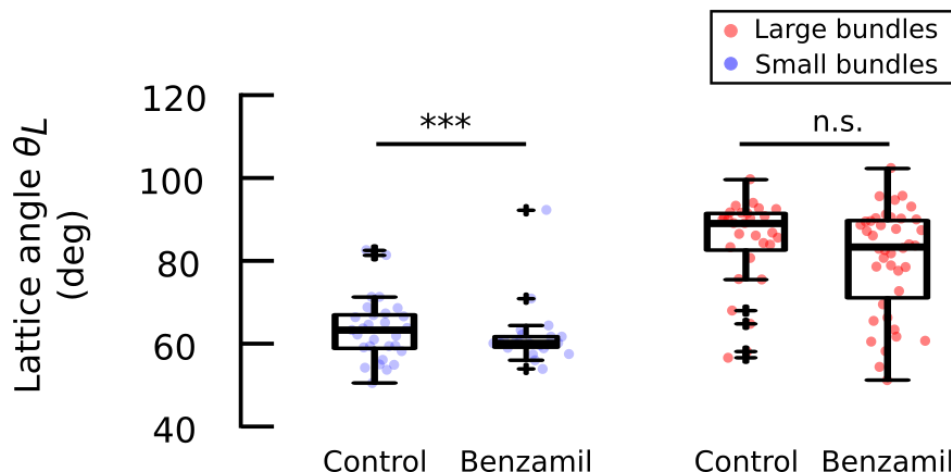
Figure III-19: LATTICE ANGLE. The lattice angle did no change for large hair bundles, whereas for small hair bundles the stereociliary packing became less variable and closer to the value $\theta_L = 60°$ corresponding to hexagonal packing. Statistical significance was tested with Mann-Whitney U test, * for p-value ≤ 0.1, ** for p-value ≤ 0.01, and *** for p-value ≤ 0.001, whereas N.S. (non-significance) for p-value > 0.1.

SUMMARY

Table III.7 summarizes the characterization of the hair-bundle imprints and the stereociliary insertions in the control and after pharmacological perturbation of the mechano-electrical transduction.

	Hair-bundle	Control	Benzamil	Statistical significance
Apical surface diameter (µm)	**Small**	**3.22 ± 0.43 µm** (*N* = 29)	**3.90 ± 0.38 µm** (*N* = 23)	***
	Large	**6.03 ± 0.49 µm** (*N* = 30)	**7.44 ± 0.89 µm** (*N* = 43)	***
Imprint diameter (µm)	**Small**	**1.59 ± 0.24 µm** (*N* = 29)	**2.22 ± 0.30 µm** (*N* = 23)	***
	Large	**3.13 ± 0.43 µm** (*N* = 30s)	**3.93 ± 0.50 µm** (*N* = 43)	***
Bundle occupancy (%)	**Small**	**50 ± 7** (*N* = 29)	**57 ± 6** (*N* = 23)	***
	Large	**52 ± 6** (*N* = 30)	**52 ± 6** (*N* = 43)	n.s.
Insertion diameter (nm)	**Small**	**132 ± 16 nm** (*N* = 29)	**164 ± 21 nm** (*N* = 23)	***
	Large	**188 ± 24 nm** (*N* = 30)	**212 ± 31 nm** (*N* = 43)	***
Insertion spacing (nm)	**Small**	**246 ± 58 nm** (*N* = 29)	**337 ± 89 nm** (*N* = 30)	***
	Large	**489 ± 75 nm** (*N* = 30)	**548 ± 74 nm** (*N* = 43)	***
Lattice angle (deg)	**Small**	**63 ± 8 °** (*N* = 29)	**62 ± 7 °** (*N* = 23)	***
	Large	**85 ± 11 °** (*N* = 29)	**80 ± 13 °** (*N* = 40)	n.s.

Table III.7: HAIR-BUNDLE IMPRINTS AND STEREOCILIARY INSERTIONS AFTER 1 H BLOCKING OF THE TRANSDUCTION CHANNELS. All data represented as mean ± SD with the number *N* of cells indicated. Statistical significance was tested with Mann-Whitney U test, * for *p*-value ≤ 0.1, ** for *p*-value ≤ 0.01, and *** for *p*-value ≤ 0.001, whereas n.s. (non-significance) for *p*-value > 0.1.

B.3 Actin core of the stereocilia.

As we have seen, blocking the transduction channels or disrupting the tip links (Fig. III-10 and III-14) resulted in an increased volume of the stereocilia, which could be explained by three possible changes in their actin core:

(i)   **More actin filaments.** New actin filaments are added into the stereociliary core

(ii)   **Larger actin spacing.** The number of actin filaments remains the same but the actin inter-filament spacing gets larger.

(iii)   **Both.** More actin filament and larger actin inter-filament spacing.

To test these hypotheses, I used transmission electron microscopy to examine the ultrastructure of the stereociliary actin core and, in particular, to measure the actin inter-filament spacing. I found that the filaments still displayed liquid packing and the average inter-filament spacing in the actin core of the stereocilia did not change (*t*-test, *p*-value = 0.52) after blocking the transduction channels, remaining at 12.0 ± 0.5 nm (Table II-1 and Fig. III-20). Thus, it is most likely that the stereocilia widen because more actin filaments were added into the stereociliary core.

	Control	Benzamil 1 h
Actin inter-filament spacing	12.0 ± 0.5 nm ($N = 43$)	12.0 ± 0.6 nm ($N = 38$), n.s.

Table III.8: ACTIN INTER-FILAMENT SPACING. Statistical significance (control vs. benzamil) was tested with Student's t-test, n.s. (non-significance) for *p*-value > 0.1. N is the number of stereocilia.
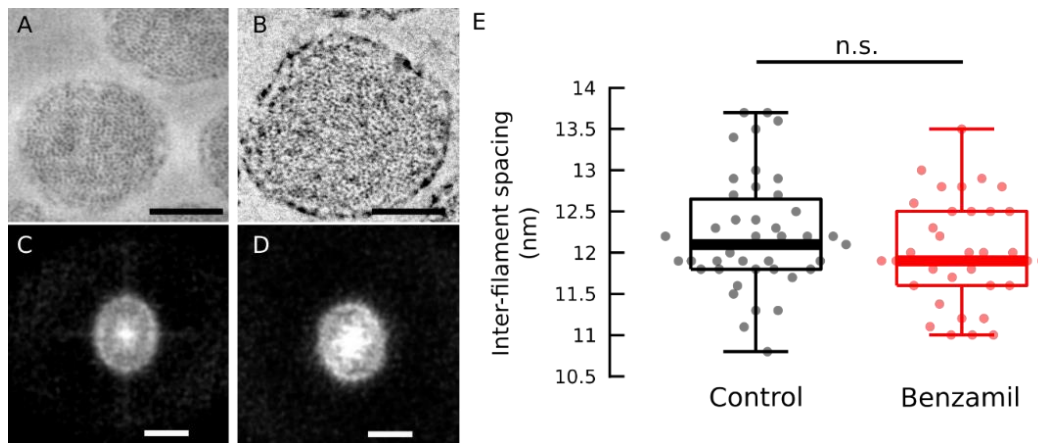
Figure III-20: INTER-FILAMENT SPACING OF IN THE ACTIN CORE OF STEREOCILIA. Transmission electron micrographs showing transverse sections of stereocilia under control conditions **(A)** and for benzamil-treated hair bundles **(B).** The corresponding 2D-FFT images, respectively **(C)** and **(D),** show ring-like patterns, corresponding to liquid packing, with the same radius. The inter-filament spacing was thus the same under the two conditions. **(E)** Boxplot of the inter-filament spacing for control (black; $N = 43$ stereocilia from 15 cells) and benzamil-treated (red; $N = 38$ stereocilia from 15 cells) hair bundles. Scale bar (A-B) 200 nm and (C-D) 0.2 nm^{-1}. Statistical significance was tested with Student's t-test, n.s. (non-significance) for *p*-value > 0.1.

B.4 Hair-bundle stiffness

The actin filaments that contribute to the stereocilia rootlets dictate the pivotal stiffness of the stereocilia. I wondered whether the stiffness of the hair bundle had changed as the result of stereocilia widening and of the corresponding increase of the number of actin filaments in the stereociliary core. To probe the hair-bundle stiffness, I attached a calibrated flexible fibre to the hair bundle's tip. I then applied a series of displacement steps at the fibre's base (Fig. III-21.A) and measured the displacement of the hair bundle (Fig. III-21.B). It is clear that with the same level of stimulation, the hair bundles that had been exposed to the channel blocker could move by a much smaller magnitude, demonstrating that they were stiffer than hair bundles under the control condition. On average over an ensemble of hair cells, I found that the hair-bundle stiffness increased by 91%, from 0.64 ± 0.51 mN/m ($N = 53$ cells) under the control condition to 1.22 ± 0.34 mN/m ($N = 32$ cells) after transduction-channel blocking with benzamil (Fig. III-21.C-D).
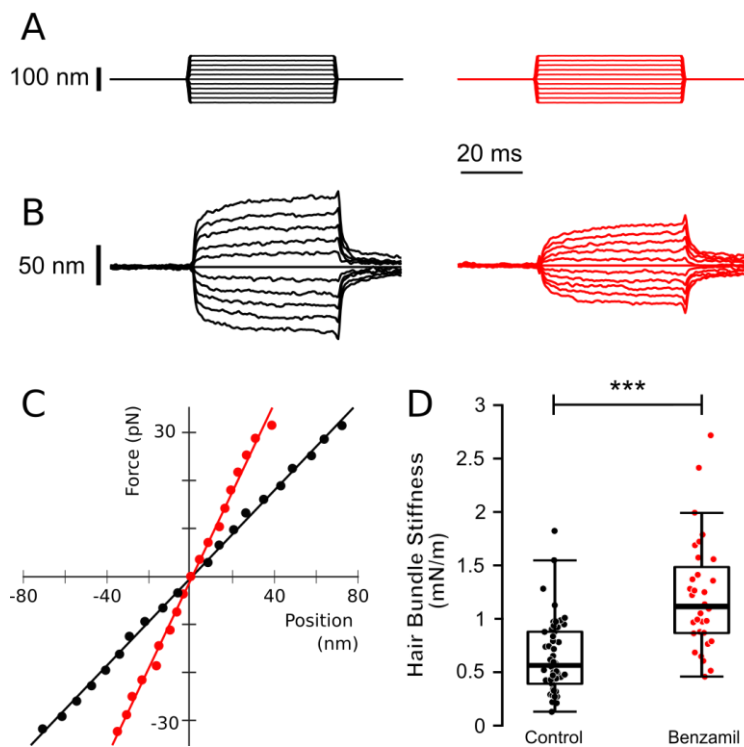
Figure III-21: HAIR-BUNDLE STIFFENENING AFTER BLOCKING THE TRANSDUCTION CHANNELS. (A) Series of step displacements at the base of a flexible fibre with the fibre's tip attached to the kinociliary bulb of a hair bundle under control condition (black) or after incubation with the channel blocker benzamil for 1 hr (red). **(B)** Hair-bundle movement in response to the mechanical stimulation shown in (A). **(C)** Force-displacement relations for the data shown in (A) and (B). The slope of curves provides the hair-bundle stiffness under the two conditions. **(D)** Box plot of the hair-bundle stiffness under control conditions (black) and for hair bundles that had been exposed to benzamil (red). Statistical significance was tested with Student's t-test, * for p-value ≤ 0.1, ** for p-value ≤ 0.01, and *** for p-value ≤ 0.001, whereas n.s. (non-significance) for p-value > 0.1.

C. Probing the role of formins for actin polymerization in stereocilia

Prompted by the observations that overexpression of Dia1 and Diaph3 results in morphological defects of inner hair-cell bundles (Fig. I-21 in the Introduction) (Schoen, Burmeister, and Lesperance 2013; Ninoyu et al. 2020), I examined the localization of formins in the hair bundle and tested the implication of formin mediated actin-nucleation on stereocilia widening upon blocking the transduction channels.

C.1 Localization of formins in the stereocilia

I used a fluorescently labelled antibody raised in rabbits against a region within amino acids 981–1272 of the human formin DIAPH1. I found that the antibody labelled the supporting cells' microvilli, the hair bundle, and the kinocilia (Fig. III-22), with a stronger fluorescence signal in the microvilli and the kinocilia than in the stereocilia (Fig. III-22.G). The reason why the antibody labelled the kinocilium, especially the kinociliary bulb, is unclear. I could rule out the possibility of non-specific binding due to the secondary antibody, for I did not detect such signals in negative controls with no primary antibodies. However, we cannot exclude at this stage the unspecific labelling of the primary antibodies. To our knowledge, the kinocilium, with its axonemal structure based on microtubules, does not contain actin or actin-binding proteins.

Labelling in the kinociliary bulb made observation of the stereociliary tips of the taller stereocilia difficult. To be able to easily distinguish the labelling in the stereociliary tips from that of the kinocilium, I detached the kinocilia from the hair bundles. This was done mechanically during the dissection by pulling the otolithic membrane to which the kinociliary bulbs are attached, without prior incubation of the sensory tissue in a solution containing the protease that is normally used to digest kinociliary links. This technique proved to be very efficient as most of the hair bundles had detached or displaced kinocilia.
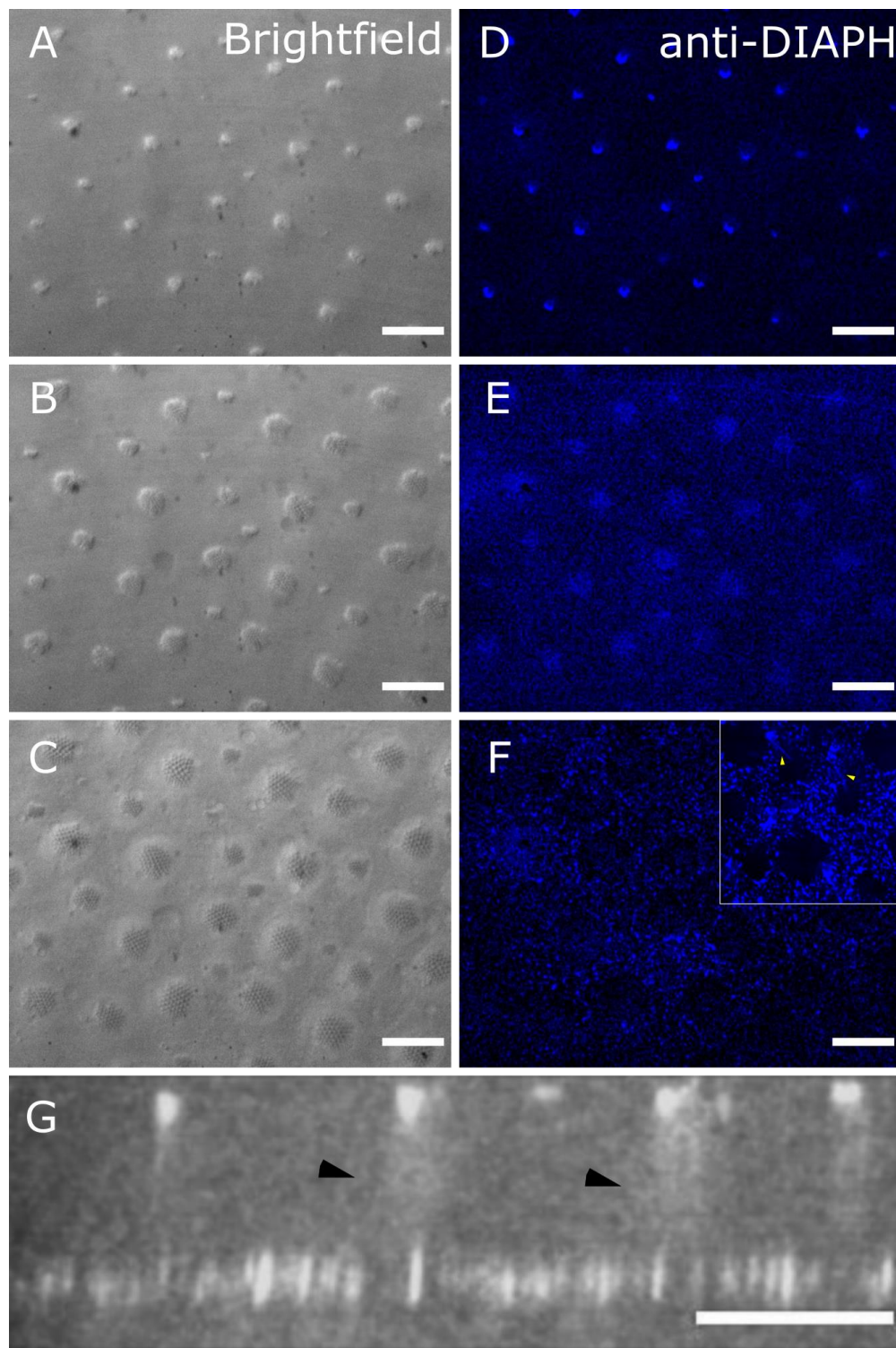
Figure III-22: LABELLING FORMINS IN FROG SACCULAR HAIR BUNDLES. Brightfield microscopy of the sensory epithelium along the hair-bundle height: **(A)** at the tip, **(B)** in the middle of the hair-bundle, and **(C)** at the apical surface. **(D-F)** Confocal images at the same z-positions as in (A-C). The inset image in **(F)** shows the labelling of the kinocilia both along their shafts and in their bulbs. **(G)** Labelling by Alexa Fluor 594-conjugated anti-DIAPH1 along the hair-bundle height. The immunoreactivity appeared at the kinociliary bulb, the hair bundle (see arrows), and the numerous microvilli of the supporting cells. The x-z slice was generated from a 3D projection of confocal image stacks in the x-y plane. The x-y confocal images were acquired from wholemount tissues. Scale bar 10 µm.

After detaching the kinocilium from the hair bundles, the antibody clearly labelled the stereociliary tips and the labelling appeared as broad puncta in all stereociliary rows (Fig. III-23). In a few stereocilia, I also observed labelling slightly further down the tip of the stereocilia (Fig. III-23.G). These observations suggest that there are formin homologs in the stereocilia of frog saccular hair bundles.
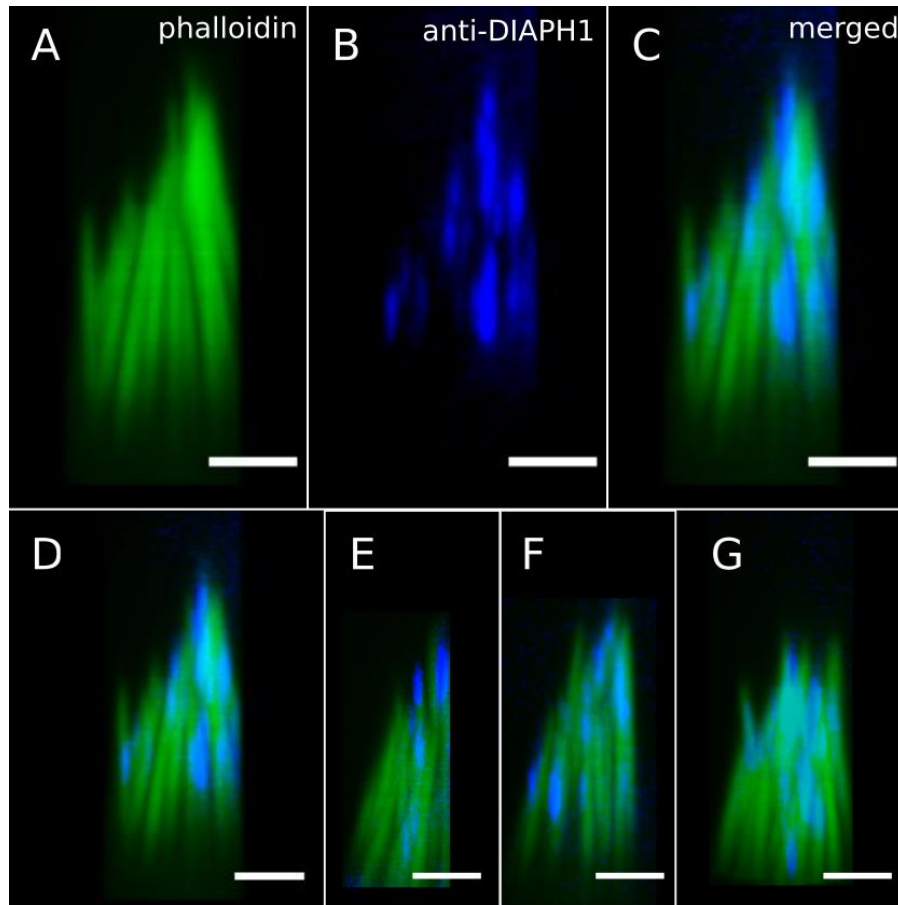
Figure III-23: IMMUNOLOCALISATION OF FORMINS AT THE TOPS OF THE FROG SACCULAR HAIR BUNDLES. (A) Labelling of actin filaments by Alexa Fluor 488-conjugated phalloidin (green). **(B)** Labelling by Alexa Fluor 594-conjugated anti-DIAPH1 (blue). The immunoreactivity appeared mostly at the stereociliary tips. **(C)** The merged image was generated from (A) and (B). **(D-H)** Different hair bundles labelled with Alexa Fluor 488-conjugated phalloidin and Alexa Fluor 594-conjugated anti-DIAPH1. These x-z slices were generated from a 3D projection of confocal image stacks in the x-y plane. The x-y confocal images were acquired from wholemount tissues. Scale bar (A-G) 3 µm.

C.2 Effects of formin inhibition on hair-bundle morphology

By exposing the hair bundles to the generic formin inhibitor SMIFH2 (for 1 hr at 250 µM), I aimed at testing whether reducing formin activity resulted in modifications of the hair-bundle morphology. At first glance, the hair bundles looked just like those under control conditions (Fig. III-24.A). However, some hair bundles, about 14% or 10 from 70 hair bundles observed, clearly

displayed stereocilia with abnormally thin tips and wavy stereociliary tapers (Fig. III-24.B-E). Such morphological abnormalities were never observed in the control. In these hair bundles, the shape of the abnormal stereocilia was not biconical anymore, with irregular variations of the stereociliary diameter along the height.
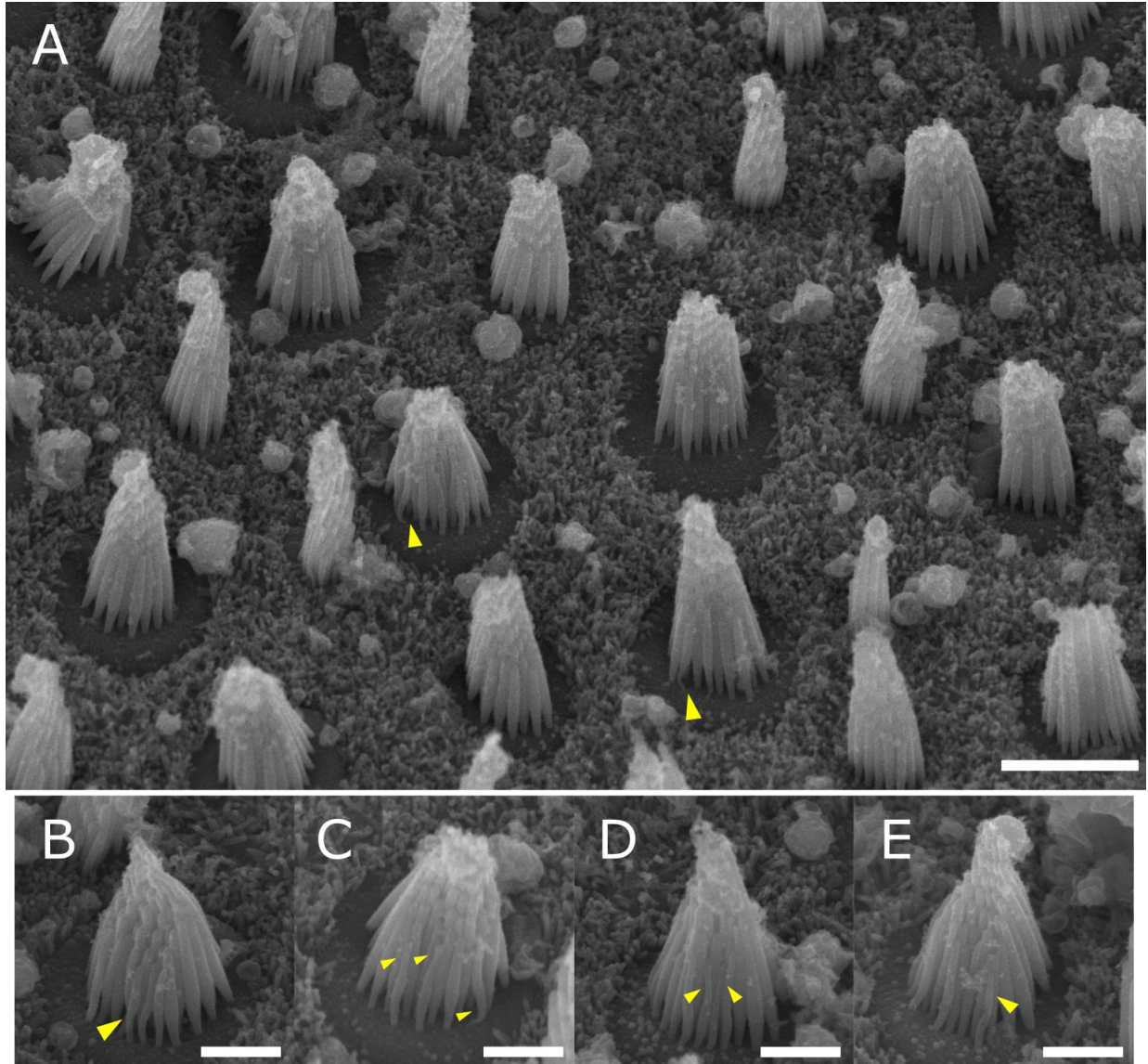
Figure III-24: EFFECTS OF FORMIN INHIBITION ON HAIR-BUNDLE MORPHOLOGY. (A) Scanning electron micrograph of the sensory epithelium after incubation for 1hr in 4-mM Ca2+ perilymph supplemented with the formin inhibitor SMIFH2 at a concentration of 250 μM. Some hair bundles (arrowheads) show stereocilia with abnormally thin tips and wavy tapers. Scale bar 5 μm. **(B-E)** Scanning electron micrographs of hair bundles with unusually thin stereociliary tips and wavy stereocilia (arrowheads). Scale bar (B-E) 3 μm.

In the shortest row of stereocilia, where stereocilia are most easily visualized, the mean of the stereociliary width measured at the taper's top did not change in the presence of SMIFH2, with taper-width values of 350 ± 50 nm ($N = 35$ stereocilia from 29 cells) in the control and of $342 \pm$

68 nm (N = 97 stereocilia from 44 cells) in the presence of the drug (Fig. III-25). The standard deviation was, however, significantly larger after exposure to formin inhibitor (p-value < 0.05). Similar to the stereociliary width measured at the taper's top, although the mean value of the width at the stereociliary tips did not change, the standard deviation was significantly larger after exposure to the formin inhibitor (Fisher's test: p-value < 0.001), with tip-width values of 285 ± 35 nm (N = 45 stereocilia from 26 cells) in the control and of 275 ± 61 nm (N = 44 stereocilia from 25 cells) in the presence of the drug (Fig. III-25).
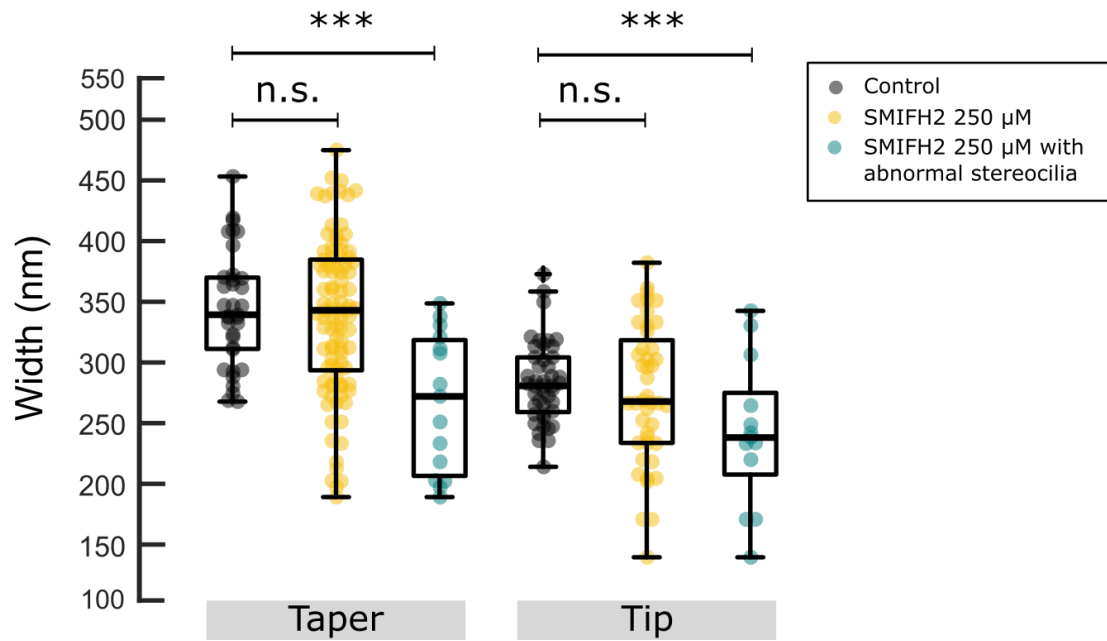
Figure III-25: STEREOCILIA THINNING UPON EXPOSURE TO FORMIN INHIBITOR. Stereocilia thinning observed in some hair bundles resulted in larger variability of stereociliary widths measured at the taper's top (p-value < 0.05) and the stereociliary tip (p-value < 0.001) but the mean width values were not statistically different. However, after restricting the analysis to the hair bundles with clear morphological abnormalities upon visual inspection, stereocilia thinning in the taper region and at the stereociliary tips were significantly different (p-value < 0.001). Statistical significance was tested with Student's t-test, * for p-value ≤ 0.1, ** for p-value ≤ 0.01, and *** for p-value ≤ 0.001, whereas N.S. (non-significance) is for p-value > 0.05.

Because morphological abnormalities were clearly observed in a small fraction (14%) of the hair bundles only, ensemble averages failed to reflect these abnormalities in mean values of the stereociliary width. However, the increased variance of taper-width and tip-width values betrayed an effect of formin inhibition. In addition, restricting the analysis to the hair bundles with clear morphological abnormalities upon visual inspection, stereocilia thinning in the taper region and at the stereociliary tips became obvious. The stereociliary width measured at the taper's top reduced from 350 ± 50 nm (N = 35 stereocilia from cells 29 cells) in the control to 268 ± 60 nm (N = 15 stereocilia from 5 cells) while the tip-width reduced from 285 ± 35 nm (N = 13 stereocilia from 5 cells) in the control to 241 ± 64 nm (N = 13 stereocilia from 5 cells). I had observed earlier that blocking the transduction channels evoked widening of the stereocilia (Fig. III-10).

Remarkably, blocking the transduction channels in the presence of SMIFH2 resulted in no clear morphological defect (Fig. III-26.A-C). In particular, the stereociliary width remained, on average, the same as under control conditions. Thus, blocking the channels and inhibiting formin had antagonistic effects (Fig. III-26.D). In the shortest stereocilia, the stereociliary width measured at the taper was 386 ± 40 nm ($N = 17$ cells) in the control and 350 ± 43 ($N = 20$ cells) when blocking the transduction channels in the presence of SMIFH2.
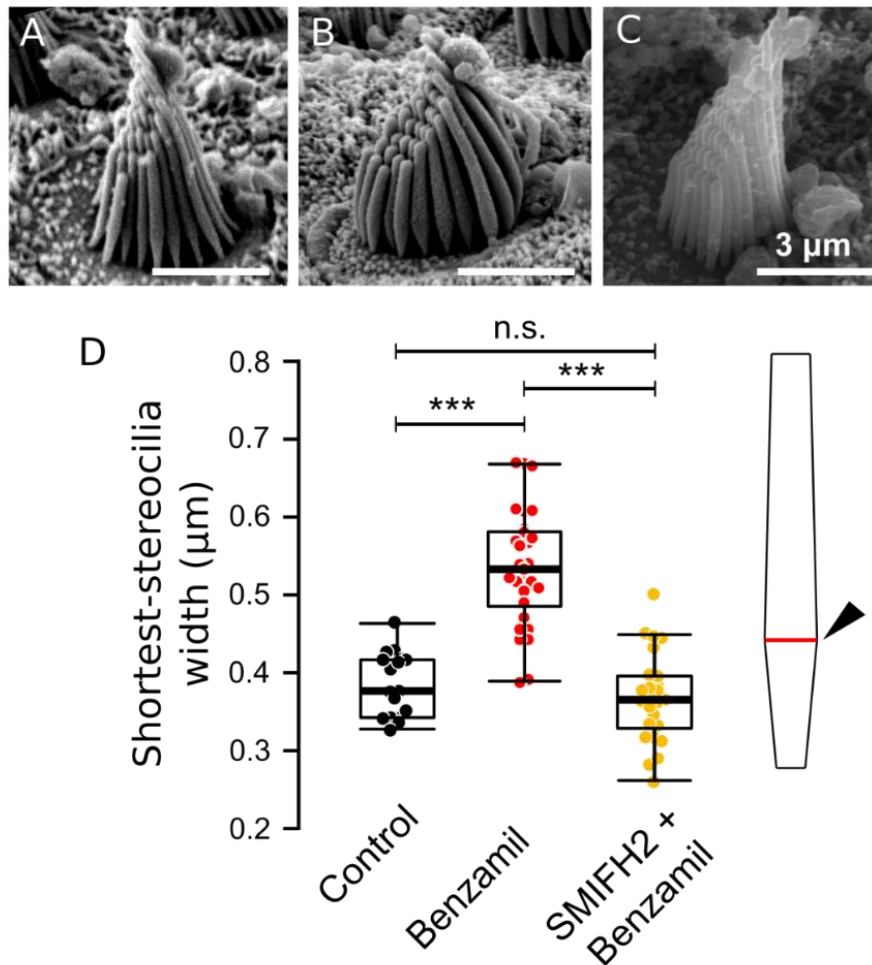
Figure III-26: EFFECTS OF FORMIN INHIBITION IN THE PRESENCE OF TRANSDUCTION CHANNEL BLOCKERS. Scanning electron micrographs of hair bundles from **(A)** the control **(B)** after 1 hr incubation in the channel blocker benzamil, and **(C)** after 1 hr incubation in benzamil with the presence of the formin inhibitor SMIFH2. **(D)** Co-application of benzamil in the presence of SMIFH2 at 250 µM produced antagonist effects resulting in the stereociliary width with similar dimensions to the control. Statistical significance was tested with Student's t-test, * for p-value ≤ 0.1, ** for p-value ≤ 0.01, and *** for p-value ≤ 0.001, whereas N.S. (non-significance) is for p-value > 0.05.

Altogether, our observations can be reconciled if the widening of the stereocilia upon blocking of the transduction channels had resulted from nucleation of new actin filaments and incorporation in the actin core of the stereocilia via a formin-dependent pathway. Within this simple framework,

the activity of formin would be enhanced by a reduction of the Ca^{2+} influx through the transduction channels, which is expected to happen both when the channels are blocked or when the tip links are disrupted. Under control conditions, formin activity would be low, so that formin inhibition would not result in dramatic remodelling of the stereocilia (Fig. III-24). However, as also observed in other species (Vélez-Ortega et al. 2017; Krey et al. 2020), blocking the transduction channels or disrupting the tip links results in remodelling of the stereocilia—here mostly stereociliary widening, demonstrating that actin dynamics is turned on by such perturbation, possibly via the increased activity of formins.

Chapter 4

IV.   Discussion and Conclusions

In this thesis, using hair cells in an excised preparation of the saccule from the inner ear of adult frogs, I studied the effects of blocking the transduction channels and, to a lesser extent, of disrupting the tip links on the morphology of the hair bundle. Adding to the available evidence in mouse and rat cochlear hair cells (Caberlotto et al. 2011; Vélez-Ortega et al. 2017; Krey et al. 2020), my observations confirm the existence of a feedback mechanism between the morphology of the hair bundle and mechanoelectrical transduction by the hair bundle. Yet, as discussed below, hair bundles in adult frogs responded differently to perturbations of mechanotransduction than hair bundles in neonatal mice or rats, providing new insight into this feedback mechanism.

Only one hour after exposing the hair cells to a drug blocking the transduction channels or after disrupting the tip links, I observed dramatic remodelling of the hair bundle. The stereocilia became substantially wider and only slightly shorter. As a result, the volume of the stereocilia increased and the hair bundle occupied a larger space at the apical surface of the hair cell. Stereocilia widening was associated with increased spacing of the stereociliary insertions, which also increased in diameter. Interestingly, the effect was not confined to the hair bundle only. I also observed that the actin-rich apical surface of the hair cell—corresponding to the cuticular plate—expanded, whereas the cell body did not.

Using transmission electron microscopy to characterize the ultrastructure of the actin core of the stereocilia, I found that spacing between neighbouring actin filaments within the parallel network remained the same as the stereocilia got wider. This key observation led to the conclusion that stereocilia widening must have resulted from the incorporation of additional actin filaments in the stereociliary core rather than from an increase of the inter-filament spacing. As a result of the observed morphological changes, the stiffness of the hair bundles nearly doubled. Although direct evidence is lacking (we looked at the actin ultrastructural organization in the stereociliary shafts only), stiffening is likely to have resulted from an increased number of actin filaments contributing to the stereociliary rootlets, as suggested by the increased diameter of the stereociliary insertions.

In addition, we gathered evidence implicating actin nucleators belonging to the formin family in the process that led to the remodelling of the stereocilia—stereociliary widening—upon blocking of the transduction channels. First, immunolabelling of actin nucleators belonging to the formin family showed localization at the tips of the stereocilia and in the numerous microvilli of the supporting cells. Because labelling was also observed in kinocilia, which to our knowledge do not contain actin filaments, and because we could not perform a control experiment with a formin knockout frog, we cannot strictly exclude (at least some) non-specific binding of the antibody. Any conclusion from our immunolabelling data must thus be taken with some caution. However, several members of the formin family have been shown to bind to microtubules (Zhou, Leder, and Martin 2006; Rosales-Nieves et al. 2006; Bartolini et al. 2008; Young et al. 2008). There is also evidence that formins may regulate microtubule-dependent processes such as meiotic spindle alignment and chromosome congression at mitosis (Bartolini et al. 2008; Leader et al. 2002; S. Yasuda et al. 2004). Formin binding was shown to stabilize microtubules by preventing depolymerisation and also to foster microtubule bundling, at least *in vitro* (Bartolini et al. 2008). Thus, localizing immunolabeling of formins in kinocilia of hair bundles might not be so surprising after all. In addition, in my work, inhibiting formin activity led to two additional observations that give credit to the implication of formins in regulating actin dynamics in the hair bundle.

First, exposing the hair cells to a formin inhibitor resulted in stereocilia with thinner tips and wavy tapers. However, these effects were clear in a small fraction of the hair bundles only, whereas most of the hair bundles remained seemingly unaffected. This behaviour may indicate that formin activity is quiescent in most but not all hair bundles under control conditions, so that inhibiting activity only marginally affects the hair-bundle morphology. This inference is consistent with the available evidence from other species, for instance in American bullfrog saccular hair bundles and mouse utricular hair bundles (Zhang et al. 2012), indicating that the actin core of the stereocilia is stable under control conditions. Second, and quite remarkably, blocking the transduction channels in the presence of the formin inhibitor did not affect the hair-bundle morphology, in striking contrast with our observations in the absence of the inhibitor. Blocking the channels and inhibiting formins thus had antagonistic effects. If widening happened as a result of actin nucleation by formins, then it would make sense that inhibiting formins would have an antagonistic effect (lower formin activity and thus reduce actin nucleation) to blocking the channels (incorporation of new actin filaments in the stereociliary core by increasing formin activity). By introducing formins as a possible player in the complex machinery that controls and maintains the morphology of the hair bundle, this work opens a novel avenue for future research.

Altogether, our observations implicate formins in the pathway that ensures maintenance of stereocilia. Within this framework, formins are expected to be quiescent under control conditions but their activity ought to increase when the transduction channels are blocked by a channel blocker or close upon of tip-link disruption, likely by reducing the Ca^{2+} influx through the transduction channels is interrupted (Vélez-Ortega et al. 2017).

The following discussion is organized into two sections. First, I discuss what I learned about the morphology of the hair bundle and the ultrastructure of its actin core under control conditions in relation to published data with hair bundles from the American bullfrog. Second, I further discuss the effects of blocking the transduction channels or disrupting the tip links on the morphology of the hair bundle, speculating on possible control mechanisms of actin dynamics in the hair bundle.

A. Comparing Rivan 92's to American bullfrogs' hair bundles

Hair bundles of the frog Rivan 92 are smaller and more compact: Compared to hair bundles of the American bullfrog, hair bundles of the frog Rivan 92, the animal model used in this thesis, are smaller and more compact. In particular, the stereociliary spacing (~490 nm) and the number of stereocilia (~33) measured here were about half those reported in American bullfrogs (Jacobs and Hudspeth 1990). A typical hair bundle of the frog Rivan 92 also showed a non-monotonic variation of stereociliary widths along the bundle's axis of mechanosensitivity: the width increased from the shortest stereociliary row toward the middle rows, before decreasing from the middle rows toward the tallest row. This morphological feature may be species-specific, or at least more pronounced in this species, for scanning and transmission electron micrographs of American bullfrogs' hair bundles showed stereocilia with more similar widths across rows (Jacobs and Hudspeth 1990). Individual stereocilia of Rivan 92's hair bundles also showed biconical shapes rather than cylindrical shapes with a conical taper. Nevertheless, these differences in morphology do not seem to contribute to a large difference in hair-bundle stiffness. I found a similar hair-bundle stiffness, ~640 $\mu N \cdot m^{-1}$, in Rivan 92 as those reported for bullfrog's hair bundles under the same ionic condition (Marquis and Hudspeth 1997).

Dimorphism of saccular hair cells: Based on the diameter of their apical surface in the central region of the saccular macula, I could distinguish "small" and "large" hair cells. This dimorphism likely corresponds to the two types of hair cells previously described in American bullfrogs (Chabbert 1997) as the Central Flask-shaped Hair Cells (CFHCs) and the Central Cylindrical Hair Cells (CCHCs), which are endowed with small and large hair bundles, respectively (Fig. IV-1)[10]. The diameter of these cells' apical surface, 5-7 μm for CFHCs and 8-11 μm for CCHCs, are slightly larger in bullfrogs than in Rivan 92 frogs, for which I measured diameter of ~3 μm for small hair cells of ~6 μm for large hair cells. Although these diameters were measured with fresh tissues in the first case and with chemically fixed tissues in the second, the difference in size remains significant even after correction for the 30% shrinkage that is expected in fixed tissues (Gale, Meyers, and Corwin 2000). CCHCs and CFHCs have been shown to be endowed with distinct physiological properties, specifically larger Ca^{2+} conductance in the soma of CCHCs and distinct distribution of different types of intracellular Ca^{2+} buffers (Chabbert 1997; Heller et al.

---

[10] Chabbert (1997) also described another type of hair cells localized along the periphery of the sensory epithelium, called the peripheral elongated hair cells (PEHCs). The PEHCs can be identified by their elongated kinocilia. In this study, I worked only within the central region of the sacular macula and therefore no peripheral elongated hair cells were included.

2002; Edmonds et al. 2000; Yamoah et al. 1998). In particular, the distribution of the plasma membrane Ca^{2+} ATPase (PMCA), the transmembrane protein in charge of actively pumping Ca^{2+} ions from inside the hair bundle to the extracellular medium, is more homogeneously distributed along the height of the hair bundle of large CCHCs than small CFHCs, where PMCA are more localized near the tips and just above the taper region (Yamoah et al. 1998). Although there is no quantification for the density of PMCA for each hair-cell type[11], having more Ca^{2+} pumping would lower the intracellular Ca^{2+} concentration. Based on our observations, a lower intracellular Ca^{2+} concentration would be expected to result in wider stereocilia.
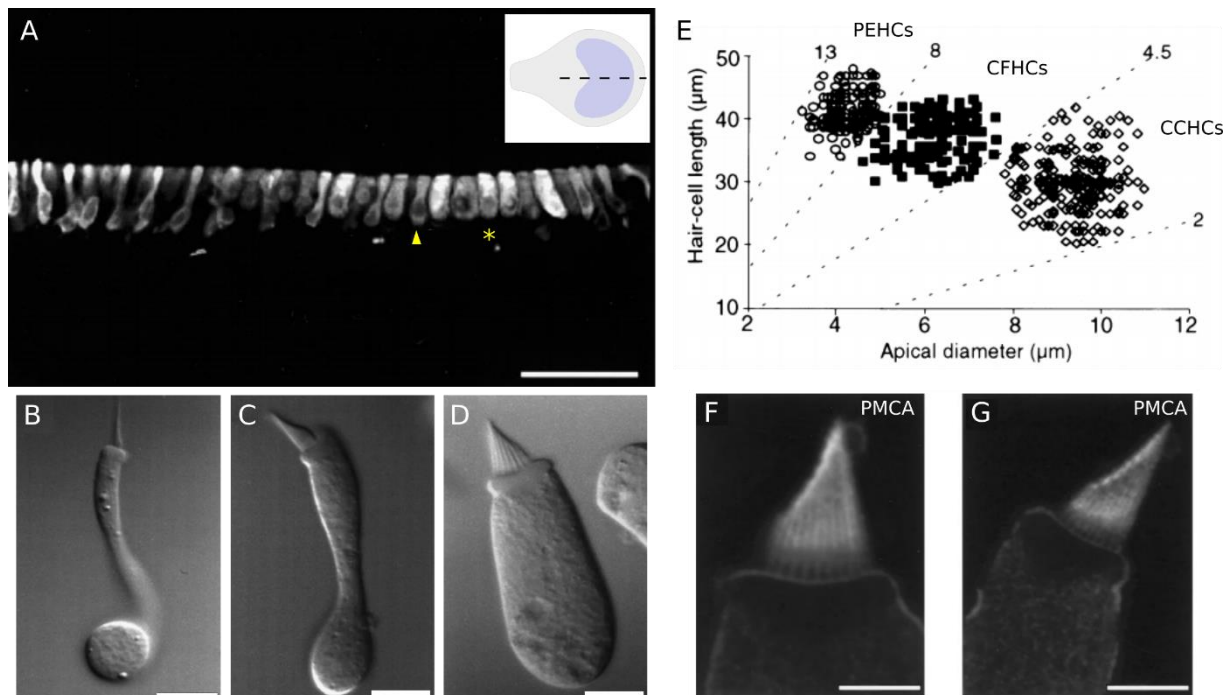
Figure IV-1: DIMORPHISM OF FROG SACCULAR HAIR CELLS IN THE CENTRAL REGION OF THE MACULA. (A) An optical section across the middle of the saccular macula (as indicated in an inset image). Hair cells are immuno-stained against S-100, small EF-hand Ca^{2+} binding proteins that are enriched in the cytoplasm of frog hair cells. There are two types of hair cells in the central region of the macula: Central Flask-shaped Hair Cells (CFHCs, see arrowhead) and Central Cylindrical Hair Cells (CCHCs, see asterisk). At the edge of the macula (on the left), are Peripheral Elongated Hair Cells (PEHCs). Light micrographs of **(B)** PEHCs, **(C)** CFHCs, and **(D)** CCHCs at a higher magnification. **(E)** The three types of hair cells are well distinguished when hair-cell lengths are plotted as a function of the cell's apical diameters. Fluorescence immunolabelling of plasma membrane Ca^{2+} ATPase or PMCA in the hair bundles of **(F)** a central cylindrical hair cell and **(G)** and a central flask-shaped hair cell. Scale bar (A) 60 µm, (B-D) 10 µm, and (F-G) 5 µm. Figures (A-E) adapted from (Chabbert 1997). Figures (F-G) adapted from (Yamoah et al. 1998).

Square and hexagonal stereociliary packing: In the frog Rivan 92, I observed two types of stereociliary packing at the stereociliary insertions: square and hexagonal. There was also a strong correlation between the hair-bundle type and the stereociliary packing, with small (probably

---

[11] The average density of PMCA of a hair cell is about 2,000 molecules per µm^2 (Yamoah et al. 1998).

CFHCs) and large (probably CCHCs) hair bundles showing hexagonal and square packing, respectively. To my knowledge, only hexagonal packing was reported in American bullfrogs or other animals. For instance, the stereociliary insertions of chick cochlear hair bundles were reported to show only hexagonal packing (Lewis G Tilney and Saunders 1983). Because hexagonal packing emerges naturally when forcing parallel cylindrical rods together, the insertions of smaller hair bundles may have been distributed on a hexagonal lattice because their thin (and more cylindrical?) stereocilia are tightly packed. With thin and tightly packed stereocilia, the convexity of the cuticular plate may not be high enough to exert a mechanical constraint on the stereocilia, and push their base away from one another. However, even if the wider stereocilia of large hair bundles are more loosely packed, the reason why their insertions adopt square packing is unclear. Perhaps, with square packing, where the number of nearest neighbours is smaller (4 neighbours instead of 6 in hexagonal packing), the loosely packed hair bundles may require fewer inter-stereociliary links at the ankle regions. The implication of the types of insertion packing for hair-bundle mechanics would deserve further investigation.

Liquid packing of actin filaments in the stereociliary core: To my knowledge, no systematic description of the stereociliary actin core has been made in American bullfrogs. However, liquid packing of actin filaments has been observed in stereocilia of other species, such as in mouse inner hair cells (Mogensen, Rzadzinska, and Steel 2007), in mouse utricular hair cells (Krey et al. 2016), and in lizard cochlea hair cells (L G Tilney, Derosier, and Mulroy 1980). In contrast, chick cochlea and utricles exhibit hexagonal packing of actin filaments in their stereocilia.
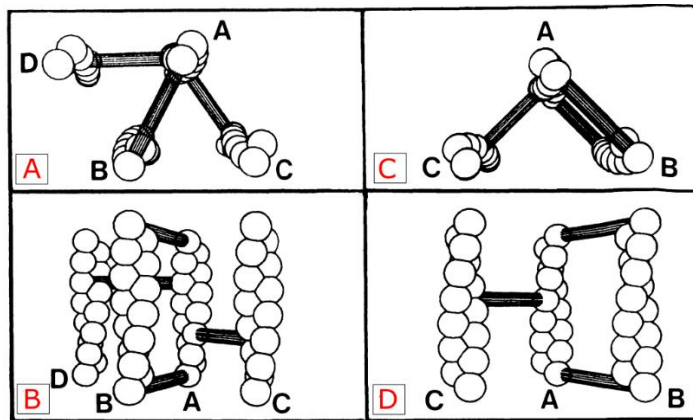
Figure IV-2: BONDING IN ACTIN BUNDLES. In the simplest model where there is only one type of cross-linkers and that the cross-link must be formed with another actin filament within the multiples of either **(A-B)** 60° (hexagonal packing) or **(C-D)** 90° (square packing), there should be 3 cross-linkers per repeat in hexagonal packing as shown in **(B)** and 2 cross-linkers per repeat in tetragonal packing as shown in **(D)**. Liquid packing, which is an intermediary between square and hexagonal packing, has on average 2.5 cross-linkers per repeat. Figure adapted from (DeRosier and Tilney 1984).

Liquid packing observed here in the stereociliary core of the frogs Rivan 92 or elsewhere in other species has been proposed to be advantageous (Krey et al. 2016). First, liquid packing is expected to reduce by about 20% the maximal number of cross-linkers to interconnect the filaments compared to hexagonal packing (DeRosier and Tilney 1984) (Fig. IV-2). In addition,

forming a paracrystal with hexagonal packing is expected to twist the filaments, imposing internal mechanical stress that may result in more fragility in response to vibrations of the hair bundle (R. Yasuda, Miyata, and Kinosita 1996). This is because adjacent filaments are not optimally positioned to be bridged by a cross-linker, which then must be twisted to allow a (rigid) crosslink to form (DeRosier and Tilney 1984; Claessens et al. 2008). Interestingly, hexagonal packing is observed in *Pls1* knockout mice, for which ESPN—a short and thus rigid molecule—provides the main crosslinker (Krey et al. 2016).

B. Stereocilia widening and shortening upon perturbation of the mechano-electrical transduction machinery

Based on previous observations with mammalian (mouse) hair bundles (see Fig. 5 in (Vélez-Ortega et al. 2017)), I expected to see *thinning* of the stereociliary tips after blocking the transduction channels for only 1 hr. To my surprise, I instead observed dramatic *widening* of the stereocilia and in turn of the hair bundle as a whole. Because widening was associated with only moderate shortening of the stereocilia, the stereociliary volume increased by 60 - 100% in the stereocilia of the shortest row. Disrupting the tip links evoked qualitatively similar morphological effects. Under both conditions, the stereocilia widened in all rows and the stereocilia shortened, except those of the tallest row. The increase in stereociliary volume was, however, more pronounced upon blocking the transduction channels (+36 to 60% in experiments using benzamil; Fig. III-10 and III-12) than upon disrupting the tip links (+16%). With the transduction channels blocked, tip-link tension is expected to remain and even to increase (Hacohen et al. 1989; Hudspeth and Gillespie 1994a; Tobin et al. 2019), pulling on the membrane of the stereociliary tips, whereas there is obviously no tension in the tip links after tip link disruption. Tension at the stereociliary tips, where G-actin incorporation to the F-actin core most likely happened, may have favoured actin polymerization. Interestingly, in line with our observations indicating that formins might be involved (Section III.C in the Results, p. 99 - 105), applying a pulling force to the mammalian formin mDia1 was shown to increase the elongation rate of actin filaments by about two-fold[12], demonstrating that formins can be mechanosensitive (Jégou, Carlier, and Romet-Lemonne 2013; M. Yu et al. 2017). Perhaps, the tension in the tip links is necessary to fully activate formin-based actin polymerization upon blocking the transduction channels.

---

[12] Of note, the magnitude of pulling force in this experiment (~ 10 pN) (Jégou, Carlier, and Romet-Lemonne 2013) is within the lower range of resting tip-link tension in bullfrogs (8-20 pN) (Alonso et al. 2020).

Blocking the transduction channels in cochlear hair bundles from mice about one week of age has been reported to result first in thinning of the stereociliary tips within the first few hours after application of the channel blocker, leading to shortening of the stereocilia in the short and middle rows of the hair bundle (which harbour transduction channels), but not of the tallest row (which do not), after about 24 hrs of cell culture (Vélez-Ortega et al. 2017). On the basis of these observations and others, it was proposed that Ca^{2+} entry through the transduction channels regulates elongation of the stereocilia and that functional channels are necessary to ensure the stability of the hair-bundle morphology. Blocking the Ca^{2+} influx led to a *reduction* of the stereociliary volume (less actin), with no obvious change in the stereociliary width but instead shortening of the stereocilia. Remarkably, repeating similar experiments with saccular hair cells from adult frogs led to markedly different observations. I did observe some shortening of the stereocilia (Fig. III-10 and III-13) but this effect was offset by a dramatic increase of the stereociliary width, resulting in an *increase* of the stereociliary volume (more actin). Of course, we worked in different organs (a hearing organ (cochlea) *versus* a vestibular organ (saccule)), species (rat/mouse *versus* frog) and at different maturation stages (immature (P6) cochlea in rat/mouse *versus* adult saccules in frog) than in the published study.

Due in particular to the availability of genetic tools, our understanding of the molecules involved in stereocilia development and maintenance is much more advanced in the mammalian cochlea (see Table I-1 in the Introduction, p. 48) than in the frog saccule. It remains possible that the two types of hair bundles react differently to blocking the transduction channels simply because the molecular players underlying actin dynamics are different. For instance, it may be that formins control actin dynamics in hair bundles of the frog saccule, as our data suggest and as observed in other actin-based protrusions such as filopodia and dendritic spines (Ljubojevic, Henderson, and Zurzolo 2021) (see Fig. I-29 in the Introduction, p. 51), but not in mammalian hair bundles. There, no actin nucleators have yet been implicated. Instead, ESP8/WHRN/MYO15-A are known to be the main proteins of the stereocilia tip complex, although other proteins such as capping proteins (CAPZ/TWF2 and severing proteins (ADF/CFL1) also play a role (Krey et al. 2020; Peng et al. 2009; McGrath et al. 2021) (see Fig. I-19 in the Introduction, p. 36).

In a simple scenario, blocking the transduction channels in frog hair bundles would result in increased tension at the stereociliary tips, enhancing the activity of formins there and resulting in an increased rate of actin elongation (Jégou, Carlier, and Romet-Lemonne 2013). Because the processivity of the formin is reduced by several orders of magnitudes upon application of

piconewton tensile forces, one would also expect polymerization of shorter filaments (Cao et al. 2018). However, one should bear in mind that stereocilia in the tallest row also widen although there is no tension applied at their tips. In addition, widening is also observed, upon disrupting the tip links, albeit with a smaller magnitude, which releases tension in the tip links (Jaramillo and Hudspeth 1993; Tobin et al. 2019). Thus, tip-link tension may play an important role but is not sufficient, by itself to explain the data. As already demonstrated in mammalian hair bundles (Vélez-Ortega et al. 2017; Krey et al. 2020), it is likely that the Ca^{2+} influx through the transduction channels is key.

What could be the possible target of Ca^{2+} ions entering the stereocilia through the transduction channels? Although to our knowledge, the activity of formins does not directly depend on Ca^{2+}, formin-dependent assembly of a perinuclear actin rim in NIH3T3 cell, has been shown to be triggered by an *increase* in the intracellular Ca^{2+} concentration, (Shao et al. 2015). However, this effect is opposite to that required in our experiments, where incorporation of new actin filaments results from a *decrease* of the Ca^{2+} influx through the transduction channels. The severing protein cofilin has been shown to be (indirectly) activated by Ca^{2+} (Yan Wang, Shibasaki, and Mizuno 2005), likely increasing the availability of G-actin and free barbed ends of F-actin for polymerization (Yan Wang, Shibasaki, and Mizuno 2005). This observation is consistent with the larger availability of free barbed ends in stereocilia of row 2 in cochlear inner hair cells, which harbour transduction channels providing a Ca^{2+} influx at the stereociliary tips and also show a larger concentration of ADF/CFL1, compared to the non-transducing stereocilia in row 1 (Fig. I-34 in Introduction, p. 58). Blocking the transduction channels in these hair cells results in a redistribution of ADF/CFL1 between the two rows of stereocilia as well as of the free barbed ends of actin filaments, but again with no obvious change in stereociliary width (McGrath et al. 2021). Interestingly, the same study revealed that the loss of both ADF and CFL1 (double knockout) leads to the widening of row-3 stereocilia in inner hair cells and of stereocilia in all rows in outer hair cells. This surprising phenotype qualitatively resembles that observed upon blocking the Ca^{2+} influx in saccular hair bundles from adult frogs, which would make sense if cofilin were deactivated at low Ca^{2+} levels (in frog) to mimic the effect of a knockout (in mouse). Of note, actin filaments fully decorated by ADF/cofilin undergo depolymerisation from both ends even in the presence of capping proteins and actin monomers (Wioland et al. 2017). Reducing the levels of these proteins may thus, counterintuitively, lead to the presence of more actin filaments.

Another putative target of Ca^{2+} ions might be the myosin motors that pull on the tip links to set the resting open probability of the transduction channels (Fig. I-10 in the Introduction, p. 21), as well as those implicated in the transport of actin-binding proteins to the stereociliary tips (Fig. I-19 in the Introduction, p. 36). In hair cells from the frog saccule, myosin 1c has been implicated as the motor pulling on the tip links (Hudspeth and Gillespie 1994a). The motor's activity is thought to be regulated by Ca^{2+} via the calmodulin-binding IQ domains of the motor's neck: Ca^{2+} binding to calmodulin is expected to release calmodulin from myosin, increasing the flexibility of the neck and reducing active force production by the motor. Conversely, blocking the Ca^{2+} influx through the transduction channels would increase the activity of the motors and in turn tip-link tension. As mentioned earlier, an increased tension at the stereociliary tips would be expected to affect the dynamics of formin-based actin polymerization. In addition, myosin 15 (MYO15A) is a major component of a protein complex at the stereociliary tips of mammalian cochlear hair bundles that is associated with the development and maintenance of the hair bundle (Section B.3 in Introduction, p. 36 - 49). The activity of MYO15A is reduced at increased calcium concentrations (Krementsov, Krementsova, and Trybus 2004), again via binding to calmodulin associated with the IQ domains in the neck of the motor. The observation that short and long isoforms of MYO15A localize predominantly in stereocilia of row 1 (not transducing - low Ca^{2+}) and row 2 (transducing - high Ca^{2+}), respectively, may be indicative of different Ca^{2+} sensitivities (Krey et al. 2020). Reducing the Ca^{2+} influx through the transduction channels is likely to modify the interplay between nucleating, capping, severing and crosslinking of actin filaments by affecting protein transport to the stereociliary tips, even in the case where tip-links are disrupted. In mutant *shaker 2* mice, which are endowed with a defective form of MYO15A, the capping protein ESP8 and severing proteins ADF/CFL1 fail to localize at the stereociliary tips (McGrath et al. 2021). It remains to be seen, however, whether MYO15A is also at work in saccular hair bundles from frogs.

Identifying the mechanisms required to specify and maintain the length, width and shape of a single actin-based protrusion, as well as their collective organization in rows of graded height within a hair bundle, still constitutes an outstanding problem (Barr-Gillespie 2015). Understanding why blocking the transduction channels in hair bundles from adult frogs results predominantly in stereocilia widening, whereas the same experiments in hair bundles from young rats or mice, predominantly result in stereocilia shortening would certainly constitute a significant step toward this goal. Our finding of a formin-dependent mechanism in frogs sheds light on the importance of actin nucleators in this process. Future experiments ought to determine how formins

modulate the localization and activity of other actin-binding proteins in the frog, as well as whether mammalian hair cells also use similar actin nucleators in the complex process of stereocilia maintenance.

Perspectives: In this work, I have introduced formins as a possible player in stereocilia maintenance. However, proteomic analysis of frog hair-bundle proteins ought to confirm the presence of formins in the stereocilia of frog saccular hair bundles. In addition, testing whether some tip-complex and row identity proteins that have been identified in mammalian hair bundles, such as ESP8, WHRN, MYO15A, and CAPZ/TWF2, are also present in frog saccular hair bundles would greatly improve our general understanding of stereocilia maintenance. Conversely, it would be desirable to test for the presence of formins and the effects of their inhibition in mammalian cochlear hair bundles. Finally, the differential effects on stereocilia widening that I observed upon blocking the transduction channels (tension at the stereociliary tips) and disrupting the tip links (no tension) may implicate a possible role of tip-link tension. A more direct study of tip-link tension on hair-bundle morphology, possibly using magnetic tweezers to pull on magnetic beads attached to the stereociliary tips or the recently developed acoustic force spectroscopy (Sitters et al. 2015), would help to elucidate the role of tip-link tension in stereocilia maintenance.

V.   Appendix

A. Lattice packing of circular disks

A

$D_{insertion}$

$S_{insertion}$

$$Packing\ Density = \left(\frac{D_{insertion}}{S_{insertion}}\right)^2 \cdot \frac{\pi}{4}$$

$$= \left(\frac{D_{insertion}}{S_{insertion}}\right)^2 \cdot 0.785$$

B

$D_{insertion}$

$S_{insertion}$

$$Packing\ Density = \left(\frac{D_{insertion}}{S_{insertion}}\right)^2 \cdot \frac{\sqrt{3}\pi}{2}$$

$$= \left(\frac{D_{insertion}}{S_{insertion}}\right)^2 \cdot 0.907$$
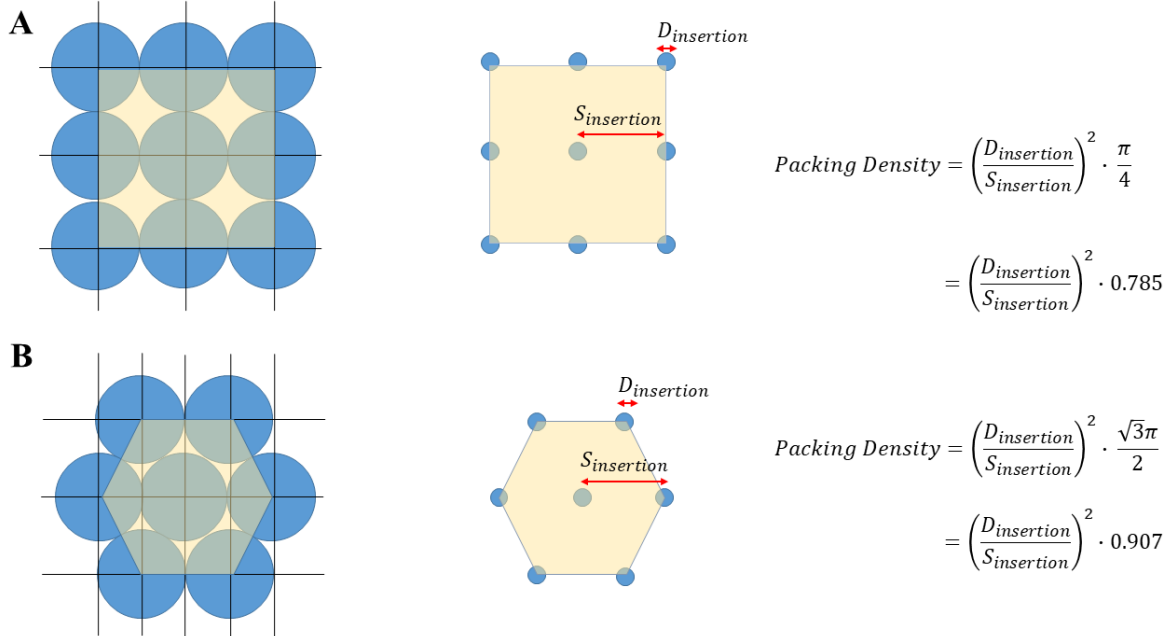
Figure V-1: PACKING OF SQUARE AND HEXAGONAL LATTICES. Lattice packing of circular disks in **(A)** square and **(B)** hexagonal lattices. In the case where the diameter of the disks is equal to that of the spacing between each disk, the packing density, defined as a fraction of the area in which the disks occupy within the lattice, is 0.79 for square packing and 0.91 for hexagonal packing.

B. Scanning electron microscopy: sample preparation

Caution: Every step must be done in a fume hood with appropriate Personal Protective Equipment (PPEs)

Fixation and staining with OTOTO		
No.	**Procedures**	**Duration**
1.	Primary fixation in **2.5% glutaraldehyde** in **0.1 M sodium cacodylate buffer** (or in DI Water)	1 hr
2.	Rinse in **0.1 M sodium cacodylate buffer**	3 x 5 min
3.	Stain in **1% osmium tetroxide (OsO₄)** in **0.1 M sodium cacodylate buffer** (OsO$_4$ is reactive to light. The media must be covered with aluminium foil.)	1 hr
4.	Rinsed in **0.1 M sodium cacodylate buffer**	3 x 5 min
5.	Stain in **0.1 M thiocarbohydrazide** (filter before use)	20 min
6.	Repeat steps 2-5 and then followed by step 3.	2 hr 20 min

Serial dehydration		
No.	**Procedures**	**Duration**
7.	• Ethanol 35% > 50% > 70% > 80% > 90% > 100%	30 min

HMDS dehydration		
No.	**Procedures**	**Duration**
8.	Submerge in **HMDS (hexamethyldisilazane)**	10 min
9.	Leave the Eppendorf tubes open for **HMDS** to evaporate	10 min

C. Transmission electron microscopy

Caution: Every step must be done in a fume hood with appropriate Personal Protective Equipment (PPEs)

C.1 Sample preparation

No.	Procedures	Duration
1.	**Primary fixation** • 2.5% Glutaraldehyde • 0.5% Paraformaldehyde • 0.5 mM CaCl$_2$ • 100 uM tannic acid **In 0.1 M Sodium cacodylate buffer, pH ~7.5**	1 hr at room temperature or overnight at 4 °C
2.	**Wash with sodium cacodylate buffer**	3 x 5 min
3.	**Primary staining: Osmication** • 1% OsO$_4$ in 0.1 M sodium cacodylate buffer	1 hr at 4 °C
4.	Rinse with sodium cacodylate buffer	3 x 5 min
5.	**Secondary staining: Uranyl acetate** • 0.5% uranyl acetate in 0.1M sodium cacodylate buffer	3 hr at room temperature
6.	**Serial dehydration** • Ethanol 35% > 50% > 70% > 80% > 90% > 100% • Acetone 100%	35 min
7.	**Epoxy infiltration**: mix B into A and turn for 10 mins + 170 µL DMAE accelerator and turn for 10 mins - Acetone 2: Epoxy 1 - Acetone 1: Epoxy 1 - Acetone 1: Epoxy 2 - Epoxy - Epoxy	 1 hr 1 hr 1 hr 1 hr Overnight
8.	**Hardening:** transfer samples into blocs and incubate at 60 °C	48 hr
9.	**Sectioning with ultramicrotome**	

C.2 Preparation of pioloform-treated grids

No.	Procedures
Prepare pioloform coated glass slides	
1.	Rinse the film caster (Fig. V-2.A) with chloroform twice to clean the glassware
2.	Pour 1 % pioloform in chloroform solution into the film caster
3.	Gently drop a clean glass and immediately release pioloform solution from the chamber at a constant rate
4.	Remove the glass slide from the film caster and store it in a glass slide holder
5.	Repeat steps 1 - 5 to prepare several glass slides. One glass slide is preferable for ~ 20 grids
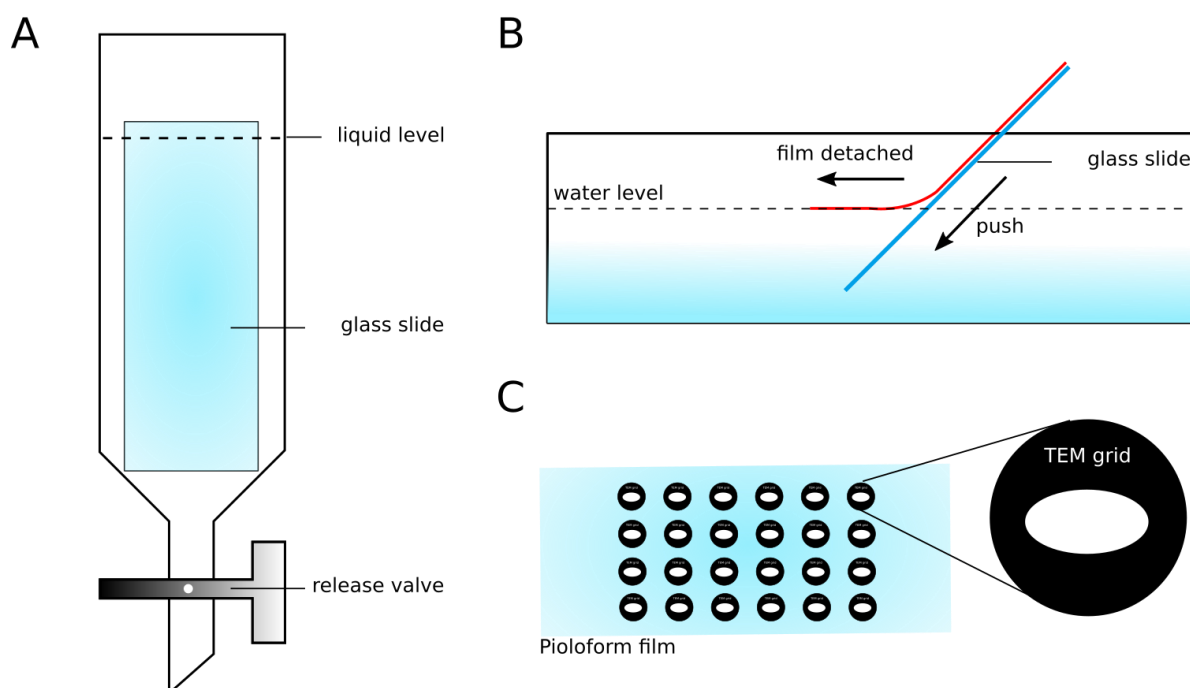
Figure V-2: PREPARATION OF PIOLOFORM-TREATED GRIDS. (A) Film caster. The 1% pioloform in chloroform solution is filled in the film caster until reaching the marked level and a clean glass slide is gently dropped into the liquid. The pioloform solution is released immediately by the release valve and when left to dry the glass slide will be coated with thin pioloform film. **(B)** Detaching the pioloform film from a glass slide by pushing the glass slide into the water. After the pioloform film is completely detached from the glass slide, the film will float on the surface of the water. **(C)** TEM grids are placed onto a floating pioloform film.

Coating TEM grids with pioloform	
No.	**Procedures**
1.	Use a razor blade to cut the edges of the pioloform film to allow for the film to detach more easily from a glass slide
2.	Prepare a water container filled with DI water
3.	Push the glass slide slowly into the water at an angle (see Fig. V-2.B). The pioloform film will start to detach from the glass slide. Continue to push the glass slide until the film is completely detached
4.	Place TEM grids (G2010-Cu, Ni, EMS, USA) onto the film in the region with homogenous thickness, usually in the middle (see Fig. V-2.C).
5.	Gently place a piece of parafilm on top of the pioloform film. When the parafilm completely covers the film, lift them out of the water.
6.	Leave them to dry in a fume hood overnight.

Bibliography

Alberts, Bruce, ed. 2008. *Molecular Biology of the Cell*. 5th ed. New York: Garland Science.

Alonso, R. G., M. Tobin, P. Martin, and A. J. Hudspeth. 2020. "Fast Recovery of Disrupted Tip Links Induced by Mechanical Displacement of Hair Bundles." *Proceedings of the National Academy of Sciences* 117 (48): 30722–27. https://doi.org/10.1073/pnas.2016858117.

Araya-Secchi, Raul, Brandon L. Neel, and Marcos Sotomayor. 2016. "An Elastic Element in the Protocadherin-15 Tip Link of the Inner Ear." *Nature Communications* 7 (1): 13458. https://doi.org/10.1038/ncomms13458.

Arruda, M V de, S Watson, C S Lin, J Leavitt, and P Matsudaira. 1990. "Fimbrin Is a Homologue of the Cytoplasmic Phosphoprotein Plastin and Has Domains Homologous with Calmodulin and Actin Gelation Proteins." *Journal of Cell Biology* 111 (3): 1069–79. https://doi.org/10.1083/jcb.111.3.1069.

Assad, John A., Gordon M.G. Shepherd, and David P. Corey. 1991. "Tip-Link Integrity and Mechanical Transduction in Vertebrate Hair Cells." *Neuron* 7 (6): 985–94. https://doi.org/10.1016/0896-6273(91)90343-X.

Avenarius, Matthew R., Jocelyn F. Krey, Rachel A. Dumont, Clive P. Morgan, Connor B. Benson, Sarath Vijayakumar, Christopher L. Cunningham, et al. 2017. "Heterodimeric Capping Protein Is Required for Stereocilia Length and Width Regulation." *Journal of Cell Biology* 216 (11): 3861–81. https://doi.org/10.1083/jcb.201704171.

Avenarius, Matthew R., Katherine W. Saylor, Megan R. Lundeberg, Phillip A. Wilmarth, Jung-Bum Shin, Kateri J. Spinelli, James M. Pagana, et al. 2014. "Correlation of Actin Crosslinker and Capper Expression Levels with Stereocilia Growth Phases." *Molecular & Cellular Proteomics: MCP* 13 (2): 606–20. https://doi.org/10.1074/mcp.M113.033704.

Aydin, Fikret, Naomi Courtemanche, Thomas D Pollard, and Gregory A Voth. 2018. "Gating Mechanisms during Actin Filament Elongation by Formins." Edited by Anna Akhmanova. *ELife* 7 (July): e37342. https://doi.org/10.7554/eLife.37342.

Banerjee, Shiladitya, Margaret L. Gardel, and Ulrich S. Schwarz. 2020. "The Actin Cytoskeleton as an Active Adaptive Material." *Annual Review of Condensed Matter Physics* 11 (1): 421–39. https://doi.org/10.1146/annurev-conmatphys-031218-013231.

Barr-Gillespie, Peter-G. 2015. "Assembly of Hair Bundles, an Amazing Problem for Cell Biology." *Molecular Biology of the Cell* 26 (15): 2727–32. https://doi.org/10.1091/mbc.E14-04-0940.

Bartles, James R., Lili Zheng, Anli Li, Allison Wierda, and Bin Chen. 1998. "Small Espin: A Third Actin-Bundling Protein and Potential Forked Protein Ortholog in Brush Border Microvilli." *Journal of Cell Biology* 143 (1): 107–19. https://doi.org/10.1083/jcb.143.1.107.

Bartolini, Francesca, James B. Moseley, Jan Schmoranzer, Lynne Cassimeris, Bruce L. Goode, and Gregg G. Gundersen. 2008. "The Formin MDia2 Stabilizes Microtubules Independently of Its Actin Nucleation Activity." *Journal of Cell Biology* 181 (3): 523–36. https://doi.org/10.1083/jcb.200709029.

Bartsch, Tobias F., Felicitas E. Hengel, Aaron Oswald, Gilman Dionne, Iris V. Chipendo, Simranjit S. Mangat, Muhammad El Shatanofy, Lawrence Shapiro, Ulrich Müller, and A. J. Hudspeth. 2019. "Elasticity of Individual Protocadherin 15 Molecules Implicates Tip Links as the Gating Springs for Hearing." *Proceedings of the National Academy of Sciences* 116 (22): 11048–56. https://doi.org/10.1073/pnas.1902163116.

Bashtanov, Mikhail E., Richard J. Goodyear, Guy P. Richardson, and Ian J. Russell. 2004. "The Mechanical Properties of Chick (Gallus Domesticus) Sensory Hair Bundles: Relative Contributions of Structures Sensitive to Calcium Chelation and Subtilisin Treatment." *The Journal of Physiology* 559 (1): 287–99. https://doi.org/10.1113/jphysiol.2004.065565.

Belyantseva, I. A., B. J. Perrin, K. J. Sonnemann, M. Zhu, R. Stepanyan, J. McGee, G. I. Frolenkov, et al. 2009. "Gamma-Actin Is Required for Cytoskeletal Maintenance but Not Development." *Proceedings of the National Academy of Sciences* 106 (24): 9703–8. https://doi.org/10.1073/pnas.0900221106.

Belyantseva, Inna A., Erich T. Boger, Sadaf Naz, Gregory I. Frolenkov, James R. Sellers, Zubair M. Ahmed, Andrew J. Griffith, and Thomas B. Friedman. 2005. "Myosin-XVa Is Required for Tip Localization of Whirlin and Differential Elongation of Hair-Cell Stereocilia." *Nature Cell Biology* 7 (2): 148–56. https://doi.org/10.1038/ncb1219.

Beurg, Maryline, Runjia Cui, Adam C. Goldring, Seham Ebrahim, Robert Fettiplace, and Bechara Kachar. 2018. "Variable Number of TMC1-Dependent Mechanotransducer Channels Underlie Tonotopic Conductance Gradients in the Cochlea." *Nature Communications* 9 (1): 2185. https://doi.org/10.1038/s41467-018-04589-8.

Beurg, Maryline, Michael G. Evans, Carole M. Hackney, and Robert Fettiplace. 2006. "A Large-Conductance Calcium-Selective Mechanotransducer Channel in Mammalian Cochlear Hair Cells." *Journal of Neuroscience* 26 (43): 10992–0. https://doi.org/10.1523/JNEUROSCI.2188-06.2006.

Beurg, Maryline, Robert Fettiplace, Jong-Hoon Nam, and Anthony J. Ricci. 2009. "Localization of Inner Hair Cell Mechanotransducer Channels Using High-Speed Calcium Imaging." *Nature Neuroscience* 12 (5): 553–58. https://doi.org/10.1038/nn.2295.

Beurg, Maryline, Wei Xiong, Bo Zhao, Ulrich Müller, and Robert Fettiplace. 2015. "Subunit Determination of the Conductance of Hair-Cell Mechanotransducer Channels." *Proceedings of the National Academy of Sciences* 112 (5): 1589–94. https://doi.org/10.1073/pnas.1420906112.

Blanchoin, L., K. J. Amann, H. N. Higgs, J. B. Marchand, D. A. Kaiser, and T. D. Pollard. 2000. "Direct Observation of Dendritic Actin Filament Networks Nucleated by Arp2/3 Complex and WASP/Scar Proteins." *Nature* 404 (6781): 1007–11. https://doi.org/10.1038/35010008.

Blanchoin, Laurent, Rajaa Boujemaa-Paterski, Cécile Sykes, and Julie Plastino. 2014. "Actin Dynamics, Architecture, and Mechanics in Cell Motility." *Physiological Reviews* 94 (1): 235–63. https://doi.org/10.1152/physrev.00018.2013.

Blanchoin, Laurent, and Thomas D. Pollard. 2002. "Hydrolysis of ATP by Polymerized Actin Depends on the Bound Divalent Cation but Not Profilin." *Biochemistry* 41 (2): 597–602. https://doi.org/10.1021/bi011214b.

Boeda, B. 2002. "Myosin VIIa, Harmonin and Cadherin 23, Three Usher I Gene Products That Cooperate to Shape the Sensory Hair Cell Bundle." *The EMBO Journal* 21 (24): 6689–99. https://doi.org/10.1093/emboj/cdf689.

Bretscher, A, and K Weber. 1980. "Fimbrin, a New Microfilament-Associated Protein Present in Microvilli and Other Cell Surface Structures." *Journal of Cell Biology* 86 (1): 335–40. https://doi.org/10.1083/jcb.86.1.335.

Bretscher, Anthony, and Klaus Weber. 1979. "Villin: The Major Microfilament-Associated Protein of the Intestinal Microvillus." *Proceedings of the National Academy of Sciences* 76 (5): 2321–25. https://doi.org/10.1073/pnas.76.5.2321.

Caberlotto, E., V. Michel, I. Foucher, A. Bahloul, R. J. Goodyear, E. Pepermans, N. Michalski, et al. 2011. "Usher Type 1G Protein sans Is a Critical Component of the Tip-Link Complex, a Structure Controlling Actin Polymerization in Stereocilia." *Proceedings of the National Academy of Sciences* 108 (14): 5825–30. https://doi.org/10.1073/pnas.1017114108.

Cao, Luyan, Mikael Kerleau, Emiko L. Suzuki, Hugo Wioland, Sandy Jouet, Berengere Guichard, Martin Lenz, Guillaume Romet-Lemonne, and Antoine Jegou. 2018. "Modulation of Formin Processivity by Profilin and Mechanical Tension." *ELife* 7 (May): e34176. https://doi.org/10.7554/eLife.34176.

Carlier, M. F., and D. Pantaloni. 1986. "Direct Evidence for ADP-Inorganic Phosphate-F-Actin as the Major Intermediate in ATP-Actin Polymerization. Rate of Dissociation of Inorganic Phosphate from Actin Filaments." *Biochemistry* 25 (24): 7789–92. https://doi.org/10.1021/bi00372a001.

Carlsson, L., L. E. Nyström, I. Sundkvist, F. Markey, and U. Lindberg. 1977. "Actin Polymerizability Is Influenced by Profilin, a Low Molecular Weight Protein in Non-Muscle Cells." *Journal of Molecular Biology* 115 (3): 465–83. https://doi.org/10.1016/0022-2836(77)90166-8.

Castrillon, D. H., and S. A. Wasserman. 1994. "Diaphanous Is Required for Cytokinesis in Drosophila and Shares Domains of Similarity with the Products of the Limb Deformity Gene." *Development (Cambridge, England)* 120 (12): 3367–77.

Chabbert, Christian H. 1997. "Heterogeneity of Hair Cells in the Bullfrog Sacculus." *Pflgers Archiv European Journal of Physiology* 435 (1): 82–90. https://doi.org/10.1007/s004240050486.

Chan, Dylan K., and A.J. Hudspeth. 2005. "Mechanical Responses of the Organ of Corti to Acoustic and Electrical Stimulation In Vitro." *Biophysical Journal* 89 (6): 4382–95. https://doi.org/10.1529/biophysj.105.070474.

Chesarone, Melissa A., Amy Grace DuPage, and Bruce L. Goode. 2010. "Unleashing Formins to Remodel the Actin and Microtubule Cytoskeletons." *Nature Reviews Molecular Cell Biology* 11 (1): 62–74. https://doi.org/10.1038/nrm2816.

Chissoe, William F., Edward L. Vezey, and John J. Skvarla. 1995. "The Use of Osmium-Thiocarbohydrazide for Structural Stabilization and Enhancement of Secondary Electron Images in Scanning Electron Microscopy of Pollen." *Grana* 34 (5): 317–24. https://doi.org/10.1080/00173139509429065.

Chou, Shih-Wei, Philsang Hwang, Gustavo Gomez, Carol A. Fernando, Megan C. West, Lana M. Pollock, Jennifer Lin-Jones, Beth Burnside, and Brian M. McDermott. 2011. "Fascin 2b Is a Component of Stereocilia That Lengthens Actin-Based Protrusions." Edited by Robin Charles May. *PLoS ONE* 6 (4): e14807. https://doi.org/10.1371/journal.pone.0014807.

Ciganović, Nikola, Amanuel Wolde-Kidan, and Tobias Reichenbach. 2017. "Hair Bundles of Cochlear Outer Hair Cells Are Shaped to Minimize Their Fluid-Dynamic Resistance." *Scientific Reports* 7 (1): 3609. https://doi.org/10.1038/s41598-017-03773-y.

Claessens, M. M. A. E., C. Semmrich, L. Ramos, and A. R. Bausch. 2008. "Helical Twist Controls the Thickness of F-Actin Bundles." *Proceedings of the National Academy of Sciences of the United States of America* 105 (26): 8819–22. https://doi.org/10.1073/pnas.0711149105.

Coffin, Allison, Matthew Kelley, Geoffrey A. Manley, and Arthur N. Popper. 2004. "Evolution of Sensory Hair Cells." In *Evolution of the Vertebrate Auditory System*, edited by Geoffrey A. Manley, Richard R. Fay, and Arthur N. Popper, 22:55–94. Springer Handbook of Auditory Research. New York, NY: Springer New York. https://doi.org/10.1007/978-1-4419-8957-4_3.

Corey, D. P., and A. J. Hudspeth. 1983. "Analysis of the Microphonic Potential of the Bullfrog's Sacculus." *Journal of Neuroscience* 3 (5): 942–61. https://doi.org/10.1523/JNEUROSCI.03-05-00942.1983.

Courtemanche, Naomi. 2018. "Mechanisms of Formin-Mediated Actin Assembly and Dynamics." *Biophysical Reviews* 10 (6): 1553–69. https://doi.org/10.1007/s12551-018-0468-6.

Courtemanche, Naomi, and Thomas D. Pollard. 2012. "Determinants of Formin Homology 1 (FH1) Domain Function in Actin Filament Elongation by Formins." *The Journal of Biological Chemistry* 287 (10): 7812–20. https://doi.org/10.1074/jbc.M111.322958.

Crawford, A C, and R Fettiplace. 1985a. "The Mechanical Properties of Ciliary Bundles of Turtle Cochlear Hair Cells." *The Journal of Physiology* 364 (1): 359–79. https://doi.org/10.1113/jphysiol.1985.sp015750.

———. 1985b. "The Mechanical Properties of Ciliary Bundles of Turtle Cochlear Hair Cells." *The Journal of Physiology* 364 (1): 359–79. https://doi.org/10.1113/jphysiol.1985.sp015750.

Cunningham, Christopher L., Xufeng Qiu, Zizhen Wu, Bo Zhao, Guihong Peng, Ye-Hyun Kim, Amanda Lauer, and Ulrich Müller. 2020. "TMIE Defines Pore and Gating Properties of

the Mechanotransduction Channel of Mammalian Cochlear Hair Cells." *Neuron* 107 (1): 126-143.e8. https://doi.org/10.1016/j.neuron.2020.03.033.

Dallos, Peter. 2008. "Cochlear Amplification, Outer Hair Cells and Prestin." *Current Opinion in Neurobiology* 18 (4): 370–76. https://doi.org/10.1016/j.conb.2008.08.016.

Delprat, Benjamin, Vincent Michel, Richard Goodyear, Yasuhiro Yamasaki, Nicolas Michalski, Aziz El-Amraoui, Isabelle Perfettini, et al. 2005. "Myosin XVa and Whirlin, Two Deafness Gene Products Required for Hair Bundle Growth, Are Located at the Stereocilia Tips and Interact Directly." *Human Molecular Genetics* 14 (3): 401–10. https://doi.org/10.1093/hmg/ddi036.

Denk, W., W. W. Webb, and A. J. Hudspeth. 1989. "Mechanical Properties of Sensory Hair Bundles Are Reflected in Their Brownian Motion Measured with a Laser Differential Interferometer." *Proceedings of the National Academy of Sciences* 86 (14): 5371–75. https://doi.org/10.1073/pnas.86.14.5371.

Denman-Johnson, Katherine, and Andrew Forge. 1999. "Establishment of Hair Bundle Polarity and Orientation in the Developing Vestibular System of the Mouse." *Journal of Neurocytology* 28 (10): 821–35. https://doi.org/10.1023/A:1007061819934.

DeRosier, David J., and Lewis G. Tilney. 1984. "The Form and Function of Actin." In *The Cytoskeleton*, edited by Jerry W. Shay, 139–69. Boston, MA: Springer US. https://doi.org/10.1007/978-1-4684-4592-3_3.

Drummond, Meghan C., Melanie Barzik, Jonathan E. Bird, Duan-Sun Zhang, Claude P. Lechene, David P. Corey, Lisa L. Cunningham, and Thomas B. Friedman. 2015. "Live-Cell Imaging of Actin Dynamics Reveals Mechanisms of Stereocilia Length Regulation in the Inner Ear." *Nature Communications* 6 (1): 6873. https://doi.org/10.1038/ncomms7873.

Ebrahim, Seham, Matthew R. Avenarius, M'hamed Grati, Jocelyn F. Krey, Alanna M. Windsor, Aurea D. Sousa, Angela Ballesteros, et al. 2016. "Stereocilia-Staircase Spacing Is Influenced by Myosin III Motors and Their Cargos Espin-1 and Espin-Like." *Nature Communications* 7 (1): 10833. https://doi.org/10.1038/ncomms10833.

Edmonds, Brian, Rosario Reyes, Beat Schwaller, and William M. Roberts. 2000. "Calretinin Modifies Presynaptic Calcium Signaling in Frog Saccular Hair Cells." *Nature Neuroscience* 3 (8): 786–90. https://doi.org/10.1038/77687.

Farris, H. E., C. L. LeBlanc, J. Goswami, and A. J. Ricci. 2004. "Probing the Pore of the Auditory Hair Cell Mechanotransducer Channel in Turtle: Pharmacology of Mechanotransduction." *The Journal of Physiology* 558 (3): 769–92. https://doi.org/10.1113/jphysiol.2004.061267.

Fay, Richard R., and Arthur N. Popper, eds. 1994. *Comparative Hearing: Mammals*. Vol. 4. Springer Handbook of Auditory Research. New York, NY: Springer New York. https://doi.org/10.1007/978-1-4612-2700-7.

———, eds. 1999. *Comparative Hearing: Fish and Amphibians*. Vol. 11. Springer Handbook of Auditory Research. New York, NY: Springer New York. https://doi.org/10.1007/978-1-4612-0533-3.

Fettiplace, Robert, and Kyunghee X. Kim. 2014. "The Physiology of Mechanoelectrical Transduction Channels in Hearing." *Physiological Reviews* 94 (3): 951–86. https://doi.org/10.1152/physrev.00038.2013.

Flock, Åke, Anthony Bretscher, and Klaus Weber. 1982. "Immunohistochemical Localization of Several Cytoskeletal Proteins in Inner Ear Sensory and Supporting Cells." *Hearing Research* 7 (1): 75–89. https://doi.org/10.1016/0378-5955(82)90082-X.

Freed, Jerome J., and Liselotte Mezger-Freed. 1970. "Chapter 2 Culture Methods for Anuran Cells." In *Methods in Cell Biology*, 4:19–47. Elsevier. https://doi.org/10.1016/S0091-679X(08)61747-1.

Furness, David N., Stuart L. Johnson, Uri Manor, Lukas Rüttiger, Arianna Tocchetti, Nina Offenhauser, Jennifer Olt, et al. 2013. "Progressive Hearing Loss and Gradual Deterioration of Sensory Hair Bundles in the Ears of Mice Lacking the Actin-Binding Protein Eps8L2." *Proceedings of the National Academy of Sciences* 110 (34): 13898–903. https://doi.org/10.1073/pnas.1304644110.

Furness, David N., Shanthini Mahendrasingam, Mitsuru Ohashi, Robert Fettiplace, and Carole M. Hackney. 2008. "The Dimensions and Composition of Stereociliary Rootlets in Mammalian Cochlear Hair Cells: Comparison between High- and Low-Frequency Cells and Evidence for a Connection to the Lateral Membrane." *Journal of Neuroscience* 28 (25): 6342–53. https://doi.org/10.1523/JNEUROSCI.1154-08.2008.

Furness, D.N., Y. Katori, S. Mahendrasingam, and C.M. Hackney. 2005. "Differential Distribution of β- and γ-Actin in Guinea-Pig Cochlear Sensory and Supporting Cells." *Hearing Research* 207 (1–2): 22–34. https://doi.org/10.1016/j.heares.2005.05.006.

Garcia, J.A., Ann G. Yee, Peter G. Gillespie, and David P. Corey. 1998. "Localization of Myosin-Iβ near Both Ends of Tip Links in Frog Saccular Hair Cells." *Journal of Neuroscience* 18(21): 8637–8647. http://doi.org/10.1523/jneurosci.18-21-08637.1998.

Gaillard, Jeremie, Vinay Ramabhadran, Emmanuelle Nemanne, Pinar Gurel, Laurent Blanchoin, Marylin Vantard, and Henry N. Higgs. 2011. "Differential Interactions of the Formins INF2, MDia1, and MDia2 with Microtubules." *Molecular Biology of the Cell* 22 (23): 4575–87. https://doi.org/10.1091/mbc.e11-07-0616.

Gale, Jonathan E., Jason R. Meyers, and Jeffrey T. Corwin. 2000. "Solitary Hair Cells Are Distributed Throughout the Extramacular Epithelium in the Bullfrog's Saccule." *Journal of the Association for Research in Otolaryngology* 1 (2): 172–82. https://doi.org/10.1007/s101620010037.

Géléoc, G. S., G. W. Lennan, G. P. Richardson, and C. J. Kros. 1997. "A Quantitative Comparison of Mechanoelectrical Transduction in Vestibular and Auditory Hair Cells of Neonatal Mice." *Proceedings. Biological Sciences* 264 (1381): 611–21. https://doi.org/10.1098/rspb.1997.0087.

Giese, Arnaud P. J., Yi-Quan Tang, Ghanshyam P. Sinha, Michael R. Bowl, Adam C. Goldring, Andrew Parker, Mary J. Freeman, et al. 2017. "CIB2 Interacts with TMC1 and TMC2 and

Is Essential for Mechanotransduction in Auditory Hair Cells." *Nature Communications* 8 (1): 43. https://doi.org/10.1038/s41467-017-00061-1.

Goldschmidt-Clermont, P. J., L. M. Machesky, S. K. Doberstein, and T. D. Pollard. 1991. "Mechanism of the Interaction of Human Platelet Profilin with Actin." *The Journal of Cell Biology* 113 (5): 1081–89. https://doi.org/10.1083/jcb.113.5.1081.

Goode, Bruce L., and Michael J. Eck. 2007. "Mechanism and Function of Formins in the Control of Actin Assembly." *Annual Review of Biochemistry* 76 (1): 593–627. https://doi.org/10.1146/annurev.biochem.75.103004.142647.

Gorelik, Julia, Andrew I. Shevchuk, Gregory I. Frolenkov, Ivan A. Diakonov, Max J. Lab, Corné J. Kros, Guy P. Richardson, et al. 2003. "Dynamic Assembly of Surface Structures in Living Cells." *Proceedings of the National Academy of Sciences* 100 (10): 5819–22. https://doi.org/10.1073/pnas.1030502100.

Grati, M'hamed, and Bechara Kachar. 2011. "Myosin VIIa and sans Localization at Stereocilia Upper Tip-Link Density Implicates These Usher Syndrome Proteins in Mechanotransduction." *Proceedings of the National Academy of Sciences* 108 (28): 11476–81. https://doi.org/10.1073/pnas.1104161108.

Gutsche-Perelroizen, Irina, Jean Lepault, Albrecht Ott, and Marie-France Carlier. 1999. "Filament Assembly from Profilin-Actin." *Journal of Biological Chemistry* 274 (10): 6234–43. https://doi.org/10.1074/jbc.274.10.6234.

Hacohen, N., J. A. Assad, W. J. Smith, and D. P. Corey. 1989. "Regulation of Tension on Hair-Cell Transduction Channels: Displacement and Calcium Dependence." *Journal of Neuroscience* 9 (11): 3988–97. https://doi.org/10.1523/JNEUROSCI.09-11-03988.1989.

Harris, Elizabeth S., Isabelle Rouiller, Dorit Hanein, and Henry N. Higgs. 2006. "Mechanistic Differences in Actin Bundling Activity of Two Mammalian Formins, FRL1 and MDia2 *." *Journal of Biological Chemistry* 281 (20): 14383–92. https://doi.org/10.1074/jbc.M510923200.

Heller, Stefan, Andrea M. Bell, Charlotte S. Denis, Yong Choe, and A.J. Hudspeth. 2002. "Parvalbumin 3 Is an Abundant Ca2+ Buffer in Hair Cells." *JARO: Journal of the Association for Research in Otolaryngology* 3 (4): 488–98. https://doi.org/10.1007/s10162-002-2050-x.

Hertzog, Maud, Francesca Milanesi, Larnele Hazelwood, Andrea Disanza, HongJun Liu, Emilie Perlade, Maria Grazia Malabarba, et al. 2010. "Molecular Basis for the Dual Function of Eps8 on Actin Dynamics: Bundling and Capping." *PLOS Biology* 8 (6): e1000387. https://doi.org/10.1371/journal.pbio.1000387.

Höfer, D., W. Ness, and D. Drenckhahn. 1997. "Sorting of Actin Isoforms in Chicken Auditory Hair Cells." *Journal of Cell Science* 110 (Pt 6) (March): 765–70.

Holt, Jeffrey R., Susan K. H. Gillespie, D. William Provance, Kavita Shah, Kevan M. Shokat, David P. Corey, John A. Mercer, and Peter G. Gillespie. 2002. "A Chemical-Genetic Strategy Implicates Myosin-1c in Adaptation by Hair Cells." *Cell* 108 (3): 371–81. https://doi.org/10.1016/S0092-8674(02)00629-3.

Hordichok, Andrew J., and Peter S. Steyger. 2007. "Closure of Supporting Cell Scar Formations Requires Dynamic Actin Mechanisms." *Hearing Research* 232 (1–2): 1–19. https://doi.org/10.1016/j.heares.2007.06.011.

Howard, J., and J.F. Ashmore. 1986. "Stiffness of Sensory Hair Bundles in the Sacculus of the Frog." *Hearing Research* 23 (1): 93–104. https://doi.org/10.1016/0378-5955(86)90178-4.

Howard, J., and A. J. Hudspeth. 1988. "Compliance of the Hair Bundle Associated with Gating of Mechanoelectrical Transduction Channels in the Bullfrog's Saccular Hair Cell." *Neuron* 1 (3): 189–99. https://doi.org/10.1016/0896-6273(88)90139-0.

Howard, Jonathon. 2001. *Mechanics of Motor Proteins and the Cytoskeleton*. Nachdr. Sunderland, Mass: Sinauer.

Hudspeth, A. J. 2014. "Integrating the Active Process of Hair Cells with Cochlear Function." *Nature Reviews Neuroscience* 15 (9): 600–614. https://doi.org/10.1038/nrn3786.

Hudspeth, A. J., and P. G. Gillespie. 1994a. "Pulling Springs to Tune Transduction: Adaptation by Hair Cells." *Neuron* 12 (1): 1–9. https://doi.org/10.1016/0896-6273(94)90147-3.

Indzhykulian, Artur A., Ruben Stepanyan, Anastasiia Nelina, Kateri J. Spinelli, Zubair M. Ahmed, Inna A. Belyantseva, Thomas B. Friedman, Peter G. Barr-Gillespie, and Gregory I. Frolenkov. 2013. "Molecular Remodeling of Tip Links Underlies Mechanosensory Regeneration in Auditory Hair Cells." Edited by Walter Marcotti. *PLoS Biology* 11 (6): e1001583. https://doi.org/10.1371/journal.pbio.1001583.

Ireton, Keith. 2013. "Molecular Mechanisms of Cell–Cell Spread of Intracellular Bacterial Pathogens." *Open Biology* 3 (7): 130079. https://doi.org/10.1098/rsob.130079.

Itoh, Masahiro. 1982. "Preservation and Visualization of Actin-Containing Filaments in the Apical Zone of Cochlear Sensory Cells." *Hearing Research* 6 (3): 277–89. https://doi.org/10.1016/0378-5955(82)90060-0.

Jackson-Grusby, L., A. Kuo, and P. Leder. 1992. "A Variant Limb Deformity Transcript Expressed in the Embryonic Mouse Limb Defines a Novel Formin." *Genes & Development* 6 (1): 29–37. https://doi.org/10.1101/gad.6.1.29.

Jacobo, A., and A. J. Hudspeth. 2014. "Reaction-Diffusion Model of Hair-Bundle Morphogenesis." *Proceedings of the National Academy of Sciences* 111 (43): 15444–49. https://doi.org/10.1073/pnas.1417420111.

Jacobs, R. A., and A. J. Hudspeth. 1990. "Ultrastructural Correlates of Mechanoelectrical Transduction in Hair Cells of the Bullfrog's Internal Ear." *Cold Spring Harbor Symposia on Quantitative Biology* 55: 547–61. https://doi.org/10.1101/sqb.1990.055.01.053.

Jaramillo, F., and A. J. Hudspeth. 1993. "Displacement-Clamp Measurement of the Forces Exerted by Gating Springs in the Hair Bundle." *Proceedings of the National Academy of Sciences* 90 (4): 1330–34. https://doi.org/10.1073/pnas.90.4.1330.

Jégou, Antoine, Marie-France Carlier, and Guillaume Romet-Lemonne. 2013. "Formin MDia1 Senses and Generates Mechanical Forces on Actin Filaments." *Nature Communications* 4 (1): 1883. https://doi.org/10.1038/ncomms2888.

Jia, Yanyan, Yimeng Zhao, Tsukasa Kusakizako, Yao Wang, Chengfang Pan, Yuwei Zhang, Osamu Nureki, Motoyuki Hattori, and Zhiqiang Yan. 2020. "TMC1 and TMC2 Proteins Are Pore-Forming Subunits of Mechanosensitive Ion Channels." *Neuron* 105 (2): 310-321.e3. https://doi.org/10.1016/j.neuron.2019.10.017.

Johnson, Stuart L., Maryline Beurg, Walter Marcotti, and Robert Fettiplace. 2011. "Prestin-Driven Cochlear Amplification Is Not Limited by the Outer Hair Cell Membrane Time Constant." *Neuron* 70 (6): 1143–54. https://doi.org/10.1016/j.neuron.2011.04.024.

Kabsch, Wolfgang, Hans Georg Mannherz, Dietrich Suck, Emil F. Pai, and Kenneth C. Holmes. 1990. "Atomic Structure of the Actin: DNase I Complex." *Nature* 347 (6288): 37–44. https://doi.org/10.1038/347037a0.

Kachar, B., M. Parakkal, M. Kurc, Y.-d. Zhao, and P. G. Gillespie. 2000. "High-Resolution Structure of Hair-Cell Tip Links." *Proceedings of the National Academy of Sciences* 97 (24): 13336–41. https://doi.org/10.1073/pnas.97.24.13336.

Kachar, Bechara, Marianne Parakkal, and Jorgen Fex. 1990. "Structural Basis for Mechanical Transduction in the Frog Vestibular Sensory Apparatus: I. The Otolithic Membrane." *Hearing Research* 45 (3): 179–90. https://doi.org/10.1016/0378-5955(90)90119-A.

Kalay, Ersan, Yun Li, Abdullah Uzumcu, Oya Uyguner, Rob W. Collin, Refik Caylan, Melike Ulubil-Emiroglu, et al. 2006. "Mutations in the Lipoma HMGIC Fusion Partner-like 5 (LHFPL5) Gene Cause Autosomal Recessive Nonsyndromic Hearing Loss." *Human Mutation* 27 (7): 633–39. https://doi.org/10.1002/humu.20368.

Kawashima, Yoshiyuki, Gwenaëlle S. G. Géléoc, Kiyoto Kurima, Valentina Labay, Andrea Lelli, Yukako Asai, Tomoko Makishima, et al. 2011. "Mechanotransduction in Mouse Inner Ear Hair Cells Requires Transmembrane Channel-like Genes." *The Journal of Clinical Investigation* 121 (12): 4796–4809. https://doi.org/10.1172/JCI60405.

Kato, Watanabe, Naoki Watanabe, Yosuke Morishima, Akiko Fujita, Toshimasa Ishizaki and Shuh Narumiya. 2001. "Localization of a mammalian homolog of diaphanous, mDia1, to the mitotic spindle in HeLa cells." *Journal of Cell Science.* Feb;114(Pt 4):775-84. PMID: 11171383.121. https://doi.org/10.1242/jcs.114.4.775.

Kim, Kyunghee X., Maryline Beurg, Carole M. Hackney, David N. Furness, Shanthini Mahendrasingam, and Robert Fettiplace. 2013. "The Role of Transmembrane Channel-like Proteins in the Operation of Hair Cell Mechanotransducer Channels." *The Journal of General Physiology* 142 (5): 493–505. https://doi.org/10.1085/jgp.201311068.

Kim, Kyunghee X., and Robert Fettiplace. 2013. "Developmental Changes in the Cochlear Hair Cell Mechanotransducer Channel and Their Regulation by Transmembrane Channel-like Proteins." *The Journal of General Physiology* 141 (1): 141–48. https://doi.org/10.1085/jgp.201210913.

Kim, Moon, Yunho Jang, and Jayil Jeong. 2006. "Using Harmonic Analysis and Optimization to Study Macromolecular Dynamics." *International Journal of Control, Automation and Systems* 4 (June).

Kohno, H., K. Tanaka, A. Mino, M. Umikawa, H. Imamura, T. Fujiwara, Y. Fujita, et al. 1996. "Bni1p Implicated in Cytoskeletal Control Is a Putative Target of Rho1p Small GTP Binding Protein in Saccharomyces Cerevisiae." *The EMBO Journal* 15 (22): 6060–68.

Kozlov, Andrei S, Thomas Risler, and A J Hudspeth. 2007. "Coherent Motion of Stereocilia Assures the Concerted Gating of Hair-Cell Transduction Channels." *Nature Neuroscience* 10 (1): 87–92. https://doi.org/10.1038/nn1818.

Krementsov, Dimitry N., Elena B. Krementsova, and Kathleen M. Trybus. 2004. "Myosin V : Regulation by Calcium, Calmodulin, and the Tail Domain." *Journal of Cell Biology* 164 (6): 877–86. https://doi.org/10.1083/jcb.200310065.

Krey, Jocelyn F., Paroma Chatterjee, Rachel A. Dumont, Mary O'Sullivan, Dongseok Choi, Jonathan E. Bird, and Peter G. Barr-Gillespie. 2020. "Mechanotransduction-Dependent Control of Stereocilia Dimensions and Row Identity in Inner Hair Cells." *Current Biology* 30 (3): 442-454.e7. https://doi.org/10.1016/j.cub.2019.11.076.

Krey, Jocelyn F., Evan S. Krystofiak, Rachel A. Dumont, Sarath Vijayakumar, Dongseok Choi, Francisco Rivero, Bechara Kachar, Sherri M. Jones, and Peter G. Barr-Gillespie. 2016. "Plastin 1 Widens Stereocilia by Transforming Actin Filament Packing from Hexagonal to Liquid." *The Journal of Cell Biology* 215 (4): 467–82. https://doi.org/10.1083/jcb.201606036.

Krey, Jocelyn F., Nicholas E. Sherman, Erin D. Jeffery, Dongseok Choi, and Peter G. Barr-Gillespie. 2015. "The Proteome of Mouse Vestibular Hair Bundles over Development." *Scientific Data* 2 (1): 150047. https://doi.org/10.1038/sdata.2015.47.

Kruth, Karina A., and Peter A. Rubenstein. 2012. "Two Deafness-Causing (DFNA20/26) Actin Mutations Affect Arp2/3-Dependent Actin Regulation *." *Journal of Biological Chemistry* 287 (32): 27217–26. https://doi.org/10.1074/jbc.M112.377283.

Kurima, Kiyoto, Seham Ebrahim, Bifeng Pan, Miloslav Sedlacek, Prabuddha Sengupta, Bryan A. Millis, Runjia Cui, et al. 2015. "TMC1 and TMC2 Localize at the Site of Mechanotransduction in Mammalian Inner Ear Hair Cell Stereocilia." *Cell Reports* 12 (10): 1606–17. https://doi.org/10.1016/j.celrep.2015.07.058.

LaFountain, James R., C. Richard Zobel, Herbert R. Thomas, and Christopher Galbreath. 1977. "Fixation and Staining of F-Actin and Microfilaments Using Tannic Acid." *Journal of Ultrastructure Research* 58 (1): 78–86. https://doi.org/10.1016/S0022-5320(77)80009-9.

Leader, Benjamin, Hyunjung Lim, Mary Jo Carabatsos, Anne Harrington, Jeffrey Ecsedy, David Pellman, Richard Maas, and Philip Leder. 2002. "Formin-2, Polyploidy, Hypofertility and Positioning of the Meiotic Spindle in Mouse Oocytes." *Nature Cell Biology* 4 (12): 921–28. https://doi.org/10.1038/ncb880.

Lewis, Edwin R., Ellen L. Leverenz, and Hironori Koyama. 1982. "The Tonotopic Organization of the Bullfrog Amphibian Papilla, an Auditory Organ Lacking a Basilar Membrane."

Journal of Comparative Physiology ? A 145 (4): 437–45. https://doi.org/10.1007/BF00612809.

Li, Sihan, Andrew Mecca, Jeewoo Kim, Giusy A. Caprara, Elizabeth L. Wagner, Ting-Ting Du, Leonid Petrov, et al. 2020. "Myosin-VIIa Is Expressed in Multiple Isoforms and Essential for Tensioning the Hair Cell Mechanotransduction Complex." *Nature Communications* 11 (1): 2066. https://doi.org/10.1038/s41467-020-15936-z.

Lippman, Jocelyn, and Anna Dunaevsky. 2005. "Dendritic Spine Morphogenesis and Plasticity." *Journal of Neurobiology* 64 (1): 47–57. https://doi.org/10.1002/neu.20149.

Ljubojevic, Nina, J. Michael Henderson, and Chiara Zurzolo. 2021. "The Ways of Actin: Why Tunneling Nanotubes Are Unique Cell Protrusions." *Trends in Cell Biology* 31 (2): 130–42. https://doi.org/10.1016/j.tcb.2020.11.008.

Lynch, E. D. 1997. "Nonsyndromic Deafness DFNA1 Associated with Mutation of a Human Homolog of the Drosophila Gene Diaphanous." *Science* 278 (5341): 1315–18. https://doi.org/10.1126/science.278.5341.1315.

Machesky, Laura M., R. Dyche Mullins, Henry N. Higgs, Donald A. Kaiser, Laurent Blanchoin, Robin C. May, Margaret E. Hall, and Thomas D. Pollard. 1999. "Scar, a WASp-Related Protein, Activates Nucleation of Actin Filaments by the Arp2/3 Complex." *Proceedings of the National Academy of Sciences* 96 (7): 3739–44. https://doi.org/10.1073/pnas.96.7.3739.

Manor, Uri, Andrea Disanza, M'Hamed Grati, Leonardo Andrade, Harrison Lin, Pier Paolo Di Fiore, Giorgio Scita, and Bechara Kachar. 2011. "Regulation of Stereocilia Length by Myosin XVa and Whirlin Depends on the Actin-Regulatory Protein Eps8." *Current Biology* 21 (2): 167–72. https://doi.org/10.1016/j.cub.2010.12.046.

Marchand, J. B., D. A. Kaiser, T. D. Pollard, and H. N. Higgs. 2001. "Interaction of WASP/Scar Proteins with Actin and Vertebrate Arp2/3 Complex." *Nature Cell Biology* 3 (1): 76–82. https://doi.org/10.1038/35050590.

Marquis, R. E., and A. J. Hudspeth. 1997. "Effects of Extracellular Ca2+ Concentration on Hair-Bundle Stiffness and Gating-Spring Integrity in Hair Cells." *Proceedings of the National Academy of Sciences* 94 (22): 11923–28. https://doi.org/10.1073/pnas.94.22.11923.

Martin, P., A. D. Mehta, and A. J. Hudspeth. 2000. "Negative Hair-Bundle Stiffness Betrays a Mechanism for Mechanical Amplification by the Hair Cell." *Proceedings of the National Academy of Sciences* 97 (22): 12026–31. https://doi.org/10.1073/pnas.210389497.

Martin, Pascal. 2007. "Active Hair-Bundle Motility of the Hair Cells of Vestibular and Auditory Organs." In *Active Processes and Otoacoustic Emissions in Hearing*, edited by Geoffrey A. Manley, Richard R. Fay, and Arthur N. Popper, 30:93–143. Springer Handbook of Auditory Research. New York, NY: Springer New York. https://doi.org/10.1007/978-0-387-71469-1_4.

Martin, Pascal, and A.J. Hudspeth. 2021. "Mechanical Frequency Tuning by Sensory Hair Cells, the Receptors and Amplifiers of the Inner Ear." *Annual Review of Condensed Matter Physics* 12 (1): 29–49. https://doi.org/10.1146/annurev-conmatphys-061020-053041.

Mass, R. L., R. Zeller, R. P. Woychik, T. F. Vogt, and P. Leder. 1990. "Disruption of Formin-Encoding Transcripts in Two Mutant Limb Deformity Alleles." *Nature* 346 (6287): 853–55. https://doi.org/10.1038/346853a0.

Matsudaira, P., E. Mandelkow, W. Renner, L. K. Hesterberg, and K. Weber. 1983. "Role of Fimbrin and Villin in Determining the Interfilament Distances of Actin Bundles." *Nature* 301 (5897): 209–14. https://doi.org/10.1038/301209a0.

Mauriac, Stephanie A., Yeri E. Hien, Jonathan E. Bird, Steve Dos-Santos Carvalho, Ronan Peyroutou, Sze Chim Lee, Maite M. Moreau, et al. 2017. "Defective Gpsm2/Gαi3 Signalling Disrupts Stereocilia Development and Growth Cone Actin Dynamics in Chudley-McCullough Syndrome." *Nature Communications* 8 (April): 14907. https://doi.org/10.1038/ncomms14907.

McGrath, Jamis, Pallabi Roy, and Benjamin J. Perrin. 2017. "Stereocilia Morphogenesis and Maintenance through Regulation of Actin Stability." *Seminars in Cell & Developmental Biology* 65 (May): 88–95. https://doi.org/10.1016/j.semcdb.2016.08.017.

McGrath, Jamis, Chun-Yu Tung, Xiayi Liao, Inna A. Belyantseva, Pallabi Roy, Oisorjo Chakraborty, Jinan Li, et al. 2021. "Actin at Stereocilia Tips Is Regulated by Mechanotransduction and ADF/Cofilin." *Current Biology* 31 (6): 1141-1153.e7. https://doi.org/10.1016/j.cub.2020.12.006.

Michalski, Nicolas, and Christine Petit. 2015. "Genetics of Auditory Mechano-Electrical Transduction." *Pflugers Archiv* 467 (1): 49–72. https://doi.org/10.1007/s00424-014-1552-9.

Michel, Vincent, Kevin T Booth, Pranav Patni, Matteo Cortese, Hela Azaiez, Amel Bahloul, Kimia Kahrizi, et al. 2017. "CIB2, Defective in Isolated Deafness, Is Key for Auditory Hair Cell Mechanotransduction and Survival." *EMBO Molecular Medicine* 9 (12): 1711–31. https://doi.org/10.15252/emmm.201708087.

Michelot, Alphée, Emmanuel Derivery, Rajaa Paterski-Boujemaa, Christophe Guérin, Shanjin Huang, François Parcy, Christopher J. Staiger, and Laurent Blanchoin. 2006. "A Novel Mechanism for the Formation of Actin-Filament Bundles by a Nonprocessive Formin." *Current Biology* 16 (19): 1924–30. https://doi.org/10.1016/j.cub.2006.07.054.

Mogensen, Mette M., Agnieszka Rzadzinska, and Karen P. Steel. 2007. "The Deaf Mouse Mutant Whirler Suggests a Role for Whirlin in Actin Filament Dynamics and Stereocilia Development." *Cell Motility and the Cytoskeleton* 64 (7): 496–508. https://doi.org/10.1002/cm.20199.

Mulhall, Eric M., Andrew Ward, Darren Yang, Mounir A. Koussa, David P. Corey, and Wesley P. Wong. 2021. "Single-Molecule Force Spectroscopy Reveals the Dynamic Strength of the Hair-Cell Tip-Link Connection." *Nature Communications* 12 (1): 849. https://doi.org/10.1038/s41467-021-21033-6.

Mullins, R. Dyche, John A. Heuser, and Thomas D. Pollard. 1998. "The Interaction of Arp2/3 Complex with Actin: Nucleation, High Affinity Pointed End Capping, and Formation of Branching Networks of Filaments." *Proceedings of the National Academy of Sciences* 95 (11): 6181–86. https://doi.org/10.1073/pnas.95.11.6181.

Naraghi, Mohammad. 1997. "T-Jump Study of Calcium Binding Kinetics of Calcium Chelators." *Cell Calcium* 22 (4): 255–68. https://doi.org/10.1016/S0143-4160(97)90064-6.

Narayanan, Praveena, Paul Chatterton, Akihiro Ikeda, Sakae Ikeda, David P. Corey, James M. Ervasti, and Benjamin J. Perrin. 2015. "Length Regulation of Mechanosensitive Stereocilia Depends on Very Slow Actin Dynamics and Filament-Severing Proteins." *Nature Communications* 6 (1): 6855. https://doi.org/10.1038/ncomms7855.

Naz, S., A. J. Griffith, S. Riazuddin, L. L. Hampton, J. F. Battey, S. N. Khan, S. Riazuddin, E. R. Wilcox, and T. B. Friedman. 2004. "Mutations of ESPN Cause Autosomal Recessive Deafness and Vestibular Dysfunction." *Journal of Medical Genetics* 41 (8): 591–95. https://doi.org/10.1136/jmg.2004.018523.

Neveu, André. 2009. "Suitability of European Green Frogs for Intensive Culture: Comparison between Different Phenotypes of the Esculenta Hybridogenetic Complex." *Aquaculture* 295 (1–2): 30–37. https://doi.org/10.1016/j.aquaculture.2009.06.027.

Ninoyu, Yuzuru, Hirofumi Sakaguchi, Chen Lin, Toshiaki Suzuki, Shigeru Hirano, Yasuo Hisa, Naoaki Saito, and Takehiko Ueyama. 2020. "The Integrity of Cochlear Hair Cells Is Established and Maintained through the Localization of Dia1 at Apical Junctional Complexes and Stereocilia." *Cell Death & Disease* 11 (7): 536. https://doi.org/10.1038/s41419-020-02743-z.

Nishimura, Yukako, Shidong Shi, Fang Zhang, Rong Liu, Yasuharu Takagi, Alexander D. Bershadsky, Virgile Viasnoff, and James R. Sellers. 2021. "The Formin Inhibitor SMIFH2 Inhibits Members of the Myosin Superfamily." *Journal of Cell Science* 134 (jcs253708). https://doi.org/10.1242/jcs.253708.

Oda, Toshiro, Mitsusada Iwasa, Tomoki Aihara, Yuichiro Maéda, and Akihiro Narita. 2009. "The Nature of the Globular- to Fibrous-Actin Transition." *Nature* 457 (7228): 441–45. https://doi.org/10.1038/nature07685.

Oertner, Thomas G., and Andrew Matus. 2005. "Calcium Regulation of Actin Dynamics in Dendritic Spines." *Cell Calcium* 37 (5): 477–82. https://doi.org/10.1016/j.ceca.2005.01.016.

Pacentine, Itallia, Paroma Chatterjee, and Peter G. Barr-Gillespie. 2020. "Stereocilia Rootlets: Actin-Based Structures That Are Essential for Structural Stability of the Hair Bundle." *International Journal of Molecular Sciences* 21 (1). https://doi.org/10.3390/ijms21010324.

Pan, Bifeng, Nurunisa Akyuz, Xiao-Ping Liu, Yukako Asai, Carl Nist-Lund, Kiyoto Kurima, Bruce H. Derfler, et al. 2018. "TMC1 Forms the Pore of Mechanosensory Transduction Channels in Vertebrate Inner Ear Hair Cells." *Neuron* 99 (4): 736-753.e6. https://doi.org/10.1016/j.neuron.2018.07.033.

Pan, Bifeng, Gwenaelle S. Géléoc, Yukako Asai, Geoffrey C. Horwitz, Kiyoto Kurima, Kotaro Ishikawa, Yoshiyuki Kawashima, Andrew J. Griffith, and Jeffrey R. Holt. 2013. "TMC1 and TMC2 Are Components of the Mechanotransduction Channel in Hair Cells of the Mammalian Inner Ear." *Neuron* 79 (3): 504–15. https://doi.org/10.1016/j.neuron.2013.06.019.

Paul, Aditya S., Aditya Paul, Thomas D. Pollard, and Thomas Pollard. 2008. "The Role of the FH1 Domain and Profilin in Formin-Mediated Actin-Filament Elongation and Nucleation." *Current Biology: CB* 18 (1): 9–19. https://doi.org/10.1016/j.cub.2007.11.062.

Paul, Aditya S., and Thomas D. Pollard. 2009a. "Review of the Mechanism of Processive Actin Filament Elongation by Formins." *Cell Motility* 66 (8): 606–17. https://doi.org/10.1002/cm.20379.

———. 2009b. "Review of the Mechanism of Processive Actin Filament Elongation by Formins." *Cell Motility and the Cytoskeleton* 66 (8): 606–17. https://doi.org/10.1002/cm.20379.

Peng, Anthony W., Inna A. Belyantseva, Patrick D. Hsu, Thomas B. Friedman, and Stefan Heller. 2009. "Twinfilin 2 Regulates Actin Filament Lengths in Cochlear Stereocilia." *The Journal of Neuroscience* 29 (48): 15083–88. https://doi.org/10.1523/JNEUROSCI.2782-09.2009.

Peng, Anthony W., Felipe T. Salles, Bifeng Pan, and Anthony J. Ricci. 2011. "Integrating the Biophysical and Molecular Mechanisms of Auditory Hair Cell Mechanotransduction." *Nature Communications* 2 (1): 523. https://doi.org/10.1038/ncomms1533.

Perrin, B. J., D. M. Strandjord, P. Narayanan, D. M. Henderson, K. R. Johnson, and J. M. Ervasti. 2013. "β-Actin and Fascin-2 Cooperate to Maintain Stereocilia Length." *Journal of Neuroscience* 33 (19): 8114–21. https://doi.org/10.1523/JNEUROSCI.0238-13.2013.

Perrin, Benjamin J., Kevin J. Sonnemann, and James M. Ervasti. 2010. "β-Actin and γ-Actin Are Each Dispensable for Auditory Hair Cell Development But Required for Stereocilia Maintenance." Edited by Bruce L. Tempel. *PLoS Genetics* 6 (10): e1001158. https://doi.org/10.1371/journal.pgen.1001158.

Phillips, Rob. 2013. *Physical Biology of the Cell*. Second edition. London : New York, NY: Garland Science.

Pickles, James O. 2012. *An Introduction to the Physiology of Hearing*. 4. ed. London: Emerald.

Pickles, J.O., S.D. Comis, and M.P. Osborne. 1984. "Cross-Links between Stereocilia in the Guinea Pig Organ of Corti, and Their Possible Relation to Sensory Transduction." *Hearing Research* 15 (2): 103–12. https://doi.org/10.1016/0378-5955(84)90041-8.

Pollard, T D. 1986. "Rate Constants for the Reactions of ATP- and ADP-Actin with the Ends of Actin Filaments." *Journal of Cell Biology* 103 (6): 2747–54. https://doi.org/10.1083/jcb.103.6.2747.

Pollard, T. D., and J. A. Cooper. 1986. "Actin and Actin-Binding Proteins. A Critical Evaluation of Mechanisms and Functions." *Annual Review of Biochemistry* 55: 987–1035. https://doi.org/10.1146/annurev.bi.55.070186.005011.

Pollard, Thomas D., and Gary G. Borisy. 2003. "Cellular Motility Driven by Assembly and Disassembly of Actin Filaments." *Cell* 112 (4): 453–65. https://doi.org/10.1016/s0092-8674(03)00120-x.

Rizvi, Syed A., Erin M. Neidt, Jiayue Cui, Zach Feiger, Colleen T. Skau, Margaret L. Gardel, Sergey A. Kozmin, and David R. Kovar. 2009. "Identification and Characterization of a Small Molecule Inhibitor of Formin-Mediated Actin Assembly." *Chemistry & Biology* 16 (11): 1158–68. https://doi.org/10.1016/j.chembiol.2009.10.006.

Rosales-Nieves, Alicia E., James E. Johndrow, Lani C. Keller, Craig R. Magie, Delia M. Pinto-Santini, and Susan M. Parkhurst. 2006. "Coordination of Microtubule and Microfilament Dynamics by Drosophila Rho1, Spire and Cappuccino." *Nature Cell Biology* 8 (4): 367–76. https://doi.org/10.1038/ncb1385.

Rüsch, A, C J Kros, and G P Richardson. 1994. "Block by Amiloride and Its Derivatives of Mechano-Electrical Transduction in Outer Hair Cells of Mouse Cochlear Cultures." *The Journal of Physiology* 474 (1): 75–86.

Rzadzinska, Agnieszka K., Elisa M. Nevalainen, Haydn M. Prosser, Pekka Lappalainen, and Karen P. Steel. 2009. "MyosinVIIa Interacts with Twinfilin-2 at the Tips of Mechanosensory Stereocilia in the Inner Ear." Edited by Magdalena Bezanilla. *PLoS ONE* 4 (9): e7097. https://doi.org/10.1371/journal.pone.0007097.

Rzadzinska, Agnieszka K., Mark E. Schneider, Caroline Davies, Gavin P. Riordan, and Bechara Kachar. 2004. "An Actin Molecular Treadmill and Myosins Maintain Stereocilia Functional Architecture and Self-Renewal." *The Journal of Cell Biology* 164 (6): 887–97. https://doi.org/10.1083/jcb.200310055.

Scheffer, Déborah I., Duan-Sun Zhang, Jun Shen, Artur Indzhykulian, K. Domenica Karavitaki, Yichao Joy Xu, Qinchuan Wang, Jim Jung-Ching Lin, Zheng-Yi Chen, and David P. Corey. 2015. "XIRP2, an Actin-Binding Protein Essential for Inner Ear Hair-Cell Stereocilia." *Cell Reports* 10 (11): 1811–18. https://doi.org/10.1016/j.celrep.2015.02.042.

Schneider, Mark E., Inna A. Belyantseva, Ricardo B. Azevedo, and Bechara Kachar. 2002. "Rapid Renewal of Auditory Hair Bundles." *Nature* 418 (6900): 837–38. https://doi.org/10.1038/418837a.

Schoen, Cynthia J., Margit Burmeister, and Marci M. Lesperance. 2013. "Diaphanous Homolog 3 (Diap3) Overexpression Causes Progressive Hearing Loss and Inner Hair Cell Defects in a Transgenic Mouse Model of Human Deafness." Edited by Gayle E. Woloschak. *PLoS ONE* 8 (2): e56520. https://doi.org/10.1371/journal.pone.0056520.

Schönichen, André, Hans Georg Mannherz, Elmar Behrmann, Antonina J. Mazur, Sonja Kühn, Unai Silván, Cora-Ann Schoenenberger, et al. 2013. "FHOD1 Is a Combined Actin Filament Capping and Bundling Factor That Selectively Associates with Actin Arcs and Stress Fibers." *Journal of Cell Science* 126 (8): 1891–1901. https://doi.org/10.1242/jcs.126706.

Sekerková, Gabriella, Claus-Peter Richter, and James R. Bartles. 2011. "Roles of the Espin Actin-Bundling Proteins in the Morphogenesis and Stabilization of Hair Cell Stereocilia Revealed in CBA/CaJ Congenic Jerker Mice." *PLOS Genetics* 7 (3): e1002032. https://doi.org/10.1371/journal.pgen.1002032.

Sept, D, and J A McCammon. 2001. "Thermodynamics and Kinetics of Actin Filament Nucleation." *Biophysical Journal* 81 (2): 667–74.

Shabbir, M I, Z M Ahmed, S Y Khan, Saima Riazuddin, A M Waryah, S N Khan, R D Camps, et al. 2006. "Mutations of Human TMHS Cause Recessively Inherited Non-syndromic Hearing Loss." *Journal of Medical Genetics* 43 (8): 634–40. https://doi.org/10.1136/jmg.2005.039834.

Shao, Xiaowei, Qingsen Li, Alex Mogilner, Alexander D. Bershadsky, and G. V. Shivashankar. 2015. "Mechanical Stimulation Induces Formin-Dependent Assembly of a Perinuclear Actin Rim." *Proceedings of the National Academy of Sciences* 112 (20): E2595–2601. https://doi.org/10.1073/pnas.1504837112.

Shawlot, W., J. M. Deng, L. E. Fohn, and R. R. Behringer. 1998. "Restricted Beta-Galactosidase Expression of a Hygromycin-LacZ Gene Targeted to the Beta-Actin Locus and Embryonic Lethality of Beta-Actin Mutant Mice." *Transgenic Research* 7 (2): 95–103. https://doi.org/10.1023/a:1008816308171.

Shin, Jung-Bum, Jocelyn F. Krey, Ahmed Hassan, Zoltan Metlagel, Andrew N. Tauscher, James M. Pagana, Nicholas E. Sherman, et al. 2013. "Molecular Architecture of the Chick Vestibular Hair Bundle." *Nature Neuroscience* 16 (3): 365–74. https://doi.org/10.1038/nn.3312.

Shin, Jung-Bum, Chantal M. Longo-Guess, Leona H. Gagnon, Katherine W. Saylor, Rachel A. Dumont, Kateri J. Spinelli, James M. Pagana, et al. 2010. "The R109H Variant of Fascin-2, a Developmentally Regulated Actin Crosslinker in Hair-Cell Stereocilia, Underlies Early-Onset Hearing Loss of DBA/2J Mice." *The Journal of Neuroscience* 30 (29): 9683–94. https://doi.org/10.1523/JNEUROSCI.1541-10.2010.

Shively, Shawn, and William R. Miller. 2009. "The Use of HMDS (Hexamethyldisilazane) to Replace Critical Point Drying (CPD) in the Preparation of Tardigrades for SEM (Scanning Electron Microscope) Imaging." *Transactions of the Kansas Academy of Science* 112 (3–4): 198–200. https://doi.org/10.1660/062.112.0407.

Shotwell, S. L., R. Jacobs, and A. J. Hudspeth. 1981. "Directional Sensitivity of Individual Vertebrate Hair Cells to Controlled Deflection of Their Hair Bundles." *Annals of the New York Academy of Sciences* 374 (1 Vestibular an): 1–10. https://doi.org/10.1111/j.1749-6632.1981.tb30854.x.

Sitters, Gerrit, Douwe Kamsma, Gregor Thalhammer, Monika Ritsch-Marte, Erwin J. G. Peterman, and Gijs J. L. Wuite. 2015. "Acoustic Force Spectroscopy." *Nature Methods* 12 (1): 47–50. https://doi.org/10.1038/nmeth.3183.

Sotomayor, Marcos, David P Corey, and Klaus Schulten. 2005. "In Search of the Hair-Cell Gating Spring: Elastic Properties of Ankyrin and Cadherin Repeats," 14.

Sotomayor, Marcos, Wilhelm A Weihofen, Rachelle Gaudet, and David P Corey. 2010. "Structural Determinants of Cadherin-23 Function in Hearing and Deafness," 16.

Sotomayor, Marcos, Wilhelm A. Weihofen, Rachelle Gaudet, and David P. Corey. 2012. "Structure of a Force-Conveying Cadherin Bond Essential for Inner-Ear Mechanotransduction." *Nature* 492 (7427): 128–32. https://doi.org/10.1038/nature11590.

Spoon, C., and W. Grant. 2011. "Biomechanics of Hair Cell Kinocilia: Experimental Measurement of Kinocilium Shaft Stiffness and Base Rotational Stiffness with Euler-Bernoulli and Timoshenko Beam Analysis." *Journal of Experimental Biology* 214 (5): 862–70. https://doi.org/10.1242/jeb.051151.

Stauffer, Eric A., John D. Scarborough, Moritoshi Hirono, Emilie D. Miller, Kavita Shah, John A. Mercer, Jeffrey R. Holt, and Peter G. Gillespie. 2005a. "Fast Adaptation in Vestibular Hair Cells Requires Myosin-1c Activity." *Neuron* 47 (4): 541–53. https://doi.org/10.1016/j.neuron.2005.07.024.

———. 2005b. "Fast Adaptation in Vestibular Hair Cells Requires Myosin-1c Activity." *Neuron* 47 (4): 541–53. https://doi.org/10.1016/j.neuron.2005.07.024.

Steyger, P. S., S. L. Peters, J. Rehling, A. Hordichok, and C. F. Dai. 2003. "Uptake of Gentamicin by Bullfrog Saccular Hair Cells in Vitro." *JARO - Journal of the Association for Research in Otolaryngology* 4 (4): 565–78. https://doi.org/10.1007/s10162-003-4002-5.

Strelioff, David, and Åke Flock. 1984. "Stiffness of Sensory-Cell Hair Bundles in the Isolated Guinea Pig Cochlea." *Hearing Research* 15 (1): 19–28. https://doi.org/10.1016/0378-5955(84)90221-1.

Tadenev, Abigail L.D., Anil Akturk, Nicholas Devanney, Pranav Dinesh Mathur, Anna M. Clark, Jun Yang, and Basile Tarchini. 2019. "GPSM2-GNAI Specifies the Tallest Stereocilia and Defines Hair Bundle Row Identity." *Current Biology : CB* 29 (6): 921-934.e4. https://doi.org/10.1016/j.cub.2019.01.051.

Tang, Yi-Quan, Sol Ah Lee, Mizanur Rahman, Siva A. Vanapalli, Hang Lu, and William R. Schafer. 2020. "Ankyrin Is An Intracellular Tether for TMC Mechanotransduction Channels." *Neuron* 107 (1): 112-125.e10. https://doi.org/10.1016/j.neuron.2020.03.026.

Tilney, G, and Mary S Tilney. 1988. "The Actin Filament Content of Hair Cells of the Bird Cochlea Is Nearly Constant Even Though the Length, Width, and Number of Stereocilia Vary Depending on the Hair Cell Location." *The Journal of Cell Biology* 107: 12.

Tilney, L G, D J Derosier, and M J Mulroy. 1980. "The Organization of Actin Filaments in the Stereocilia of Cochlear Hair Cells." *Journal of Cell Biology* 86 (1): 244–59. https://doi.org/10.1083/jcb.86.1.244.

Tilney, L. G., M. S. Tilney, and D. A. Cotanche. 1988. "Actin Filaments, Stereocilia, and Hair Cells of the Bird Cochlea. V. How the Staircase Pattern of Stereociliary Lengths Is Generated." *The Journal of Cell Biology* 106 (2): 355–65. https://doi.org/10.1083/jcb.106.2.355.

Tilney, Lewis G, and James S Saunders. 1983. "Actin Filaments, Stereocilia, and Hair Cells of the Bird Cochlea I. Length, Number, Width, and Distribution of Stereocilia of Each Hair Cell Are Related to the Position of the Hair Cell on the Cochlea," 15.

Tilney, Lewis G, Mary S Tilney, James S Saunders, and J Derosier. 1986. "Actin Filaments, Stereocilia, and Hair Cells of the Bird Cochlea III : The Development and Differentiation of Hair Cells and Stereocilia," 19.

Tobin, Mélanie, Atitheb Chaiyasitdhi, Vincent Michel, Nicolas Michalski, and Pascal Martin. 2019. "Stiffness and Tension Gradients of the Hair Cell's Tip-Link Complex in the Mammalian Cochlea." Edited by Doris K Wu, Andrew J King, and Anthony J Ricci. *ELife* 8 (April): e43473. https://doi.org/10.7554/eLife.43473.

Tocchetti, Arianna, Charlotte Blanche Ekalle Soppo, Fabio Zani, Fabrizio Bianchi, Maria Cristina Gagliani, Benedetta Pozzi, Jan Rozman, et al. 2010. "Loss of the Actin Remodeler Eps8 Causes Intestinal Defects and Improved Metabolic Status in Mice." *PLOS ONE* 5 (3): e9468. https://doi.org/10.1371/journal.pone.0009468.

Tompkins, Nathan, Kateri J. Spinelli, Dongseok Choi, and Peter G. Barr-Gillespie. 2017. "A Model for Link Pruning to Establish Correctly Polarized and Oriented Tip Links in Hair Bundles." *Biophysical Journal* 113 (8): 1868–81. https://doi.org/10.1016/j.bpj.2017.08.029.

Tona, Yosuke, and Doris K Wu. 2020. "Live Imaging of Hair Bundle Polarity Acquisition Demonstrates a Critical Timeline for Transcription Factor Emx2." *ELife* 9 (September): e59282. https://doi.org/10.7554/eLife.59282.

Tsien, Roger Y. 1980. "New Calcium Indicators and Buffers with High Selectivity against Magnesium and Protons: Design, Synthesis, and Properties of Prototype Structures." *Biochemistry* 19 (11): 2396–2404. https://doi.org/10.1021/bi00552a018.

Vandekerckhove, Joel, and Klaus Weber. 1978. "At Least Six Different Actins Are Expressed in a Higher Mammal: An Analysis Based on the Amino Acid Sequence of the Amino-Terminal Tryptic Peptide." *Journal of Molecular Biology* 126 (4): 783–802. https://doi.org/10.1016/0022-2836(78)90020-7.

Vélez-Ortega, A Catalina, Mary J Freeman, Artur A Indzhykulian, Jonathan M Grossheim, and Gregory I Frolenkov. 2017. "Mechanotransduction Current Is Essential for Stability of the Transducing Stereocilia in Mammalian Auditory Hair Cells." *ELife* 6 (March): e24661. https://doi.org/10.7554/eLife.24661.

Vélez-Ortega, A. Catalina, and Gregory I. Frolenkov. 2019. "Building and Repairing the Stereocilia Cytoskeleton in Mammalian Auditory Hair Cells." *Hearing Research*, Annual Reviews 2019, 376 (May): 47–57. https://doi.org/10.1016/j.heares.2018.12.012.

Vignjevic, Danijela, Shin-ichiro Kojima, Yvonne Aratyn, Oana Danciu, Tatyana Svitkina, and Gary G. Borisy. 2006. "Role of Fascin in Filopodial Protrusion." *The Journal of Cell Biology* 174 (6): 863–75. https://doi.org/10.1083/jcb.200603013.

Volkmann, Niels, David DeRosier, Paul Matsudaira, and Dorit Hanein. 2001. "An Atomic Model of Actin Filaments Cross-Linked by Fimbrin and Its Implications for Bundle Assembly and Function." *Journal of Cell Biology* 153 (5): 947–56. https://doi.org/10.1083/jcb.153.5.947.

Wang, Yan, Futoshi Shibasaki, and Kensaku Mizuno. 2005. "Calcium Signal-Induced Cofilin Dephosphorylation Is Mediated by Slingshot via Calcineurin." *The Journal of Biological Chemistry* 280 (13): 12683–89. https://doi.org/10.1074/jbc.M411494200.

Wang, Yanfei, Jie Li, Xuerui Yao, Wei Li, Haibo Du, Mingliang Tang, Wei Xiong, Renjie Chai, and Zhigang Xu. 2017. "Loss of CIB2 Causes Profound Hearing Loss and Abolishes Mechanoelectrical Transduction in Mice." *Frontiers in Molecular Neuroscience* 10: 401. https://doi.org/10.3389/fnmol.2017.00401.

Wioland, Hugo, Berengere Guichard, Yosuke Senju, Sarah Myram, Pekka Lappalainen, Antoine Jégou, and Guillaume Romet-Lemonne. 2017. "ADF/Cofilin Accelerates Actin Dynamics by Severing Filaments and Promoting Their Depolymerization at Both Ends." *Current Biology: CB* 27 (13): 1956-1967.e7. https://doi.org/10.1016/j.cub.2017.05.048.

Wolf, K., and M. C. Quimby. 1964. "Amphibian Cell Culture: Permanent Cell Line from the Bullfrog (Rana Catesbeiana)." *Science* 144 (3626): 1578–80. https://doi.org/10.1126/science.144.3626.1578.

Wright, A. 1983. "Scanning Electron Microscopy of the Human Organ of Corti." *Journal of the Royal Society of Medicine* 76 (4): 269–78.

Wright, A. 1984. "Dimensions of the Cochlear Stereocilia in Man and the Guinea Pig." *Hearing Research* 13 (1): 89–98. https://doi.org/10.1016/0378-5955(84)90099-6.

Xiong, Wei, Nicolas Grillet, Heather M. Elledge, Thomas F.J. Wagner, Bo Zhao, Kenneth R. Johnson, Piotr Kazmierczak, and Ulrich Müller. 2012. "TMHS Is an Integral Component of the Mechanotransduction Machinery of Cochlear Hair Cells." *Cell* 151 (6): 1283–95. https://doi.org/10.1016/j.cell.2012.10.041.

Yamoah, Ebenezer N., Ellen A. Lumpkin, Rachel A. Dumont, Peter J. S. Smith, A. J. Hudspeth, and Peter G. Gillespie. 1998. "Plasma Membrane Ca2+-ATPase Extrudes Ca2+from Hair Cell Stereocilia." *Journal of Neuroscience* 18 (2): 610–24. https://doi.org/10.1523/JNEUROSCI.18-02-00610.1998.

Yasuda, Ryohei, Hidetake Miyata, and Jr Kinosita Kazuhiko. 1996. "Direct Measurement of the Torsional Rigidity of Single Actin Filaments." *Journal of Molecular Biology* 263 (2): 227–36. https://doi.org/10.1006/jmbi.1996.0571.

Yasuda, Shingo, Fabian Oceguera-Yanez, Takayuki Kato, Muneo Okamoto, Shigenobu Yonemura, Yasuhiko Terada, Toshimasa Ishizaki, and Shuh Narumiya. 2004. "Cdc42 and MDia3 Regulate Microtubule Attachment to Kinetochores." *Nature* 428 (6984): 767–71. https://doi.org/10.1038/nature02452.

Yin, H. L., J. H. Hartwig, K. Maruyama, and T. P. Stossel. 1981. "Ca2+ Control of Actin Filament Length. Effects of Macrophage Gelsolin on Actin Polymerization." *The Journal of Biological Chemistry* 256 (18): 9693–97.

Young, Kevin G., Susan F. Thurston, Sarah Copeland, Chelsea Smallwood, and John W. Copeland. 2008. "INF1 Is a Novel Microtubule-Associated Formin." *Molecular Biology of the Cell* 19 (12): 5168–80. https://doi.org/10.1091/mbc.e08-05-0469.

Yu, Miao, Xin Yuan, Chen Lu, Shimin Le, Ryo Kawamura, Artem K. Efremov, Zhihai Zhao, et al. 2017. "MDia1 Senses Both Force and Torque during F-Actin Filament Polymerization." *Nature Communications* 8 (1): 1650. https://doi.org/10.1038/s41467-017-01745-4.

Yu, X. L., E. R. Lewis, and D. Feld. 1991. "Seismic and Auditory Tuning Curves from Bullfrog Saccular and Amphibian Papillar Axons." *Journal of Comparative Physiology. A, Sensory, Neural, and Behavioral Physiology* 169 (2): 241–48. https://doi.org/10.1007/BF00215871.

Zhang, Duan-Sun, Valeria Piazza, Benjamin J. Perrin, Agnieszka K. Rzadzinska, J. Collin Poczatek, Mei Wang, Haydn M. Prosser, James M. Ervasti, David P. Corey, and Claude P. Lechene. 2012. "Multi-Isotope Imaging Mass Spectrometry Reveals Slow Protein Turnover in Hair-Cell Stereocilia." *Nature* 481 (7382): 520–24. https://doi.org/10.1038/nature10745.

Zhao, Y.-d., E. N. Yamoah, and P. G. Gillespie. 1996. "Regeneration of Broken Tip Links and Restoration of Mechanical Transduction in Hair Cells." *Proceedings of the National Academy of Sciences* 93 (26): 15469–74. https://doi.org/10.1073/pnas.93.26.15469.

Zheng, Lili, Gabriela Sekerková, Kelly Vranich, Lewis G. Tilney, Enrico Mugnaini, and James R. Bartles. 2000. "The Deaf Jerker Mouse Has a Mutation in the Gene Encoding the Espin Actin-Bundling Proteins of Hair Cell Stereocilia and Lacks Espins." *Cell* 102 (3): 377–85. https://doi.org/10.1016/S0092-8674(00)00042-8.

Zheng, Wang, and Jeffrey R. Holt. 2021. "The Mechanosensory Transduction Machinery in Inner Ear Hair Cells." *Annual Review of Biophysics* 50 (1): annurev-biophys-062420-081842. https://doi.org/10.1146/annurev-biophys-062420-081842.

Zhou, Fen, Philip Leder, and Stuart S. Martin. 2006. "Formin-1 Protein Associates with Microtubules through a Peptide Domain Encoded by Exon-2." *Experimental Cell Research* 312 (7): 1119–26. https://doi.org/10.1016/j.yexcr.2005.12.035.

Zigmond, Sally H. 2004. "Formin-Induced Nucleation of Actin Filaments." *Current Opinion in Cell Biology* 16 (1): 99–105. https://doi.org/10.1016/j.ceb.2003.10.019.

Zwaenepoel, Ingrid, Alexandra Naba, Marcel Menezes Lyra Da Cunha, Laurence Del Maestro, Etienne Formstecher, Daniel Louvard, and Monique Arpin. 2012. "Ezrin Regulates Microvillus Morphogenesis by Promoting Distinct Activities of Eps8 Proteins." *Molecular Biology of the Cell* 23 (6): 1080–95. https://doi.org/10.1091/mbc.E11-07-0588.

RÉSUMÉ

Les cellules ciliées de l'oreille interne convertissent les vibrations induites par le stimulus sonore en signaux électriques. Chaque cellule ciliée est dotée d'une touffe de 'stéréocils' cylindriques remplis de filaments d'actine. Une déflexion de la touffe ciliaire module la tension dans les liens de bout-de-cil qui interconnectent les stéréocils et transmettent une force à des canaux ioniques, entraînant l'apparition d'un courant. La morphologie de la touffe ciliaire est étroitement liée à la fonction des cellules ciliées: les touffes ciliaires sont plus courtes pour la détection des hautes fréquences et des défauts morphologiques de la touffe ciliaire sont associés à des pertes auditives. Le mécanisme qui maintient la morphologie de la touffe ciliaire tout au long de la vie est donc d'une grande importance mais demeure obscur. Ce projet de thèse vise à étudier une rétroaction entre la transduction mécanoélectrique et la morphologie de la touffe ciliaire. Nous avons observé chez la grenouille que bloquer les canaux de transduction ou couper les liens de bout-de-cil entraîne un raccourcissement (~15%) et un épaississement (~17-60%) des stéréocils. En conséquence, la rigidité de la touffe ciliaire est deux fois plus grande que dans les cellules non perturbées. La microscopie électronique a de plus révélé que l'espacement entre filaments d'actine dans chaque stéréocil n'est pas modifié. L'épaississement d'un stéréocil résulte donc d'une augmentation du nombre de filaments d'actine. Enfin, l'inhibition des formines—des protéines impliquées dans la polymérisation de l'actine—produit des stéréocils plus minces dans les cellules témoins et aboli presque complètement l'épaississement des stéréocils résultant du blocage des canaux de transduction. Ces observations sont suggèrent que le contrôle de la polymérisation de l'actine par les canaux de transduction pourrait dépendre de la formine.

MOTS CLÉS

L'audition, les cellules ciliées, les touffes ciliaires, le cytosquelette d'actine, la transduction mécanoélectrique

ABSTRACT

Hair cells of the inner ear operate as cellular microphones that convert sound-evoked vibrations into electrical signals. Each hair cell is endowed with a mechanosensitive hair bundle—a tuft of actin-filled and cylindrical stereocilia. Hearing starts when sound evokes deflections of the hair bundle. Deflections modulate tension in the tip links that interconnect stereocilia and convey force to mechanosensitive ion channels, resulting in ionic influx. The hair-bundle morphology is tightly coupled to hair-cell function as a frequency-selective detector: high-frequency hair cells have shorter hair bundles and morphological defects in the hair bundles are associated with deafness. Because hair cells do not regenerate in mammals, the mechanisms that maintain the hair-bundle morphology throughout life are of great importance, yet have remained elusive. This PhD project aims at studying a feedback mechanism between mechanoelectrical transduction and hair-bundle morphology. With hair cells excised from a frog's ear, we found that blocking the transduction channels or disrupting the tip links resulted in shortening (~15%) and widening (~17-60%) of the stereocilia. Hair bundles with blocked transduction channels showed a 2-fold increase in their stiffness, a change too large to be explained by shortening only. Electron microscopy revealed that spacing of the parallel actin filament in the core of the stereocilia does not change with blocked transduction channels or disrupted tip links. Widening thus probably resulted from an increase in the number of actin filaments constituting the stereociliary core. Inhibiting formins— proteins that promote actin polymerization—resulted in thinner stereocilia in control cells and nearly abolished stereocilia widening upon blockage of the MET channels. These observations suggest that the control of actin polymerization by the transduction channels is likely to be formin-dependent.

KEYWORDS

hearing, hair cell, hair bundle, actin cytoskeleton, mechanoelectrical transduction